Humidity sensing by optically interfacing with spectrally absorptive materials

A thesis submitted to Brunel University
for the degree of Doctor of Philosophy

By

Ahmad H.Kharaz

Department of Manufacturing and Engineering Systems,
Brunel University, Uxbridge Middlesex UB8 3PH.

1999

Abstract

The measurement of humidity is rapidly increasing in importance in physical, chemical and biological processes as industry attempts to improve quality and production rates by better control of relative humidity (RH).

A novel optical fibre humidity sensor suitable for use in an optical fibre multi-point distributed sensing system has been developed, thus for the first time allowing multi-point measurements of humidity along an optical fibre which can be distributed within an industrial plant or machine without the need for electrical power supplies.

The novel point sensor is based on the principle of using the absorption spectrum of a colorimetric reagent (cobalt chloride) immobilised on the surface of the core of a multimode optical fibre by employing a thin gelatin film. The single point sensor has an insertion loss of less than 0.2 dB. Two-wavelength detection is employed to provide referencing to eliminate common mode intensity variation.

The basic design, construction and testing of an experimental sensor in the humidity region 20 to 80% RH and temperature range 25 to 50 °C is described. Resolution and Repeatability can be better than 2% RH with a time constant of 0.5 second.

A two-wavelength optical time domain reflectometer (OTDR) has been developed and a four-sensor network has been built. The resolution of measurement on the network can be better than 4% RH, but because of noise in the OTDR the resolution value is dependant on averaging time in the instrument.

Acknowledgements

I would like to express my deepest thanks and appreciation to Professor Barry E. Jones for his continuous help, encouragement, and valuable supervision throughout my work.

I would also like to thank; Dr. Ken Hale for his valuable support and continuous interest throughout this research work, Professor R C Spooncer for his help and all the staff of the BCMM for all their support.

I would further like to thank The UK National Physical Laboratory (NPL) for sponsoring me on this project. Special thanks are due to Stephanie Bell and Mark Stevens at NPL, for their support throughout my work and specially during my work at NPL. I would also like to thank Dr K P Birch in the Division of Mechanical and Optical Metrology at NPL for his technical help at the start of this work.

I am very grateful to the EPSRC for awarding me the PhD studentship which enabled me to undertake this work.

Last but not least I would like to thank my wife Margaret and my children Esra, Saphia, Nisreen and Adam for the sacrifices they made to make this possible. My special thanks are due to my parents, brothers and sisters for their invaluable encouragement.

CONTENTS

List of figures and tables

CHAPTER 1

Introduction

1.1 Industrial requirements

The measurement of humidity is rapidly increasing in importance in physical, chemical and biological processes as industry attempts to improve quality and production rates by better control of humidity. Typical examples occur in the food, textile, chemicals, electronics and pharmaceutical industries (Diedling 1989, Berro et al 1993, Komatsu and Tanaka 1994, Allison 1996, Bruce et al 1997). Fibre optic humidity sensors would not only have the advantages of freedom from electromagnetic interference, intrinsic safety and remote monitoring but offer the prospect of distributed sensing using the fibre itself as the sensor, and so it is not surprising that several optical fibre humidity sensing methods have been reported (Jones 1984, Jones 1985, Dakin and Culshaw 1989).

A report issued on behalf of the UK Energy Efficiency Office (ETSU 1993) has emphasised the importance of investing in new sensor technology. It stated that

"Improved process control is a means of saving energy but is often limited by the sensor technology available".

The International Energy Agency believes savings between 5% and 20% can be achieved in any individual industry by this method; with humidity control in the various industries the savings could be over 20% (see Table 1.1). Averaged across all industry this gives scope for energy consumption to be cut by at least 10%. In the UK,

this saving equates to approximately 200 PJ/year for primary energy, worth in excess of £500 million. This energy saving will reduce carbon dioxide emissions to the atmosphere by two million tonnes (ETSU 1993).

Table 1. 1 Potential energy savings by employing humidity sensing (ETSU 1993).

Requirement	*Applications*	*Total market PJ/yr*	*Market penetration of application*	*Energy saving*	*Resultant saving PJ/yr*
Cheap durable air humidity	Tumble dryers and textile dryers	40	20%	20%	2
Reliable, high temperature air humidity	Cement, ceramic and paper drying	100	10%	20%	2
Bulk moisture content unaffected by composition, etc.	Ceramic, food, chemicals & textiles	80	5%	20%	0.8
Humidity profile across a wide area	Drying processes	100	2%	20%	0.4

The need for strategic research and development (R&D) to improve energy efficiency has been highlighted by research experts in a Commission of the European Communities study (Reay and Pilavachi 1989) which states:

"A general consensus was found among industrial companies that sensor development has lagged seriously behind control theory development. The consequence is that implementation of advanced control strategies, which could improve energy efficiency significantly, is hampered by lack of adequate sensors to make the on-line measurement needed by such control systems".

In industrial drying processes reliable sensors are needed for the measurement of the water content of the exhaust gas (Kuisma 1988). To see how that is related to some industries, examples are given below.

In the ceramics industry the bulk moisture content of clay must be carefully controlled on-line (Itaya and Hasatani 1996) because time and energy are wasted in removing excess moisture during the drying stage. Although humidity is the best parameter to monitor, drying kilns are often controlled on a temperature/time basis, because reasonably cheap, durable humidity sensors which operate at 400 °C in industry environments are not generally available (Kemp 1998).

In food and drink drying operations, such as grain drying and malting, humidity measurements at around 200 °C are required (Estrada and Litchfield 1993). Energy is saved if heating is discontinued once the product is dry and additional savings can be made if the drying system recycles hot air, providing it is below certain humidity (Bakker-Arkema 1983).

The most important area for sensors in the textiles industry is the residual moisture content of fabric in a tumble dryer (Slater 1979, Diedling 1989). Without such control, the tumble dryers run on a very simple temperature /time basis. Sensors for this application should be durable and unaffected by dust and lint. Some systems are available for large commercial laundries, but low cost sensors for use in small laundries are not available.

In paper manufacture, temperature and humidity need to be controlled and it is important to maintain uniformity of product along its length and its width. Humidity sensors in this industry may have to withstand temperature as high as 400 °C. They must not be susceptible to other gases or contamination with fibres and dust (Castelli and Tenney 1996). Some sensors are available for operation under these conditions, but

they are expensive (several thousand pounds) and still suffer from drift and contamination problems.

The importance of humidity measurement in industry can readily be determined by noting the number of humidity related British Standard specifications published for various industries. Some of the areas covered are; testing vulcanised rubber, high voltage testing, colour fastness of textile, use of desiccants in packaging, electroplated coatings of cadmium and zinc on iron and steel, testing plastics, solid electrical insulating materials, automatic analysis of flue gases, analysis of fuel gases, specification for laboratory humidity ovens, methods of test for paints, determination of resistance to humidity (cyclic condensation), etc. [see Appendix II for more examples].

Existing methods of humidity measurement are by no means adequate to meet the needs identified above, and this will be discussed later in the thesis. The purpose of the research investigation reported upon in this thesis has been to explore a completely new way of making humidity measurement which could have relevance to these needs.

1.2 Aim of Research Work

The aim of the research reported in this thesis has been to develop a novel optical fibre humidity sensor suitable for use in an optical fibre distributed sensing system, thus for the first time allowing multi-point measurements of humidity along an optical fibre which can be distributed within an industrial plant or machine without the need for electrical power supplies. It is believed that such an approach would open-up new prospects for improving manufacturing quality and efficiency as well as energy efficiency in many industrial situations.

1.3 Overview of the thesis

The thesis is structured in the following manner.

Chapter 2 deals with the fundamentals of humidity measurement. It explains the various parameters and their definitions and how they are related. It goes on to discuss the existing humidity measurement methods and their limitations. Possible optical fibre measurement methods are then introduced and their potential advantages are considered.

Chapter 3 introduces the theory of optical fibre transmission, fibre losses and the various mechanisms that may limit the minimum pulse width that can propagate through a fibre. How light is coupled into the fibre and the different ways of connecting the fibres together are discussed next. Optical sources and detectors are then reviewed. Optical fibre sensing systems are introduced and intrinsic and extrinsic sensors are defined. The various transduction mechanisms that may be employed to make an optical fibre sensor are pointed out. Some examples of optical fibre sensors are then given. Various intensity referencing techniques are discussed. The prospect for distributed optical fibre sensors is introduced and various possible schemes are briefly considered.

Having looked at various optical fibre sensing methods, Chapter 4 introduces the novel sensor employed in the present work. It shows how the sensor is physically configured and then using geometric optics and the theory of absorption and scattering a model of sensor operation is developed. The power budget of the sensor is calculated, and its installation in a distributed sensing system is examined.

Chapter 5 explains the experiments carried out to select the various components of the new sensor. It explains the general arrangement and describes the initial experiments

carried out on different materials. It concludes with a basic design for the thin film to be used.

Having carried out the initial experiments, a complete intrinsic optical fibre humidity sensor was built and tested (described in Chapter 6). A stabilised LED transmitter-receiver module was designed and constructed to enable an evaluation of the sensor time constant. The sensor was tested using a two-wavelength method (one wavelength being a reference). It has also been evaluated against temperature variations. A portable system was also built for field testing.

Chapter 7 deals with a new distributed optical fibre humidity sensing system. This system is based on the point sensor developed in the previous chapters. The design, construction and testing of the experimental system are described. This is followed by a description of the basic design of a new 670nm laser driver and a two-wavelength optical time domain reflectometer (OTDR). A four sensor network has been built and tested and this work is presented in Chapter 7.

Finally, in Chapter 8 the conclusions of the research investigation are outlined. The basic characteristics of the new humidity and the distributed humidity sensing system are summarised, and there is a discussion of future work needed to produce fully engineered sensors and systems for use as demonstration in relatively low temperature industrial applications. A new reflective optical fibre humidty sensing system is proposed. Such a system has the potential of multiplexing much more sensors along a single fibre. The thesis is concluded by the reference list and appendices.

CHAPTER 2

Humidity measurement

2.1 Introduction

Humidity is a measure of water vapour in a gas. It may be expressed in a variety of ways depending on the needs of the particular process and the measuring instrumentation utilised. For example it can be described in terms of relative humidity, dew-point temperature, mass ratio or partial pressure. The term hygrometry is often used when talking about humidity. It is derived from the Greek word hygros, which means moist, and is defined as that branch of science which is concerned with the measurement of moisture content (Harrison 1965).

Most materials, whether natural or synthetic, react to the humidity of the atmosphere. This can be seen by changes in their physical, electrical and chemical characteristics. Consequently, measurement of these changes can serve as an indication of the humidity of the surrounding atmosphere.

2.2 Humidity parameters and definitions

2.2.1 Vapour pressure

The water vapour in the atmosphere behaves like any other gases present in that it exerts a pressure which makes up part of the total pressure of air. This partial pressure of the water vapour is known as the vapour pressure (e), and may be measured in any of the usual units of pressure (Meteorological Office 1981).

At constant temperature, free evaporation of water or ice from a plane surface into a space containing only water vapour ceases, and equilibrium is reached, when the pressure exerted by the water vapour attains a certain maximum value which depends on the temperature. This pressure is known as the saturated vapour pressure (e_S) and the space is said to be saturated (Harrison 1965, BS 1339). Saturation vapour pressure is a function of temperature as shown in Fig.2.1.

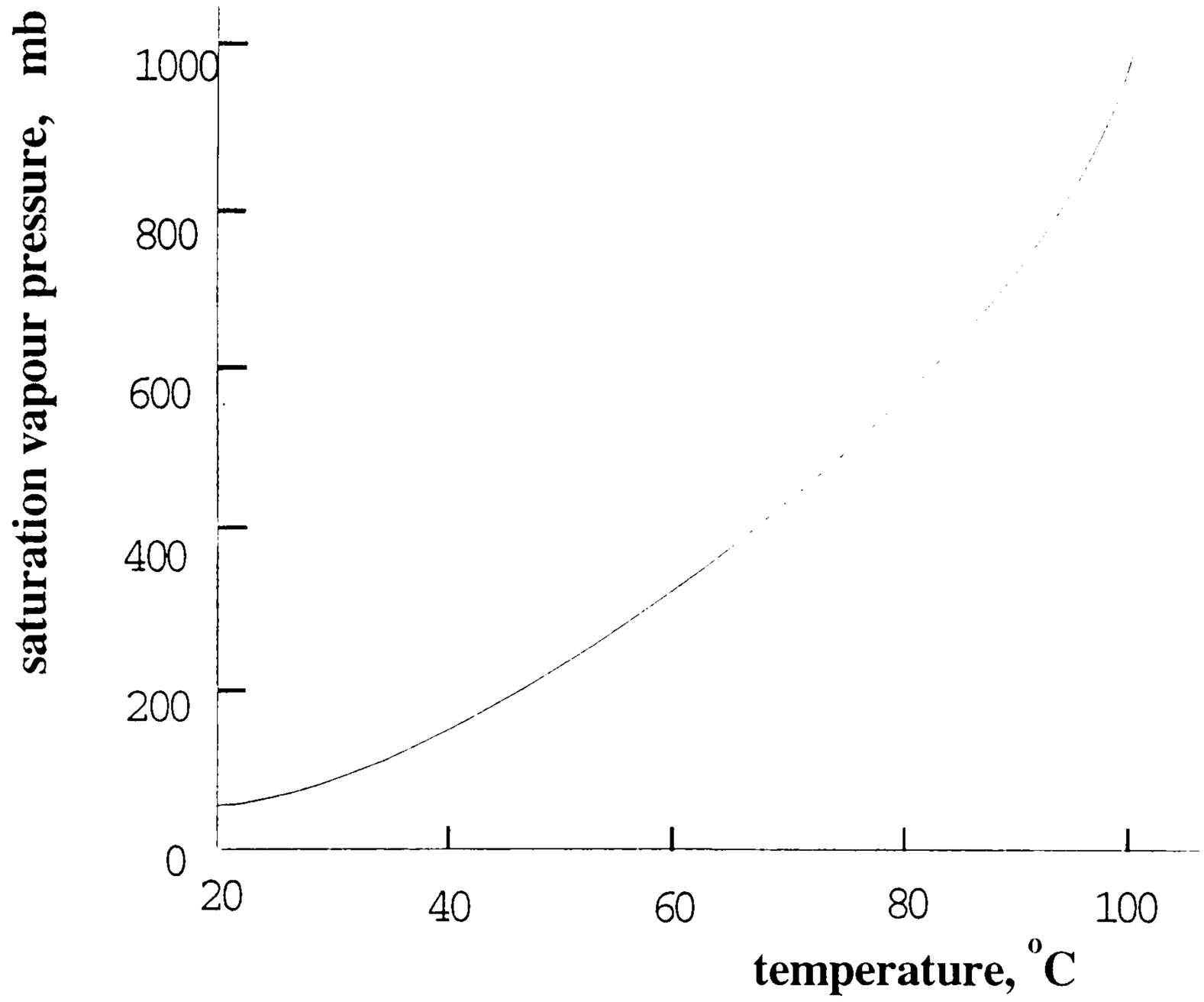

Figure 2. 1 The variation of saturation water vapour pressure with temperature (Sira 1991).

2.2.2 Absolute humidity

Absolute humidity (d_V) is sometimes known as vapour concentration, or vapour density, and is defined as the mass of water vapour present in unit volume of moist air and is normally expressed in kilogram per cubic metre of moist air (BS1339 1965, Harrison 1965, Meteorological Office 1981).

i.e.

$$d_v = \frac{m_v}{V} \qquad (2.1)$$

m_V = mass of water vapour contained in the sample of moist air, and V = total volume occupied by the sample of moist air.

It is equivalent to water vapour density or vapour concentration (Hickman 1970) and increases rapidly as temperature increases, as shown in Fig. 2.2.

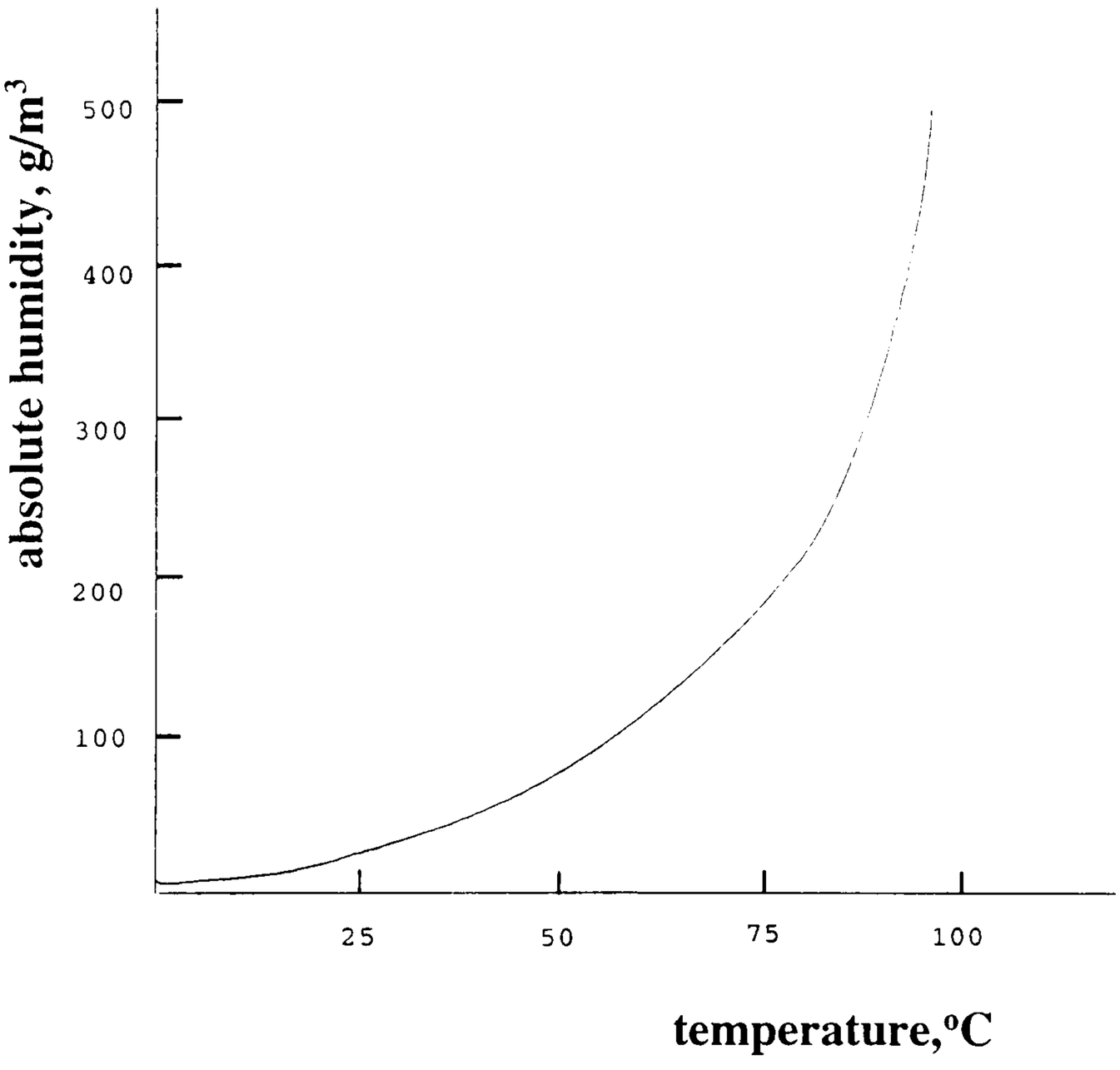

Figure 2. 2 The absolute humidity of saturated air from 0°C-100°C (Hickman 1970).

For dry air the relationship between pressure (p), density (d_a) and temperature T is given by the ideal gas equation

$$p = RTd_a \qquad (2.2)$$

where R = 2.87 for dry air and p in mb, T in K and d_a in kg/m^3. Water vapour has a density of 0.662 of the dry air density. Applying this equation to moist air (assuming water vapour to act as an ideal gas (Loughlin 1993), water vapour density is given by

$$d_v = 0.662\frac{e_d}{RT} \qquad (2.3)$$

Thus the absolute humidity d_v is proportional to the vapour pressure at a given temperature.

2.2.3 Mixing ratio

The mixing ratio (r) of moist air is the ratio of the mass of water vapour (m_v) per unit mass of dry air (m_a) (Harrison 1965, BS1339).

$$r = \frac{m_v}{m_a} \qquad (2.4)$$

Mixing ratio can also be calculated using the previous gas equations;

$$r = \frac{m_v}{m_a} = \frac{\frac{0.622e_d}{RT}}{\frac{p - e_d}{RT}}$$

$$\text{i.e.} \qquad r = \frac{0.622e_d}{p - e_d} \qquad (2.5)$$

where e_d = vapour pressure of the air and p = pressure.

2.2.4 Mole fraction of water vapour

The mole fraction of water vapour is the ratio of the number of moles of the water vapour to the total number of moles present (Harrison 1965, BS1339 1965). To every mixing ratio there is a corresponding mole fraction.

2.2.5 Specific humidity

The specific humidity (q) is defined as the ratio of the mass of water vapour (m_v) to the mass of moist air (m_a) with which it is associated (Meteorological Office 1981):

$$q = \frac{m_v}{m_v + m_a} = \frac{r}{1+r} \qquad (2.6)$$

where r = mixing ratio.

2.2.6 Dew-point

The dew-point is the temperature (^oC dp) at which condensation occurs when a gas is cooled (at constant pressure). The gas is then saturated with respect to water. It is called the frost point when the gas is saturated with respect to ice, although the term 'dew-point' is usually used (Harrison 1965, BS1339 1965).

2.2.7 Relative humidity (RH)

Relative humidity is the ratio of the actual vapour pressure (e) to the saturated vapour pressure (e_S) over a plane liquid water surface at the same temperature, expressed as a percentage (Harrison 1965, BS1339 1965). Its importance arises because many systems (including the human body) respond to it;

$$\%RH = \frac{e}{e_s} \times 100\% \qquad (2.7)$$

Fig.2.3 shows the relationship between relative humidity, dew-point and ambient temperature.

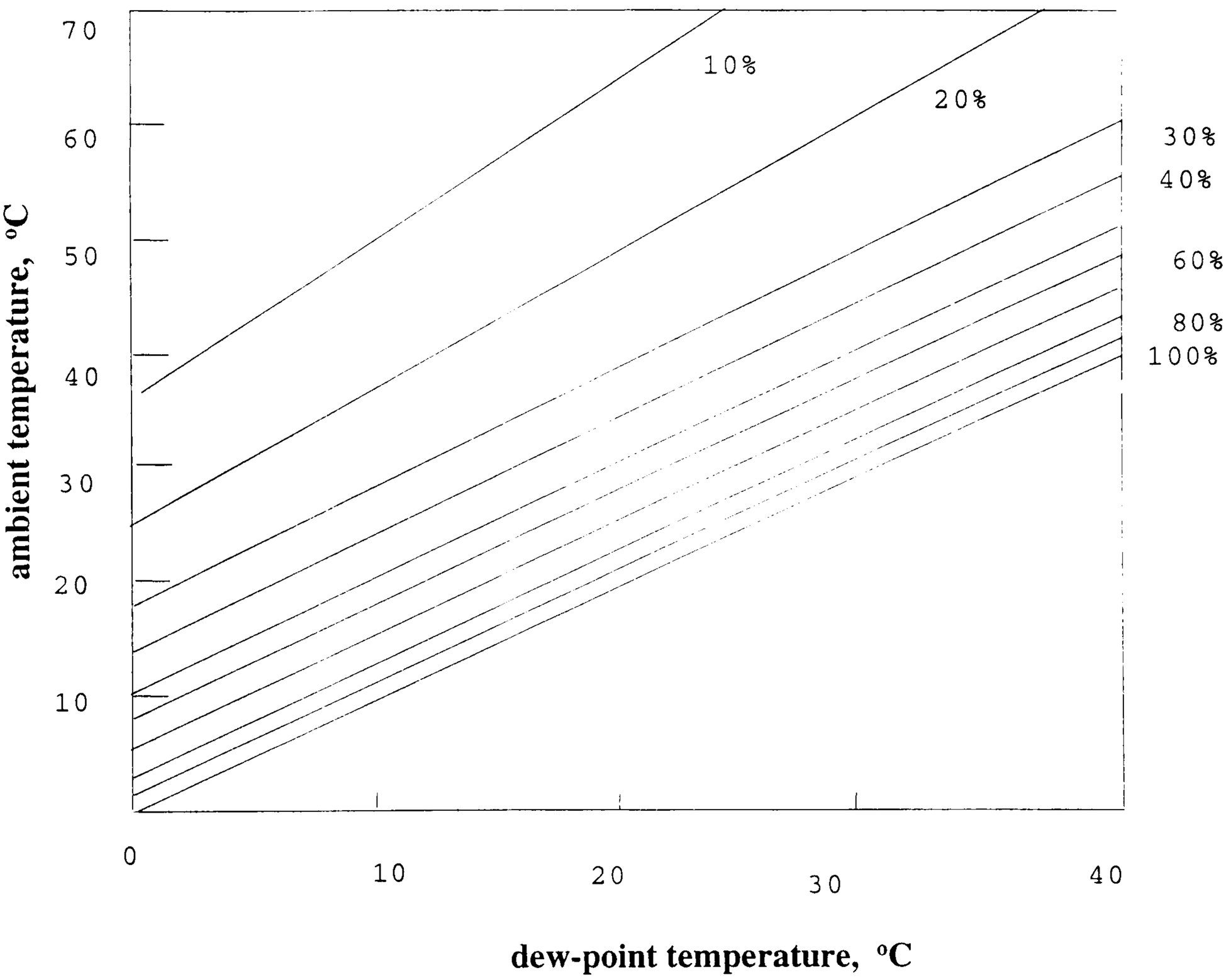

Figure 2. 3 Relative humidity against dew-point and ambient temperature (Sira 1991).

2.3 Existing measurement methods

Great many different methods of humidity measurement have been used, and the most common methods are described below.

2.3.1 Mechanical hygrometer

Traditionally, the mechanical hygrometer relied on the change in length of a human hair or animal membrane with humidity. Latterly various plastic materials and textiles are used. Usually a simple mechanical linkage moves a pointer and today a few instruments have electrical or pneumatic outputs (Pragnell 1986).

It operates over a limited temperature range. The typical measurement range is 25 to 80 % RH, but response is relatively slow, hysteresis is usually several percent RH, and accuracy is unlikely to be better than $\pm$ 6% RH (Hichman 1970). Even this accuracy is only normally possible over the mid-range, because many of the materials used have a very non-linear response at high and low humidities (Pragnell 1986).

2.3.2 Psychrometer (wet and dry hygrometer)

Psychrometers measure humidity by measuring the ambient (dry bulb) temperature, and the temperature of an evaporating water source (wet-bulb) temperature. In practice the source of moisture is usually a moistened wick surrounding a thermometer. The reservoir, which provides water to the wick, requires regular filling with distilled water.

The method is simple and cheap, but is very sensitive to small temperature errors which may occur for several reasons, including thermometer inaccuracy. An air-stream of speed 3 to 5 m/sec is essential for accurate measurement (Croft 1986). The rate of evaporation from the wick can be reduced by deposition from the air stream thus effecting the accuracy. With the proper air-stream flow and the use of high accuracy thermometers, accuracy can be better than $\pm$3% (Croft 1986, Pragnell 1986).

2.3.3 Electrolytic hygrometer

The electrolytic hygrometer relies on phosphorus pentoxide, which is a very powerful desiccant, to absorb all of the moisture from the gas sample. The phosphorus pentoxide is supported on a substrate between electrodes (usually platinum), and the water is electrolysed to form hydrogen and oxygen. Theoretically the electrolysis current is related by Faraday's law to the rate of water uptake, however in practice, incomplete absorption and recombination of the hydrogen and oxygen lead to errors. Accuracy is normally about $\pm$10 %, but with high precision gas flow rate measurement and proper precautions when recoating the cell electrodes, an accuracy of $\pm$5 % can be achieved (Walker and Campion 1965, Pragnell 1986). The measuring cell needs regenerating or replacing roughly every three months depending on operating conditions.

2.3.4 Saturated (heated) lithium chloride hygrometer

Above approximately 10% RH, lithium chloride adsorbs water and becomes conductive. A large current is passed via the electrodes on a non-conductive substrate. As a result the lithium chloride is heated and moisture is driven off. An equilibrium temperature is established which depends on the ambient humidity. The sensor temperature can be converted to a dew-point using a characteristics curve. Accuracy is typically about $\pm$1 ^{o}C dp (Pragnell 1986). The lithium chloride element needs renewing when its performance deteriorates and also it must be re-moistened at regular intervals (Carr-Brion 1986).

2.3.5 The condensation hygrometer

Measurement of condensation temperature is almost as old as humidity measurement itself. Early instruments relied on cooling a surface of something similar to a test tube. Cooling was achieved by means of evaporating alcohol, ether, or by other means.

depending on the temperature required and the formation of dew was observed by the operator. An automatic dew-point hygrometer using Peltier cooling was first reported in 1959 (Gerthsen *et al* 1959).

The development of an efficient dew-point hygrometer followed the comparatively recent development of efficient Peltier coolers and reliable opto-electronics. A Peltier cooler is used to cool a mirror. Formation of dew point on the mirror surface is detected by means of an optical sensor and the rate of cooling is controlled to maintain a constant dew layer. A temperature sensor (normally a platinum resistance thermometer) in intimate contact with the mirror surface is used to measure the condensation temperature (Loughin 1993). An accuracy of $\pm$0.2 °C dp is possible with reproducibility better than $\pm$0.05 °C dp, and so the condensation hygrometer is the most accurate instrument available commercially at the present time (Pragnell 1986, Sira 1991, Loughlin 993). The mirror requires regular cleaning and require a filtered gas to minimise contamination and give long periods between cleaning.

2.3.6 Gravimetric hygrometer

The gravimetric hygrometer is the ultimate standard for calibration of humidity-measuring devices, and is strictly a laboratory apparatus. The water content of the sample gas is separated from the gas, and weighed. The quantity of the remained dry gas is measured. This give a direct measure of the amount of water present. It is used as the primary humidity standard by both the UK National Physical Laboratory (NPL) and the USA National Bureau Standard (NBS) (Hickman 1970). The NPL humidity calibration facility currently offers an uncertainty of $\pm$0.1 °C dp (95% confidence) in the mid-range, with increased uncertainty at higher and lower humidities.

Gravimetric hygrometers are very slow in operation and tedious to use: they measure the average humidity over a period of time, which may be up to 18 hours in case of the NPL standard, or up to 35 hours in the case of the NBS standard. They can only be used under ideal conditions when very stable humidity can be maintained for long periods. They also have a limited measurement range -30 to +30 ^{o}C dp for NBS and -50 to +80^{o}C dp for NPL (Pragnell 1986).

2.3.7 Quartz crystal oscillator

The oscillation frequency of a quartz crystal coated with a hygroscopic material such as aluminium oxide can provide a very sensitive output for humidity detection. The additional mass of the absorbed water onto the surface alters the oscillation frequency, with the frequency reducing as the moisture content rises.

The instrument makes use of two simple crystal-controlled oscillators having nearly identical temperature/frequency characteristics. One of the quartz plates is coated with the hygroscopic film and exposed to the atmosphere. The difference in frequency of the two oscillators is a function of humidity, and measurement resolution can be about 4 % RH with a time-constant of less than 1 second (Gjessing *et al* 1967).

A dew-point hygrometer using quartz crystal has also been reported (Inamatsu and Takashi 1985). In this case there is a decrease in the resonant frequency with the condensation of water vapour on the surface of the quartz crystal and the temperature of the surface is controlled to keep the mass of the condensation constant.

2.3.8 Microwave techniques

There are certain bands in the microwave spectrum between 2.6 to 3.95 GHz (S band) and 8.2 to 12.4 GHz (X band), where microwaves are absorbed by water molecules.

The attenuation of microwave signals in these bands can be used to determine moisture content (Sira 1991, Loughlin 1993, Toropainen and Vainikainen 1998)

2.3.9 Electrical impedance sensors

The presence of moisture modifies the electrical impedance of many substances. Modern electronic moisture sensors are normally constructed using thin-film technology, and the sensor configuration may be resistive, capacitive, or some combination of electrical parameters (Pragnell 1986, Boyle 1992).

A direct relative-humidity sensor usually consists of a hygroscopic material whose electrical impedance varies with relative humidity. Often the material used is lithium chloride or another salt, which may be held in a gel or matrix structure.

Many sensors have a limitation on the measurement range either near to 100% RH, or near to 0% RH. This may cause a severe non-linearity in the measurement characteristic and sensor damage in some cases. An accuracy of about $\pm$3% of reading is possible, although $\pm$4% is a more realistic limit for most instruments of this type (Pragnell 1986, Sira 1991). Most sensors could not handle wet conditions (i.e. accidental immersion in water).

Most dew-point (vapour pressure) sensors are based on the impedance change of an aluminium oxide capacitor as moisture penetrates the pore structure. The accuracy of a dew-point instrument is unlikely to be better than $\pm$2 ^{o}C, and will usually be greater than $\pm$3 ^{o}C dp for humidities above -30 ^{o}C dp. At lower humidities uncertainties may be much worse (Norton 1969, Pragnell 1986).

The main problems associated with thin-film sensors in a wide range of humidities have been long-term stability and drift at humidities above 85% or 90% (Visscher and Kornet 1994).

2.3.10 Summary

A summary of the humidity instruments in use, their principles of operation, measurement response times and typical accuracies are shown in Table 2.1.

Table 2. 1 Characteristics of humidity sensors (Pragnell 1986, Carr-Brion 1986, Toropainen and Vainikainen 1998).

Type	***Principle***	***Response time***	***Typical accuracy***
Mechanical	Change in physical size	>20 min.	$\pm$10% RH
Psychrometer	Temperature change due to evaporation		$\pm$3 % RH
Dew-point sensor (capacitance)	Change in impedance. often aluminium oxide. Change proportional to vapour pressure.	<10 s	$\pm$3 % (^{o}C dp)
Electrolytic	Electrolysis of water absorbed by phosphorus pentoxide	2-3 min	$\pm$10 % (ppm_v)
Relative humidity sensor	Change in impedance of a hygroscopic material. Often lithium chloride.	<10 sec	$\pm$4% RH
Condensation	Measurement of condensation temperature.	2-30 min.	$\pm$0.3 ^{o}C dp
Microwave sensor	Attenuation of microwave transmitting along a dielectric substrate	few seconds	±2% RH

In 1980 the UK Department of Trade and Industry, via the NPL, commissioned a survey from Sira Ltd (formerly the British Scientific Instrument Research Association) to assess the need for a UK national humidity standard and to recommend the specifications, in terms of range and accuracy, of any facility that was required (Poulter *et al* 1985). Although the survey was done some 15 years ago it still gives an indication of the application areas. However, recently I have contacted major humidity instrument suppliers in the UK. As a result, it can be estimated that thin film capacitive sensors now account for more than 70% of the total instruments sold. Some of the results of the Department of trade and industry survey are tabulated in Tables 2.2-2.4.

Table 2. 2 Hygrometer distribution by industries (Poulter *et al* 1985).

Sector	***Proportion %*** *(to nearest 5%)*
Electricity Generation	45
Food	35
Oil and Chemical	15
Photographic and Pharmaceuticals	5
Radio and electronics	<5
others	<5

Table 2. 3 Distribution of the types of hygrometers used in the UK in 1980 (Poulter *et al* 1985).

Type	***Proportion %***
Mechanical	45
Wet and Dry	15
Capacitance	12
Electrolytic	11
Conductance	11
Condensation	3
Spectroscopic	1
Dew cell	1
Others	2

Table 2. 4 Applications for hygrometers (Poulter *et al* 1985).

Application	***Industry %*** *(to nearest 5%)*	***Research %*** *(to nearest 5%)*
Environmental control	50	30
Automatic process control	5	5
Manual in-line quality control	25	25
Off-line quality control	15	-
Indirect measurement of moisture in solids	-	15
Scientific, research and development, test work	10	20

The development of humidity sensors with high sensitivity (≈0.1% RH), long-term stability (<2% RH), fast response time (<1 sec) and a wide temperature range (up to 800 °C) is strongly desired. However such sensors are not readily available.

Existing humidity sensors have problems ranging from drift to hysteresis, nonlinearity, and operation over a limited temperature range. Some require constant gas flow, the more accurate (optical dew-point) require regular cleaning of the mirror. Others require regular cell replacement. Some can be destroyed by accidental immersion in water. Most require regular calibration. Some need temperature control at high temperature and some are sensitive to the presence of some gases or to dust.

At present humidity sensors are too expensive for multipoint (typically 6 to 10) applications and often are not reliable or accurate. Although the ideal range of operating temperature, in industry, is 100 to 800 °C many applications could benefit with a range 100 to 200 °C (Kemp 1998).

The output of many sensors used in the measurement of humidity is in analogue voltage form. This may be converted to current and transmitted in traditional format as

4-20mA signal. However such signals are more prone to electromagnetic interference (emi) than either frequency or digital signals. Routing data transmission cables can be restricted as this should not, for example, be running alongside heavy motor starters. Even with very careful planning emi can still be a serious problem. In hazardous zones, the transmission cables have to conform to the required code of practice and some sort of protection is required such as Zener barriers or galvanic isolators (Bass 1984).

The use of fibre optic transmission is very attractive in such zones since optical fibres require no electrical supply and they are immune from electromagnetic interference. An even more attractive proposition is to develop optical fibre humidity sensors thus eliminating, completely, the need for electrical signals. Optical fibre sensors offer also the prospect of muli-point sensing on a single fibre (Kharaz and Jones 1995).

2.4 Optical Fibre measurement methods

The explosive growth of optical fibres for use in telecommunications and the associated development of cheap solid-state optical sources and detectors has enabled optical fibre technology to be utilised in novel optical fibre sensors (Jones and Spooncer 1984, Jones 1985, Miller and Hirschfeld 1986, Dakin and Culshaw 1989, Udd 1991, Wang 1992, Sadaoka *et al* 1993). Several optical fibre humidity sensing methods have been reported. These methods are mainly based on one of the following phenomena: -

2.4.1 Colorimetric reagents that change colour with relative humidity

Certain chemicals change colour as the relative humidity of the surrounding air changes, and hygrometric indicators have been devised which use this effect by immobilising the reagents on filter paper (Hickman 1970). Over the last decade optical

fibre sensors, using this phenomena, have been reported (Russell and Fletcher 1985, Morisawa *et al* 1992, Kharaz and Jones 1993).

2.4.2 Change in physical size with humidity

The dimensions of many natural and synthetic materials, e.g. human hair, animal membrane, various plastics, textiles and polymers, change in response to humidity. This phenomenon can easily be exploited optically to give a measure of humidity (Psaila *et al* 1990). Another example is using a wavelength-dependent holographic filter (Spooncer *et al* 1992). Whichever material and method is used, it is inevitable that temperature has also an effect on the material dimensions and this can cause some measurement error.

2.4.3 Change of refractive index with humidity

Some materials have a certain degree of porosity that moisture from the atmosphere can diffuse into the pores thus changing the effective refractive index of the material. In 1926 the change in the refractive index of a thin film of glycerine was used to measure the relative humidity (Griffiths and Awbery 1926); an Abbe' refractometer was used to measure the refractive index. Several optical fibre sensors based on refractive index change and using thin films and porous material have been reported (Tiefenthaler and Lukosz 1989, Mitschke 1989, Dakin and Culshaw 1989). Takeo and Hattori (1991) suggested using a U-shaped optical fibre, based on refractive index change, as a dew point hygrometer. The main disadvantages of these methods are; first: - refractive index is temperature dependent, second: - where intensity modulation is employed referencing is difficult to achieve.

2.4.4 Change of reflectivity of thin metal films with humidity

Metal thin films are known to vary in conductivity with varying relative humidity (Tanaka and Iwata 1981), while reflectivity from a metallic surface is strongly dependent upon the conductivity of the metal (Hadley and Dennison 1947). Using a silver coated glass, its reflectance has been shown to be dependent upon relative humidity (Park and Day 1986). It has also been shown that metal coated optical fibres can be used as relative humidity sensors, metals used have been copper, chromium, silver, gold and nickel, with silver showed the best sensitivity (Stuart and Grazier 1988). The main disadvantages of such sensors are the fast deterioration of the film (Park and Day 1986), and its temperature dependence.

2.4.5 Change of florescence intensity with humidity

As a result of the absorption of visible or ultraviolet light certain materials emit radiation at a different wavelength, this effect is known as fluorescence; the emitted radiation is usually of greater wavelength than that of the absorbed radiation (Barrow 1979). An extensive list of fluorescent materials can be found in Lange's handbook of chemistry (Dean 1990). The radiation of some fluorescent material does vary with humidity changes, and humidity and pH optical fibre sensors using such materials have been reported (Sydenham 1983, Zhu *et al* 1989).

2.5 Advantages of optical fibre methods

The potential advantages of a passive optical fibre humidity sensor would be as follows:-

(i) Freedom from electromagnetic interference (optical fibres are made from dielectric materials).

(ii) Intrinsic safety (Hale 1984).

(iii) The potential for high reliability and security.

(iv) High voltage insulation and absence of electrical ground loops (hence obviating any necessity for isolation devices such as optocouplers and isolating transformers).

(v) The potential for small size and lightweight.

(vi) The potential for resistant to nuclear or ionising radiation.

(vii) Remote sensing capability, since such a sensor can easily be interfaced with low-loss optical fibre and allow the control electronics for LED/lasers and detectors to be a considerable distance from the sensor head.

(viii) Offers the prospect of distributed sensing and the possibility of multiplexing a large number of individually addressed point sensors.

(ix) Can be chemically inert and they can be readily employed in chemical, process and biomedical instrumentation due to their small size and mechanical flexibility.

(x) No requirement for an electrical supply to be provided at the sensor.

2.6 Chosen approach

Sensors based on approaches (2)-(4), in section 2.4 above, seem to have one or more of the following problems; (i) strong temperature dependence in approach (2)-(3); (ii) rapid deterioration of sensing area as in (4)-(5) (iii) when utilised using intensity based approach (as is normally) it is difficult to devise a referencing method.

Therefore, the method selected here for the development of an optical fibre humidity sensor has been based on colorimetric interaction of a reagent with water molecules. This approach offers the prospect of having a wavelength band within which the active measuring signal may lie, while having a second wavelength band that can accommodate a reference signal to enable reduction in the effects of common-mode variations. There appeared to be a good prospect for developing suitable sensing thin film using this approach which could be deposited on an optical fibre.

In the following chapter optical fibre sensing systems are discussed.

CHAPTER 3

Optical fibre sensing

3.1 Introduction

The progress of optical fibre technology during the past 25 years has been aided enormously by the realisation of its tremendous potential as a transmission media because of its high bandwidth capability. The invention of the laser in 1960 and the demonstration of the first room-temperature continuous-wave semiconductor laser at Bell Laboratories in 1970 (Hayashi *et al* 1970) were most important.

The first near infrared optical fibre was fabricated in 1965 (Waynant and Ediger 1993), but it had transmission loss of more than 10,000 dB/km. Koa and Hockham studied the loss mechanisms in optical fibres and proposed the utilization of optical fibres for communications applications (Kao and Hockman 1966). By 1970 Corning Glass Works was manufacturing step-index fibres which had attenuation values of less than 20 dB/km. In due course by reducing the impurities in the source materials and improving the homogeneity of the glass processing, an attenuation of 0.2 dB/km was achieved (Miya *et al* 1979). In 1978, it was proposed that an ultra-low-loss fibre with a loss less than 0.001 dB/km for heavy-metal-flouride glass fibres was theoretically possible (Waynant and Ediger 1993). Today standard silica-based optical fibre for optical communications typically has less than 0.2 dB/km attenuation at 1550nm (Buck 1995).

The basic operating principles and components available for optical fibre sensing will now be briefly described, so that subsequent use of the technology for the research investigation can be understood.

3.2 Optical fibres

3.2.1 Theory of fibre transmission

Light rays are electromagnetic waves and obey Maxwell's equations (Waynant and Ediger 1993). Reflection and refraction occur at the interface of two regions of different refractive index.

An optical fibre consists of at least two distinct regions known as the core and cladding. The refractive index of the core n_1, when made higher than the refractive index of the cladding n_2, can confine a light beam to the core region of a fibre by total internal reflection (Syms and Cozens 1992). There are two possible types of pathways that may be followed by rays travelling down the fibre (Senior 1992, Syms and Cozens 1992). Meridional rays follow pathways that can be drawn on a single plane as shown in Fig. 3.1 (a). These are directly analogous to the rays that propagate in planar slab guides. Skew rays on the other hand, do not travel in the exact centre of the fibre, but propagate in an annular region near the outer edge of the core, following off-axis helical paths that effectively circle the fibre axis after a finite number of reflections as shown in Fig. 3.1 (b). The existence of such rays implies that the analysis of an optical fibre will be more difficult than a simple extension to cylindrical geometry would suggest (Senior 1992). However it is adequate to consider only the meridional rays for the purpose of this work.

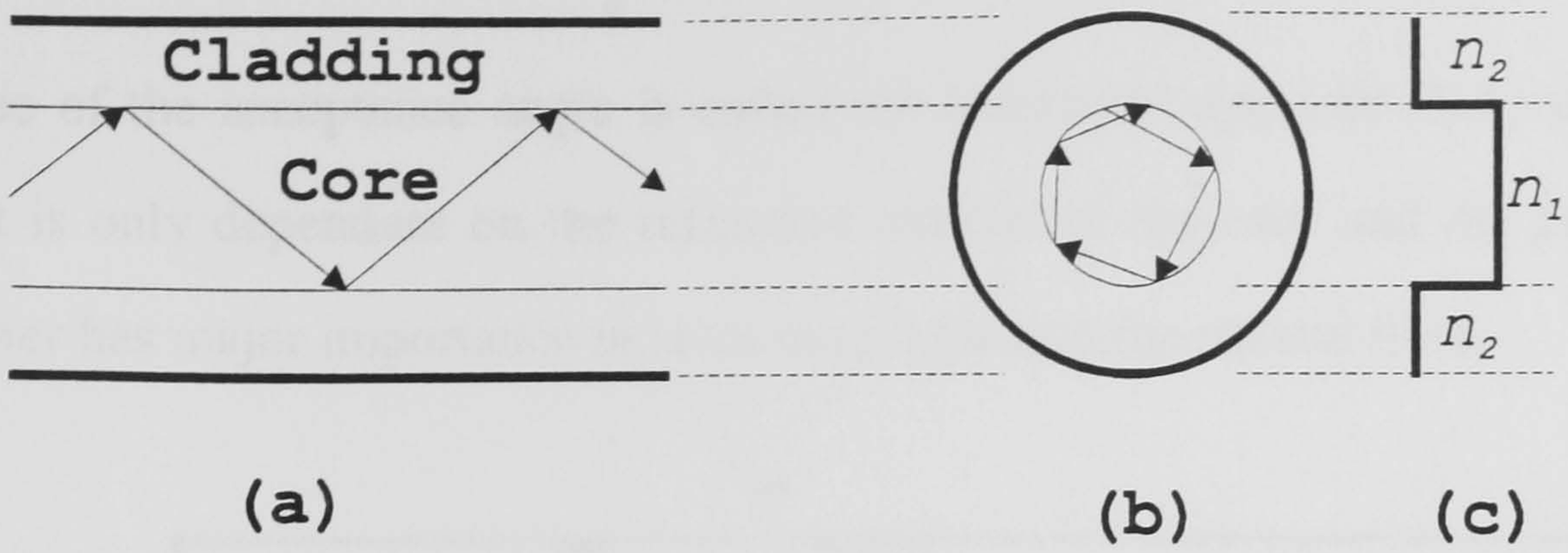

Figure 3. 1 Light propagation in a step-index optical fibre (a) propagation of meridional rays (b) skew rays (c) refractive index profile.

Looking at Fig. 3.2, in order to launch light from outside (air with refractive index n_0=1) into the core, the launch angle θ must satisfy Snell's law, so we must have

$$\frac{\sin\theta}{\sin(90-\alpha_o)} = \frac{n_1}{n_o}$$

hence

$$\sin\theta = n_1\cos\alpha_o = n_1\sqrt{1-\sin^2\alpha_o} \qquad (3.1)$$

The greatest possible launch angle (θ_{max}), is called the acceptance angle, and occurs when α equals the critical angle (α_c) at the core-to-cladding interface.

The critical angle is given by

$$\sin\alpha_c = \frac{n_2}{n_1} \qquad (3.2)$$

and by substitution into the above equation we get

$$\sin\theta_{max} = \sqrt{n_1^2 - n_2^2} \qquad (3.2)$$

The sine of the acceptance angle is called the numerical aperture (NA) of the optical fibre; it is only dependant on the refractive indices of the core and the cladding. This parameter has major importance in launching light into the optical fibre.

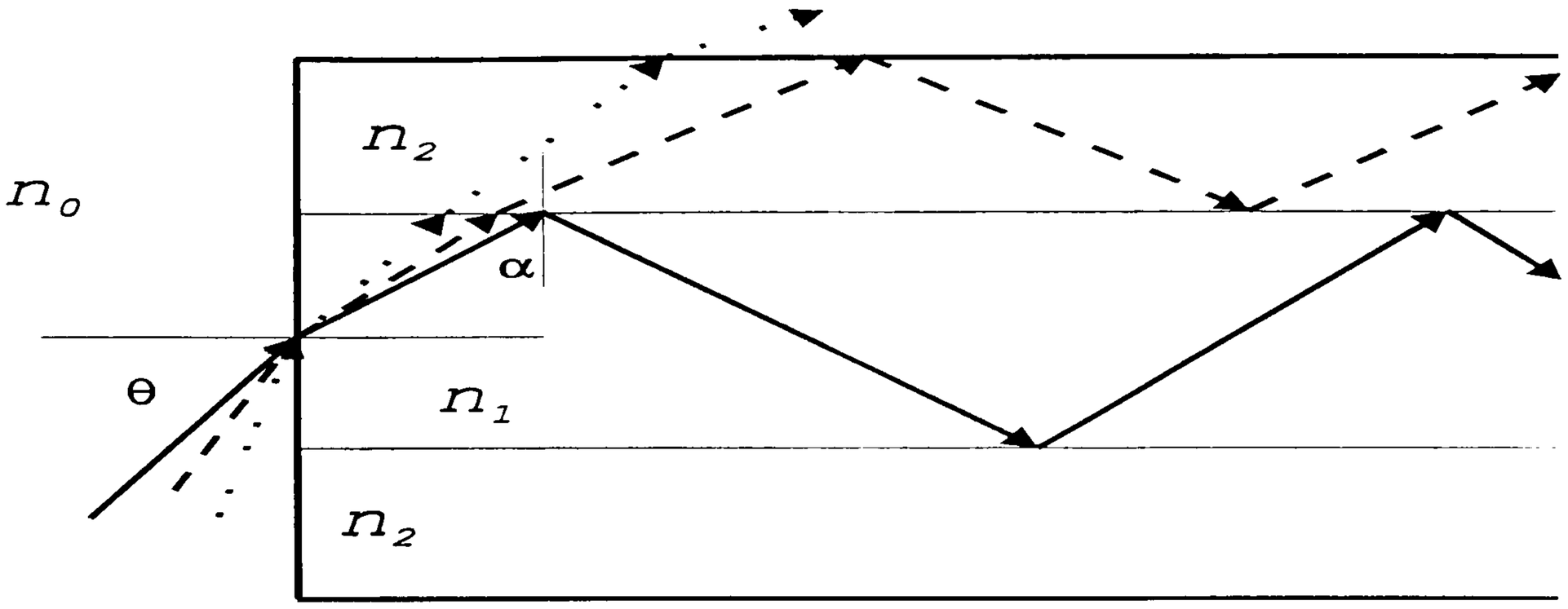

Figure 3. 2 Light transmission in a step index fibre.

Light guided down the fibre core is known as 'guided or bound mode' light which has an angle of incidence at the core/cladding interface of less than the critical angle is unguided and escapes into the cladding. Some of this light also escapes from the cladding in 'radiative modes'. In between, some rays escape from the core but are reflected at the air/cladding interface; these are termed 'cladding modes', but because of the lossy nature of the cladding they gradually die away. Cladding modes may introduce inaccuracies into any sensor which depends upon intensity modulation of light (Spooncer 1989).

Optical fibres may be classified as follows. First, optical fibre is generally either a single mode (core diameter < 10μm), allowing only one pathway for rays to be transmitted, or a multi-mode (core diameter > 40μm) which can support a larger number of pathways. Second, the core may be defined either by an abrupt increase in the refractive index (step-index fibre), or by a gradual variation in index, which is

typically parabolic (graded index fibre). Only multimode step-index fibres are used in this work. The other types are included for completeness. These fibre types are illustrated in Fig. 3.3.

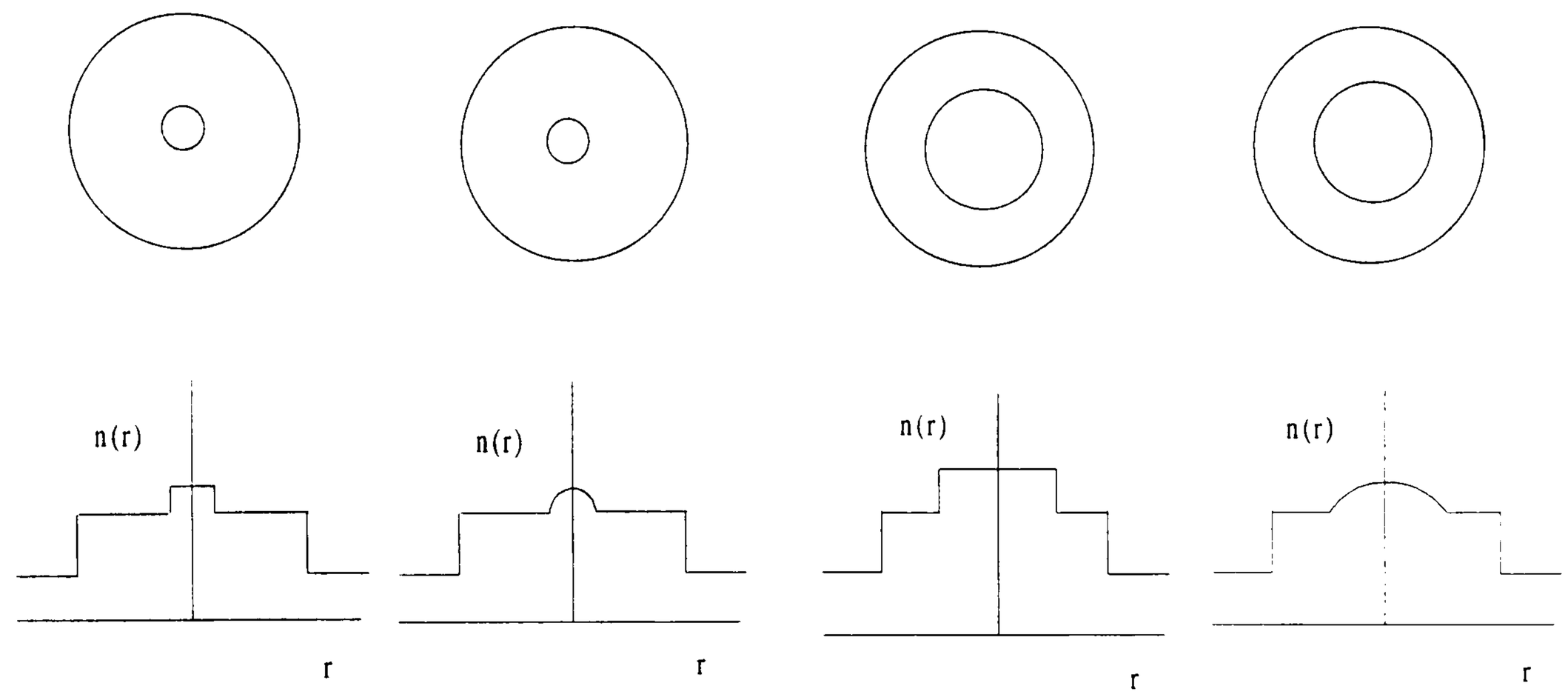

(a) Step index, single mode

(b) Graded index, single mode

(c) Step index, multi-mode

(d) Graded index, multi-mode

Figure 3. 3 Optical fibre types (cross-section).

The refractive index of a material n is given by the expression

$$n = \frac{v_{medium}}{c} \tag{3.4}$$

where v_{medium} is the velocity of light in the medium and c is the speed of light in a vacuum ($c = 3 \times 10^8 m/s$). The refractive index is a measure of the relative speed of light in the material as compared with light travelling in vacuum (Smith and Thomson 1971). The larger the refractive index of a material, the more slowly the light travels within it.

3.2.2 Fibre losses

One of the most important features of the optical fibre is its exceptionally low propagation loss, which is normally quoted in units of decibels (dB/distance), defined as (Buck 1995)

$$loss = -10\log(\frac{P_{out}}{P_{in}}) \text{ dB/km} \qquad (3.3)$$

where P_{in} = optical power launched into the fibre.

P_{out} = output optical power.

There are three main loss mechanisms in optical fibres: absorption, scattering and bending.

(1) Rayleigh Scattering

Rayleigh scattering is caused by the interaction of light and the granular appearance of atom and molecules on a microscopic scale. The scattering sites are much smaller than the wavelength of the light. Rayleigh scattering is proportional to λ^{-4} (Waynant and Ediger 1993) (λ is wavelength).

(2) Absorption losses

Absorption losses in the visible and near-infrared regions arise mainly from the presence of impurities, particularly traces of transition metal ions (e.g. Fe^{3+},Cu^{2+}) or hydroxyl (OH^-) ions. The latter have strong absorption peaks at 0.95 μm, 1.24 μm and

1.39 μm. Most of the dramatic successes in reducing the fibre losses to date have come about because of better control of the impurity concentrations.

At wavelengths greater than about 1.6 μm the main loses are due to transitions between vibrational states of the lattice. Although the actual fundamental absorption peaks occur at wavelength well into the infrared (in SiO_2, for example, the main peak is at 9μm), the anharmonic nature of the inter atomic forces causes combination and overtone bands extend all the way down to 3 μm with appreciable absorption still occurring below 2 μm (Buck 1995). To date, some of lowest optical fibre attenuation of about 0.2 dB/km occur at a wavelength of 1.55 μm. This figure is quite close to the limit set by Rayleigh scattering. A typical attenuation curve is shown in Fig. 3.4.

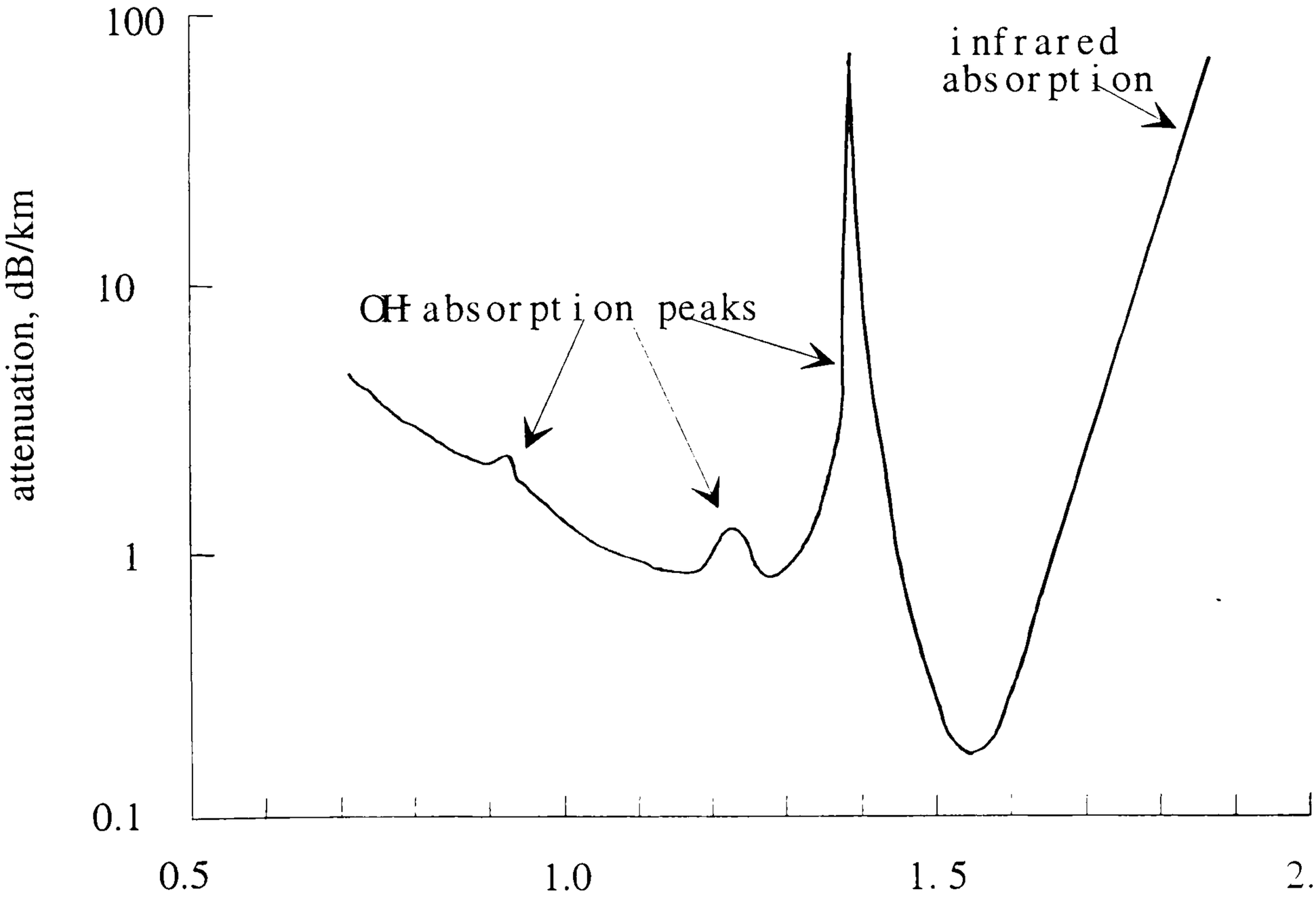

Figure 3. 4 Typical attenuation characteristics for silica-based optical fibre (Syms and Cozens 1992).

(3) Mode conversion

Although optical fibre is normally made with a uniform cross-section, there will inevitably be small irregularities (e.g. at the interface between core and cladding, as shown in Fig. 3.5(a)). Any change in ray direction resulting from scattering by such an irregularity then corresponds to mode conversion and can lead to light loss. Slight change in direction (Fig. 3.5(b)) (bending) lead to similar effects (Syms and Cozens 1992).

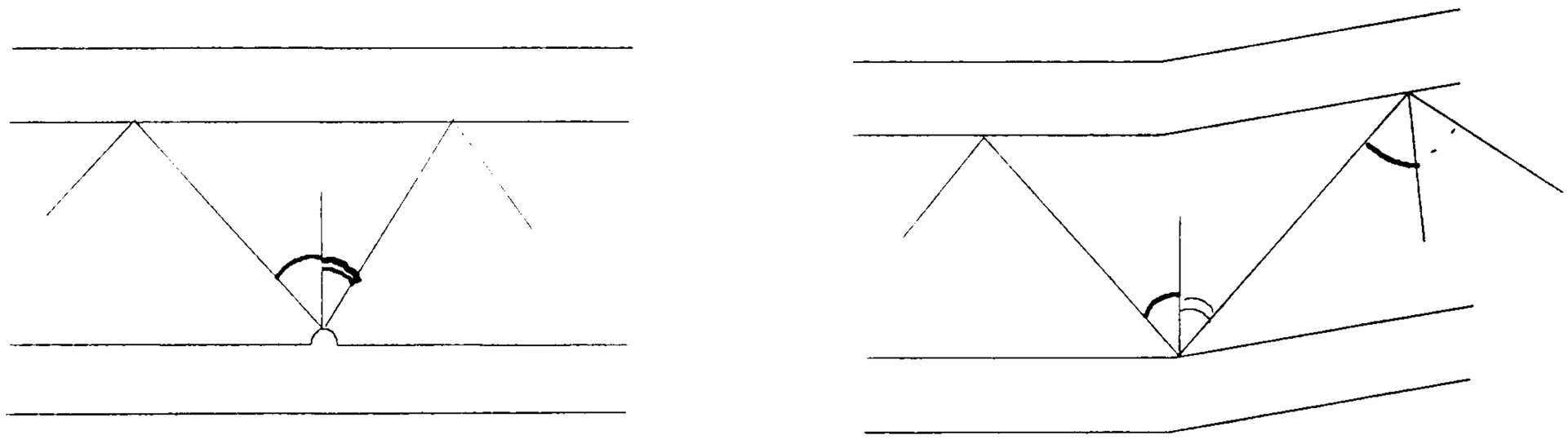

(a) small irregularity (b) slight change in direction

Figure 3. 5 Illustration of mode conversion.

3.2.3 Pulse broadening

During transmission of a light pulse down an optical fibre, pulse broadening can occur due to three main types of dispersion.

(i) Material dispersion

This is the most fundamental type of dispersion and is caused by the wavelength dependence of the refractive index i.e. the speed of light. All optical sources such as

light emitting diodes (LEDs), semiconductor lasers and even gas lasers have finite spectral widths, and the lower optical frequencies travel faster than the higher optical frequencies so as to cause the light pulse to be spread out (Spooncer 1989). The wider the spectral width of the source, the greater the spread, so that for high speed systems LEDs cannot be used. Fig. 3.6 shows the variation of the refractive index with wavelength for pure SiO_2 as calculated using Sellmiere formulae .

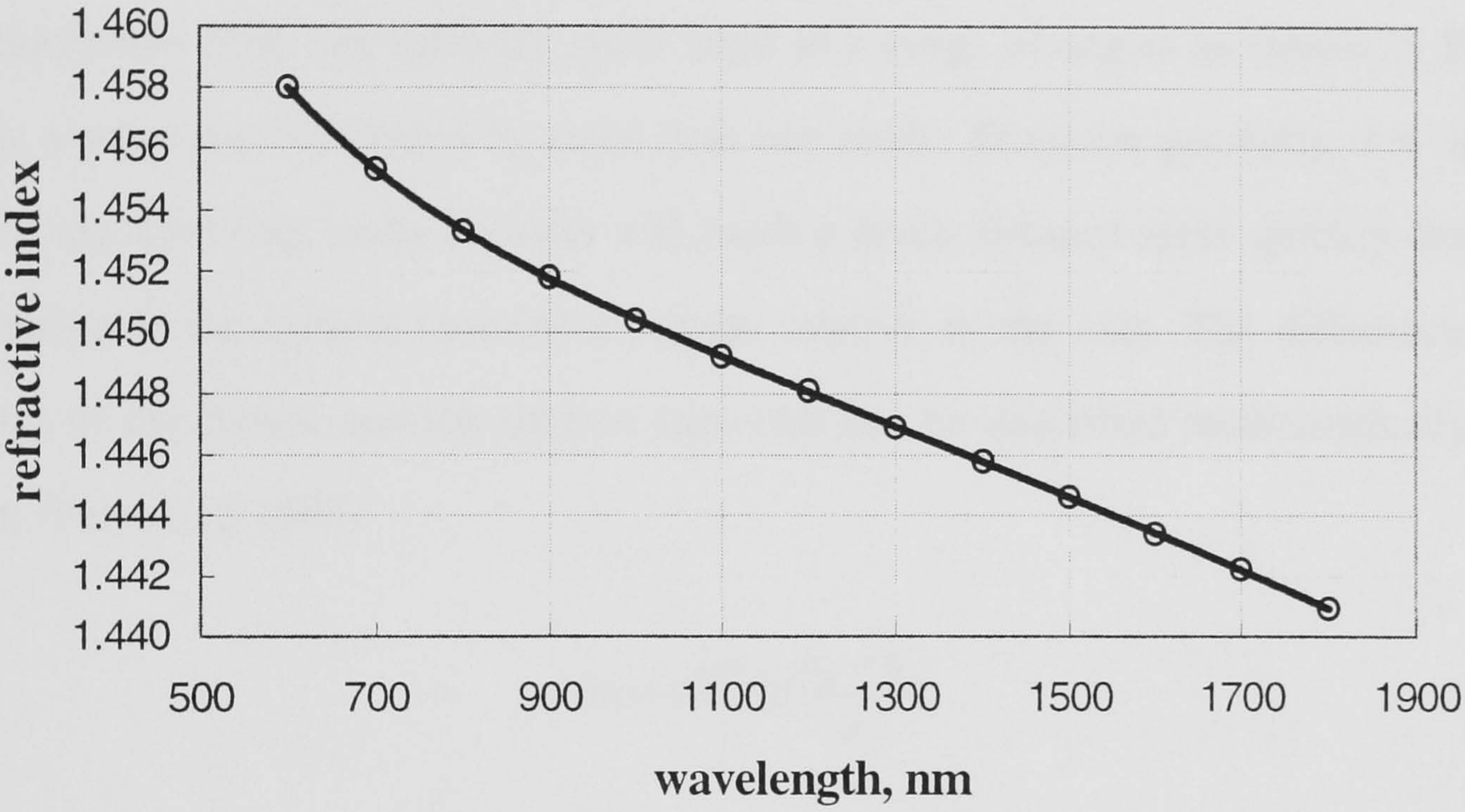

Figure 3. 6 Wavelength versus refractive index n for SiO_2.

(ii) Waveguide dispersion

Waveguide dispersion arises because the mode velocity depends on wavelength. This is independent of material dispersion i.e. this would remain true even if the refractive index were independent of wavelength (Snyder and Love 1983). Provided the guide dimensions are not close to cut off, then the waveguide dispersion is usually much less than material dispersion (Wilson and Hawkes 1983).

(iii) Intermodal dispersion

The first two types of dispersions have most relevance to single mode fibres where material dispersion plays the dominant role. In multimode step index fibres, material dispersion is overshadowed by another effect; intermodal dispersion.

A multimode fibre can typically guide light in a range of angles as shown in Fig. 3.2. Thus a pulse can be formed by more than one mode. From the geometry it is apparent that a ray travelling along the axis will reach a given distance more quickly than a ray travelling at the critical (maximum) angle relative to the axis. The difference in the delays of the fastest and the slowest rays (Δt) can be described mathematically in the form (Personick 1985)

$$\Delta t = (\frac{Ln_c}{c})(\frac{n_c - n}{n}) \qquad (3.4)$$

L = length of fibre

where the first term in this product is the delay along the axis and the second term is the fractional index difference between the core and the cladding.

3.2.4 Launching light into fibres

The procedure for launching light into an optical fibre is very important as regards the further distribution of the light power in the fibre, because in multimode fibres the power of the launched light is distributed over the individual modes. In the case of single-mode fibres light is partly launched into the fundamental mode and partly

radiated. Depending on the launching conditions, when light is launched into multimode and single-mode fibres, the fibres will guide the light power differently.

Sources normally emit light in a diverging cone with a numerical aperture that is normally much larger than that of the fibre. So a lens or some optical arrangement is often used to collect the light and redirect it into the fibre end; some of these arrangements are shown in Fig. 3.7 below (Keiser 1991, Senior 1992, Wood 1994, Shi and Jannson 1994).

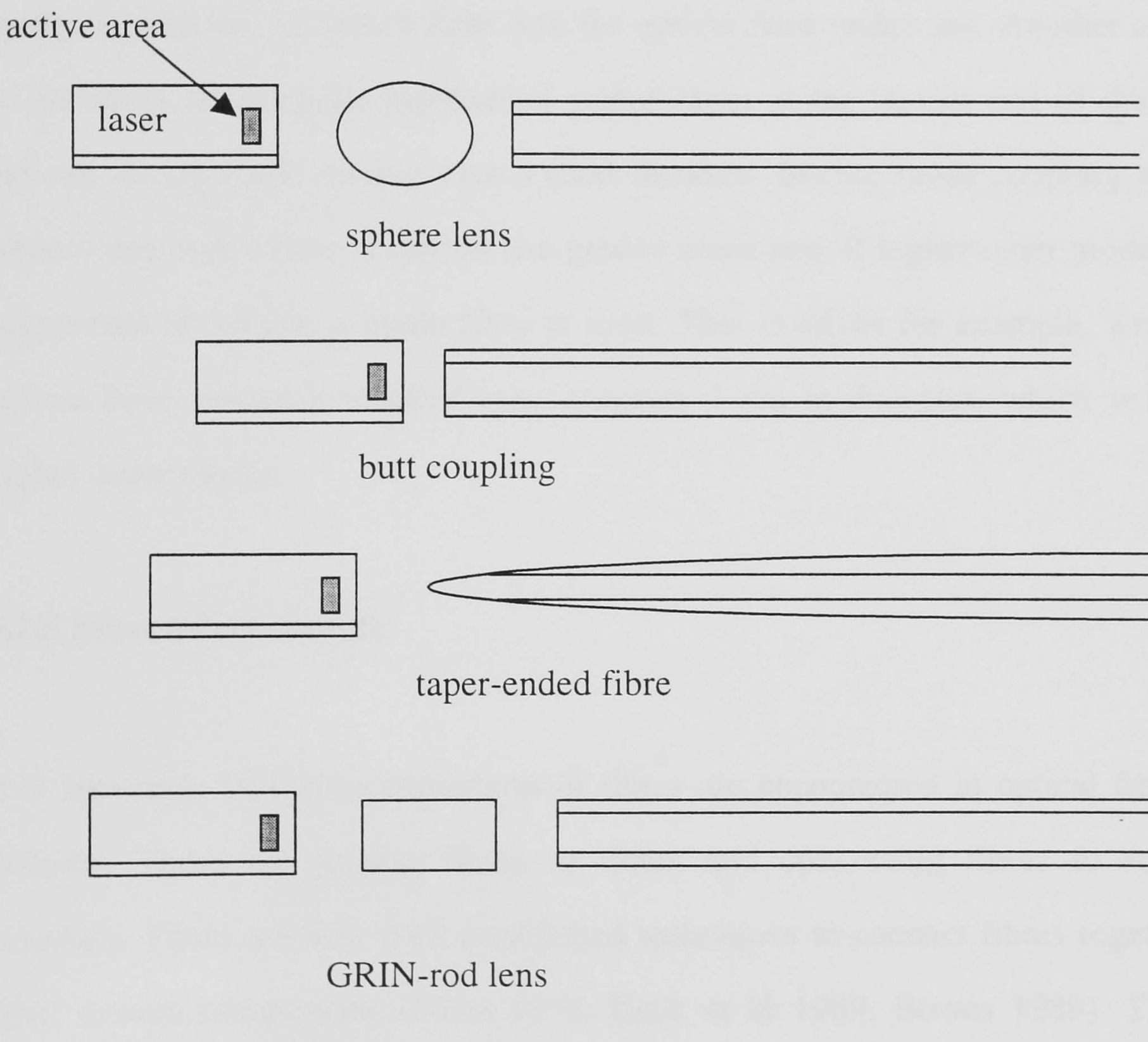

Figure 3. 7 Source to fibre connection schemes.

In multimode fibres, when the entire core of the fibre is flooded with light (full flood launch), all guided modes and also the leaky modes get excited. Because different modes have different attenuations and in addition mode mixing takes place, power distribution varies along the fibre. A steady state or equilibrium mode distribution is reached after a certain length, beyond which the energy distribution remains constant over the modes. In optical fibre sensors which utilise the fibre for sensing purposes it is important to take this into consideration in order to get accurate measurements. There are different techniques for reaching this equilibrium state within the fibre. One way is to use a dummy fibre of sufficient length, which has already established the equilibrium mode distribution, to launch light into the optical fibre under test. Another approach is to introduce an irregular mechanical perturbation at the launch end of the fibre that induces strong mode mixing over a short distance. Intense mode coupling also results when a step-index fibre is spliced to a graded index one. If higher order modes are to be suppressed at launch, a mode filter is used. This involves for example, wrapping the optical fibre around a mandrel approximately 1 cm in diameter, which strips off the higher order modes.

3.2.5 Fibre interconnects

It is inevitable that interconnections of fibres are encountered in optical fibre sensing systems. These are joining fibres to fibres and connecting fibres to sources and detectors. There are now well established techniques to connect fibres together and to other system components (Nicia 1978, Keck et al 1989, Bowes 1989). The type of connector used is dependant on the application. For less demanding applications mechanical splices are often used where the fibres are placed in a precision assembly and kept in position either by mechanical means or by epoxy resin. High precision demountable connectors are widely available for both monomode and single-mode fibres. For more demanding applications fusion splicing is used. Fusion splicing is

permanent and is made by first aligning two fibre ends and then fusing them together using an electric arc or a gas flame (Harbison 1989). Commercial programmable microprocessor controlled fusion splicers are widely available.

3.3 Optical sources and detectors

Fibre optic sensors exploit a very wide range of operating principles. Consequently the range of optical sources for such sensors is also diverse. Three types of light source which are relevant to the work in this thesis are discussed below.

3.3.1 Light emitting diode (LED)

Spontaneous emission of radiation from a forward biased p-n junction forms the basis of operation of LED's (Senior 1992, Wood 1994). The LEDs are solid-state semiconductor devices which can be fabricated from various semiconductor materials to give the desired wavelength of emission. The centre emission wavelength λ depends on the bandgap energy E_g of the semiconductor material.

Four materials are commonly used to produce LEDs : GaP (emits at 700nm), GaAlAs (emits at 650-850nm), GaAs (emits at 900nm) and InGaAs (emits at 1200-1700) (Dakin and Culshaw 1989). A normal LED has a spectral width in the range 30-100 nm depending on the material.

LEDs can be modulated by varying the electrical current used to power them. Achievable modulation rates range from 20 MHz to beyond 1 GHz (Kazovsky et al 1996). The maximum output power of LEDs is normally in the region 1 to 10 mW (Boisde and Harmer 1996). Some of the advantages of the LED as a light source are

simpler fabrication procedures, lower cost, and simpler drive circuitry. LEDs are, in general, more reliable than lasers because they operate at lower powers and therefore do not suffer catastrophic degradation or even gradual degradation prevalent in lasers. The light-current characteristic is also less sensitive to temperature than that in a laser. Some of the disadvantages are the low power output, harmonic distortion due to the multimodal output, and a smaller modulation bandwidth.

3.3.2 Incandescent sources

The incandescent source produces light because its metal element (tungsten) is heated as electric current flows through it. This light source has a continuous-shaped output spectrum as shown in Fig. 3.8.

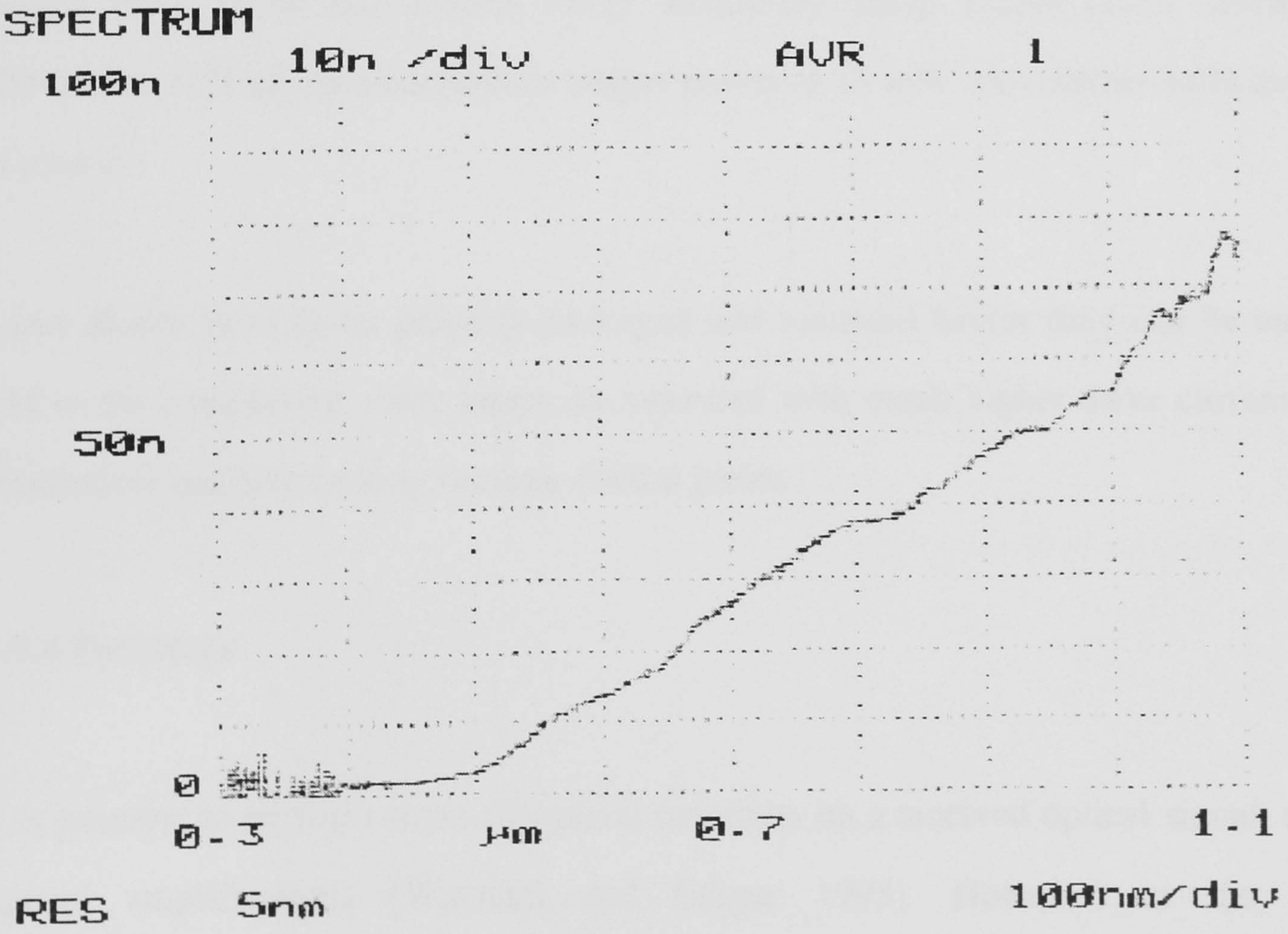

Figure 3. 8 Incandescent source spectrum.

3.3.3 Semiconductor laser sources

The term 'laser' is an acronym for a radiation source based on 'light amplification by stimulated emission'.

Semiconductor diode lasers have many characteristics that make them one of the most attractive types of laser. They are small and efficient, have long operating lifetimes. and in many cases are inexpensive. They are also capable of high powers of up to several watts continuous-wave from a very small laser. Unfortunately most semiconductor lasers operate in the near-infrared spectral region owing to the inherent nature of their energy levels. However, in recent years significant progress has been made in engineering special semiconductor materials that have provided energy levels in the visible spectral region which can lead to population inversions and gain (Hecht 1992, Senior 1992, Syms and Cozens 1992). Relatively cheap visible lasers operating at 635nm and 670 nm with continuous output power of 15 mW are commercially available at present.

Laser diodes have to be properly packaged and mounted before they can be used. To add to the complexity, since lasers are operated with much higher drive currents, heat dissipation and heat sinking become critical issues.

3.3.4 Detectors

It is possible to perform some all-optical functions on a received optical signal, such as optical amplifications (Waynant and Ediger 1993). However, in the optical communication and sensing systems used today information is extracted from the optical signal by converting it into an electrical signal using an optical detector (Billings 1993). All the detectors used for fibre optic applications are invariably semiconductor p-n junction devices. These devices may be operated either in the photovoltaic mode in

which the junction is treated as an open circuit to measure the voltage across the junction (as in solar cells) or in the photoconductive mode as a reverse-biased photodiodes in which the current is made to flow externally to complete the circuit between the two junctions. The latter configuration is preferred for better sensitivity and fast response; the devices are called PIN photodiodes and avalanche photodiode (APD) respectively (Syms and Cozens 1992). The choice of a photodiode depends mainly on the wavelength of operation. Table 3.1 shows some of the general characteristics of commonly used photodiodes.

Table 3. 1 General characteristics of commonly used photodiodes (Keiser 1991, Billings 1993).

Type of diode	***Wavelength (μm)***	***Quantum efficiency (%)***	***Response time***	***Dark current***
SiPIN	0.4-1.1	90	0.1-5 ns	1-50nA
SiAPD	0.4-1.1	85	0.05-0.3 ns	20-100nA
GeAPD	0.6-1.6	85	0.1 ns	20-100nA
GePIN	1.0-1.6	60	2.5 ns	100nA
III-V	0.92-1.65	50-70	10-100 ps	10^{-5}-10^{-1} A/cm^2

3.4 Sensing systems

In an optical fibre sensor (OFS) light is guided by an optical fibre and modulated in response to an external physical, chemical, biological or similar influences. Light can be modulated while confined to the fibre and such a sensor is termed "intrinsic" as shown in Fig. 3.9(a). Light may be modulated outside the fibre then relaunched back again into

the same or another optical fibre and this sensor would be called "extrinsic" as shown in Fig. 3.9 (b).

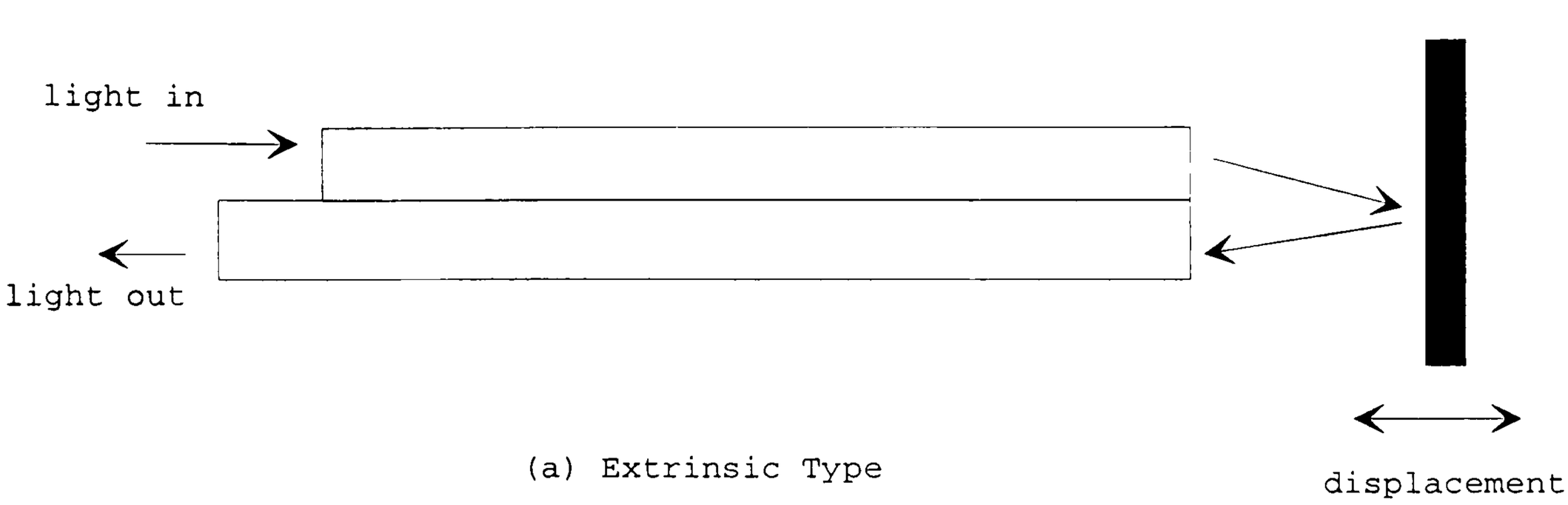

Figure 3. 9 (a) Extrinsic optical fibre sensor and (b) intrinsic optical fibre sensor.

3.4.1 Light Modulation Methods

The methods for light modulation by the measurand may be divided into the following categories:

1. Intensity modulation. Changes in the parameter being measured results in variations in optical intensity.

2. Wavelength modulation. Wavelength modulation sensors are based on the detection of radiation whose wavelength is a function of the measurand (McKellar and Allen 1979, Culshaw and Dakin 1989).

3. Phase modulation. Phase modulation is one of the most sensitive techniques available in optical fibre sensors. They generally require single-mode fibre, other single-mode optical components and complex electronics. The optical signal is diverted into two different paths: one path is allowed to be modulated by the measurand (phase modulation) while the other path is used as a reference. The two signals are then combined and interfere to give a quantitative measure of the phase difference (Culshaw and Dakin 1989).

4. Polarisation. Polarisation modulation can be used in a very similar manner to that of phase modulation (Culshaw and Dakin 1989, Udd 1991, Waynant and Ediger 1993).

For the purpose of the work done in the thesis we are going to concentrate on the intensity modulation method.

3.4.2 Intensity modulation

This is the simplest form of modulation and was employed in the earliest optical fibre sensor developments (Krohn 1986). It offers the advantages of simplicity, reliability and low cost. Changes in the parameter being measured results in variations in optical intensity. While the intensity modulation takes place as a result of the measurand, additional variations may arise from source intensity variations, variable losses in fibres and connectors, and sensitivity changes in detectors. This is a serious disadvantage that directly affects the accuracy of the measurement. To remedy this problem, several

referencing techniques have been developed (Jones et al 1989), some will be illustrated later in this section.

There is a large number of intensity-modulation techniques reported in the literature. Some examples, which could be employed in humidity measurement, are presented here to illustrate the concept.

Fig. 3.10(a) shows a transmissive intensity modulated displacement sensor. In this example, light leaves one fibre end in a cone pattern, and strikes the end of the second fibre. The amount of light collected by the second fibre is a function of both the longitudinal and transverse distance between the fibre ends as shown in the figure. The amount of light collected by the second fibre is also dependant upon the refractive index of the gap between the fibre ends (active area). This can create another type of sensor if the active area is filled with a material whose refractive index changes with a measurand thus modulating the light intensity, see Fig. 3.10(b).

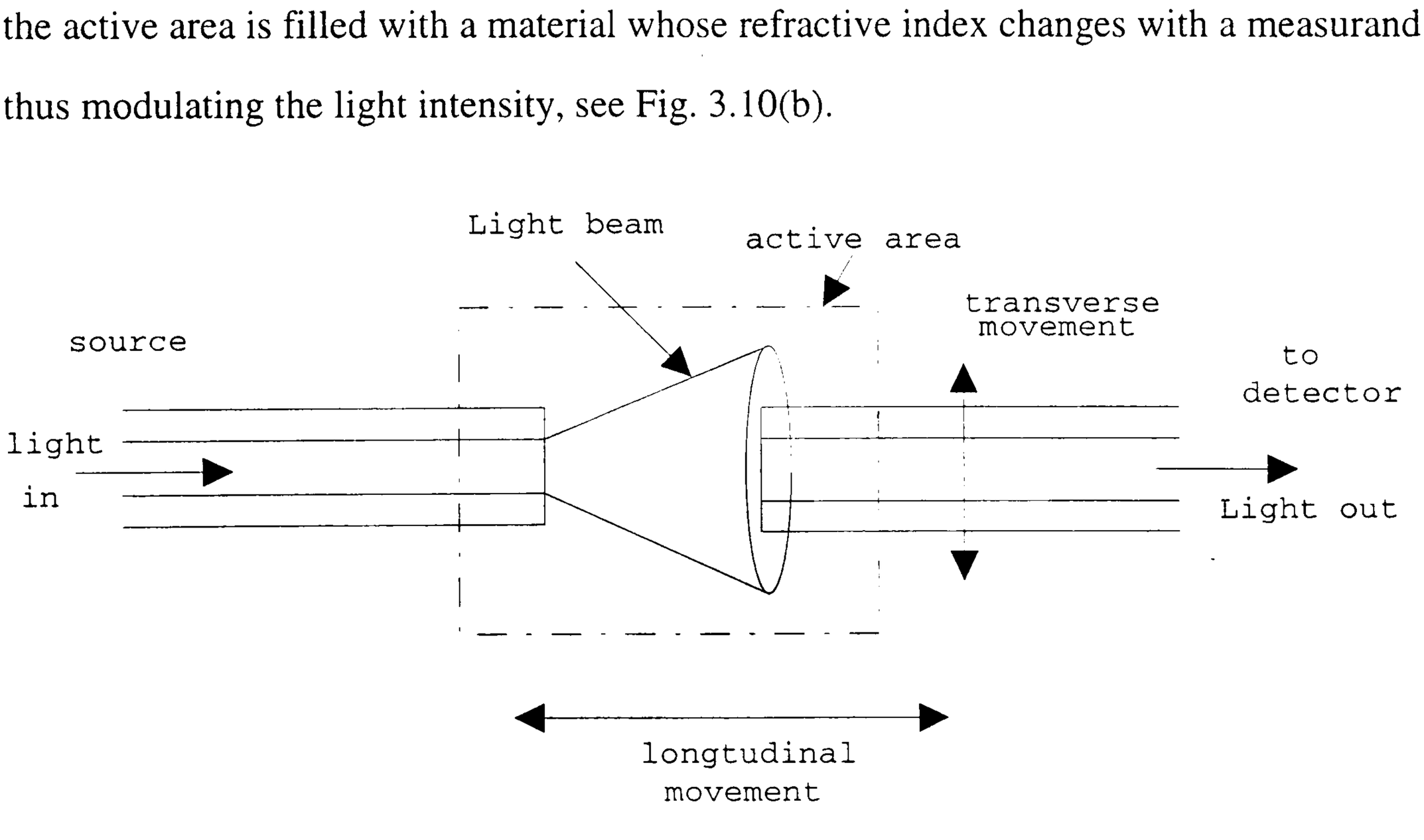

(a)

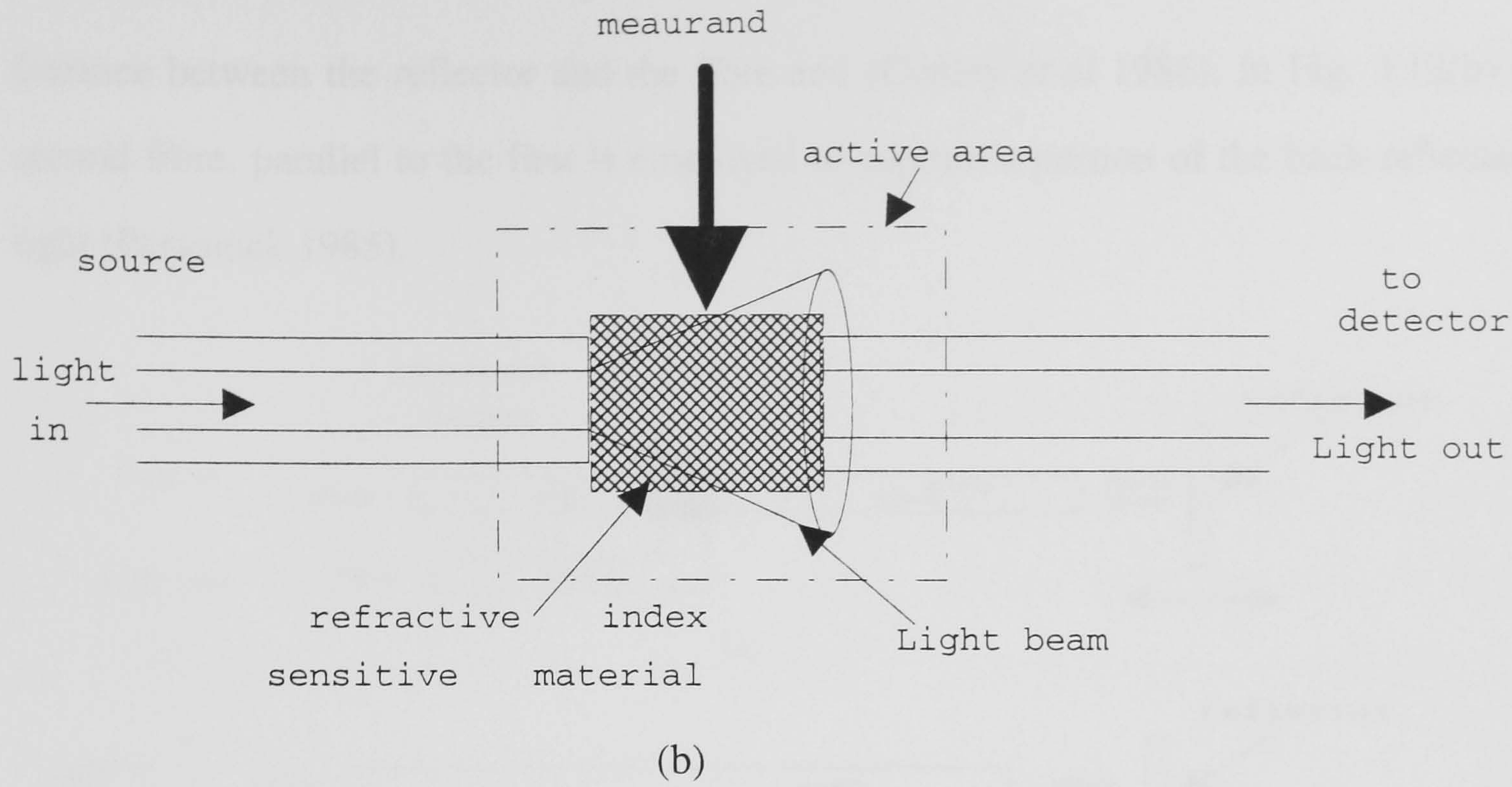

(b)

Figure 3. 10 (a) Transmissive displacement sensor (b) measurement of a refractive-index-sensitive parameter.

Fig.3.11 shows an angular displacement sensor. Here the light collected by the receiving fibre is a function of the angle θ between the axes of the fibres as shown in the figure.

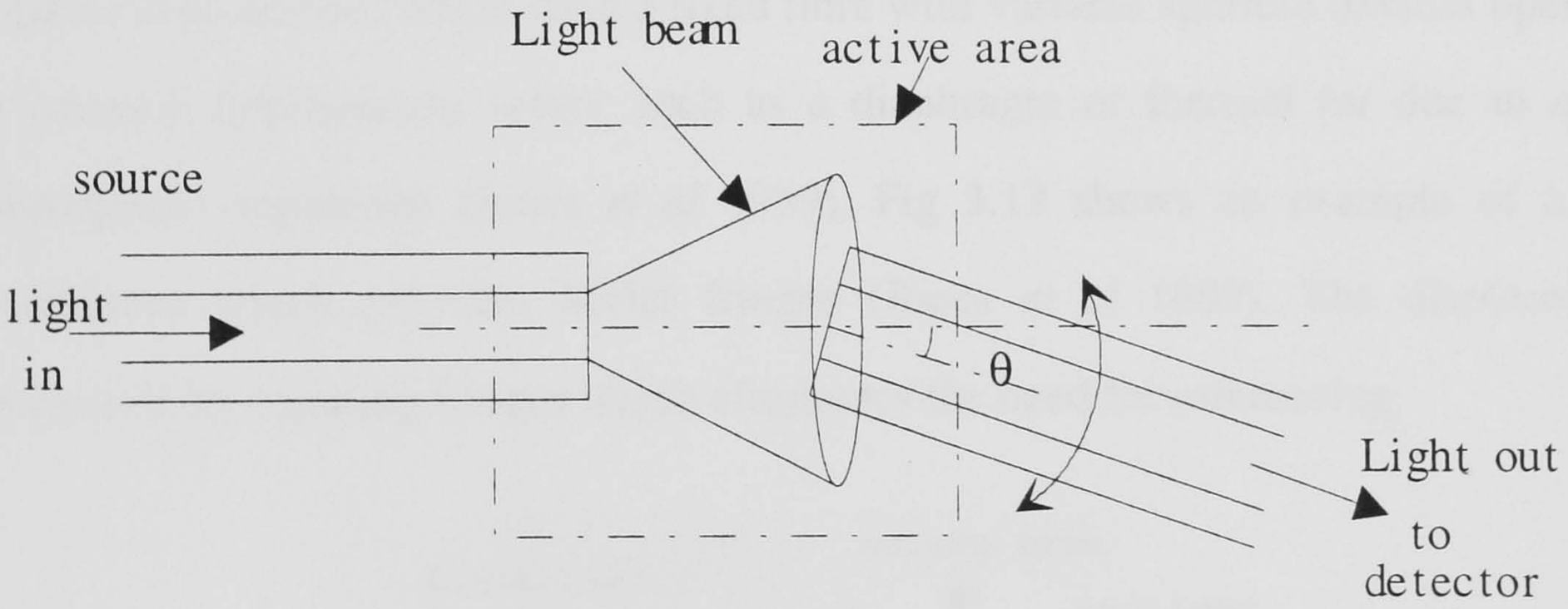

Figure 3. 11 Optical fibre angular displacement sensor.

Fig. 3.12 (a) shows an example of reflective displacement sensor. Light exits the fibre in a cone pattern and strikes a reflecting surface perpendicular to the axis of the optical fibre. A portion of the light reflected by the surface is recaptured by the fibre and propagates in the opposite direction. The amount of light recaptured is a function of the

distance between the reflector and the fibre end (Conley *et al* 1986). In Fig. 3.12(b) a second fibre, parallel to the first is employed to capture a portion of the back-reflected light (Personick 1985).

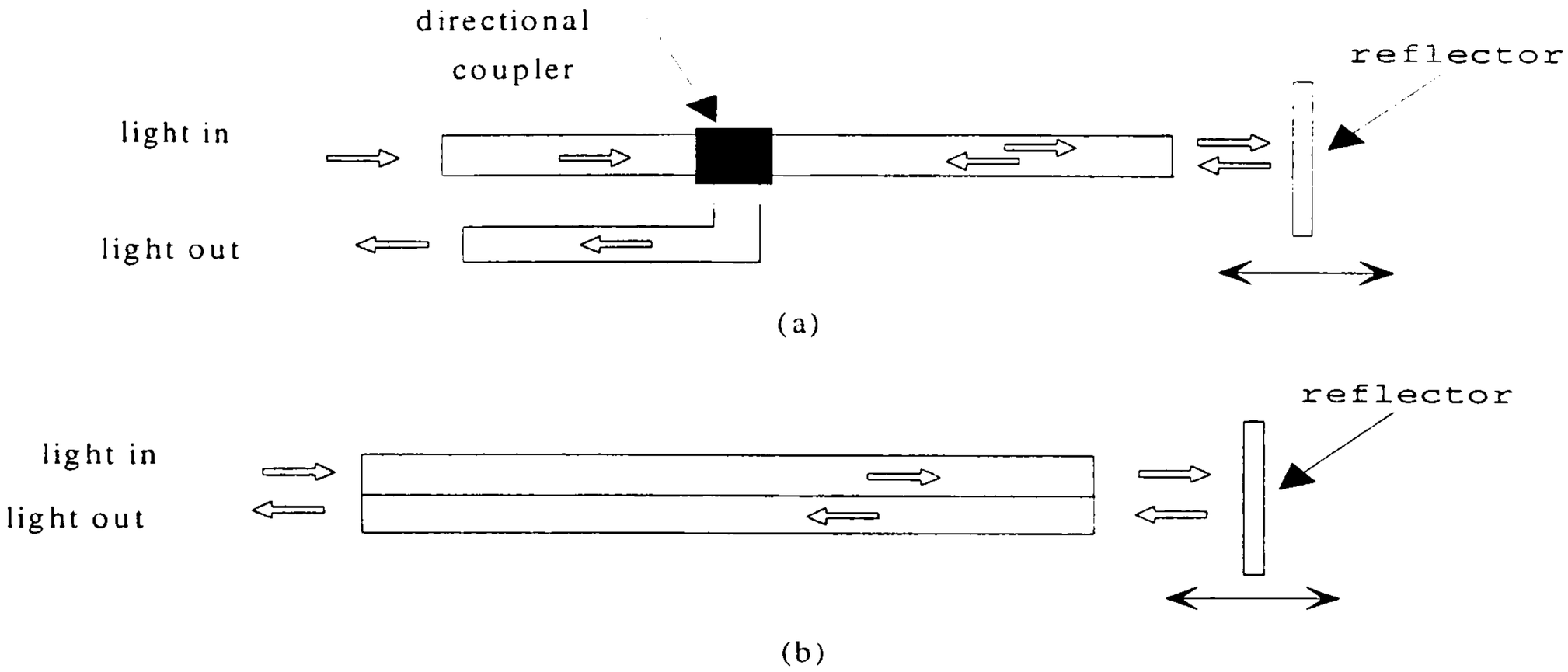

Figure 3. 12 Displacement reflective sensors (a) employing a single fibre (b) employing two fibres.

Shutter type devices which have a fixed fibre with variable aperture devices operated by a primary displacement sensor such as a diaphragm or thermal (or due to moisture absorption) expansion (Jones *et al* 1989). Fig 3.13 shows an example of a shutter modulator which provides Moiré fringes (Jones *et al* 1989). The displacement is measured by counting fringes which eliminates the need for referencing.

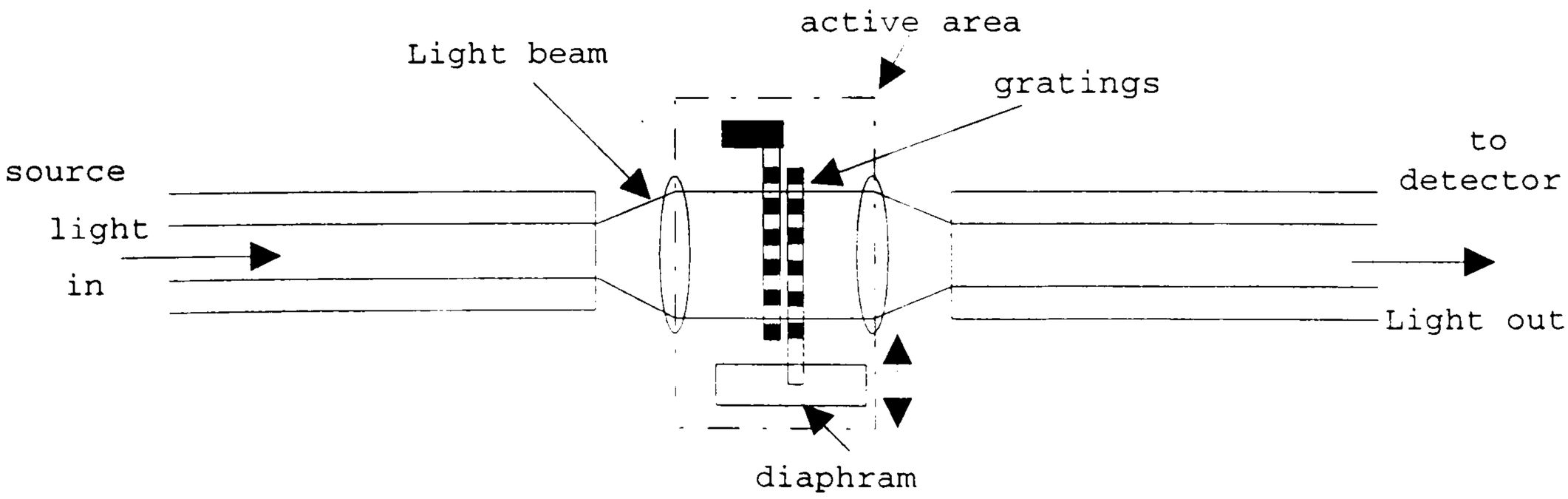

Figure 3. 13 Moiré fringe sensor.

Another class of intensity modulation sensors relies on introducing losses from the core or cladding of the optical fibre. Such sensors can be produced by causing the parameter of interest to introduce losses in the fibre.

Fig. 3.14 shows a microbend sensor. It is one the most popular technique of this class. It works by inducing periodic bend in the fibre by compression between two grooved plates. It can be shown that the attenuation is maximum, for step index fibre, when the bending is applied periodically with a bend pitch x where (Waynant and Ediger 1993)

$$x = \frac{C\pi rn}{NA} \tag{3.7}$$

where C= $\sqrt{2}$

r= the core radius,

n= refractive index of the fibre core.

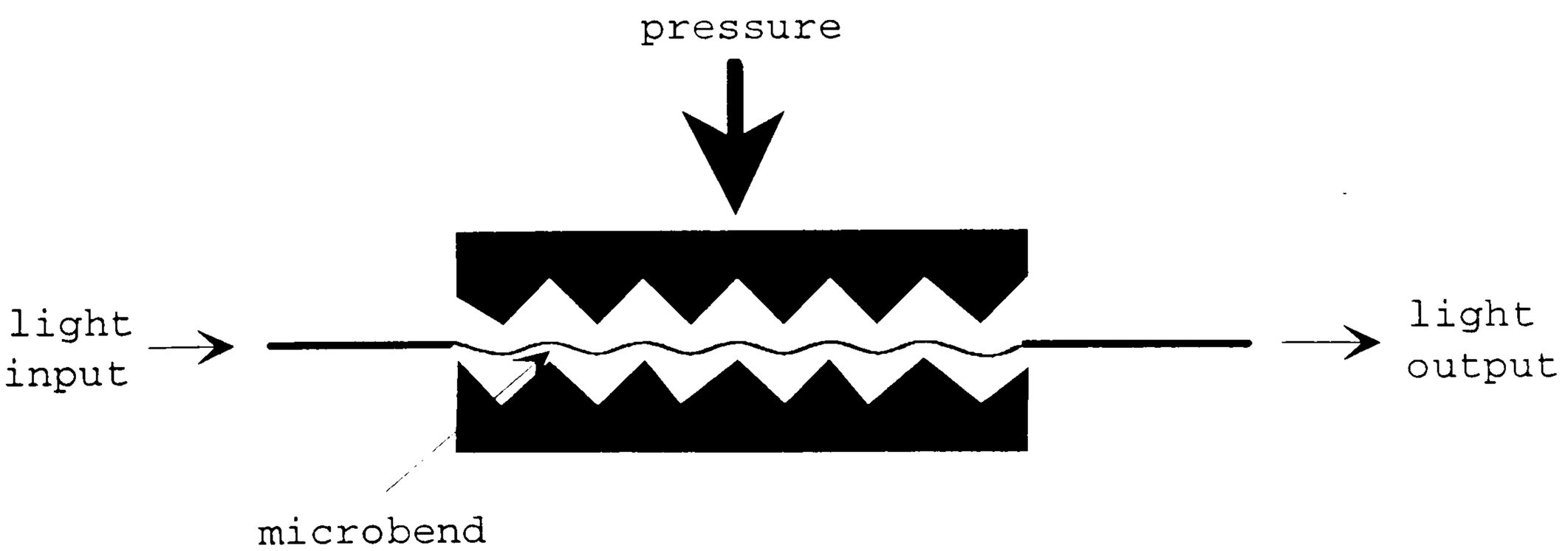

Figure 3. 14 Microbend sensor.

Fig.3.15 shows another type of sensor. Part of the cladding is removed in the sensing region. This makes the guidance properties of the fibre susceptible to changes in the refractive index of the region surrounding the unclad section. The nature of the interaction of the light with the surrounding medium depends on its refractive index. For example, evanescent field interaction occurs if the refractive index of the medium is less than that of the core (Harrick 1967). A wide range of sensors using this technique have been reported (Jones *et al* 1989).

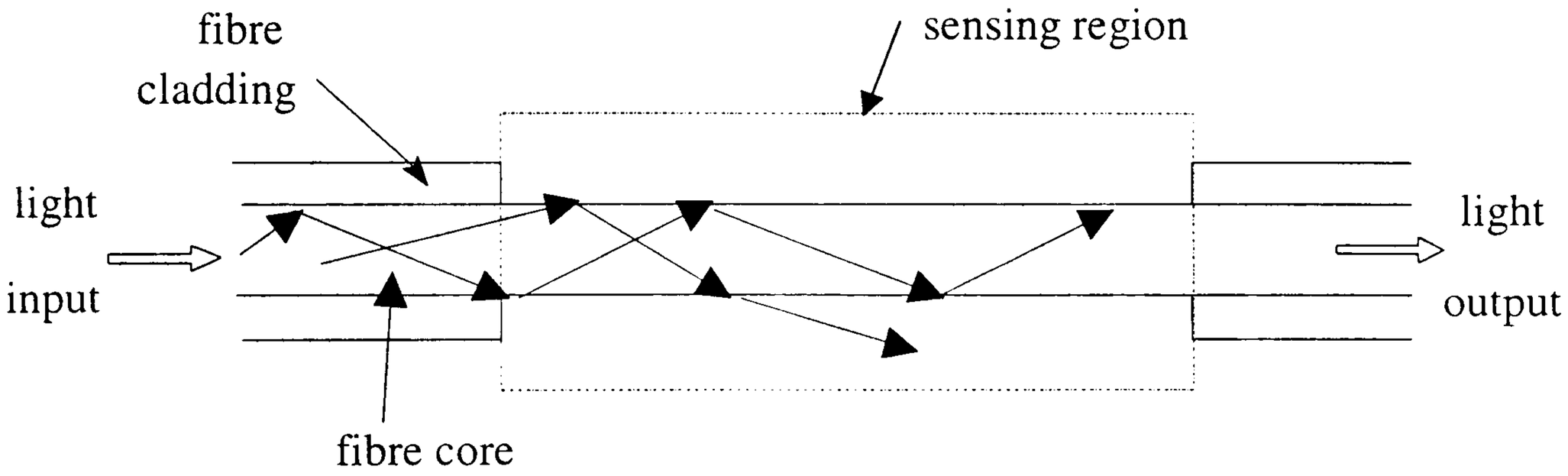

Figure 3. 15 An unclad optical fibre sensor.

Fig. 3.16 shows a sensor arrangement that uses similar principle as in above. In this case a short length of cladding from two adjacent fibres is removed. The level of cross-talk between the two fibres is determined by the refractive index of the material present in the active region as shown in the figure. This device has several applications (Jones *et al* 1989).

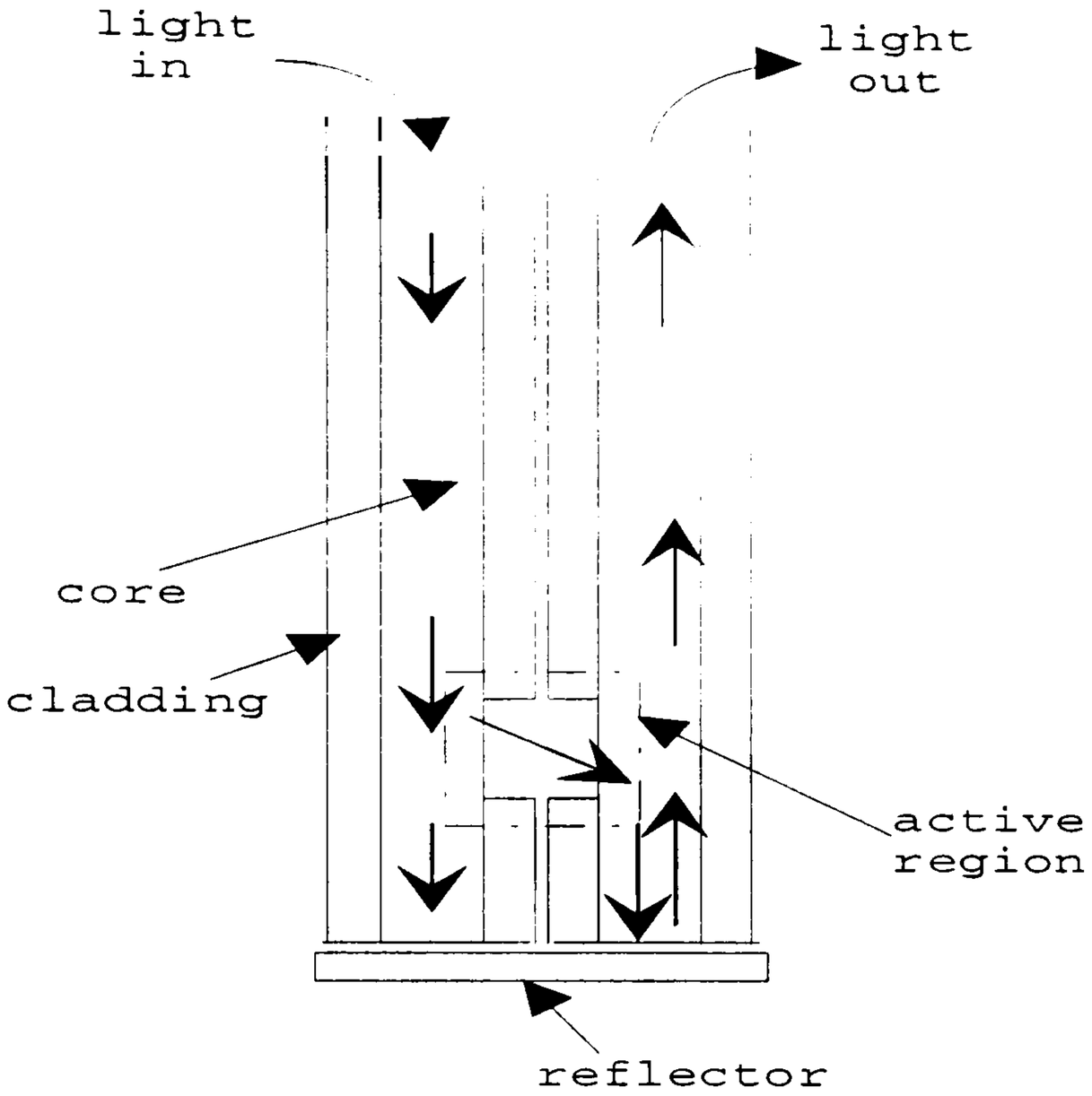

Figure 3. 16 'Cross-talk' sensor.

3.4.3 Referencing techniques for intensity based sensors

As mentioned earlier, there are errors inherently associated with intensity modulation sensors. Several referencing techniques have been developed to remedy this problem. Some of these techniques are briefly described below.

Fig.3.17 shows a balanced bridge system (Jones *et al* 1989). Two separate LEDs modulated at (typically) 1 kHz and 10 kHz provide light to the sensing head (M) via two separate multimode fibres. The light from the two outputs of the bridge goes to two separate detectors followed by electronic filters to separate the signals. It has been shown that an imbalance due to a 10 dB loss in one of the fibres causes less than 1% change in the processed output.

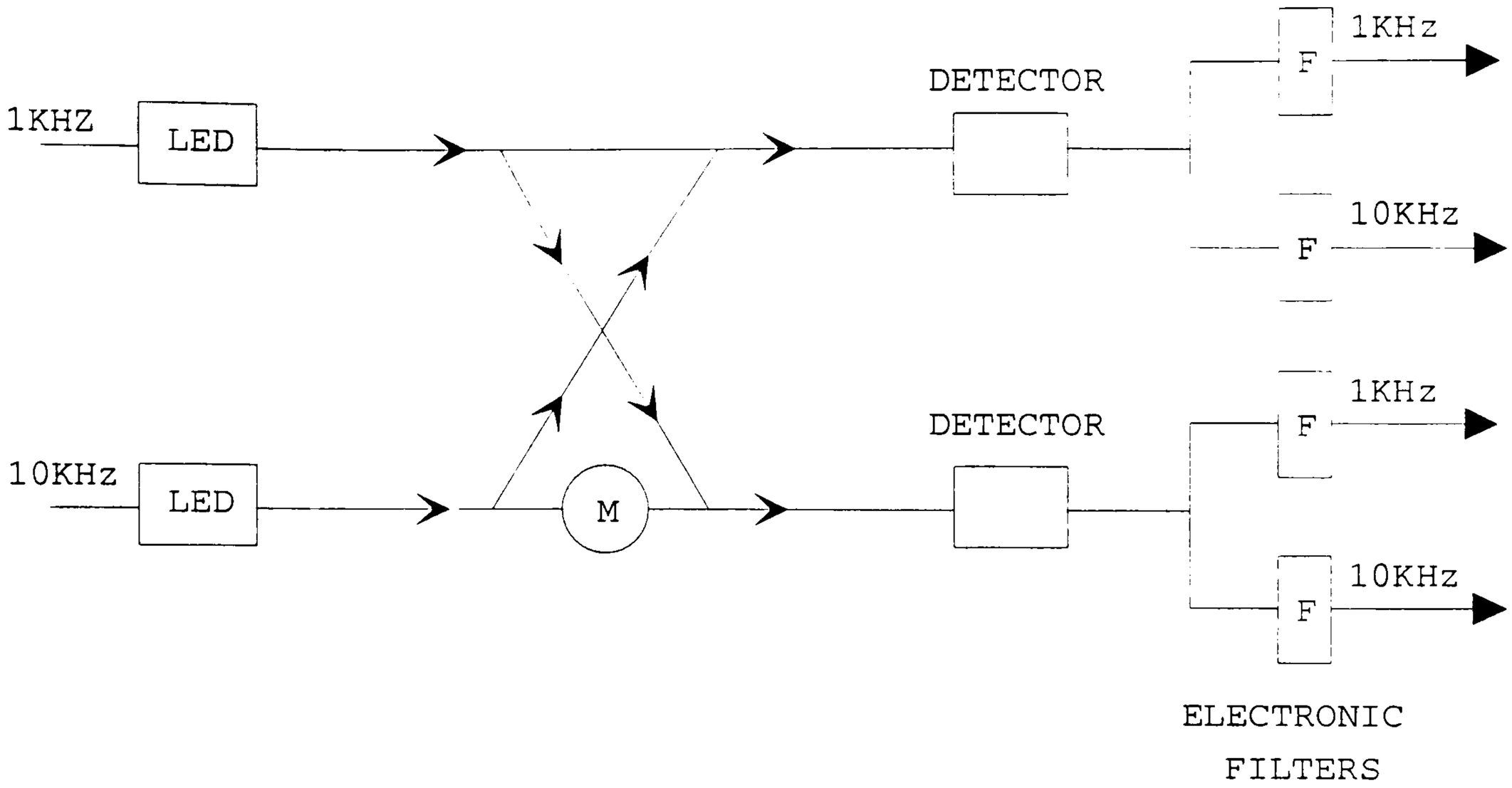

Figure 3. 17 Single-wavelength referencing using balanced bridge arrangement.

Fig.3.18 shows a modification of the reflection sensor system where the reflector is replaced by a partial reflector. in this case the beam is divided into two parts. The two beams are converted to electrical signal using two separate detectors. One beam is used as a reference (Jones *et al* 1989, Personick 1985).

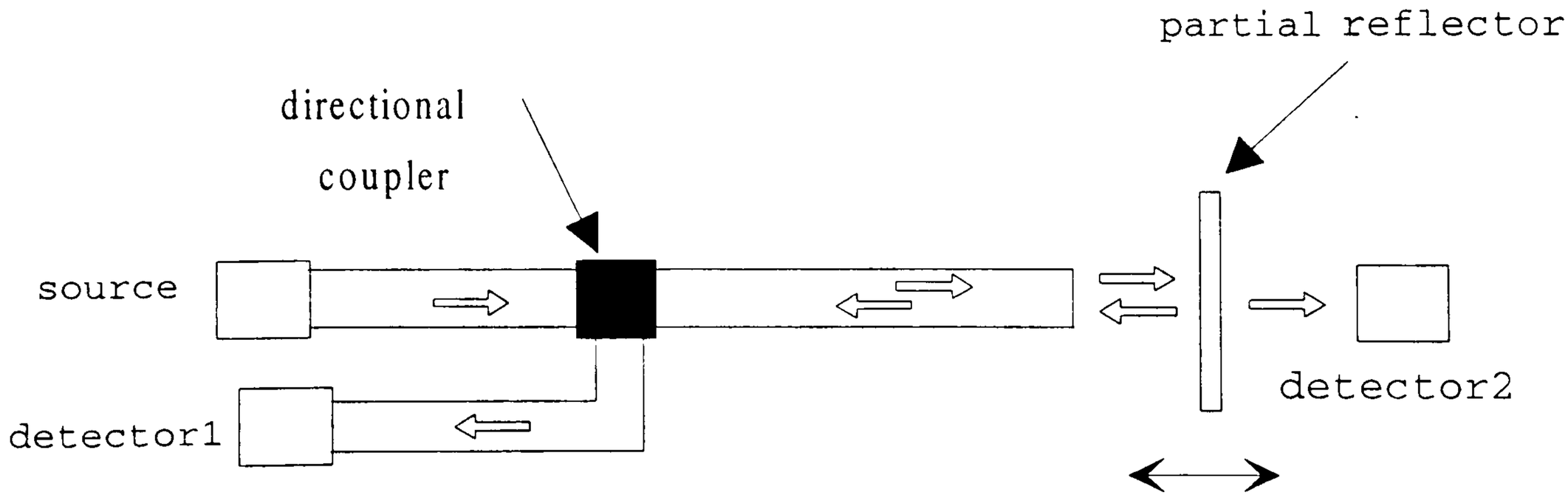

Figure 3. 18 Referencing scheme for reflective displacement sensor.

Fig. 3.19 illustrates the principle of dual wavelength referencing scheme by showing two examples. An ideal system has the following features:

(a) Losses in the system are wavelength-independent.

(b) The relative intensity of light at the two wavelengths remains constant.

(c) The relative sensitivity of the detection system at the two wavelengths remains constant.

(d) The launch conditions remain constant.

A number of optical fibre sensors using a variation of this scheme have been reported (Jones and Spooncer 1984, Murtaza and Senior 1993, Kharaz and Jones 1993). In this scheme the light intensity at one wavelength is modulated by the measurand. Light at a second wavelength, which is not affected by the measurand, is used to carry the reference signal. In Fig. 3.19(a) two independent light sources, at two different wavelengths, are used. The sources are modulated at two different frequencies. Light from the two sources are launched into two separate fibres then, using an optical coupler, combined into the sensing optical fibre. The photodiode convert the optical signal to an electrical one. The reference and the measurand signals are separated using electronic filters. The ratio of the two detected signals provide the sensor output. The disadvantage of this scheme is that it does not compensate for variation in the intensity of the sources. Fig. 3.19(b) shows an alternative scheme which uses a single source which contains both wavelengths. In this scheme the signals are received by two separate detectors. The main drawback here is that it is susceptible to any variations in the detectors characteristics.

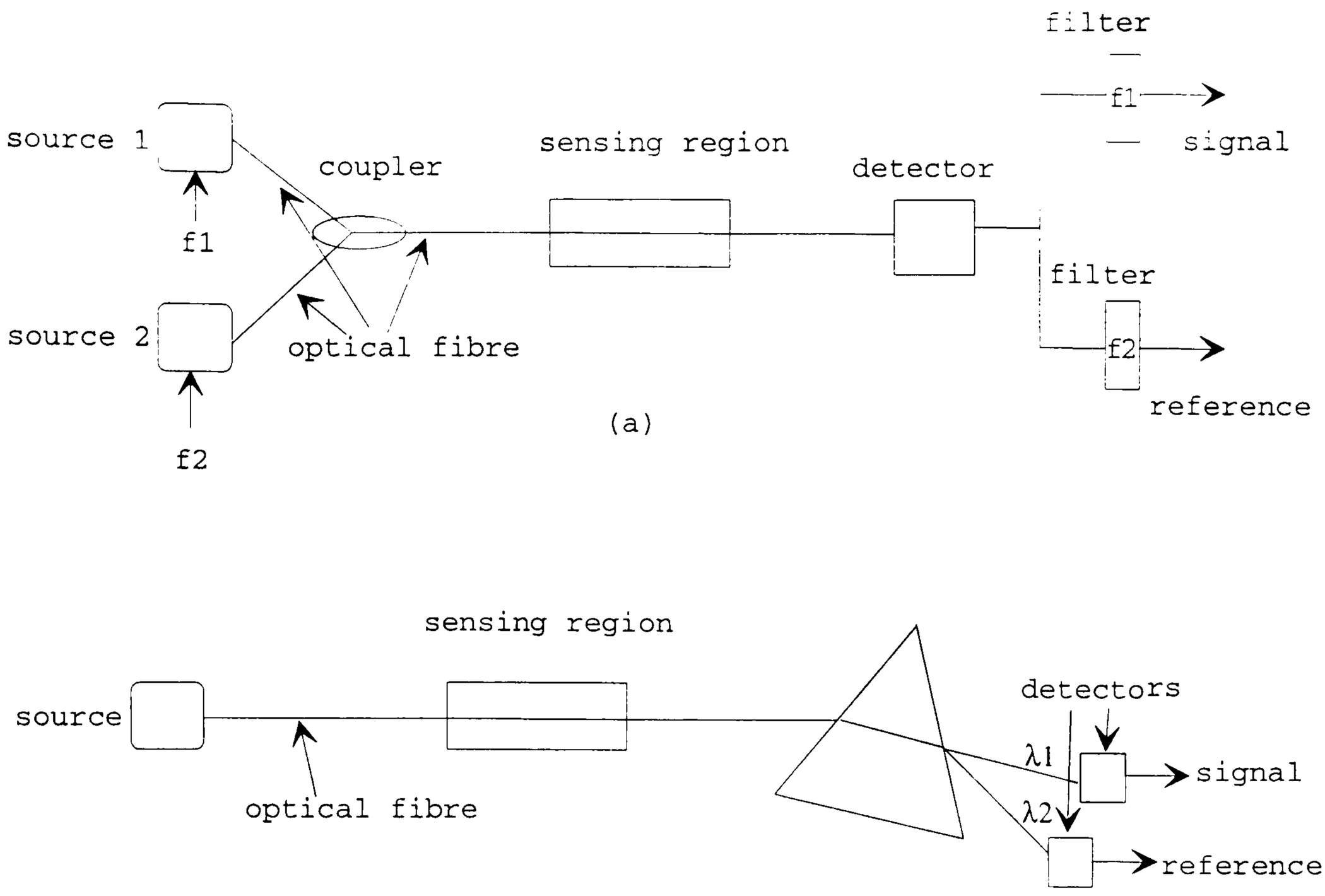

Figure 3. 19 Dual wavelength referencing schemes.

As shown in Chapter 2 section 2.6 the method selected here for the development of an optical fibre humidity sensor has been based on colorimetric interaction of a reagent with water molecules. It was also shown that this approach offers an easy implementation of a dual wavelength referencing scheme as that shown in Fig. 3.19. This method can be implemented in any of the techniques outlined in this section. However, the technique selected, for the sensor, was broadly based on the approach outlined in Fig. 3.15. This can be achieved by developing a suitable film to replace the cladding in the sensing region. This approach offers also the prospect of a multi-point distributed sensing system as discussed next.

3.5 Optical fibre multiplexing methods

Multi-optical-fibre-sensor systems can be formed in a number of ways.

1. A number of discrete sensors designed to operate as point sensors can be arranged in a network or array configuration, with the individual sensor outputs multiplexed onto the optical fibre system using conventional techniques common to electrical sensors such as frequency division multiplexing (FDM) or time-division multiplexing (TDM). Alternatively a variation specific to optical fibre sensors such as wavelength division multiplexing (Jones 1981, Kist 1989, Dakin 1990, Laude 1993).

2. The inherent distributed sensing nature of intrinsic optical fibre sensors can be used to create unique forms of sensors for which, in general, there may be no counterpart based on conventional sensor technologies. Intrinsic distributed sensors are particularly attractive for use in applications where monitoring of a single measurand is required at a large number of points or continuously over the path of the fibre. One of the earliest schemes for sensor multiplexing in optical fibre was reported by Nelson (Nelson 1980), where a fibre optic branched network was used in conjunction with an optical time domain reflectometer (OTDR) system capable of receiving and independently monitoring the separate returns from a series of reflective sensors.

3.5.1 Optical time-domain reflectometry

As shown in section 3.2, Rayleigh scattering loss arises as a result of random microscopic variations in the index of refraction of the fibre core. A fraction of the light that is scattered in a direction 180° to the propagation axis of the light (backscattered light) is recaptured by the fibre aperture and returned towards the source. By pulsing the input optical signal to a length of fibre and monitoring the variation in the returned

backscattered intensity, spatial variations in the fibre scattering coefficient or cross-section, or attenuation, can be determined. This forms the basis of optical time-domain reflectometry (OTDR), which is a well-established technique for fault/imperfection location and diagnostics in fibre communications applications (Dakin and Culshaw 1989). In sensing applications, OTDR can be used to detect localised measurand-induced variations in the loss or scattering coefficient of a continuous sensing fibre (Davies 1984).

The sensor under investigation is an intrinsic intensity based optical fibre sensor. It therefore requires an intensity-based OTDR to form a multi-point distributed optical fibre system. An OTDR, operating at the required wavelength, was developed. The theory and design is covered in Chapter 7.

3.6 Summary

In this chapter the basic theory of optical fibre transmission and the main elements of optical fibre sensors were discussed. Some intensity based optical fibre transduction mechanisms were introduced. Some intensity referencing techniques were also discussed. The method selected here for the development of an optical fibre humidity sensor is based on colorimetric interaction of a reagent with water molecules. This can be achieved by developing a suitable film to replace the cladding in the sensing region. The prospect for multi-point distributed optical fibre sensors was addressed.

In the next chapter the basic theory of the sensor design is addressed.

CHAPTER 4

Basic scheme

4.1 Introduction

Based on the discussion introduced in Chapter 2, optical fibre humidity sensors may be broadly divided into two categories: firstly, physical sensors for which the presence of water vapour does not alter the chemical structure of the sensing material but it alters one or more of its physical parameters, e.g. change in physical size or refractive index (Culshaw and Dakin 1989, Takeo and Hattori 1991, Spooncer *et al* 1992); secondly, chemical sensors in which a chemical reaction takes place due to the presence of water vapour, thus changing the chemical structure of the sensing material, e.g. chemical structure change that gives rise to colour (colorimetric) or fluorescence change (Rudolf Seitz 1984, Narayanaswamy *et al* 1988, Culshaw and Dakin 1989). The selected approach for the research work reported in this thesis is in the second category and it will now be discussed in more detail. This approach was selected because it is wavelength specific and lends itself to referencing as shown in Chapter 3 section 3.4.1.

4.2 Sensor configurations

Optical techniques are widely used in conventional chemical analysis employing bulk-optical systems (Nussbaum and Phillips 1976, Culshaw and Dakin 1989, HMSO 1992). Optically-excited transitions of an atom or molecule between the various allowed quantum states are highly specific and have the potential to yield considerable information regarding the molecule and its coupling to the surrounding medium (Dakin and Culshaw 1989, HMSO 1992). The sensing of chemical parameters via optical fibres

is usually performed by monitoring changes in a suitably selected optical property. Depending on the particular device, the optical property measured may be absorbance, reflectance, scattering, luminescence (fluorescence or phosphorescence) or refractive index (Graff 1983, Krohn 1986, Dakin and Culshaw 1989)

An optical fibre humidity sensor using a colorimetric material (reagent) may be realised in one of the following three methods.

4.2.1 Reflective method

Measurement of intensity to detect colour change of the reflected light is particularly useful when the sensing element is either opaque or a weak transmitter of light. Reflection takes place when light infringes on a boundary surface, and two distinct types of reflection are possible (Boisde and Harmer 1996). The first is a mirror type or specular reflection, which occurs at the interface of a medium with no transmission through it. The second is a diffuse reflection, where the light penetrates the medium and subsequently reappears at the surface after partial absorption within the medium.

In the reflective method the reagent may be bound to the end of the fibre using a colourless hygroscopic membrane, or it can be fixed at a small distance from the fibre end, as shown in Fig. 4.1. Transmitted light leaves one optical fibre and strikes the reagent; the reflected light may be collected by a separate fibre, as shown in Fig. 4.1 (a) & (b), or it can be collected by the same fibre, as shown in Fig. 4.1 (c).

Variation of humidity in the region of the membrane causes variation in the colour of the reagent and modulates the intensity of the reflected light.

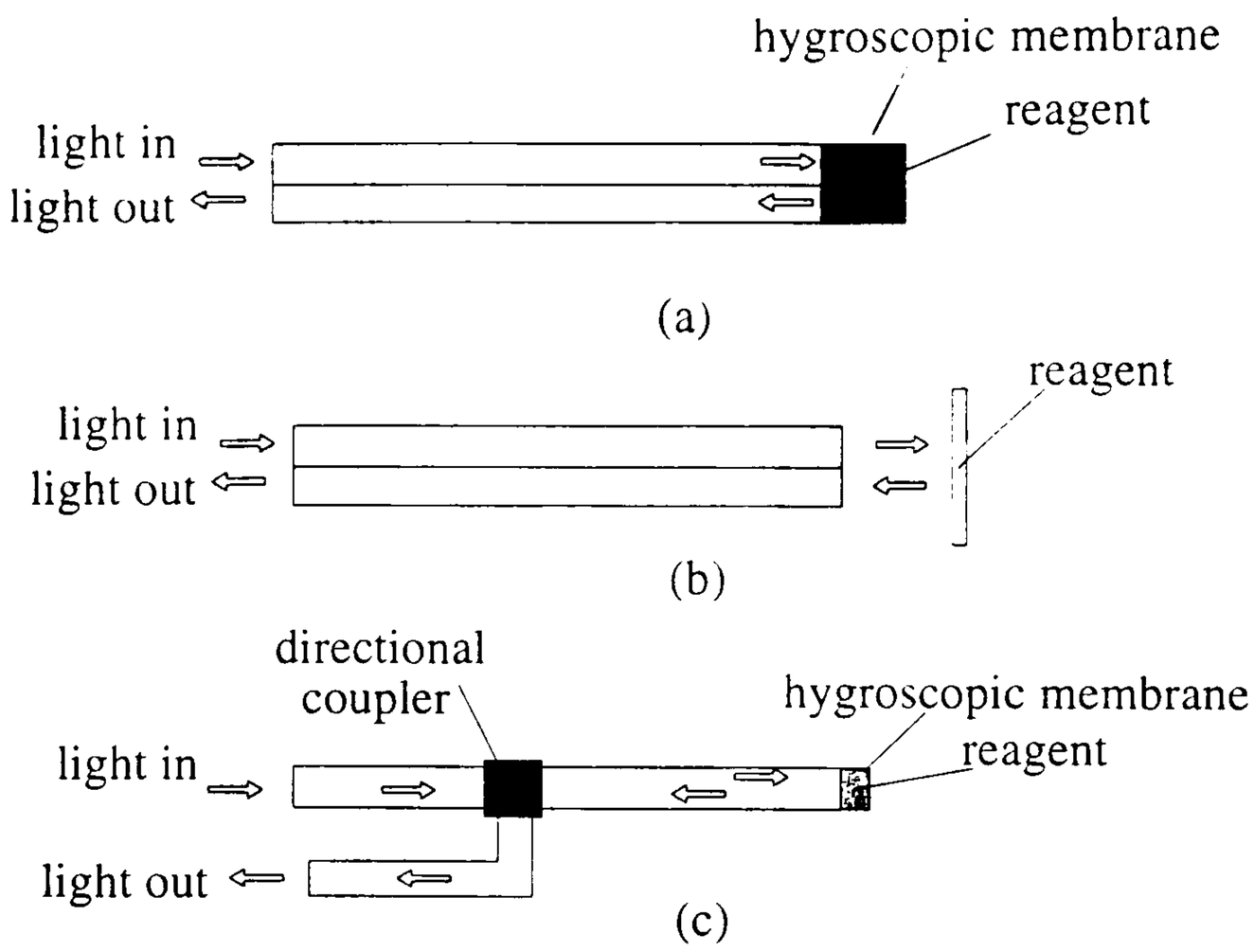

Figure 4. 1 Schemes for a reflective humidity sensor.

4.2.2 Transmissive method (core)

A transmissive method can be used by immobilising the reagent in a specially modified optical fibre which has a porous core that can entrap the reagent molecules in the pores, as shown in Fig.4.2. As light travels through the fibre it gets absorbed by the reagent molecules. One of the main disadvantages of such an arrangement is that the moisture has to diffuse deep into the fibre core, and this can take a relatively long time. This technique can be implemented by either manufacturing a special optical fibre or by the insertion of a sensing element between two fibres. The first of the two is expensive and impractical for our investigation. The second approach makes use of the commercially available optical fibres. However, it has the disadvantage of introducing additional loss as light leaves one fibre and is collected by another.

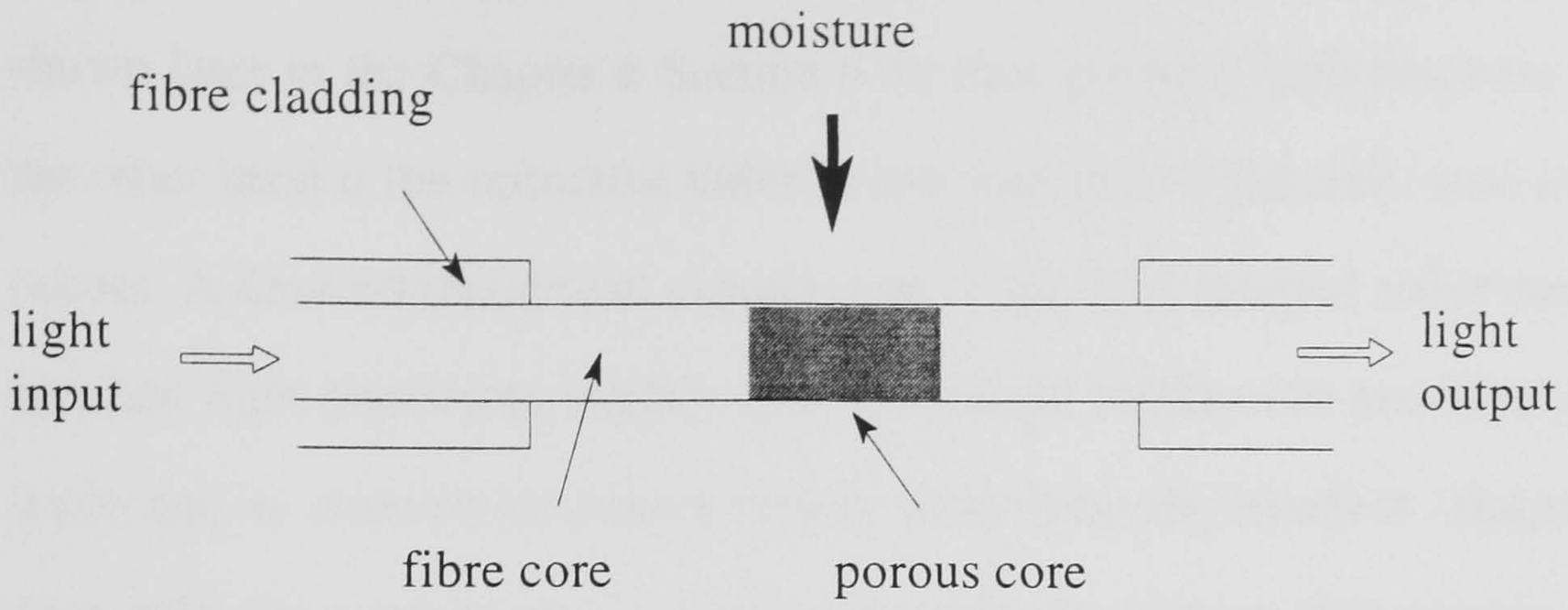

Figure 4. 2 A sensor configuration using the core as the active region.

4.2.3 Transmissive method (cladding)

A transmissive method can also be used by immobilising the reagent in the cladding of the fibre by means of a hygroscopic film or by having a porous, cladding as shown in Fig. 4.3.

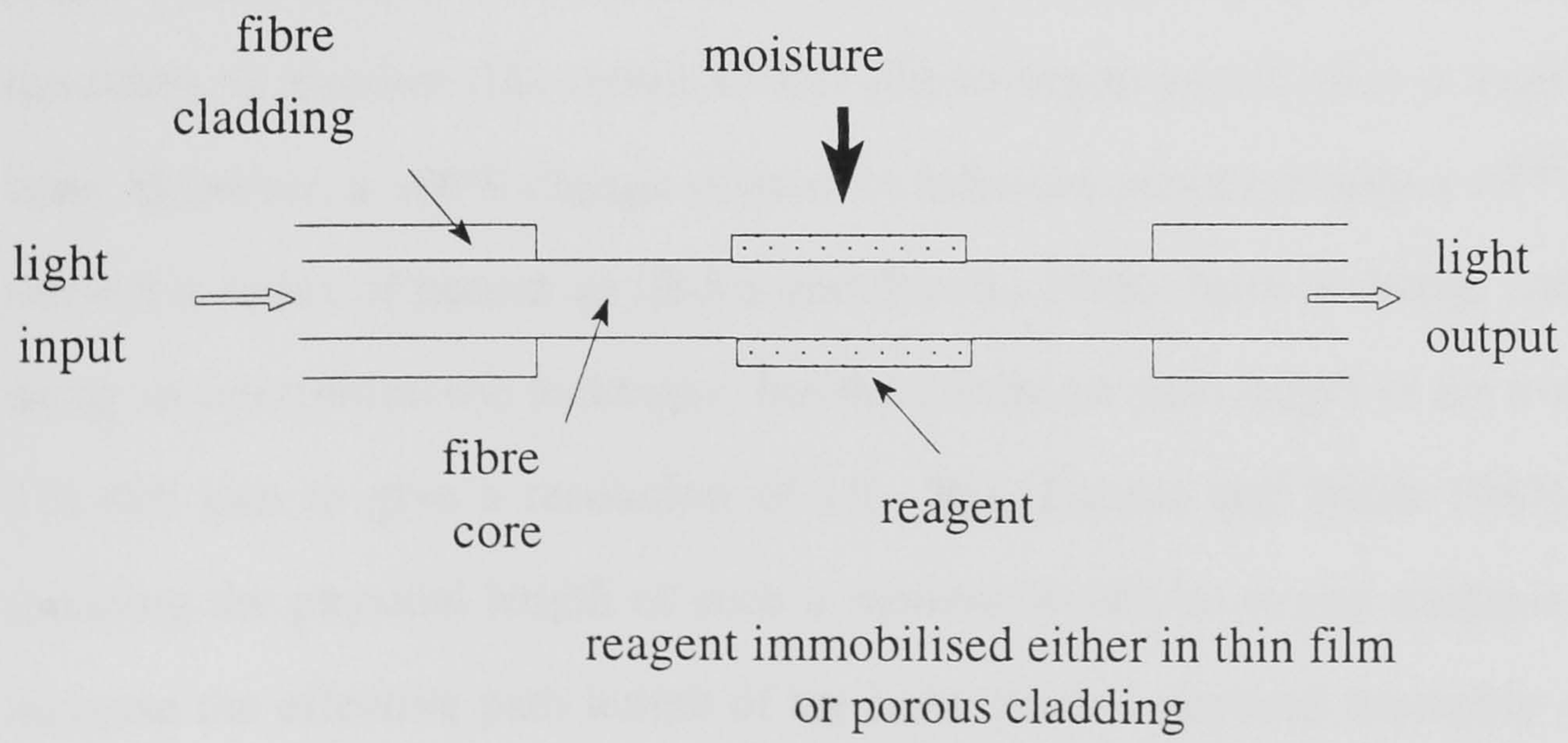

Figure 4. 3 A sensor configuration using the cladding as the active region.

In either case, if the refractive index of the cladding (porous silica or a hygroscopic film) is greater than that of the core all the light will propagate through the film (as shown later in the Chapter 6 Section 6.3), thus giving a high response to moisture. On the other hand if the refractive index is less than that of the core. total internal reflection occurs. A detailed theoretical examination of the total internal reflection reveals that the incident light penetrates slightly into the second medium in the form of an evanescent wave and its intensity decreases rapidly away from the interface (Harrick 1967). In this case only the evanescent field interacts with the reagent thus giving a much-reduced response. This method is attractive since both the sensitivity and the time constant can be controlled by careful selection of both the reagent and the immobilising agent. It also has the potential of producing a lower loss sensor than the case of methods (i) and (ii) above. In all methods above, there are other ways, in addition to that caused by humidity variation, in which the intensity of light can be altered, for example, by the variation of the intensity of the light source. Hence the need for implementing a referencing scheme as discussed in Chapter 3 section 3.4.1.2.

It is worth mentioning here that as the refractive index of air changes with humidity, it might seem obvious to use measurement of refractive index as a means of determining humidity. A monitor that relied on this phenomenon would have a very fast response time. However, a 100% change of relative humidity produces only a 10^{-6} change in the refractive index of humid air (Birch and Downs 1988). Such a change can be measured using an interferometric technique, but the minimum path length in air would have to be 316.496 mm to give a resolution of 1% RH (Downs and Birch 1983). One way of reducing the physical length of such a monitor would be to use multiple reflections to increase the effective path length of the light. Such a physical assembly would have to be very stable to about 1nm in length (Birch 1990), and this requirement is difficult to achieve. In addition, refractive index has been shown to be dependent on barometric pressure, air temperature and atmospheric constituents. For example, 1°C change in temperature causes $1x10^{-6}$ in refractive index, 100Pa change in pressure causes a

$2.7x10^{-7}$ and a 1 % RH change causes a $1x10^{-8}$. (Birch and Downs 1988). It is also interesting to note that if a core of an optical fibre of a refractive index 1.453 is exposed to air, the critical angle at the interface changes by 5.43×10^{-6} ° for 100% change in RH. So it seems impractical to use refractive index of air to monitor relative humidity.

The sensor configuration selected for this work is based on the method shown in Fig. 4.3. It makes use of the cladding as the active region. A hygroscopic thin film, of a larger refractive index than that of the core, is used to immobilise the reagent. Since the refractive index of the film is larger than that of the core, light is refracted into the film and then totally reflected at the air/film interface and refracted back again into the core, as explained below.

4.3 Theoretical analysis of the selected configuration for the sensor

4.3.1 Geometric Analysis

Light propagation through the sensor is illustrated in Fig.4.4. With reference to the figure, the refractive index of the core and the cladding are n_1 and n_2 respectively. The refractive index of air, n_o, is taken as 1.0. The numerical aperture (NA) of the optical fibre is the sine of the maximum acceptance angle θ_{max} (refer to point A) and is given by the relationship

$$NA = \sin\theta_{max} = \sqrt{n_1^2 - n_2^2} \qquad (4.1)$$

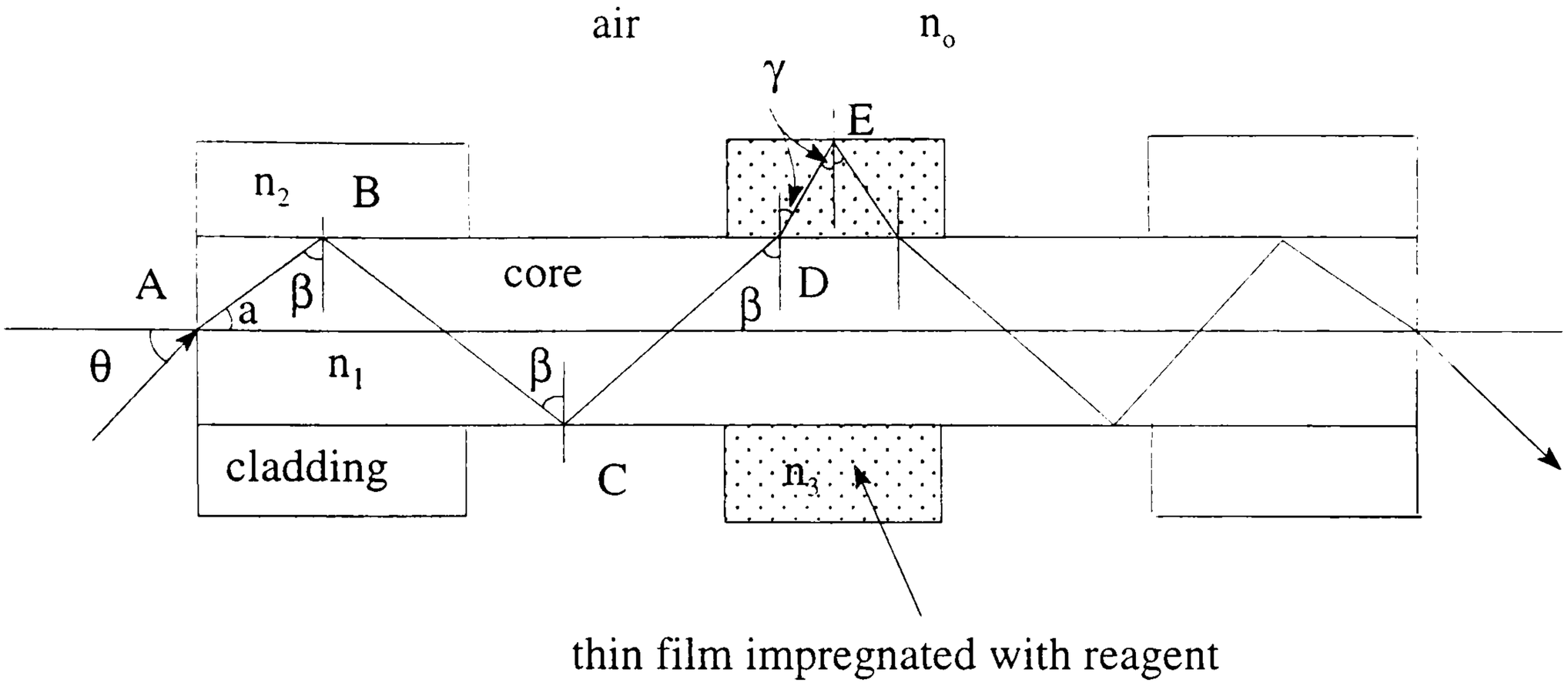

Figure 4. 4 Light propagation through the sensor.

Using Snell's law at point A for θ_{max} (angle α is also a maximum and β is a minimum since $\beta = 90 - \alpha$)

$$n_o \sin\theta_{max} = n_1 \sin\alpha$$

$$\sqrt{n_1^2 - n_2^2} = n_1 \sin\alpha$$

$$\Rightarrow \sin\alpha = \sqrt{1 - \frac{n_1^2}{n_2^2}}$$

$$\Rightarrow \cos\alpha = \frac{n_2}{n_1}$$

$$\sin\beta = \cos\alpha$$

$$\therefore \sin\beta = \frac{n_2}{n_1} \qquad (4.2)$$

At point C, core/air interface, the critical angle β_C is given by the relationship

$$n_1 \sin\beta_c = 1$$

$$\text{or} \quad \sin\beta_c = \frac{1}{n_1} \tag{4.3}$$

For all rays guided by the optical fibre the following conditions apply

$$0 \le \theta < \sin^{-1}\sqrt{(n_1^2 - n_2^2)} \tag{4.4}$$

$$0 \le \alpha < \sin^{-1}\sqrt{1 - \frac{n_1^2}{n_2^2}} \tag{4.5}$$

$$\sin^{-1}\left(\frac{n_2}{n_1}\right) < \beta \le 90^o \tag{4.6}$$

From equations 4.2 & 4.3, and since $n_2 > 1$, β will always be greater than β_C (the critical angle), i.e. all rays supported by the optical fibre are reflected at the core/air interface and will be guided through the area where the cladding has been removed.

At point E (air/film interface), the critical angle γ_C is given by the expression

$$\sin\gamma_c = \frac{1}{n_3} \tag{4.7}$$

Applying Snell's law at point D (core/film interface), it follows that

$$n_1 \sin\beta = n_3 \sin\gamma \tag{4.8}$$

From equations 4.6 & 4.8.

$$\sin^{-1}\left(\frac{n_2}{n_3}\right) < \sin^{-1}\left(\frac{n_1}{n_3}\right) \tag{4.9}$$

From equations. 4.7 & 4.9 and since n_1 and $n_2 > 1$, it can be concluded that the angle γ (at film/air interface) is always greater than the critical angle, hence all rays guided are totally internally reflected and guided back again into the core, as shown in the figure.
So far only the rays falling on the air/film interface parallel to the fibre are considered. However, some rays fall on the air/film interface perpendicular to the fibre, as illustrated in Fig. 4.5.

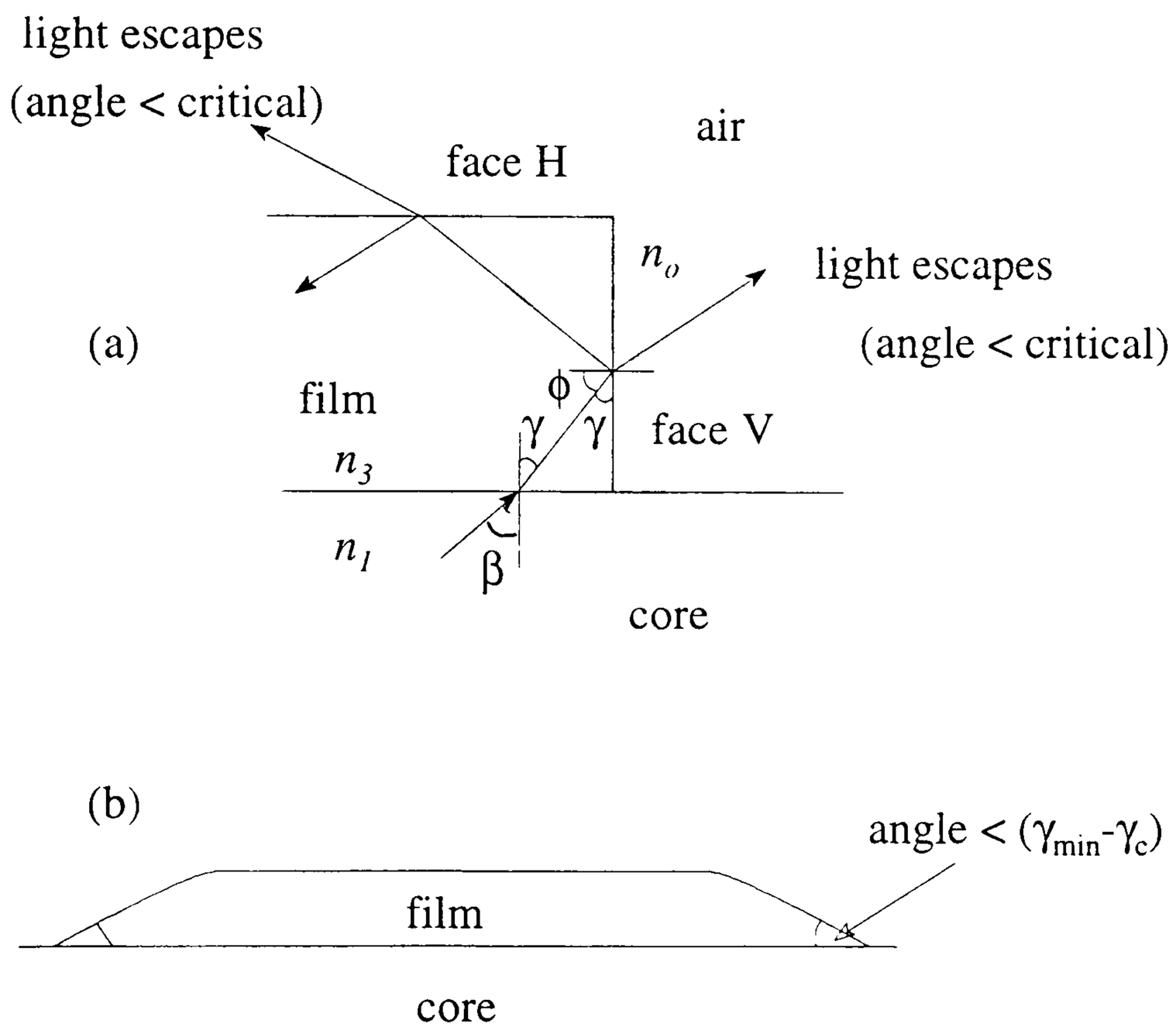

Figure 4. 5 Rays falling on the edge of the film: (a) edge perpendicular to fibre causes light loss; (b) edge at an angle to the fibre to eliminate light loss.

The minimum and maximum values of γ derived from Equations. 4.9 are given by

$$\gamma_{\min} = \sin^{-1}\left(\frac{n_2}{n_3}\right) \tag{4.10}$$

$$\gamma_{max} = \sin^{-1}\left(\frac{n_1}{n_3}\right). \qquad (4.11)$$

If the critical angle $\gamma_C < 45^O$, it is possible (depending on the values of n_1, n_2 and n_3) that light may strike the vertical face (see Fig.4.5 (a)) at an angle greater than γ_C thus allowing total internal reflection. On the other hand if $\gamma_C > 45^O$, then $\gamma > 45^O$ which makes $\phi < 45^O$, i.e. $< \gamma_C$ (since $\phi = 90 - \gamma$) thus causing light to escape into the air. Some light escapes in both cases as shown in the figure.

To solve this problem the edge of the film must be made sloping at an angle of less than $\gamma_{min} - \gamma_C$, so that the light incident angle at the air/film interface is always $> \gamma_C$.

Thus, when coating an optical fibre core with a film of higher refractive index than that of the core, all rays supported by the optical fibre will be guided into the coated region provided that the film geometry has the form shown in Fig.4.5 (b).

Example

A step index optical fibre has a core refractive index of 1.453 and a cladding refractive index 1.405. Part of the cladding is replaced by a thin film coating which has a refractive index of 1.5. What is the geometry of the thin film such that no losses occur?

Referring to Fig.4.4, n_1=1.453, n_2=1.405 and n_3=1.5.

The critical angle at the thin film/air interface,

$$\gamma_c = \sin^{-1}\frac{1}{n_3} = \sin^{-1}\left(\frac{1}{1.5}\right) = 41.81^o$$

Using equation (4.10),

$$\gamma_{\min} = \sin^{-1}\left(\frac{n_1}{n_3}\right) = \sin^{-1}\left(\frac{1.453}{1.5}\right) = 75.62^{\circ}$$

The shape of the film is given in Fig.4.5 (b) with a maximum slope to the horizontal of $\gamma_{min} - \gamma_C = 33.81^{o}$.

4.3.2 Fresnel reflection within the sensor

This occurs at the boundary between dielectrics with dissimilar refractive indexes. For normal incident it is given by (Senior 1992)

$$r = \left(\frac{n_{3-}n_1}{n_3 + n_1}\right)^2 \qquad (4.12)$$

where r = fraction of light reflected,

n_1 = refractive index of the fibre core and

n_3 = refractive index the film.

Fig.4.6 shows the transmitted and reflected rays at the core-film interface. Only the evanescent field of the reflected light at point A interacts with the reagent in the film. On the other hand at point B some of the light gets reflected back into the film thus have more interaction with the reagent, thus making up for the loss in interaction occurred as a result of the reflection at point A.

Example

For the sensor in the above example, the fraction of light, r, that gets reflected at the core/film interface is given by Eq.(4.12), as follows

$$r = \left(\frac{n_3 - n_1}{n_3 + n_1}\right)^2 = \left(\frac{1.5 - 1.453}{1.5 + 1.453}\right)^2 = 2.53 \times 10^{-4}.$$

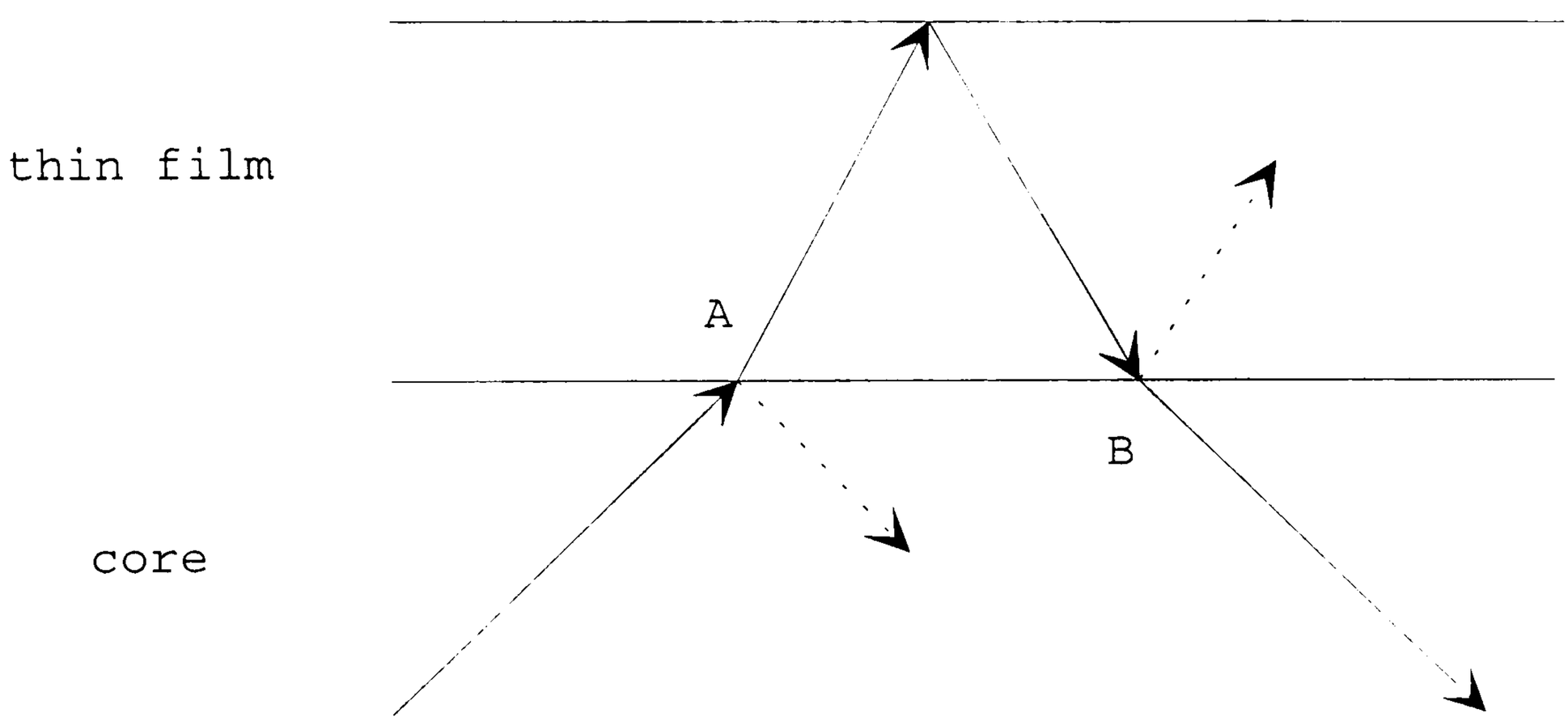

Figure 4. 6 Fresnel reflections at film-core interface.

4.3.3 Intrinsic losses

The sensing element in the optical fibre introduces two intrinsic losses.

(a) Scattering losses. These depend on the structure of the thin film. They are caused by the interaction of light and the granular appearance of atom and molecules in the thin film on a microscopic scale (see Chapter 3).

(b) Mode mismatch loss. The introduction of the thin film to the optical fibre changes the waveguiding characteristics of the sensing part of the fibre, thus changing the number of modes (Snyder and Love 1983) that can be supported. The region of the fibre into which power is injected must be capable of propagating as many modes as the region from which power is emitted. If this is not the case, losses will occur. The magnitude of this loss is given by (assuming that the power is equally distributed among the modes)

$$loss = 10\log\left(\frac{N_r}{N_t}\right) \tag{4.13}$$

where N_r and N_t are the number of modes propagated by the receiving and transmitted fibres, respectively. The number of modes (N) any fibre can support is given by (Jones *et al* 1989)

$$N \approx \frac{V^2}{2} \tag{4.14}$$

$$V \approx \frac{2\pi}{\lambda} a n_1 (2\Delta)^{\frac{1}{2}} \tag{4.15}$$

$$\Delta = \frac{n_1^2 - n_2^2}{2n_1^2}$$

where V = the normalised frequency,

a = the core radius,

Δ = relative refractive index difference and

λ = the operating wavelength.

Fig.4.7 shows the sensing fibre being divided into five regions. Regions A and E represent the unmodified fibre. In regions B and D the unclad core of the fibre is exposed to air. In region C the cladding is replaced by the thin film. Each of the above regions supports a different number of modes. As light travels through a fibre, if any of the region supports less number of modes than its predecessor loss occurs Therefore, loss is suffered at the interface between the regions.

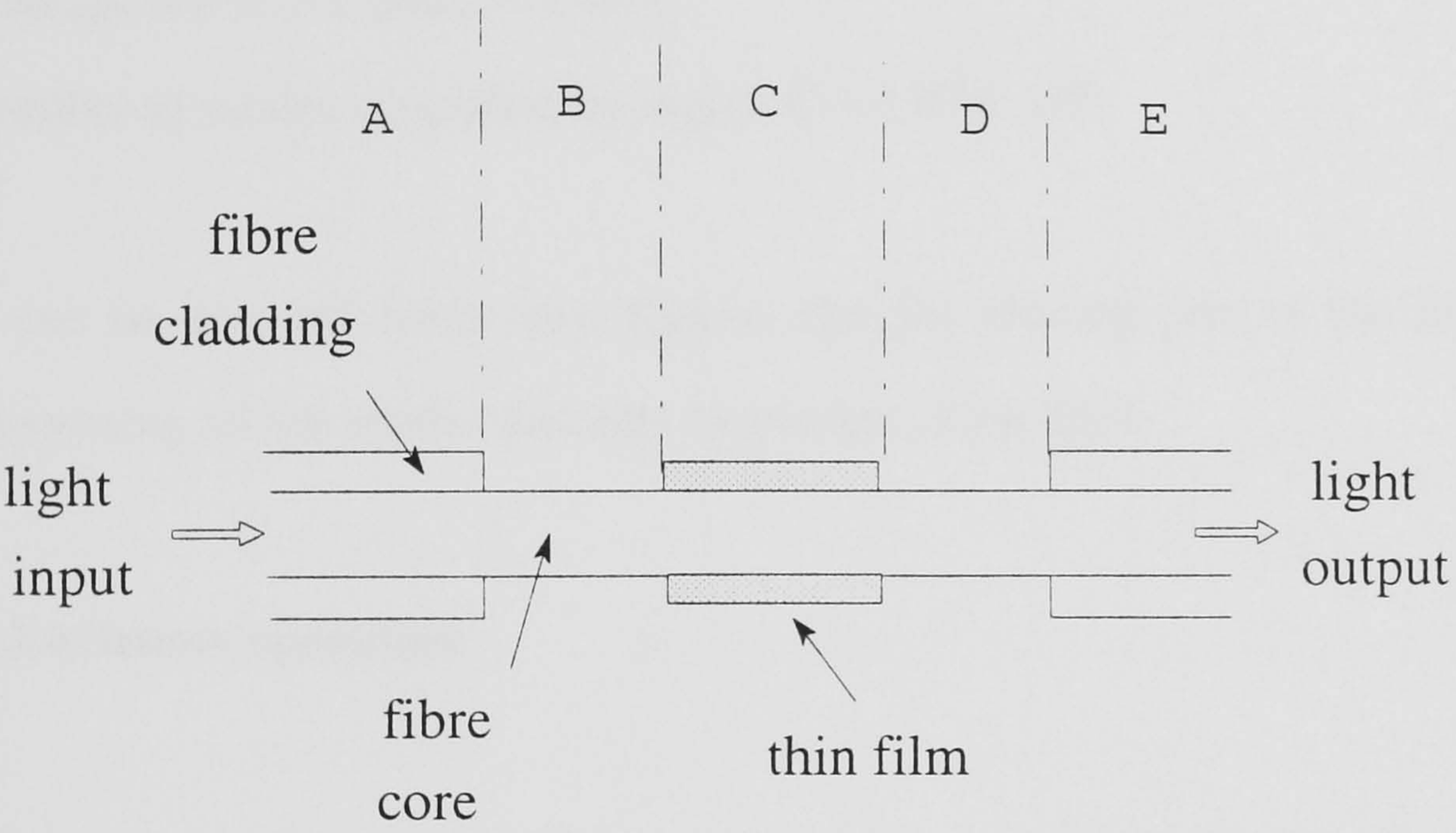

Figure 4. 7 Modal Regions for the sensor.

Example:

An optical fibre and a thin film have the same specifications as those in the previous example. The refractive index of the core n_1= 1.453, cladding n_2 = 1.405 and the thin film n_3 = 1.5. The diameter of the core is 200 μm and the operating wavelength is 670 nm.

Applying Eq. 4.14 and 4.15 the number of modes in each region can be calculated as given below.

Number of modes supported by region A $\approx 2.376 \times 10^5$

Number of modes supported by region B = 1.95×10^6

In region C, for simplicity we can take the average value of refractive index assuming the thickness of the film to be 1 μm.

Average refractive index ≈ 1.454.

Number of modes supported by region C = 1.97×10^6.

It can be deduced from these figures that the sensing part of the fibre is capable of supporting all the modes that may be present in the fibre.

4.3.4 Sensor operation

Now to consider an optical fibre humidity sensor based on the colorimetric principal. The variation of air humidity causes variation in the colour of the reagent and modulates the intensity of the transmitted light through the sensor. Light is subjected to both absorption and scattering as it propagates through the sensor.

The change in light intensity due to absorption is determined by the type of the reagent in the optical path and is related to the concentration (C) via the Beer-Lambert relationship. This law describes an exponential reduction of light intensity with distance (and concentration) along the optical path. The relationship can be expressed logarithmically as follows (Boisde and Harmer 1996):

$$A = \log \frac{I_o}{I} = \varepsilon l C \qquad (4.16)$$

Where A is the optical absorbance, l is the path length of the light, ε is the molar absorptivity, and I_O and I are the incident and the transmitted light, respectively. Materials can have a high absorption at one wavelength and a low absorption at another, because transitions of energy in atoms or molecules are specific to each material (Fowles 1968, Keitz 1971, Nussbaum and Phillips 1976).

Unlike the processes of absorption, the scattering of light need not involve a transition of energy between quantized energy levels in atoms or molecules. Instead it involves a redirection of the light radiation. For particles of sizes small compared to the wavelength of radiation, the scattering of light is described as Rayleigh scattering (described in Chapter 3). This type of scattering is exhibited by all atoms and molecules. If the particles are similar to or relatively large compared to the wavelength of radiation, the scattering of light is known as Mie scattering. In this case, the intensity of the scattered radiation can be related to the concentration of the scattering particles (Milton 1969, Keitz 1971, Bohren and Huffman 1983, Dakin and Culshaw 1989).

The absorption can be specific to a certain material, whereas scattering is not. The common mode intensity variation that may be introduced by scattering may be substantially reduced by employing a two-wavelength detection method (to be described in more detail later).

4.4 Prospects for distributed sensing

Multiplexing methods for optical fibre sensors were introduced in Chapter 3. It was pointed out that the possibility of distributed sensing is a potential feature of intrinsic

optical fibre sensors. Thus the novel intrinsic optical fibre humidity sensor described gives an opportunity to create a unique form of point-source distributed humidity measurement.

In a fibre optic sensor network only a fraction of the optical source power available can be coupled into the optical bus and distributed over the network. Each component, including both the sensor elements themselves and the optical fibres, absorb or divert a certain amount of power (insertion loss), typically between 0.1 dB and a few dB loss. Calculation of the network power budget determines the power margin available at each sensor, and hence the dynamic measurement range. It should be noted that the receiver 'noise floor', and hence the sensor dynamic range, will be a function of the method of signal encoding and the required response speed. The maximum number of sensors that can be operated within the network may be obtained, for a required dynamic measurement range at each sensor.

Commercially available OTDRs have a dynamic range higher than 15dB, for example Hewlett Packard makes OTDRs with link loss range of 34dB. Therefore, more than 10 sensors can be served by a single OTDR incorporated on a single fibre each with a dynamic range of 1.5dB (i.e. the maximum loss that can be caused by the sensor over its entire operating range).

4.5 Summary

A basic design for the sensor has been formulated in this chapter. Several possible options of implementing the sensor were considered. The method selected is such that at the sensing point a length of the cladding is to be removed and replaced by a colorimetric film which gives a measure of humidity The two attractive features of the design are that its potential for low insertion loss which makes it suitable for multi-point

distributed sensing, since optical power is at a premium, and the inherent nature of the design that lends itself to a dual wavelength referencing scheme as was discussed in Chapter 3 section 3.4.1.2. In the next chapter the various elements of the sensor are considered.

CHAPTER 5

Exploratory experiments

5.1 Introduction

The purpose of the work reported in this chapter was to select a suitable immobilising agent and a colorimetric reagent to construct an optical fibre humidity sensor based on the design established in the previous chapter.

To carry out the selection, the following steps were followed:

1. A survey was carried out of the physical and chemical properties of various materials and their suitability as immobilising agents and colorimetric reagents. As a result, a preliminary list of a number of materials was made.

2. Aqueous or organic solvent solutions (depending on the solubility of the raw material) were prepared and thin films were cast on glass plates. Optical and hygroscopic properties were examined.

3. Materials used successfully in step 2 were then used to fabricate thin films impregnated with colorimetric reagents. The samples were placed in an environmental chamber and tested over a range of % RH.

4. Films fabricated successfully on glass plates were then tried on optical fibres and the tests in step 3 were repeated.

5.2 Immobilising agents

A suitable immobilising agent should satisfy the following:

(1) The immobilising agent must be transparent and have a refractive index larger than that of the core of the optical fibre over the full operating range of the sensor.

(2) Both the raw material for making the immobilising film and the colorimetric reagent must be soluble by the same solvent to enable the formation of a homogeneous film.

(3) The immobilising film should entrap the reagent without impeding its sensing capacity.

(4) The pore structure of the film should be sufficiently permeable to allow adequate diffusion of the moisture within a required time scale (see Chapter 2 section 2.4).

There are a large number of water permeable synthetic and non-synthetic materials that might be suitable as immobilising agents for the sensor (Kesting 1971, Van Krevelen 1972, Lemstra and Kleintjens 1989, Briston and Katan 1974, Hench and West 1990, Bhave 1991). However, it has not been the aim of this work to study these materials in detail. This would warrant a research program in its own right. Therefore, three types of immobilising agents were selected for the purpose of this study. These are:

(i) **Cellulose and its derivatives**. Cellulose film, commonly known as cellophane, was the first transparent packaging film (Charrier 1990). It is also known that cellulose absorbs moisture from air even at low humidity (Nevell 1985). A cellulose film has been used to construct an optical pH sensor (Jones and Porter 1989). Cellulose acetate was selected for this study because it is an excellent transmitter of light and its refractive index is 1.47-

1.50, as shown in Table 5.1, which is higher than that of the core of the HCS (Hard Clad Silica) optical fibre used in this work as will be discussed in the next chapter. It also has the highest water vapour transmission rate and the highest ability to absorb moisture amongst popular polymers as shown in Tables 5.2 and 5.3.

(ii) **Gelatin**. It is a well established immobilising agent in photographic films since 1878 (Smith 1929, Eder 1978). Gelatin film photosensitized with ammonium dichromate has been chosen as the best material, so far, for the production of holographic mirrors. It is the only material that can produce holographic mirrors with an efficiency very close to 100%, scattering of less than 1%, high spatial resolution, and durability in the recording (Magariños and Coleman 1985). In recent years, gelatin has become increasingly important because of its potential for use in integrated optical elements (Shih *et al* 1992). It was selected for this work because it has the appropriate value for refractive index and for its ability to absorb moisture at a wide range of relative humidity values as shown in section 5.2.2.

(iii) **Sol-gel of glass**. In this process a porous silica can be produced from a low temperature solution with controllable pore size and refractive (Rabinovich et al 1983, Hench *et al* 1988, Hench and West 1990). This opens the prospect of operating at high temperatures.

5.2.1 Cellulose

Cellulose is a white powder insoluble in water, but can be dissolved by sulphuric acid. It is the main constituent of the structure of plants, which, when extracted, is employed for making paper, plastics, in many combinations. Cellulose is made up of long-chain molecules in which the complex unit $C_6H_{10}O_5$ is repeated as many as 2,000 times. It

consists of glucose molecules with hydroxyl groups for each glucose unit. These OH groups are very reactive, and an almost infinite variety of compounds may be made by grafting to other groups, either repetitively or intermittently (Young and Rowell 1986). Such a reaction occurs with acetic or nitric acids to form cellulose acetate or nitrocellulose. Unlike nitrocellulose, cellulose acetate is a transparent material and non-flammable, and it has better light and heat stability (Brady and Clauser 1992)). Cellulose acetate is water resistant and soluble in acetone (Nevell and Zeronian 1985). It has found applications in lacquers and coatings, moulding plastics and photographic films. Table 5.1 shows the optical properties of cellulose acetate amongst other polymers. Cellulose acetate has the highest ability to absorb water amongst other polymers as shown in Table 5.2. It also has a high permeability to water as shown in Table 5.3.

Table 5. 1 Optical properties of polymers, at 589.3 nm (Brydson 1969, Briston and Katan 1974, Bolton 1989).

Polymer	*Refractive index*	*Transmission %*
Acetal copolymer	1.49	0
Acrylics	1.49	>99
Cellulose acetate	1.46-1.50	>99
Nylon 66	1.45	0
Polycarbonate	1.59	0
Polyethylene, Low density	1.52	45
Polyethylene terephthalate	1.52-1.57	>90
Polymethylepenetene	1.47	99
Polypropylene	1.49	11-46
Polystyrene	1.59-1.60	11-46
Polsulphone	1.63	11-46
Polyvinylchloride (PVC)	1.54	94
Polytetrafluoroethylene	1.32	0

Table 5. 2 Water absorption of the selected polymers (Arnold 1968, Billemeyer 1971, Briston and Katan 1974).

Polymer	*Water absorption, 24 hr, %*
Acrylics	0.2
Cellulose acetate	>1.7
Polyethylene terephthalate	0.07
Polymethylepenetene	0.55
Polyvinylchloride (PVC)	0.5-0.8

Table 5. 3 Water vapour transmission for 25 μm thick films of some plastics at 90%RH and 38°C (Billmeyer 1971, Briston and katan 1974).

Material	*Transmission ($g/m^2/day$)*
Cellulose acetate	100-320
Low density Polyethylene	15-20
High density Polyethylene	5
Cast polypropylene	10-12
Oriented polypropylene	7
Rigid PVC	30-40
Oriented polystyrene	70-150
Regenerated cellulose(MS grade)	5-15
Nylon 11	40-80
EVA	50-60
Ionomer	25-35
Polycarbonate	77-93
Polyester	25-30

From Table 5.1 it can be seen that acrylics, cellulose acetate, polyethylene terephthalate. polymethylepenetene and polyvinylchloride (PVC) all have a high transmittance of light and seem to satisfy the design criteria regarding the refractive index value. Table 5.2 shows water absorption values for these polymers. It is clear from the table that cellulose acetate has the highest ability to absorb water. This is the reason why it was selected for this investigation.

In addition to the polymers mentioned above. There are other cellulose derivatives which are water-soluble, such as HEC (Hydroxyethylcellulose) and HPC (Hydroxypropycellulose), that can be used to make clear hygroscopic films.

Clear, colourless and light-stable (Davidson 1980), films can be made from HEC solutions. Such films have good resistance to many organic solvents but remain permanently water-soluble unless cross-linking additives are added before formation. Other additives can be used to modify other properties such as adhesion to metal, glass, or other surfaces. Raising the pH can also improve adhesion (Davidson 1980). Table 5.4 shows some properties of the HEC films.

Table 5. 4 Some properties of HEC film cast from aqueous solutions (Davidson 1980, Hercules 1994).

General appearance	Transparent
Refractive index (sodium "C" line, 20°C)	1.50-1.51
Equilibrium moisture content at 25°C	
10% RH	1.5-3.0%
45% RH	7.5-10.0%
65% RH	18-19.5%
90% RH	25-28%

Aqueous or organic solvent solutions of HPC can produce clear hygroscopic films. Films may be prepared by thermoforming procedures. Typical properties of thin film cast from water solutions are given in the Table 5.5 below.

Table 5. 5 Typical Properties of HPC Film (Davidson 1980, Hercules 1994).

Appearance	Clear
Refractive index	1.559
Moisture content (equilibrium) at 23°C and	
50% RH	4%
84% RH	12%
Solubility	
Water below 40°C	Soluble
Water above 45°C	Insoluble

The above cellulose based films satisfy the criteria stated at the beginning of this section. However, HEC and HPC films are prepared from an aqueous solution while cellulose acetate is from an acetone-based solution. In addition, as shown in the next section, gelatin films are prepared from aqueous solution and have higher moisture absorption ability than both HEC and HPC films. Therefore gelatin was chosen to represent water soluble materials. Cellulose acetate is insoluble in water and sensitive to moisture absorption at various values of relative humidity (Briston and Katan 1974) and was therefore selected for the exploratory experiments.

5.2.2 Gelatin

Gelatin is a colourless to yellowish colloidal hemicellulose which is water-soluble and can be made insoluble by chemical processing (Kenchington and Lauder 1958, Tachibana et al 1958). Gelatin has an ionic or hydrogen bonding in which the molecules are brought together into larger aggregates, and it sets to a rigid glass film with very little absorption and optical scattering (Saunders and Ward 1958, Mason 1975).

Gelatin has two extraordinary microstructural morphologies: (1) Two dimensional network-molecules are partially aligned and cross-linked with interchain hydrogen bonds to form a helical collagen-like sheet; (2) Thermoplastic, gelatin in this form can be readily transformed into a highly cross-linked and insoluble polymer using heat or UV radiation curing (Ho et al 1992).

Gelatin is obtained from bones or from skins and used as a dispersing agent, sizing medium, coating for photographic films, and stabiliser for foodstuffs and pharmaceutical preparations. In recent years, gelatin has become increasingly important because of its potential for use in integrated optical elements such as lenses, grating, couplers, multiplexed gratings and optical interconnects (Ho et al 1992).

Dried films can be prepared from the solution state by high temperature drying and from the gel state by low temperature drying. The hot dried films gave an amorphous diagram (noncrystallizing) whereas the cold dried films gave a recognisable diagram (crystallizing) (Ward 1955). The presence of crystalline regions tends to reduce the level of light transmission (Charrier 1990). The gelatin film changes dimension with relative humidity variations (Arnold and Rolls 1971).

Gelatin possesses no definite melting point, but begins to soften at about 140^{o}C (Smith 1929). The variation of the moisture content of a gelatin film with relative humidity is shown in Fig. 3. Data were extracted from (Ward and Courts 1977). Although data found in the literature, for the variation of gelatin moisture content with relative humidity vary, data presented here acts as a good indicator. Comparing the moisture absorption stated above for HEC and HPC films and the values for gelatin in Fig. 5.1. Gelatin is a better absorber of moisture than both films. Therefore gelatin was selected here.

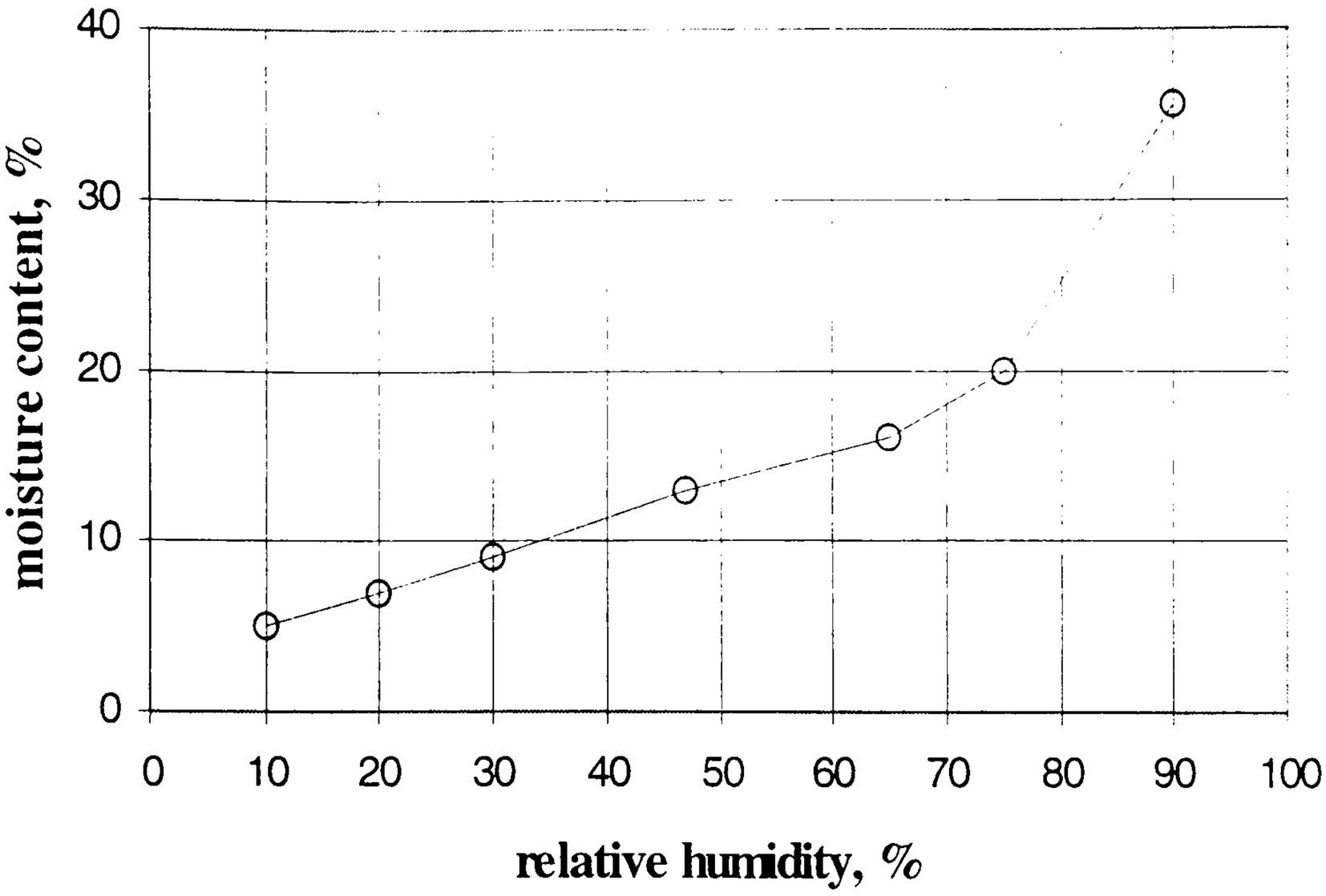

Figure 5. 1 Variation of gelatin moisture content with relative humidity at 25 °C

5.2.3 Sol-Gel process

Interest in the sol-gel processing of inorganic ceramic and glass materials began as early as mid-1800s. Early investigators observed that hydrolysis of tetraethyl orthosilicate (TEOS), $Si(OC_2H_5)_4$ under acidic conditions yielded SiO_2 in the form of a glass-like material. Extremely long drying times of 1 year or more were necessary to avoid the silica gels fracturing into fine powder and consequently there was little technological interest. At present, drying of monolithic silica optics can be achieved in hours or days (Hench and West 1990). To prevent fracture during drying, it is essential to control the chemistry of each step of the sol-gel process carefully. Materials prepared by the sol-gel process can be divided into three main categories, bulk glass, coating and fibres.

There are a number of different types of precursor materials that can be used. All should be soluble in organic solvents and easily converted to the relevant oxide preferably by hydrolysis but alternatively by chemical reaction or thermal or oxidative decomposition.

The simplest method of preparation involves making a solution of all the components as metal alkoxides precursors in a suitable organic solvent and then reacting the solution with water to form the oxide mix (Thomas 1987). Alkoxide salts and other methods can also be used. All metal alkoxides, except the alkoxides of silicon and phosphorous, are rapidly hydrolyzed to the corresponding hydroxide or oxide. Silicon alkoxides require an acid or basic catalyst for hydrolysis (Thomas 1987).

Thin glassy films have been made with refractive index 1.4-2.0 with various degrees of porosity (Stewart and Johnstone 1996). These films are characterised by their high transparency and chemical durability. The basis for the sol-gel coating process is the hydrolysis of metal compounds in alcoholic solutions. They are converted into oxides by hydrolysis and polycondensation during and after contact of the substrate with the coating solution. From a practical view, the reaction rate for the hydrolysis and condensation for the gel formation should be higher than the crystallisation rate from the solution, in order to obtain uniform, transparent coatings. For this reason alkoxides are preferred. A single oxide layer such as SiO_2 with refractive index ≤ 1.45 (depending on porosity) or with TiO_2 with refractive index ≤ 2.2 can be used. A combination of the two gives a choice of refractive index range 1.28 to 2.2. Good film adhesion to surface has been observed (Dislich 1987).

Sol-gel processing involves hydrolization and polymerization steps. Although polymerization products, reaction rates, and the effects of pH or different additives on these rates may be experimentally obtainable, the actual mechanisms of polymerization are not fully understood and can only be conjectured from experimental results (Garofalini 1987).

The general method for the preparation of an alkoxide derived silica is as follows: -

1. **Mixing**. A liquid alkoxide precursor, such as $Si(OR)_4$, where R is CH_3, C_2H_5 or C_3H_7 is diluted in ethanol.

2. Adding water (acid or base) to effect hydrolysis and condensation.

3. Mixing for a set time under defined conditions. If required, a reagent can be added at this stage.

4. **Casting**. Since the sol is a low-viscosity liquid it can be cast into a mould.

5. **Gelation**. With time the colloidal particles and condensed silica species link together to become a three-dimensional network. The physical characteristics of the gel network depend upon the size of the particles and the extent of cross-linking prior to gelation. At gelation, the viscosity increases sharply, and a solid object results in the shape of the mould. With appropriate control of the time-dependent change of viscosity of the sol, fibres can be pulled or spun and coating can be applied as gelation occurs.

6. **Ageing**. Ageing of a gel involves maintaining the cast object for a period of time, hours to days, completely immersed in liquid. During ageing, polycondensation continues along localised solution and reprecipitation of the gel network, which increases with ageing. An aged gel must develop sufficient strength to resist cracking during drying.

7. **Drying**. During drying the liquid is removed from the interconnected pore network. Large capillary stresses can develop during drying when the pores are small (< 20nm). These stresses will cause the gels to crack catastrophically unless the drying process is controlled by decreasing the liquid surface energy by obtaining monodisperse pore sizes by controlling the rates of hydrolysis and condensation.

8. **Dehydration or chemical stabilisation**. The removal of surface silanol (Si-OH) bonds from the pore network results in a chemically stable ultraporous solid. Porous gel-silica made in this manner is optically transparent with interconnected porosity and has sufficient strength to be used as unique optical components when impregnated with optically active polymer such as fluors, wavelength shifters. dyes, or non-linear polymers (Hench *et al* 1988, 1989)

9. **Densification**. Pores may be eliminated by heating at high temperatures.

The porous gel-silica is transparent because the pores have a very small radius of 1.2 nm and do not scatter visible light. There is very little change in the size of the interconnected pores for temperatures from 200 °C to 900 °C. But the number of pores decreases depending upon the heat treatment. Consequently the specific surface area of the material varies from 770 m^2/g at 200 °C to 290 m^2/g at 900 °C and down to about 10 m^2/g at 950 °C (Hench 1988). Reported refractive index of porous silica is over the range 1.28 to 1.45 (Hench 1988, Ramaswany et al 1988).

Porous silica produced by the sol-gel process is characterised by its high transparency and chemical durability. Their microstructure can be modified by several factors during the fabrication process, and they also offer the prospect of working at high temperatures. Porous sol-gel glass has been used as an immobilising agent in a number of optical fibre sensors (Boisdé and Harmer 1996). For these reasons porous sol-gel glass has been chosen for this work.

5.3 Aging

Aging is an important factor that should be considered when selecting polymeric immobilising agents. The selected films above are known for their long-term stability (Brady and Clauser 1992) but no quantitative evaluation could be found.

The physical and chemical structure and macroscopic properties of polymers change during processing, storage and use. This change, commonly referred to as ageing, is evidently a very complex process involving chemical reactions, physical structural changes and changes in properties of the material (Hedvig 1977). Prolonged exposure to light may bring about many undesirable effects in certain films. In particular, light may catalyse certain other reactions such as oxidation. Brittleness, loss of clarity, colour changes and surface imperfections are some of the undesirable effects. If a film is intended for applications involving continued use in sunlight it should contain stabilisers such as ultra-violet absorbers (Briston and Katan 1974).

Although, as mentioned earlier, there are a large number of synthetic and non-synthetic films that might be suitable as immobilising agents. Only few can be considered here for the purpose of this study. Therefore, three types of films were selected based on the arguments presented in the previous sections. These were:

1. Cellulose acetate.
2. Gelatin.
3. Sol-gel.

Evaluation of these immobilising agents is carried out in section 5.5 later in this chapter.

5.4 Colorimetric reagents

A number of hygroscopic materials change colour as they interact with water molecules. A list of these materials is shown in Table. 5.6. This list is not claimed to be exhaustive but every effort was made to include as many materials as possible.

Table 5. 6 Hygroscopic materials that change colour as they interact with water.

Material	*Dry colour*	*Wet colour*
Aluminium Iodide (AlI_3)	brown	white
Calcium Chlorate $(CaClO_3)_2$	white	yellow
Vanadium Chloride (VCl_2)	light green	yellow
Copper Chloride ($CuCl_2$)	brown-yellow	black-green
Copper Fluoride (CuF_2)	white	blue
Lanthanum Sulfate $(La_2(SO_4)_3)$	white	colourless
Cobalt Iodide (CoI_2) to	black	red-brown
Cobalt Chloride ($CoCl_2$)	Blue	pink
Titanium (III) Bromide ($TiBr_3$)	grey-black	red-violet

Cobalt Chloride is considered here since it is a well established humidity indicator, as already discussed in Chapters 2 section 2.4. Copper chloride ($CuCl_2$) and vanadium chloride (VCl_2) are also considered. All three salts are water and acetone soluble (Perry 1984, Dean 1990)

5.5 Experimental evaluation

In section 5.2, the desirable properties of an ideal immobilising agent were stated. Possible materials for use as immobilising agents were considered. After some discussion, a short list of three types of immobilising agents was formed. Also in section 5.4 above a number of reagents were considered. Again three reagents were also selected.

In this section few experiments were carried out in order to examine the suitability of these agents and immobilising agents for the fabrication of the sensor sought.

5.5.1 Cellulose acetate film fabrication and testing

In this section the steps taken to establish a procedure to make transparent cellulose acetate films are stated. Measurement of refractive index and its variation with relative humidity and simple transparency tests are also covered.

The following steps were carried out: -

1. A homogeneous acetone solution of cellulose acetate was prepared as follows. 20 ml of acetone was placed in a small beaker. Cellulose acetate powder (supplied by SIGMA Chemical Company Ltd catalogue no. C3782) was gradually added to the beaker while stirring. The solution was mixed until a uniform transparent solution was achieved. Powder continued to be added until it wasn't possible to stir efficiently to form a homogeneous and bubble free solution. The limit was found to be about 2 g in 20 ml of acetone.

2. A sample of the mixture about 2 mm deep was placed in a glass container and left to dry. A thick film, with some opaque white patches, was formed. After some investigations it was discovered that this was due to the presence of water in the solution. This was confirmed by the appearance of more white patches as some water was added to the solution.

3. The above procedure was repeated, but this time some molecular sieves were placed in acetone for several hours, which absorbed water, before it was mixed with the cellulose acetate. The result was that a transparent film was produced. Transparency at this stage was examined by the naked eye. A more quantitative method was left to a later stage when appropriate.

4. The dry film retained its transparency after being momentarily immersed in water and then left to dry in ambient air. This was repeated several times.

5. A sample of the above solution was applied onto a clean glass plate (microscope slides). When dried, a thin film with some opaque white patches was formed. This was believed to be due to the presence of moisture in the air, as mentioned above.

6. To remedy this problem, a simple chamber was constructed. It was filled with dry silica gel to absorb the moisture from the air. The chamber was then saturated with acetone vapour to reduce the moisture in contact with the sample.

7. Step 6 was repeated in the chamber and a strong (strong here means that handling did not damage it) transparent film was formed. The film retained it transparency when subjected to several cycles of immersing in water and drying.

8. The mixture was then applied to the core of a 600 μm diameter core HCS fibre inside the chamber. The cladding of the fibre was removed prior coating, see next chapter. A partially transparent coating was achieved. This was believed to be due to the presence of moisture in the chamber. It had more effect because the film on the fibre dried much more rapidly, i.e. a higher relative surface area was exposed, than that on the glass plates. Several mixing ratios (by gradually increasing the concentration of cellulose acetate) were tried with limited success. Although it was felt that with more care better results could be achieved, further work was deferred at this stage.

5.5.1.1 Refractive index measurement

As mentioned earlier in Chapter 4 section 4.2 and section 5.2 of this chapter, one of the requirements of the properties of the immobilising film is that its refractive index must

be equal to or higher than that of the core of the optical fibre over the full operating range. To establish this the following experiments were carried out.

The refractive index of the cellulose acetate film was measured using a high accuracy Abbé refractometer (Bellingham and Stanley Model 60/ED). This instrument is capable of measuring refractive index to within $\pm$0.00004 as specified by the manufacturer. The basic configuration of the instrument is shown in Fig.5.2. The instrument employs the critical angle effect marked by a demarcation line between light and dark portions of the telescope field (Bellingham and Stanley 1992).

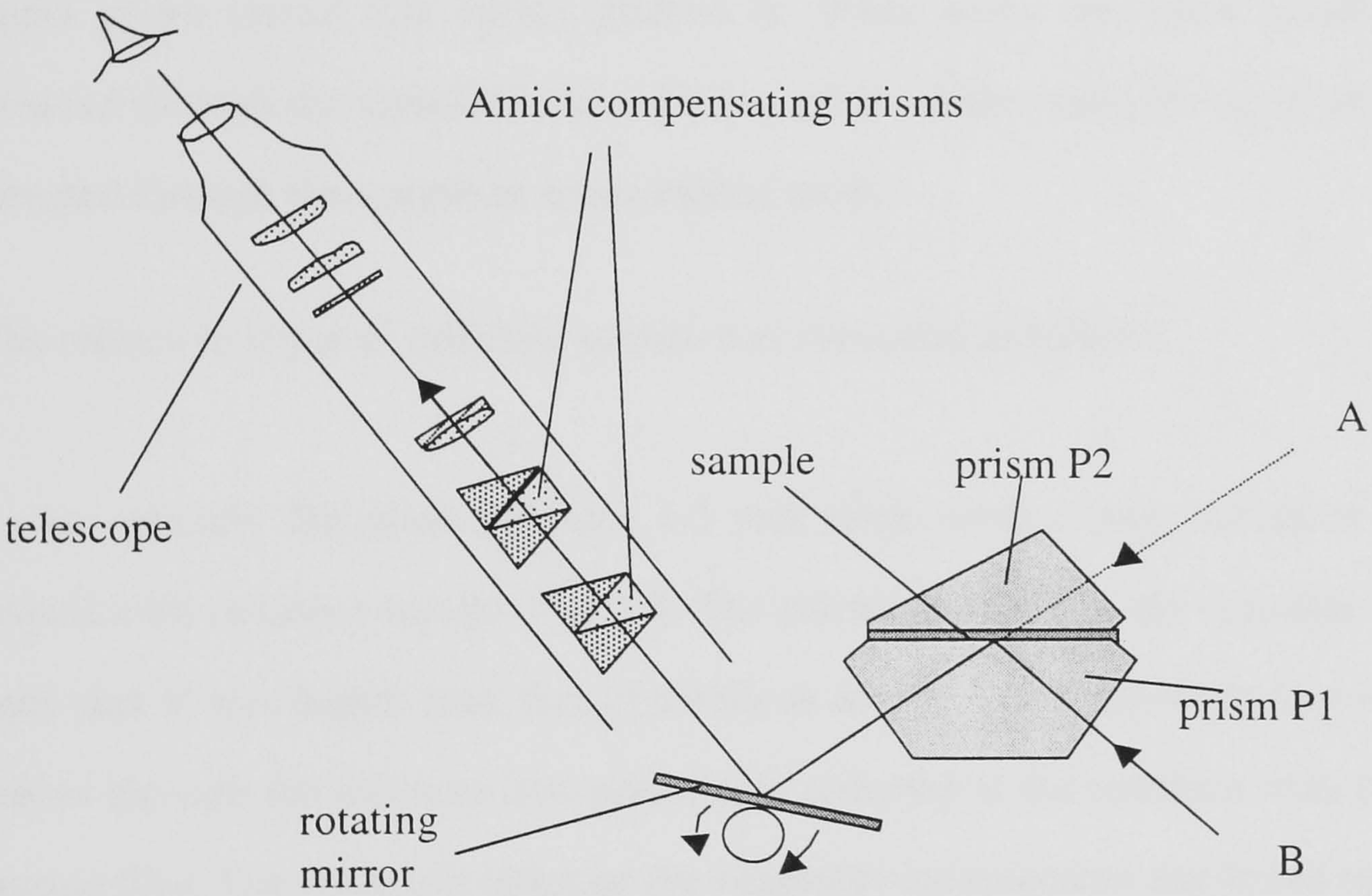

Figure 5. 2 Basic components of Abbé refractometer.

In the classical form of the Abbé refractometer, as shown in Fig. 5.2, the essential components are: - a pair of prisms one being a measuring prism and the second being used for illumination, and a simple inverting telescope in front of which is placed a pair of counter rotating Amici prisms. The two prisms P1 & P2 are made from glass with refractive index > 1.74. The illuminating prism, P2, is housed in a hinged prism box. The two prisms, when brought together, enclose a thin film of the liquid being

measured. When a solid is being measured prism P2 is left open and the solid is placed on the measuring prism with a contact liquid of high refractive index placed in between. The measuring prism and the telescope are rigidly mounted. The rotating mirror is rotated to pick up the critical-angle boundary.

The position of the rotating mirror is read off a micrometer drum. The corresponding refractive index is then found using a computer program, supplied by the manufacturer. A sodium lamp must be positioned directly in front of the instrument. Either by letting the light through the lower window (shutter open), marked B in Fig 5.2, or through the upper prism (metal flap open), marked A. When using the lower window, light is directed through the sample in the reflective mode. When using the upper prism, light is directed through the sample in a transmitted mode.

The refractive index of cellulose acetate was measured as follows:

1. An optically flat glass substrate 1.5 mm thick, with a high refractive index, was coated with cellulose acetate, Fig. 5.3. The refractive index of the substrate was chosen such that it was higher than that of cellulose acetate. This was necessary so that light passes through the substrate and gets totally reflected at the interface with the cellulose acetate film. The refractive index of the substrate was measured and found to be 1.73.

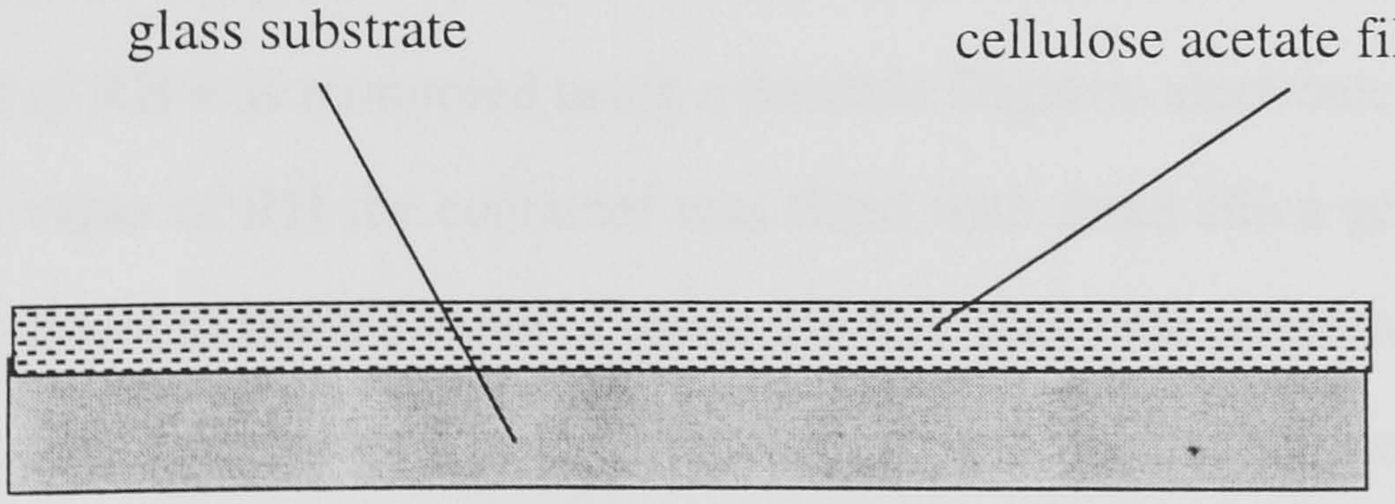

Figure 5. 3 A high refractive index glass substrate coated with a cellulose acetate film.

2. Prism P2 was moved out of the way. The slide, with the coated slide uppermost, was placed on the measuring prism P1. A contact liquid with higher refractive index was used to form good optical contact between P1 and the glass substrate.

3. Two demarcation lines were found, one corresponded to the refractive index of the glass substrate and the other to the cellulose acetate film. The reading of the rotating drum that corresponded to cellulose acetate was noted. Using the computer program supplied by the manufacturer, the corresponding refractive index of the cellulose acetate could be found.

5.5.1.2 Variation of refractive index with humidity

As mentioned earlier in Chapter 4 section 4.2, one of the requirements is that the refractive index of the immobilising film must be higher than that of the core of the optical fibre over the full operating range. The moisture content of the cellulose film increases with increasing RH. This causes the refractive index of the film to decrease since the refractive index of water is 1.33, i.e. lower than that of the film.

To measure the variation of the refractive index of the film with RH, the arrangement shown in Fig. 5.4 was constructed. With the container in the enclosure filled with water, the relative humidity rose slowly to reach a value close to 100% RH in about 2 hours. The value of RH was monitored using a portable Digitron electronic humidity meter. To get a low value of RH the container was filled with dried silica gels and again it took about two hours to reach a value of about 2% RH. Since the refractive index of cellulose acetate is well documented in the literature, it was decided to measure the refractive index at a high humidity level, which corresponds to the lowest refractive index.

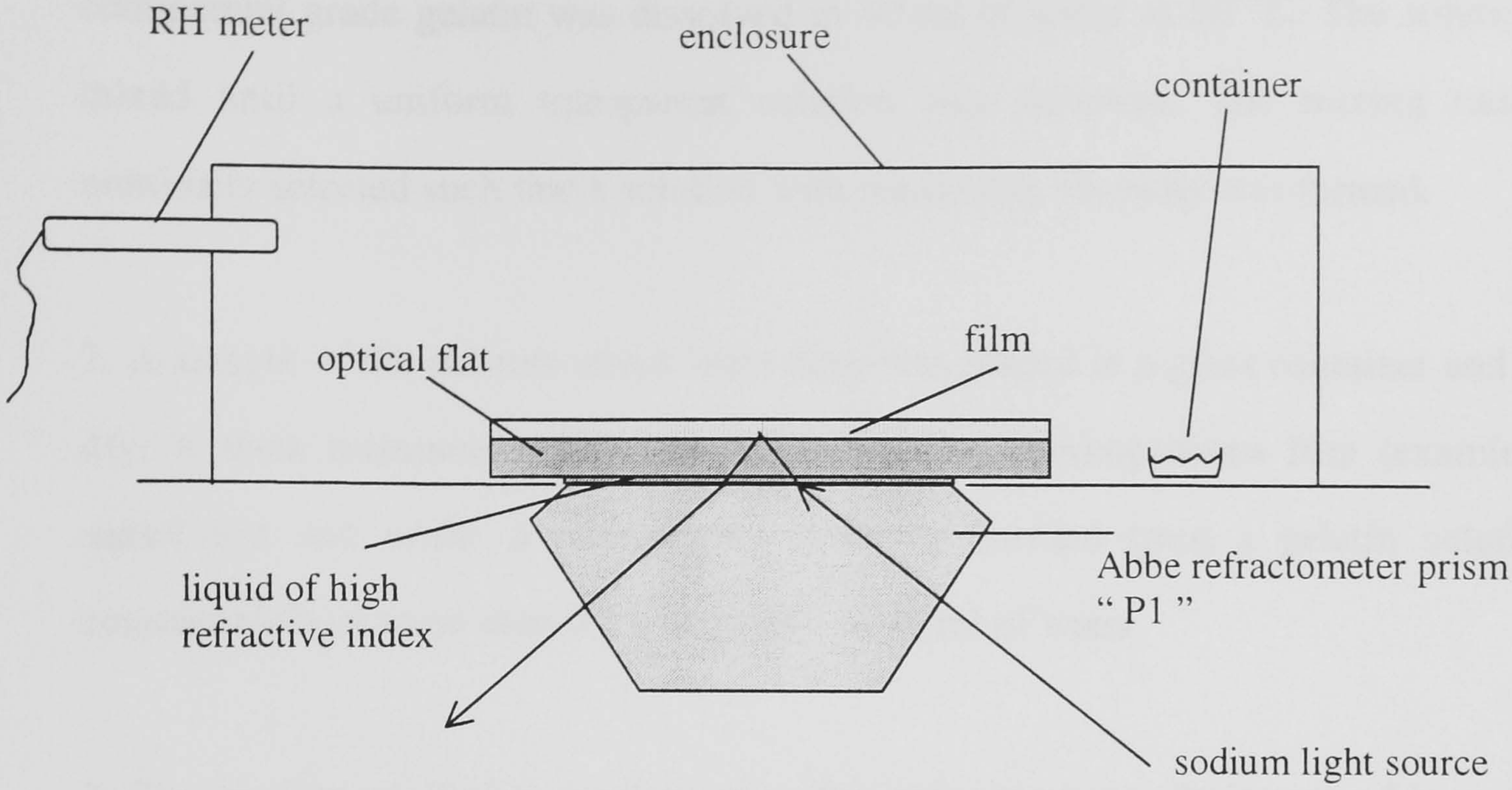

Figure 5. 4 Experimental set-up in conjunction with Abbe refractometer to measure the variation of a film refractive index with RH.

Using the above arrangement the refractive index of the cellulose acetate film was found to be 1.469 ± 0.001 at 19.1 ^{o}C and 95.7% RH. This clearly satisfies the requirement that the refractive index of the immobilising film must be higher than that of the core of the optical fibre (1.453) over the full operating range, as stated in section 4.2 Chapter 4.

5.5.2 Gelatin film fabrication and testing

In this section the steps taken to establish a procedure to make transparent gelatin films are stated. Measurement of refractive index and its variation with relative humidity and simple transparency tests are also covered.

The following set of experiments were carried out:

1. A homogeneous aqueous solution of gelatin was prepared as follows. 1.5g of Boots commercial grade gelatin was dissolved in 40 ml of water at 80 ^{o}C. The solution was mixed until a uniform transparent solution was achieved. The mixing ratio was nominally selected such that a solution with reasonable viscosity was formed.

2. A sample of the mixture about 2mm deep was placed in a glass container and left to dry. A thick transparent film was produced. Clear homogeneous film (examined by naked eye and under a microscope) could be formed from a gelatin solution of concentration of more than 0.5 g of gelatin in 40 ml of water.

3. The dry film retained its transparency after being momentarily immersed in water and then left to dry, in ambient air, several times.

4. A sample of the above solution was applied onto a clean glass plate to form a transparent film. The film retained it transparency after being momentarily immersed in water and then left to dry, in ambient air. This was repeated several times.

5. Thin films were successfully coated onto the cores of 200, 400 and 600 μm core fibres. The cladding of the fibre was removed prior coating, see Chapter 6 section 6.3 for detail. The coated fibres were exposed to 0 to 100% of relative humidity values in an environmental chamber. The spectra of white light, as expected, showed no variation with relative humidity.

5.5.2.1 Variation of refractive index with humidity

Using the arrangement described in section 5.5.1.2 above the refractive index of gelatin was measured at 29.5% RH and 25.2°C (ambient condition at the time of the experiment) and at 96% RH at the same temperature. The refractive index was found to be 1.538 and 1.500 respectively. This clearly satisfies the requirement that the refractive

index of the immobilising film must be higher than that of the core of the optical fibre over the full operating range.

5.5.3 Sol-Gel fabrication and testing

In this section the method followed to produce porous silica is detailed. Measurement of refractive index and its variation with relative humidity and simple transparency tests are also covered.

The method of fabrication is as fellows: -

Materials used:

1. Tetraethyl orthosilicate (TEOS) $Si(OC_2H_5)_4$.
2. Hydrochloric acid HCl.
3. Distilled water.
4. Ethanol.

Method

1. TEOS and Alcohol were mixed in a sealed container for 60 minutes.
2. HCl was added to some distilled water to obtain a pH value of 2.
3. The resulting acid water was added to the solution and stirred for 10 minutes.
4. The solution was left standing in a sealed container for one to seven days (depending on the mixing ratios).
5. Coating was applied to microscopic slides by dip coating. Successful coating was produced.
6. Also thick films (0.5mm thick) were prepared by casting.

The mixing ratios tried are tabulated in the table below:

Table 5. 7 Mixing ratios of Sol-Gel solution.

Sample No.	*TEOS*	*H2O (pH=2)*	*Alcohol*
A	2	4	10
B	2.5	4	10
C	3	4	10
D	3.5	4	10
E	4	4	10

For a week old sample A, the mixture retained very low viscosity and could be cast to any shape. In the extreme, sample E, the solution turned into a solid gel in less than 24 hours i.e. it could not be reshaped. All samples, if left to dry, solidified into lumps of pure silica.

5.5.3.1 Measurement of refractive index

Using the arrangement shown in Fig. 5.4 and described in section 5.5.1.2 above the refractive index of the porous silica was measured at 50% RH and 24.5 ^{o}C (ambient condition at the time of the experiment). The piece of porous silica used in this experiment was prepared from sample D shown in Table 5.7 above. The refractive index was found to be 1.3478. The value is expected to be in the range 1.28-1.45 as reported in the literature. This clearly does not satisfy the requirement that the refractive index of the immobilising film must be higher than that of the core of the optical fibre over the full operating range. However, it is expected that with the reagent embedded in the porous silica film, the total refractive index would increase. These tests are carried out in the next section.

5.5.4 Tests on colorimetric reagents

Having done the initial tests on immobilising agents, it was felt sensible to test the colorimetric reagents in conjunction with the immobilising agents. Essentially two aspects were examined: -

1. The response of the colorimetric reagent, within the immobilising agent, to relative humidity.
2. The variation of refractive index, of the resulting film, with relative humidity.

5.5.4.1 Measurement of refractive index of cobalt chloride ($CoCl_2$)

The refractive index of cobalt chloride was not readily available in the literature. Therefore it was measured using the Abbé refractometer. Cobalt chloride was supplied in the form of fine powder. To measure its refractive index it had to be dissolved in a suitable solvent (water was used here). The refractive index of the resulting solution was measured at different concentrations. Results obtained are plotted as shown in Fig. 5.5. It can be seen from the graph that the relationship between the refractive index of the solution and the concentration of cobalt chloride is a straight line. The equation of the straight line is given by: -

$$y = 0.2712x + 1.3327 \qquad (1.1)$$

where y = refractive index of solution

x = concentration of cobalt chloride.

For 100% concentration i.e. $x = 1$, $y = 1.6039$. This is the value of the refractive index corresponding to 100% concentration i.e. pure cobalt chloride.

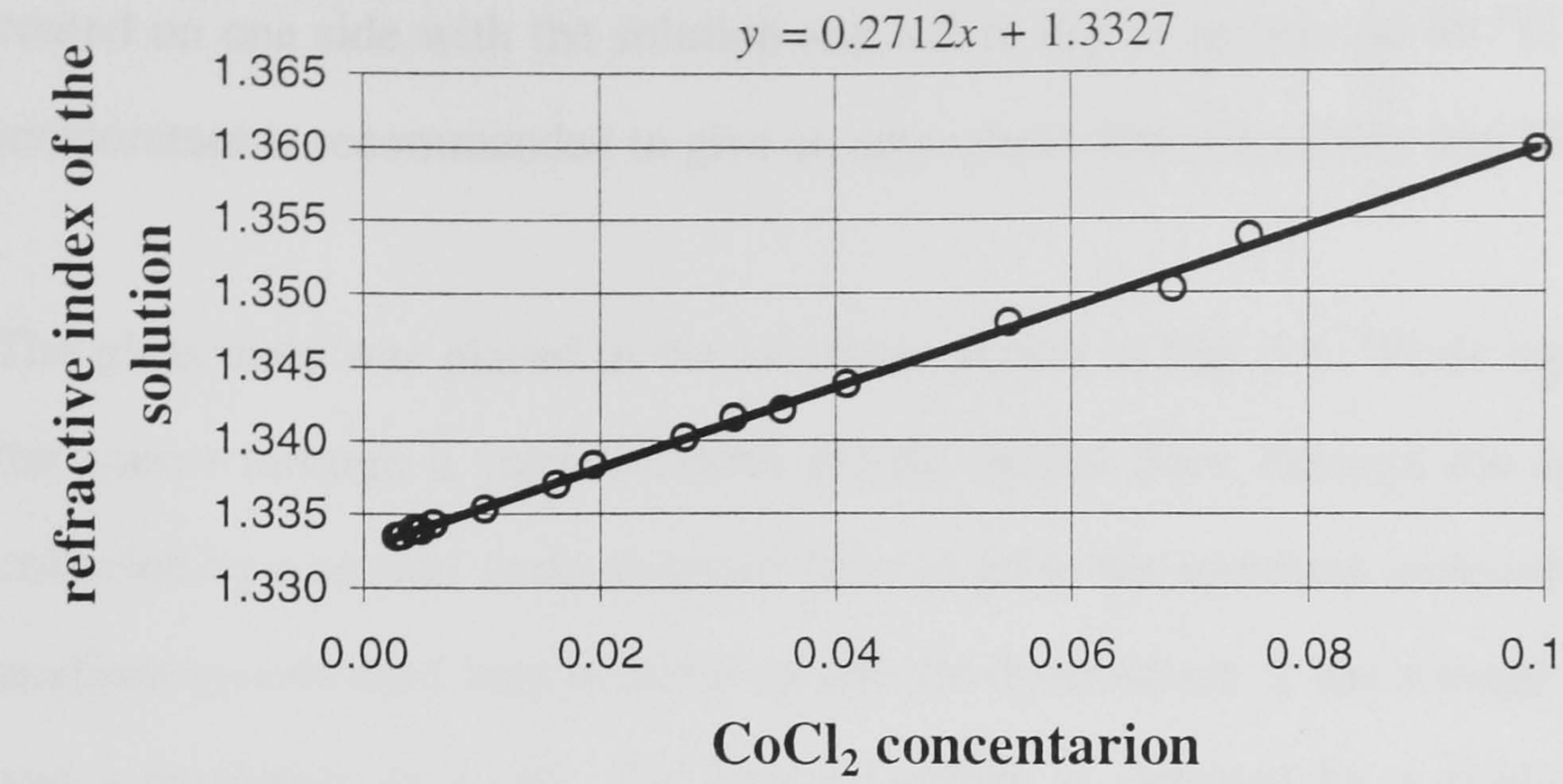

Figure 5. 5 Refractive index of the aqueous solution versus cobalt chloride concentration.

5.5.4.2 Spectral response of colorimetric reagents, within the gelatin film, to relative humidity

As mentioned in section 5.4 three colorimetric reagents were selected for this investigation. These were cobalt chloride ($CoCl_2$), copper chloride ($CuCl_2$) and vanadium chloride (VCl_2). All three salts are water and acetone soluble. A simple set-up was constructed to perform preliminary tests to establish how the films responded to relative humidity variations. Following these initial tests more detailed tests were carried out in the next chapter. Tests were carried out first with cobalt chloride and repeated for the other two salts.

An aqueous solution of cobalt chloride was prepared, consisting of 1.5 g salt, 1.5 g gelatin and 40 ml of water. This ratio was nominally selected for two reason; 1. The resulting solution was of reasonable viscosity 2. A change of colour of the film was clearly visible when relative humidity varied. A glass plate (microscope slide) was

coated on one side with the solution and left to dry in an oven at 50 °C. Drying at this temperature is recommended to give an amorphous film (Bradbury and Martin 1952).

The glass plate was placed in the assembly shown in Fig. 5.6. White light travels from the source through a 1mm diameter plastic optical fibre, through the sample and was collected by a second 1mm diameter fibre to go to the spectrum analyser. The spectrum analyser system used here is based on a Rofin Spectraliser. It has a range of 400-950 nm and a resolution of ±1nm. The spectral output is detected by a photomultiplier tube (PMT), fed to a microcomputer based system and displayed on a monitor. For later experiments an Anritsu spectrum analyser (model MS99A) was used.

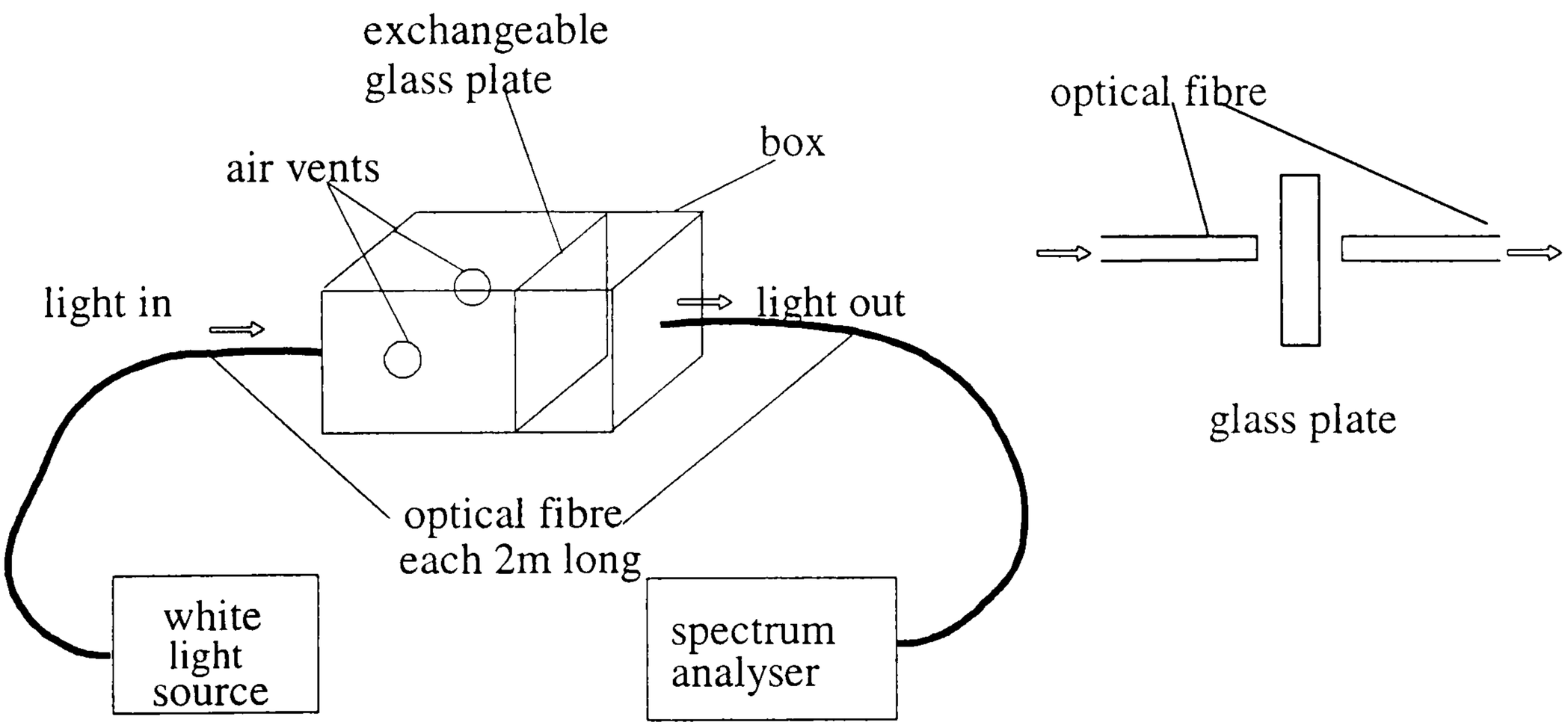

Figure 5. 6 Test assembly.

The test assembly was placed in the environmental chamber (a detailed description of the environmental chamber is given in the last section of this chapter) in which the air in the chamber was sampled by two vents in the assembly. While keeping the temperature constant, the relative humidity in the chamber was varied and the spectrum of the collected light was obtained using the spectrum analyser. A plot of the spectrum at two different humidities was obtained. The two values of RH selected, 20 and 70% RH,

because they clearly illustrate the change in the spectra. Typical results are shown in Fig 5.2. It can be seen that the spectra are modulated by humidity only in the visible region.

The above experiments were repeated for the other two salts, $CuCl_2$ and VCl_3. No change in the spectra was detected over the range 0 to 80% RH. Concentration was increased to saturation level with no noticeable change. However, in both cases, changes in spectra occurred when the film was completely immersed in water. Therefore, no further work was done on these two salts.

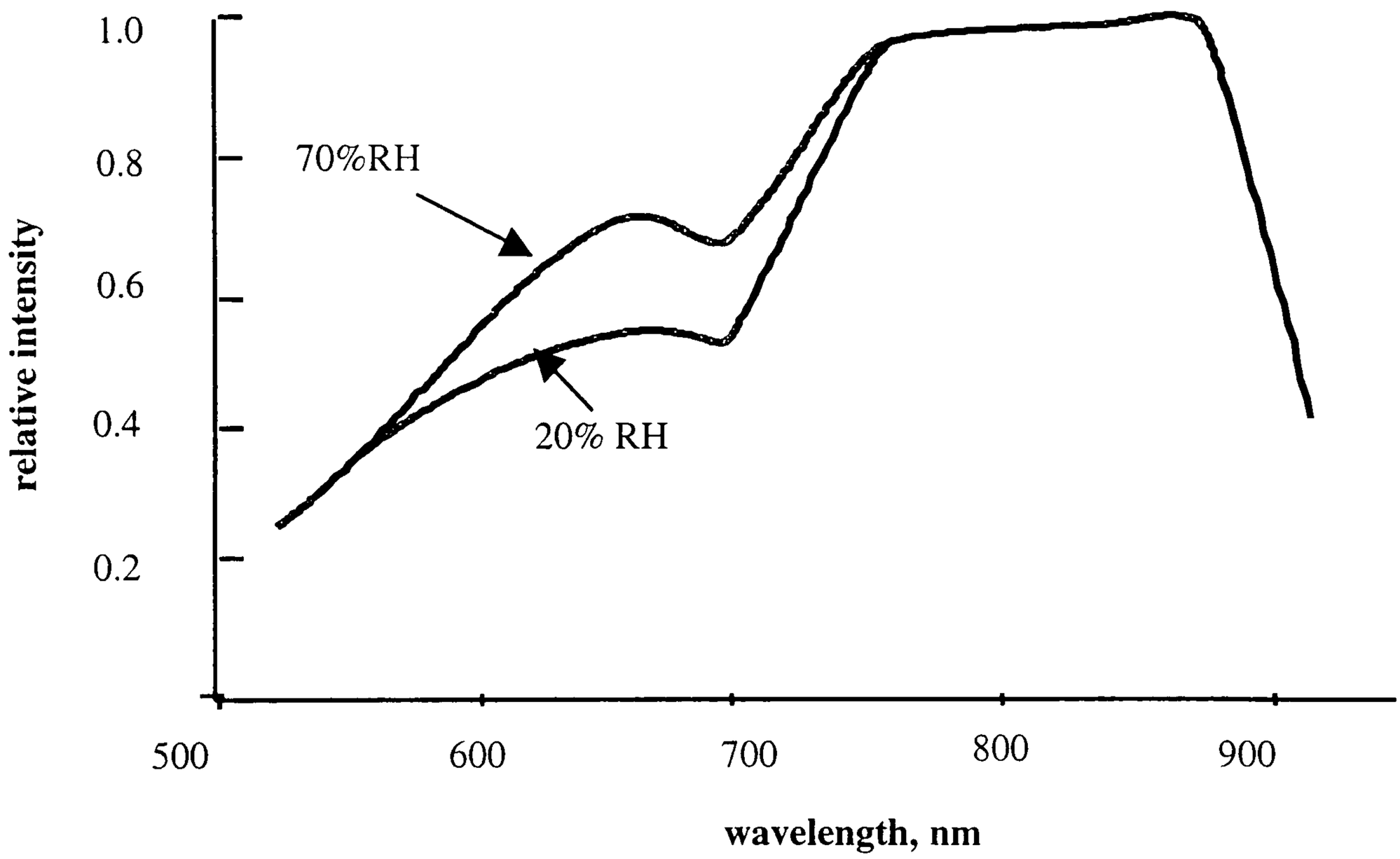

Figure 5. 7 White light spectra for cobalt chloride embedded in a thin film at different % RH.

5.5.4.3 Variation of the refractive index of cobalt chloride/gelatin film with relative humidity

The variation of refractive index of cobalt chloride/gelatin film with relative humidity, at different mixing ratios, was examined here. This was to ensure that the design criteria are met over the full operating range.

Using the arrangement shown in Fig.5.4, the container shown was filled with water. This caused the RH to increase slowly from ambient to a value approaching 100%. The refractive index of the film was measured using the Abbé refractometer and the corresponding relative humidity reading was recorded at regular intervals. Results obtained are plotted in Fig. 5.8 for mixing ratio of 2 g gelatin, 4 g cobalt chloride in 50ml of water.

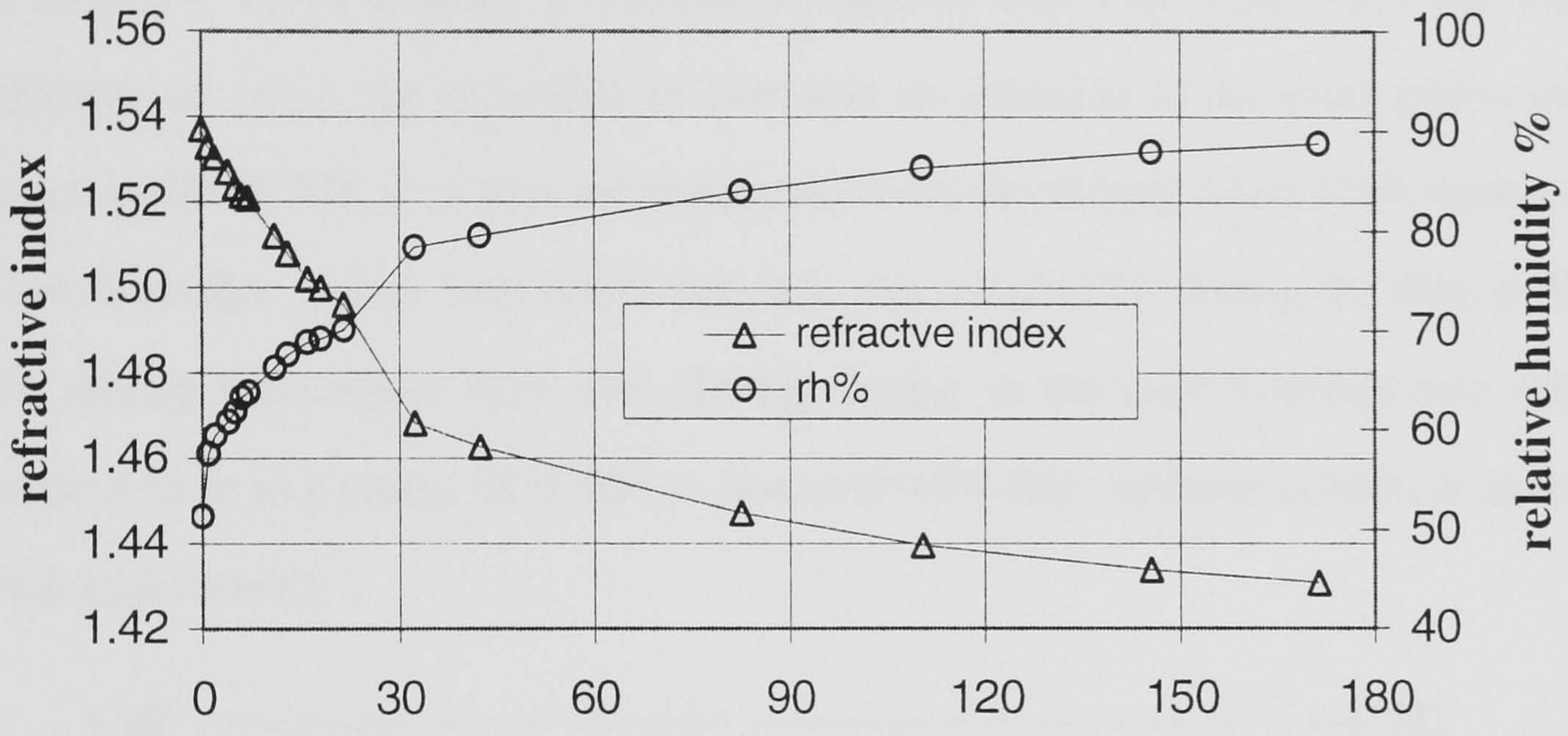

Figure 5. 8 Refractive index variation with slowly increasing relative humidity for a mixing ratio of 2g gelatin, 4 g cobalt chloride in 50 ml of water.

The intermediate values of relative humidity are only approximate. This is because the relative humidity was continuously increasing and the film used was thick hence a relatively long period was required to reach moisture equilibrium level. However, the initial and final values were accurate and gave true values since sufficient time was allowed for equilibrium to occur. This applied to all measurements taken by this arrangement throughout this chapter.

From the graph shown in Fig.5.8 it can be seen that the refractive index of the film is close to 1.54 at 45% RH (ambient) and about 1.43 at 88 % RH. This clearly shows that,

at high humidity, the refractive index is lower than that of the core. This doesn't satisfy the design criteria mentioned earlier.

Now the water container was replaced by one filled with dried silica gel. This caused the relative humidity to gradually decrease. The refractive index was measured and noted at regular intervals. The results are plotted in Fig. 5.9. It can be seen from the graph that the refractive index reached a maximum value of just over 1.56. This test was also performed to check the reversibly of film and its adhesion to the glass plates over the range 0 to 100% RH. In some circumstances cracks developed when films were exposed to low humidity. It was later found that this was avoided by drying the film at 50°C to 60°C during fabrication. Note that, during drying, at the start humidity was suddenly switched from just under 90 % RH to just over 40% RH (ambient condition at the time of the experiment).

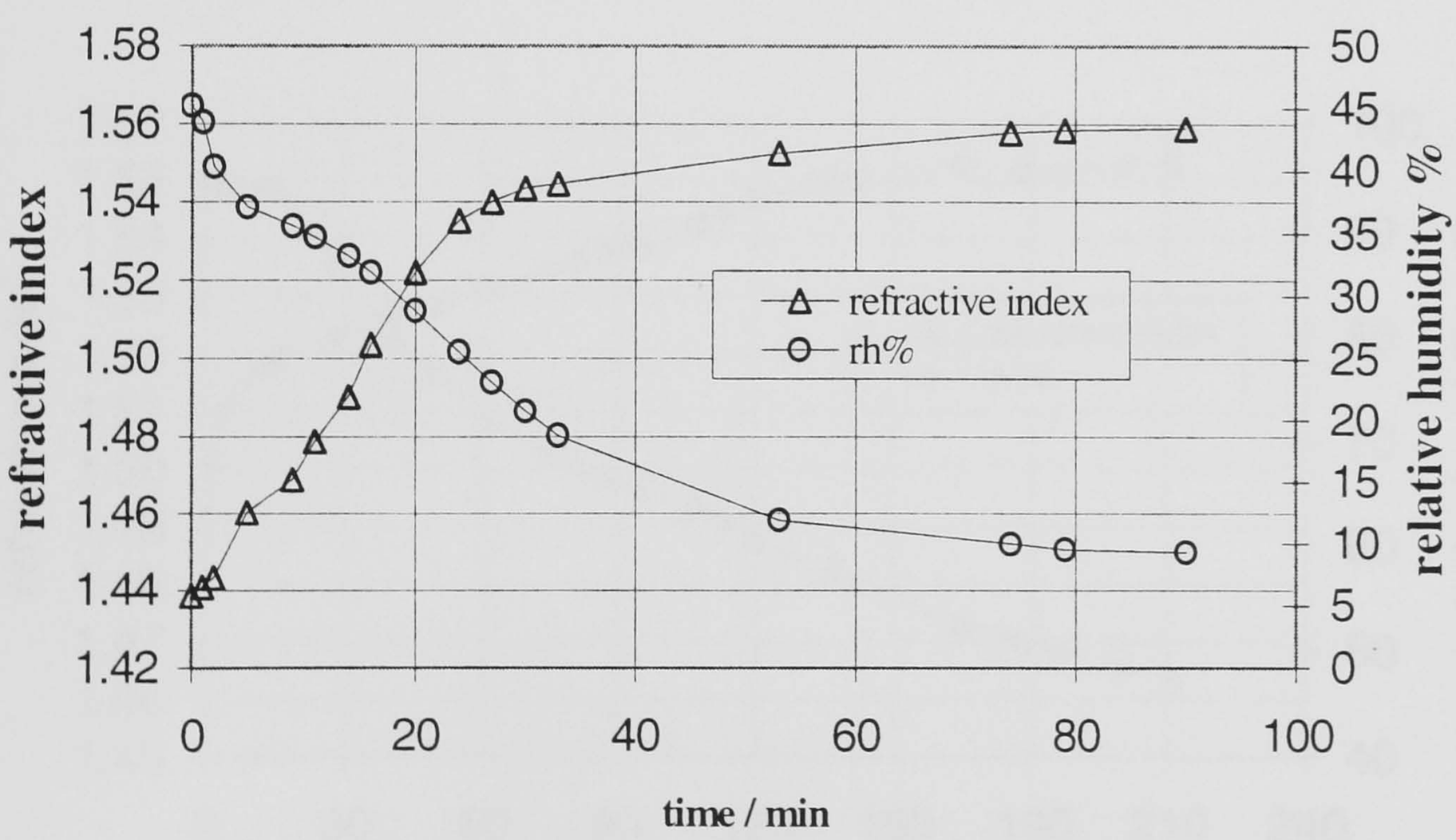

Figure 5. 9 Refractive index of film used for Fig.5.8 above as relative humidity slowly decreased.

It was shown in section 5.5.2.1 that the refractive index of the gelatin film reached a minimum of 1.500 at 96.7 % RH. The addition of cobalt chloride had the effect of reducing further the refractive index at high relative humidity. This is clearly illustrated in Fig.5.9 above. This gives a clear indication that gelatin films absorb more moisture when impregnated with cobalt chloride.

Different mixing ratios were tried to establish the maximum concentration of cobalt chloride within the gelatin film that would give a refractive index value higher than 1.453 (refractive index of the core of the fibre used) over 0 to 100% RH. This ratio, in weight, was found to be 1.2:1 cobalt chloride to gelatin. Results obtained for this mixing ratio are plotted in Fig.5.10 below. Note that the amount of water used in the solution did not affect the final ratio of the dried film. It only affected the method of fabrication and the quality of the resulting film.

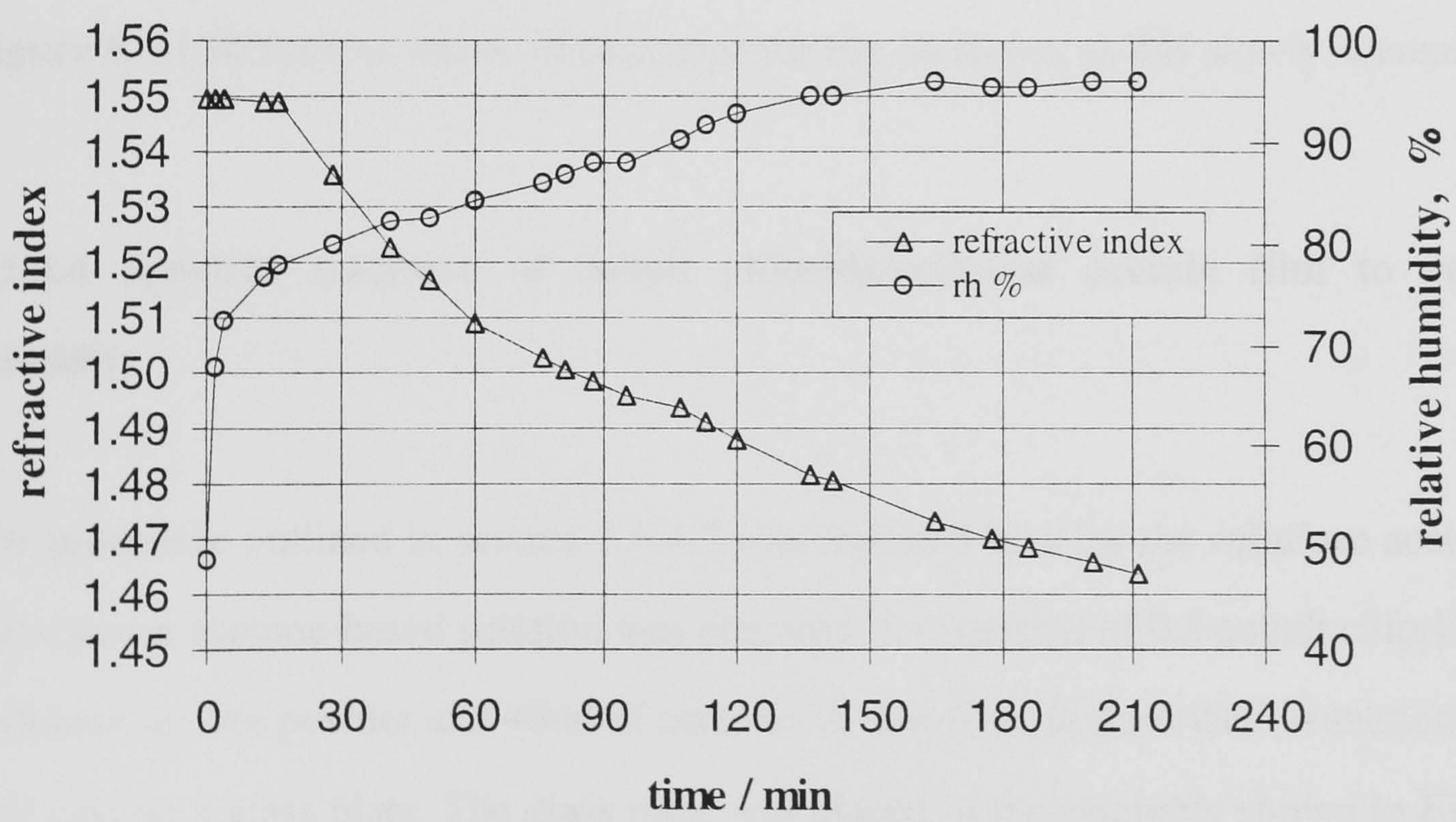

Figure 5. 10 Refractive index variation with slowly increasing relative humidity for mixing ratio of 3g gelatin, 3.6 g cobalt chloride in 50 ml of water.

Using the procedure explained above relative humidity was gradually decreased. The refractive index and the relative humidity were measured and noted at regular intervals. The results are plotted in Fig. 5.11. The maximum refractive index obtained was just over 1.55.

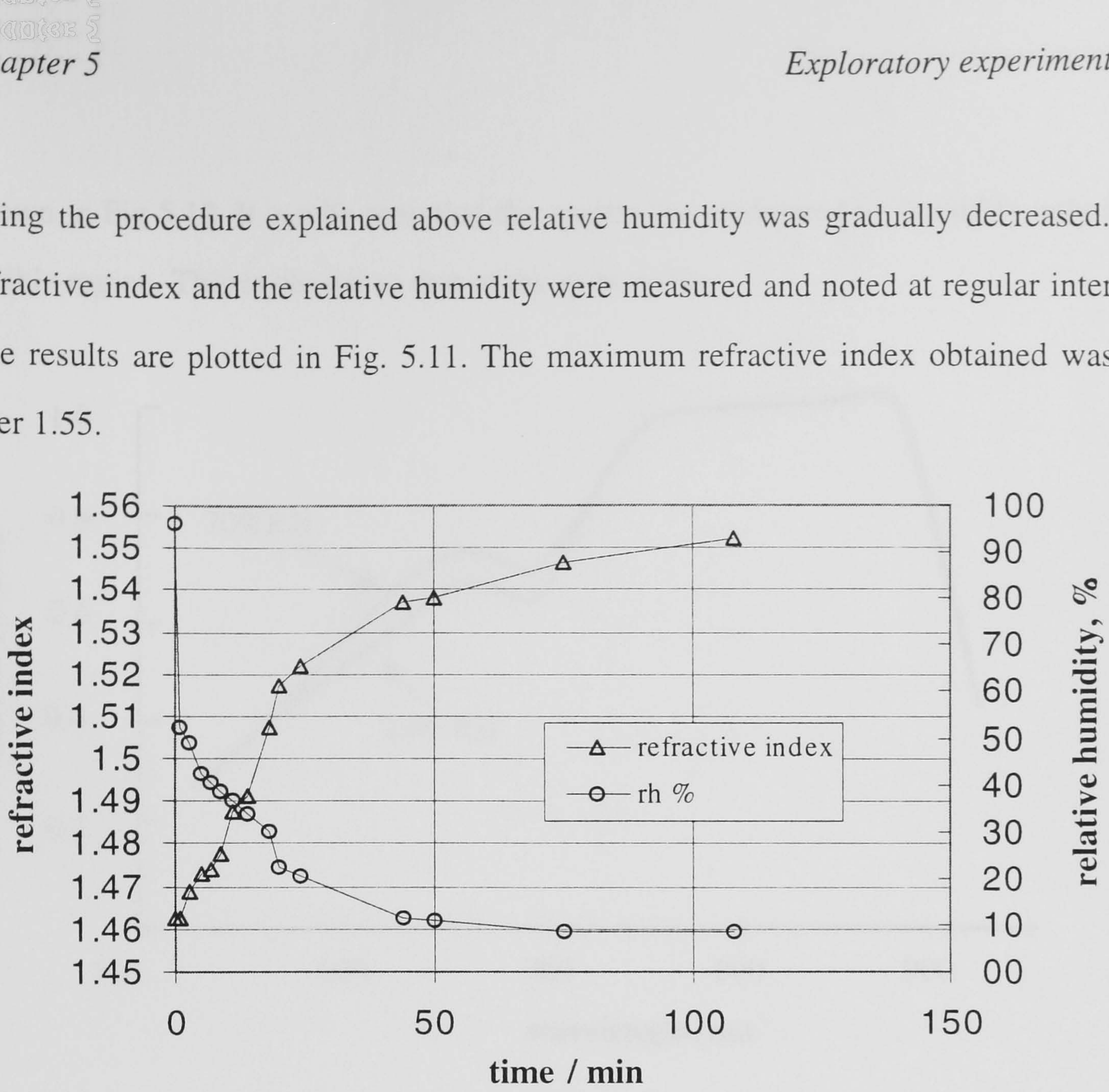

Figure 5. 11 Refractive index, of film used for Fig.10 above, as RH slowly decreased.

5.5.4.4 Spectral response of cobalt chloride/cellulose acetate film to relative humidity

The procedure outlined in section 5.5.4.2 was repeated here for the cellulose acetate. In this case an acetone-based solution was prepared. It consisted of 0.5 cobalt chloride, 3 g cellulose acetate powder and 40ml of acetone. A thin film, as described in section 5.5.1, was cast on a glass plate. The glass plate was placed in the assembly shown in Fig. 5.6. The test assembly was placed in the environmental chamber. While keeping the temperature constant, the relative humidity in the chamber was varied and the spectrum of the collected light was obtained using the spectrum analyser. A plot of the spectrum at two different humidities was obtained. The two values of RH selected were 20 and 70% RH, because they clearly illustrate the change in the spectra. Results obtained are

shown in Fig 5.12. It can be seen that the spectra are modulated by humidity only in the visible region. This is similar to that of the gelatin film.

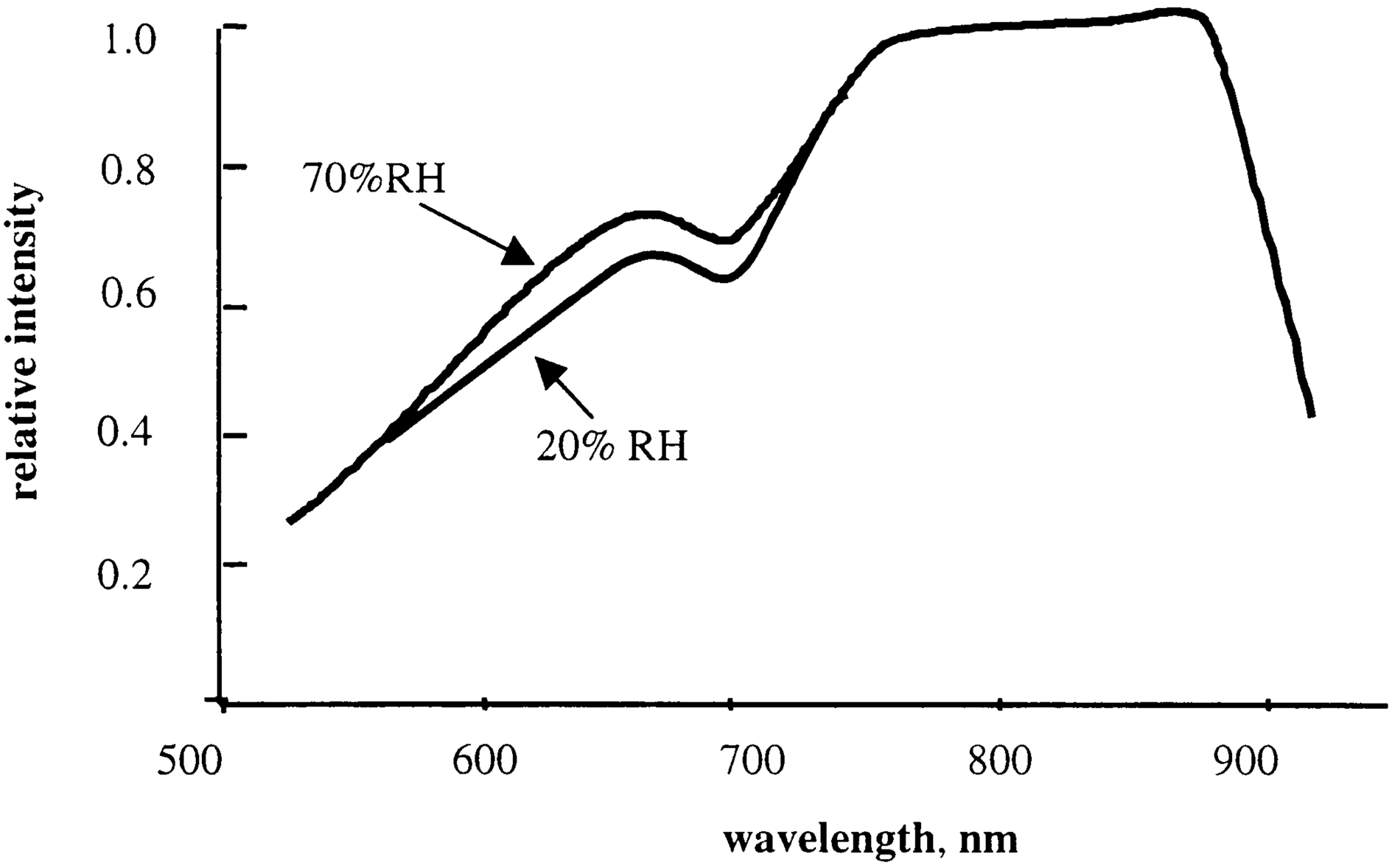

Figure 5. 12 White light spectra through cellulose acetate film at two different humidities.

5.5.4.5 Variation of the refractive index of cobalt chloride/cellulose acetate film with relative humidity

The variation of refractive index of cobalt chloride/cellulose acetate film with the relative humidity was examined here. Again this was to ensure that the design criterion is met over the full operating range. The procedure followed is the same as that followed earlier for the gelatin-based film. Results obtained for slowly increasing relative humidity are shown in Fig. 5.13.

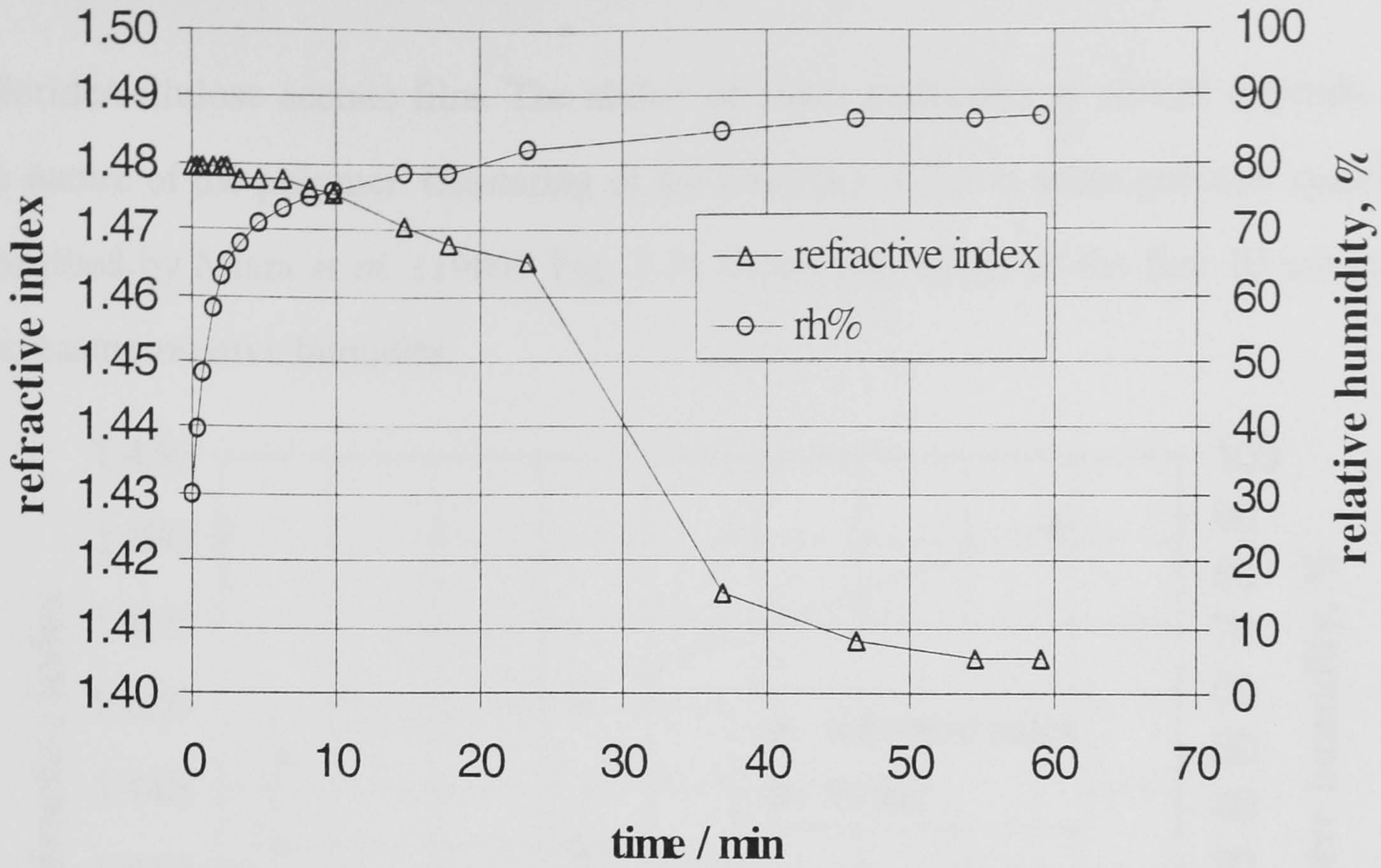

Figure 5. 13 Refractive index variation with slowly increasing relative humidity for a mixing ratio of 3g cellulose acetate, 0.5 g cobalt chloride in 40 ml of acetone.

Having reached a RH of about 90%, relative humidity was forced to decrease as explained in section 5.5.1.2 above. After 10 minutes of gradually decreasing relative humidity the film started to separate from the glass substrate. This was clearly seen through the refractometer as the demarcation line's sharpness diminished slowly.

Testing further samples revealed that some form of leaching of the cobalt chloride from the cellulose acetate film occurred. This can probably be seen by studying Fig. 13 above. From the graph it can be seen that the refractive index gradually decreases to about 1.46 then it drops suddenly to 1.41. Then it gradually falls again to just over 1.40. When examining the sample it was found to be wet. Further examination revealed that when a film of cobalt chloride/cellulose acetate film was exposed to a high relative humidity (>80%), for a prolong period (>2 hours) the cobalt chloride got completely washed away especially from the uppermost part of the film as it was suspended in humid air. This could be due to large scale clustering of the absorbed water in the cobalt

chloride/cellulose acetate film. The ability of water molecules to cluster depends upon the nature of the polymer. Clustering of the absorbed water in some polymer systems is described by Misra *et al* (1986). Fig. 5.14 shows the results of the first 10 minutes of decreasing relative humidity.

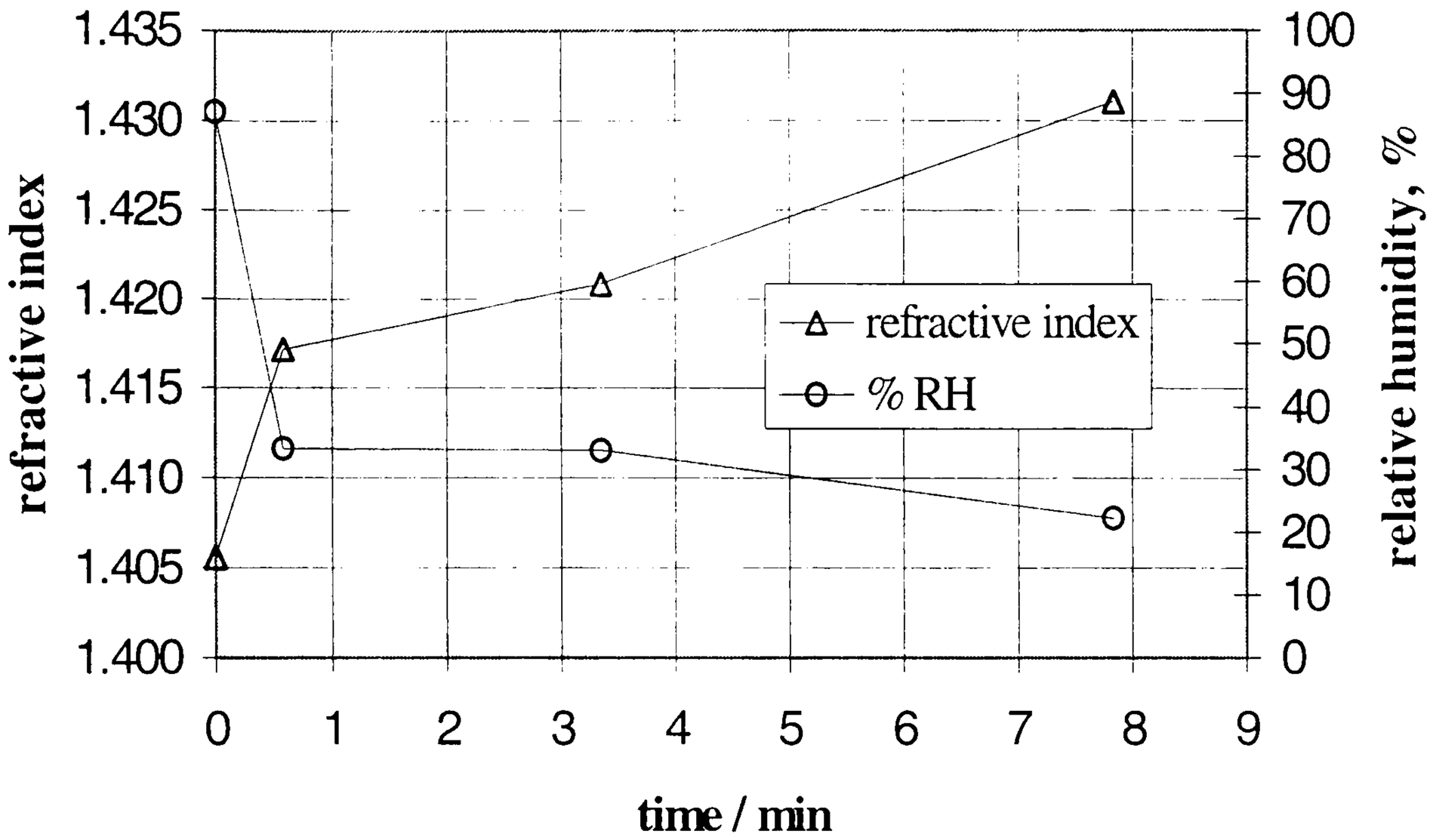

Figure 5. 14 Refractive index, of film used for Fig.13 above, as relative humidity slowly decreased.

5.5.4.6 Spectral response of cobalt chloride/porous silica film to relative humidity.

The procedure outlined in section 5.4.2.1 was repeated here for the porous silica. A solution of 0.5 g cobalt chloride, 3.5 ml of TEOS, 4 ml acid water (2 pH) and 10 ml ethanol was prepared. A thin piece of porous silica was cast as described in section 5.5.3. The piece was self-supported and was therefore placed, without additional support, in the assembly shown in Fig. 5.6. A similar procedure was followed to that outlined in section 5.5.4.2. The spectral response was monitored as the relative humidity was varied. No response was observed for values above 32% RH. This suggested that the porous film was completely saturated with water molecules at 32% RH or above.

5.5.4.7 Variation of the refractive index of cobalt chloride/porous silica film with relative humidity

Using the arrangement of Fig. 5.4 the refractive index of cobalt chloride/porous silica was measured at 50% RH and was found to be 1.465. In this case the porous silica sample was placed directly on the Abbe measuring prism with a contact liquid of high refractive index in between. The value above corresponds to the minimum value of refractive index since saturation occurred at 32% RH, as mentioned in the previous section, i.e. no extra moisture was absorbed above 32% RH.

5.5 Basic design of the thin film

The exploratory experiments carried out in the last section showed that gelatin film seemed to satisfy all the desired properties of the immobilising agent stated in section 5.2. A wide range of concentration of cobalt chloride could be used within the film. The film seemed to behave satisfactorily across the full humidity range (0 to 100% RH).

On the other hand cellulose acetate only partially satisfied the design criteria. However, it failed on two accounts; first: - it formed a weak adhesion to the glass substrate, second: - cobalt chloride leaching occurred at high humidity. In other words the film was unstable at high humidities.

Regarding the sol-gel technique, the initial work carried out here showed that it is suitable as an immobilising agent for cobalt chloride. It had the right range of refractive index and the process of water absorption was reversible. Although casting films with different concentrations of cobalt chloride was successful, film coatings could only be achieved with a very low cobalt chloride concentration. In addition there are many

factors that determine the properties of the resulting porous silica. This required a longer time to develop. Therefore, further work was deferred.

Amongst the colorimetric reagents selected for this work, cobalt chloride showed superior sensitivity to relative humidity. Therefore, the film adopted here was cobalt chloride/gelatin film.

5.6 Humidity test chamber

The environmental chamber, of 30×30×30 cm^3, described below and shown in Fig.5.15, supplied by Michell Instruments Limited, Cambridge, was designed to generate predetermined relative humidities at selected temperatures. Two temperature controllers were used to control the temperature within the chamber and at the point of generating wet air. The system operates within a relative humidity range of 2 to 100% over a temperature range of 23 to 70 °C. The relative humidity within the chamber is measured using an optical dew point hygrometer (Michell 3020) with an accuracy of ±1% RH. The temperature is also measured using the same instrument.

The system consists of the following: -

5.6.1 The optical dew point hygrometer

This type of instrument is used as a transfer standard by NPL and was calibrated against a similar instrument at NPL before measurements were carried out (calibration was valid for 12 months).

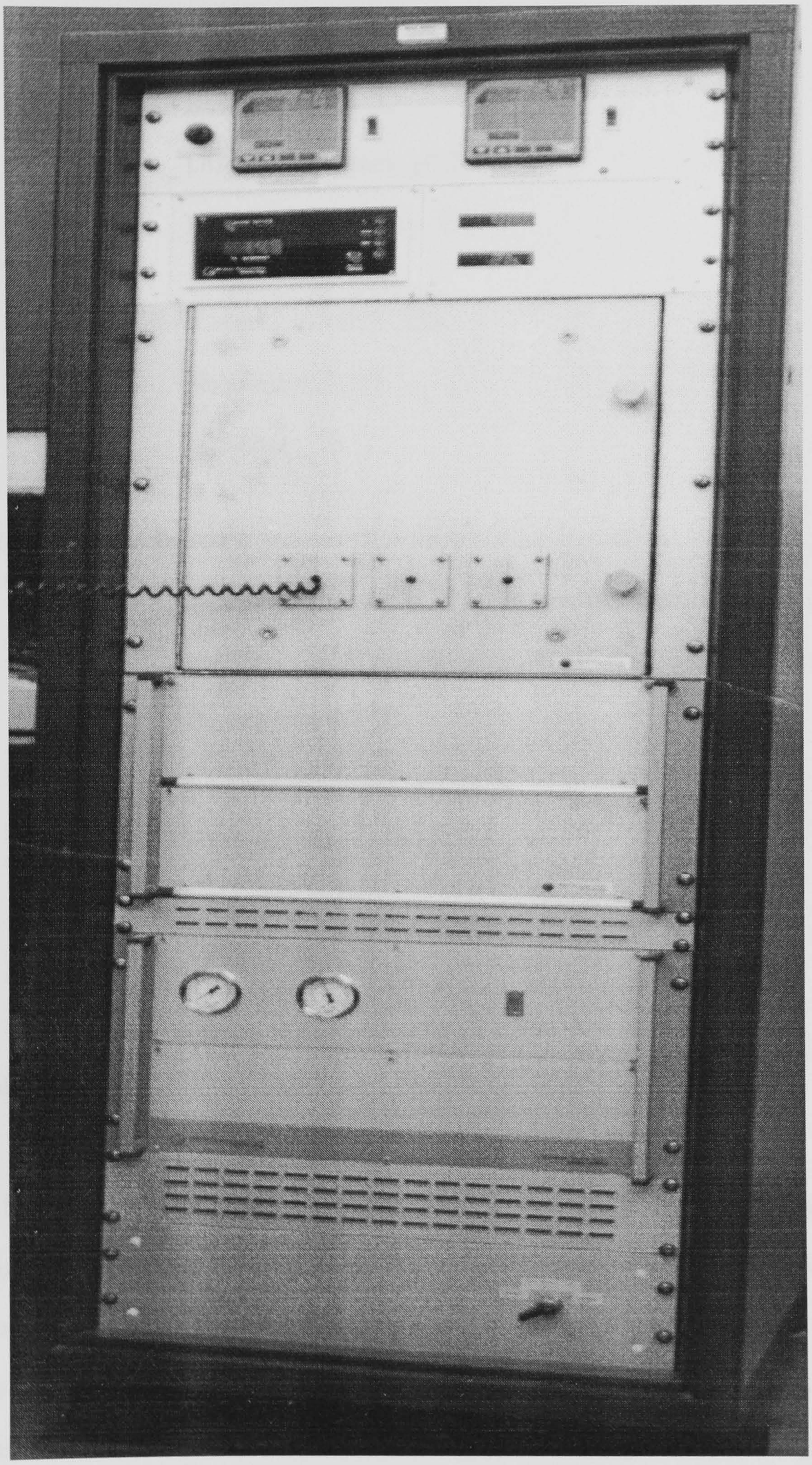

Figure 5. 15 Humidity test chamber.

The Michell series 3020 dewpoint hygrometer has the following specifications:-

Temperature

Range -75 to +80 °C

Resolution 0.1 °C

Display Accuracy ±0.26 °C

PRT Accuracy ±0.1 °C.

Relative humidity

Range 2 to 100% RH

Resolution 0.1%

Accuracy 1%

Dew point measurement

Range -53°C to 80 °C is achievable but is very much dependant on the ambient temperature where the sensor is mounted.

Resolution 0.1 °C

Display Accuracy ±0.26 °C

PRT Accuracy ±0.1 °C.

5.6.2 Air dryer

Air is dried in the system using Michell PSD-2 pressure swing dryer. Fig.5.16 shows a flow diagram of the air dryer. Wet incoming air is pressure regulated to kPa (70 psi) by PR1 and passes through the switching valve assembly formed by SV1 and SV2 into column 1 (DC1) where it passes through the desiccant. Air drying takes place by absorption which occurs when the moisture level in the gas stream is greater than the moisture level of the desiccant. A molecular sieve is used to remove water vapour from the air. These moisture levels come into equilibrium and as a result, water vapour in the

air stream condenses as a film on the desiccant. Dry air from column 1 goes to the dewpoint generator.

At the same time desiccant in column 2 (DC2) which has been wetted in the previous cycle, is being simultaneously regenerated. At the start of its regeneration cycle, column 2 is depressurised from operating pressure to atmospheric in a reversed flow direction through valve SV2, and goes out through the purge exhaust.

A portion of the dry outlet air from column 1 passes through the check valve assembly and the column being regenerated in a reversed flow direction to that of the drying cycle. The sudden pressure drop followed by this dry purge removes the moisture from the desiccant and out through the purge exhaust. The regenerating purge flow is countercurrent to the direction of drying for efficient desiccant regeneration.

When the regenerating cycle is complete. The column being regenerated is repressurised to full operating pressure by closing the purge exhaust. Purge gas continues to flow into the column until the pressure rises to system pressure, 70 psi. Inlet air is then switched over to column 2 by the switching valves for drying. Repressurisation before switch over ensures that the desiccant will not be damaged by the inrushing downward air flow.

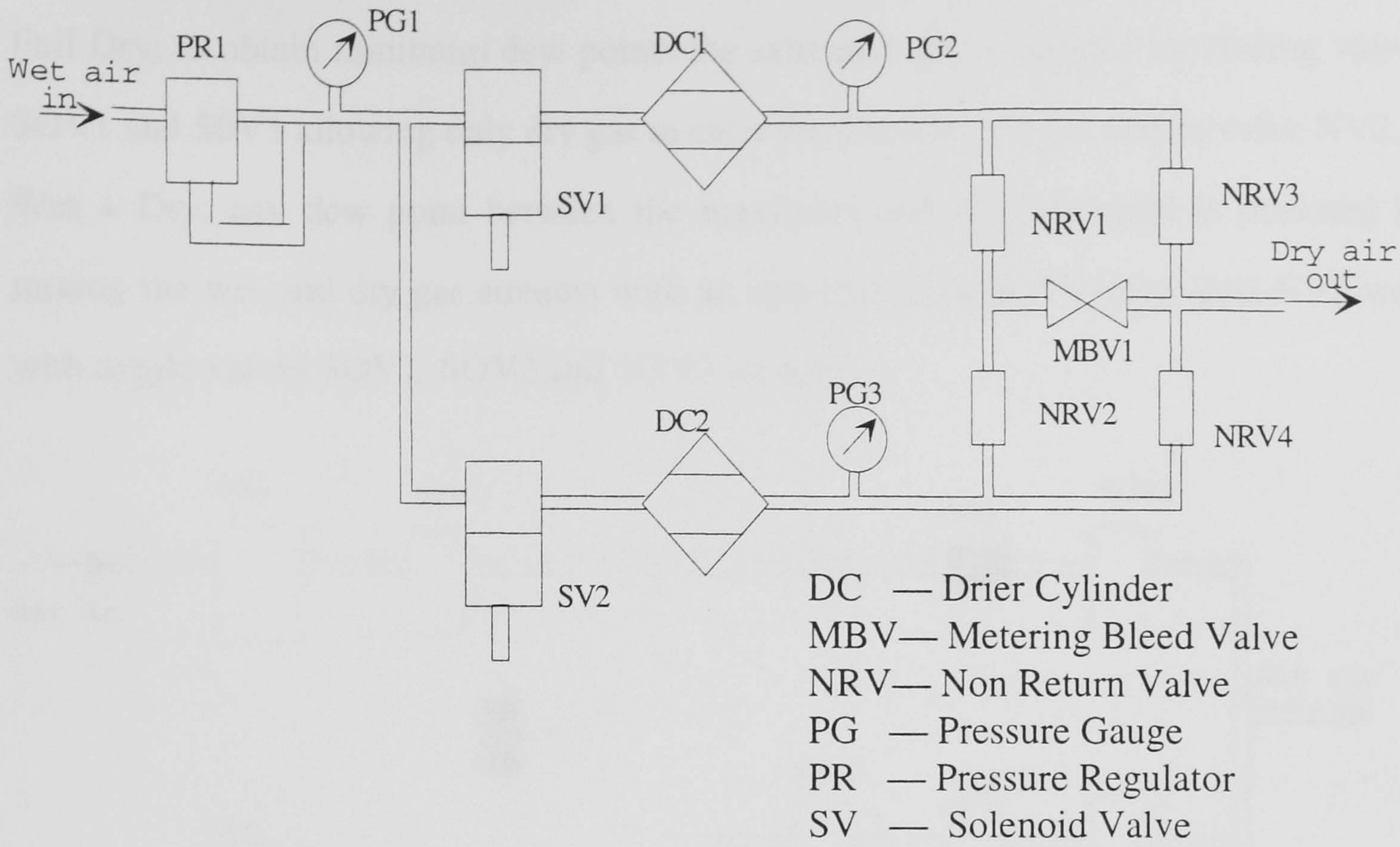

Figure 5. 16 Pressure swing dryer.

The system operates within the dewpoint range of -20 to 65^{o}C and an air temperature range of 23 to 70^{o}C.

5.6.3 Dew point generator

Dew points are generated by mixing dry gas with wet gas as shown in Fig.5.17. This is achieved by splitting the input dry gas into two streams, and bubbling one of the streams through a water saturator. The two streams are then joined together via needle valves. By changing the mixing ratios different dew points can be generated.

Full Wet: to obtain maximum dew points the dry stream is isolated by closing the toggle valve SOV2 allowing only saturated gas to enter the test chamber via the needle valve NV2.

Full Dry: to obtain minimum dew points the saturated gas is isolated by closing valves SOV1 and S0V3 allowing only dry gas to enter the chamber via the needle valve NV2.

Wet + Dry: any dew point between the maximum and the minimum is obtained by mixing the wet and dry gas streams with an appropriate ratio NV1(dry) and NV2(wet) with toggle valves SOV1, SOV2 and SOV3 all open.

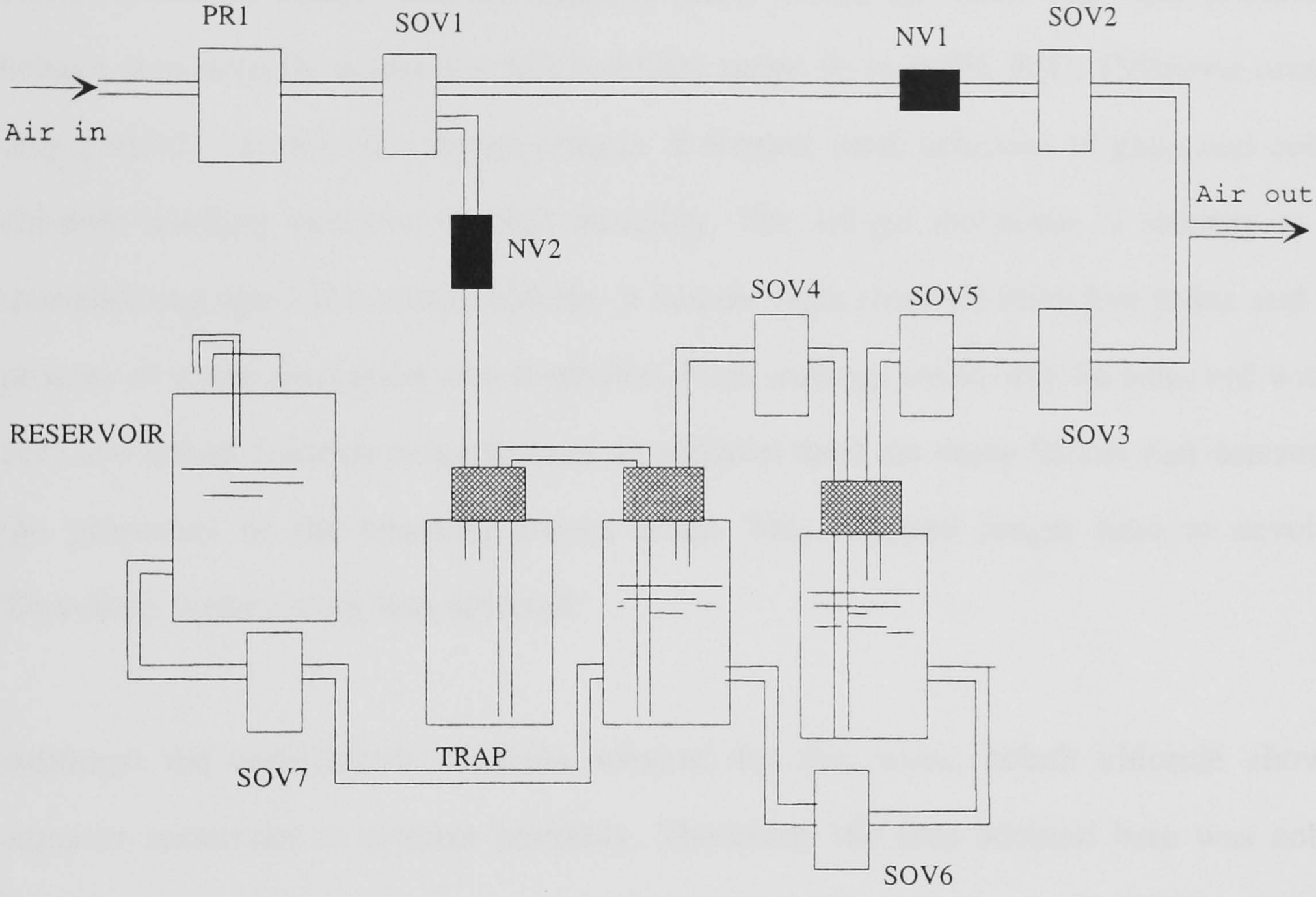

Figure 5. 17 Special dew point generator.

5.6.4 Temperature controller

The temperature is controlled by two WEST controllers. Heating is provided by two electric heating elements one for the dew point generator and one for the test chamber. The element is turned on when temperature falls below a present value. Cooling is achieved by passing cold tap water in a copper pipe. One of the drawbacks of this way of cooling is that at higher humidites, condensation occurs on the cooling pipe thus reducing the efficiency of the system.

5.7 Summary

In this chapter three immobilising agents and three colorimetric reagents were considered for this investigation. After a set of experiments it was concluded that cobalt chloride and gelatin were the most suitable for this investigation. A wide range of concentration of cobalt chloride could be used within the film. The film seemed to behave satisfactorily across the full humidity range (0 to 100% RH). Cellulose acetate only partially satisfied the design criteria. It formed weak adhesion to glass and cobalt chloride leaching occurred at high humidity. The sol-gel technique is suitable as an immobilising agent for cobalt chloride. It had the right range of refractive index and the process of water absorption was reversible. Film coatings could only be achieved with a very low cobalt chloride concentration. In addition there are many factors that determine the properties of the resulting porous silica. This required longer time to develop. Therefore, further work was deferred.

Amongst the colorimetric reagents selected for this work, cobalt chloride showed superior sensitivity to relative humidity. Therefore, the film adopted here was cobalt chloride/gelatin film.

In the next chapter optical fibre sensors were fabricated using cobalt chloride and gelatin and were tested.

CHAPTER 6

Design, construction and testing of a single point-source sensor

6.1 Introduction

In the previous chapter the reason for the choice of the immobilising agent and the colorimetric reagent were given while in Chapter 4 the basic design of the sensor has been described. In this chapter the construction and testing of a single point sensor is carried out. Range and accuracy are also examined.

6.2 An optical fibre sensor using cobalt chloride/gelatin film

In the previous chapter, cellulose acetate, gelatin and porous silica were evaluated as immobilising agents. It was concluded that gelatin film is the most suitable for this study. On the other hand cellulose acetate (impregnated with cobalt chloride) was found to be unstable at high humidities and had poor adhesion to glass. The sol-gel technique was found suitable. However, more development work was required to produce films with the desired properties. Cobalt chloride was also selected as the colorimetric reagent. Therefore, the film selected was cobalt chloride/gelatin film.

6.2.1 Variation of refractive index of the gelatin film and its adhesion to glass with RH

The gelatin used here is Boots commercial grade. As mentioned earlier in Chapter 4 section 4.2, one of the requirements of the properties of the immobilising film is that its

refractive index must be equal to or higher than that of the core over the full operating range. The moisture content of gelatin film increases with relative humidity as was shown in Chapter 5 Fig 5.1. This in turn causes the refractive index of the film to decrease since the refractive index of water is 1.33, i.e. lower than that of gelatin. Therefore, it was essential to measure the variation of refractive index of the gelatin film with relative humidity over the full range 0 to 100% RH.

Using the arrangement described in section 5.4.1.2 and shown in Fig. 5.4, the refractive index of gelatin was noted, at regular intervals, as the relative humidity was gradually increased from 2% RH to 96% RH. The results are plotted in Fig. 6.1 below.

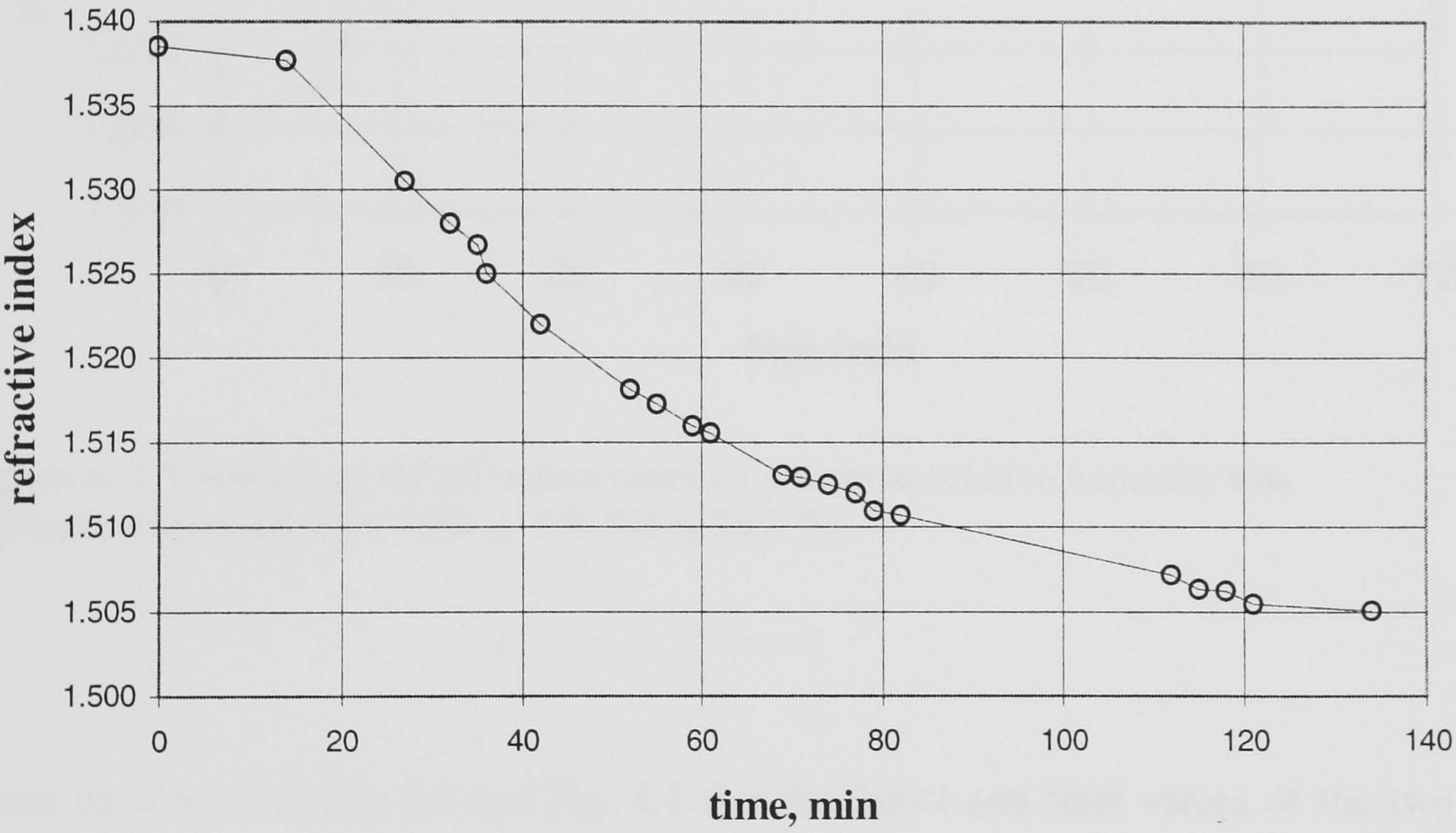

Figure 6. 1 Variation of the refractive index of gelatin as the relative humidity was gradually increased from 2% to 96% RH at 25.2 °C.

It can be seen from the graph that the refractive index had a maximum value of just under 1.54 at very low humidity. The minimum value was approaching 1.50 at 96% RH. To examine the reversibility of the process, the relative humidity was made to gradually

decrease to a final value of 2% starting from 96% RH. Again the refractive index of gelatin was noted at regular intervals. The results are plotted in Fig.6.2 below.

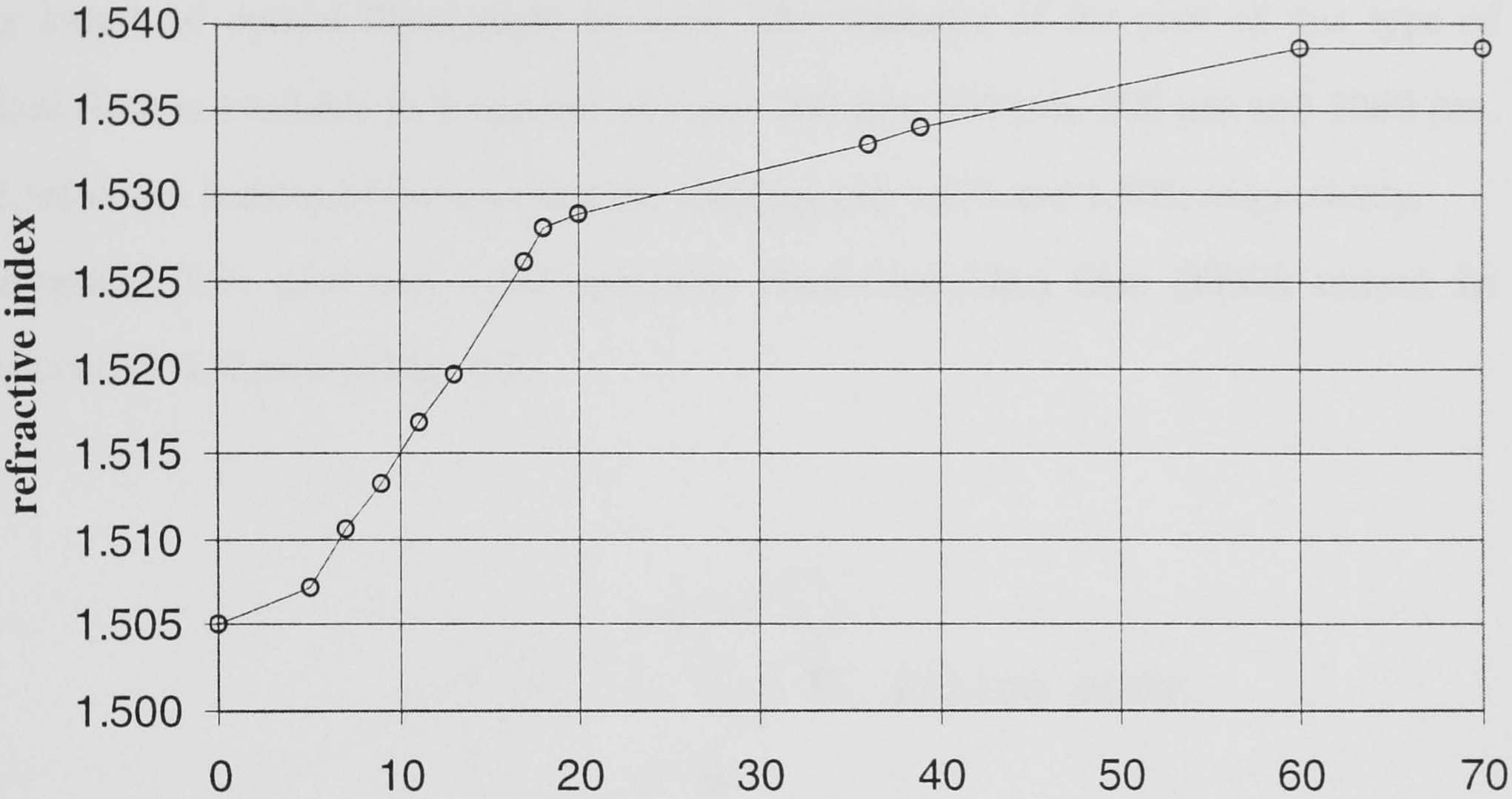

Figure 6. 2 Variation of the refractive index of gelatin as relative humidity was gradually decreased from 96% to 2% RH at 25.2 °C.

It can be seen from Fig 6.1 and Fig. 6.2 that the initial and final values of the two curves, which correspond to the same % RH values, are identical. The moisture content of the film is related somehow to the refractive index. This is outside the scope of this study. However, it is true to conclude from above, that the water absorption process of the gelatin film is reversible. This experiment also examined the adhesion behaviour of the gelatin film to glass as RH varied. Any separation of the film from the glass substrate or surface failure could be detected by the refractometer. This could clearly be seen as degradation of the demarcation line.

6.2.2 Properties of optical fibre used

A Hard Clad Silica (HCS) optical fibre was selected for this study. This type of fibre was selected because the cladding could be removed and also it had lower light attenuation than plastic clad fibre and this is important in distributed sensing where a long length of optical fibre might be used. The diameter of the core of this type of optical fibre is available in a number of sizes, 200 μm, 400 μm, 600 μm and 1000 μm. The refractive indices of the core and the cladding are 1.453 and 1.405, respectively.

The optical fibre used was a 3M speciality Hard-Clad silica fibre (TECS series); its construction is shown in Fig. 6.3.

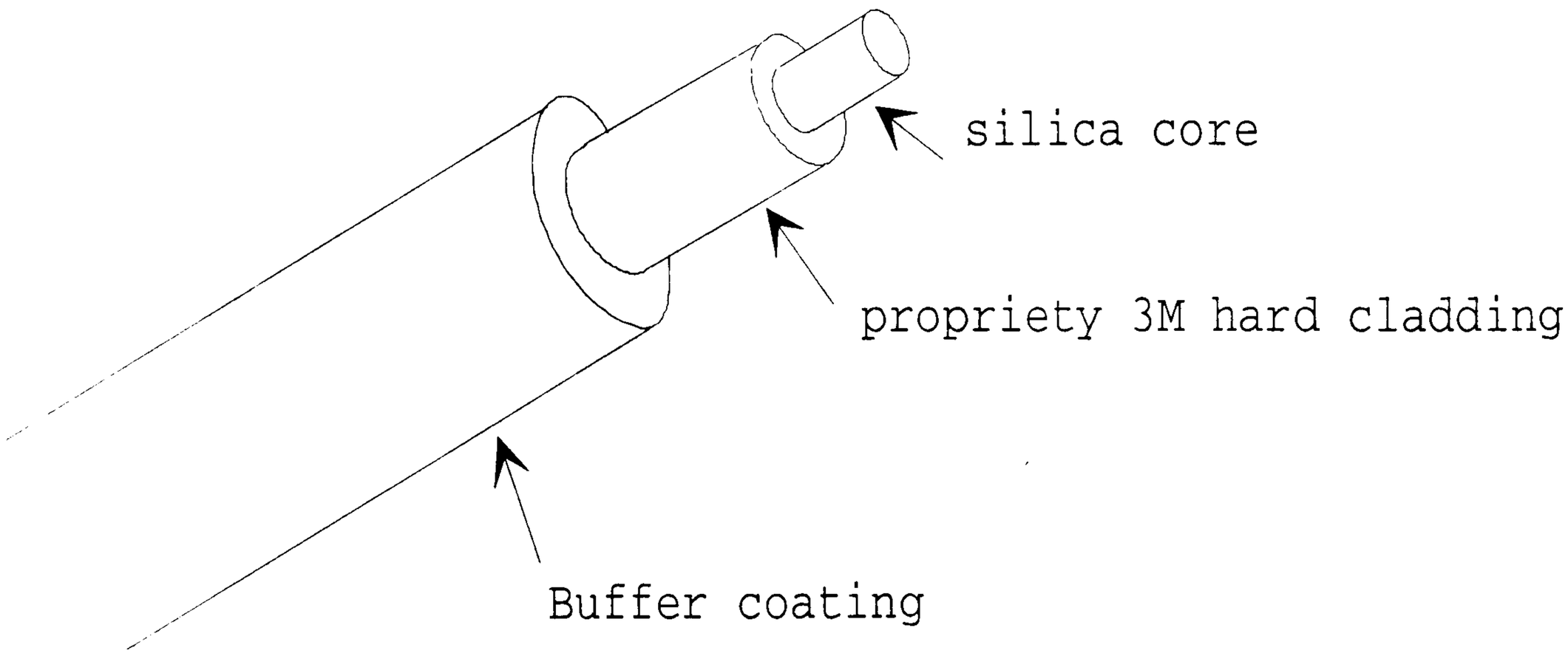

Figure 6. 3 Optical fibre construction.

Table 6.1 shows the specifications of the TECS series optical fibre used. The optical fibre has the following features as stated by the manufacturer:

1. Hard cladding gives increased fibre strength, over all-silica fibres. and reduced static fatigue in humid environment. Also protects the fibre during buffer stripping to prevent fibre breakage.

2. Efficient light coupling and superior transmission in tight bends due to its high numerical aperture.

3. Broad spectral transmission range from 220nm to 2400nm.

Table 6. 1 Optical Fibre specifications.

Type	*200 μm*	*400 μm*	*600 μm*
Core diameter (mm)	200±5	400±8	600±10
Clad diameter (mm)	230± 10	430 ±15	630±10
Buffer Diameter (mm)	500 ±30	750±30	1040±30
Numerical Aperture	0.39±0.02	0.39±0.02	0.39±0.02
Operating temperature range(^{o}C)	-65 to +125	-65 to +125	-65 to +125
Attenuation @820nm (dB/km)	<6	<8	<8
Attenuation @630 nm (dB/km)	<10	<10	<10
Minimum Bend radius (mm)			
-recommended short term	13	53	80
-recommended long term	20	80	120
-Absolute short term	5	12	18
-Absolute long term	10	20	30

6.3 Sensor construction

The following steps were followed to construct the optical fibre humidity sensor:-

(1) The optical fibre was first fitted with demountable connectors (SMA) at both ends to enable easy connection to a stabilised white light source (supplied by Lucas Control Systems Products) and a spectrum analyser (Anritsu model MS99A). SMA connectors are available in different sizes and are generally used with multimode fibres. To excite all modes a 20 m long dummy optical fibre was inserted between the source and the sensor. The optical fibre was then fitted in an assembly as shown in the Fig.6.4 below. The optical fibre was connected to a white light source and the spectrum analyser throughout the fabrication process. This enabled monitoring the process at each stage of the construction.

(2) A section of the protective coating, about 70mm long, was stripped off using a sharp scalpel. During the whole process of fabrication, the optical fibre was firmly supported in the construction assembly as shown in Fig. 6.4. This was essential to avoid fibre breakage during and after the removal of the buffer coating. It was not possible to strip the coating chemically (acetone, sulphuric acid and nitric acid were tried) since the coating was a cross-bonded polymer. It could be visibly seen, at this stage, that some light escaped at a number of discrete points within the stripped area. This was due to some damage to the cladding by the scalpel. This was accompanied by slight reduction in the optical power measured by the spectrum analyser. Typical results are shown later in the section.

(3) A 50 mm section of the cladding was removed by burning it off using a low temperature flame. The temperature of flame was set such that it was high enough to burn the cladding off but not high enough to melt the fibre. An improvement in transmission was always observed at this stage of construction. The fibre was then

cleaned with alcohol, acetone and water. The loss observed at this stage could be attributed to the fact that some light was lost due to the change in the properties of the cladding at the edge where the cladding is partially burned off. However, this light attenuation could be as low as 0.1 dB. Typical results of optical power taken at various steps during construction are shown in Table 6.2 below. These results were taken by the Amritsu spectrum analyser with average frames set to 100. The figures give the impression that the resolution was 50pW. Readings were obtained using an active cursor which had an increment of 0.05 nW for that particular setting.

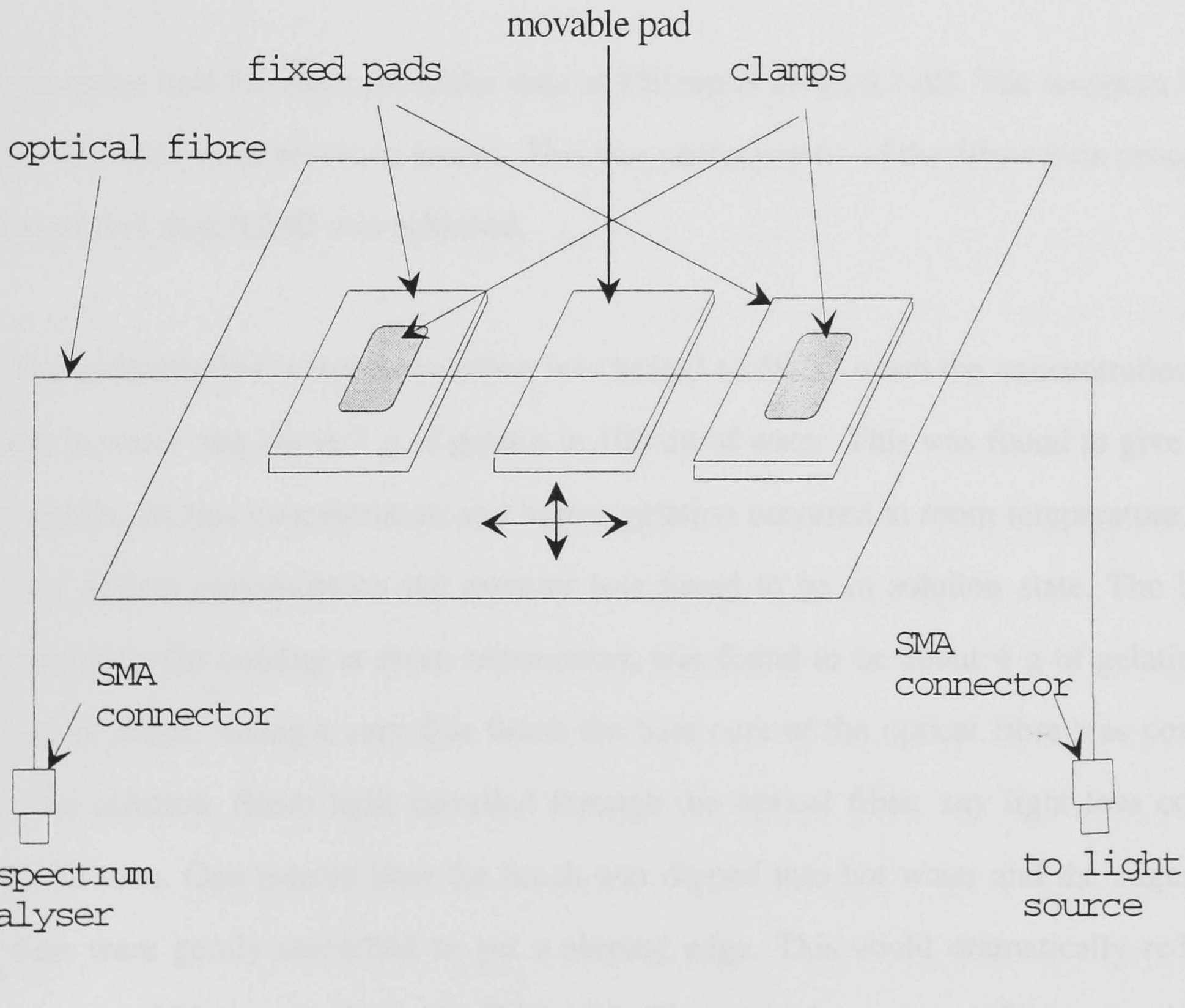

Figure 6. 4 Sensor construction assembly.

Table 6. 2 Light intensities @670nm & 850nm throughout the construction (intensity given in nW) of a cobalt chloride/gelatin based sensor.

Condition	*@ 670nm*	*@ 850nm*
Intensity before removing protective coating	20.50	36.50
Intensity after removing protective coating	19.50	34.75
Intensity after removing cladding	20.50	36.50
Intensity after initial coating	1.75	19.25
Intensity after smoothing the edge of the coating	2.75	31.25

The insertion loss for these particular data at 850 nm is about 0.7 dB. The insertion loss achieved varied from sensor to sensor. This was characteristic of the fabrication process. A loss of less than 0.2dB was achieved.

(4) The gelatin/cobalt chloride solution was heated to 50 °C when the concentration of gelatin in water was above 7 g of gelatin in 100 ml of water. This was found to give the best results. At this concentration and higher gelation occurred at room temperature. At a lower gelatin concentration the mixture was found to be in solution state. The best concentration for coating at room temperature was found to be about 4 g of gelatin in 100 ml of water. Using a very fine brush the bare core of the optical fibre was coated with the solution. Since light travelled through the optical fibre, any light loss could easily be seen. One minute later the brush was dipped into hot water and the edges of the film were gently smoothed to get a sloping edge. This could dramatically reduce light loss at 850 nm as shown in Table 6.2. The optical power at 670 nm is also a function of RH. Although coating was done using a brush, it was applied in such away to be similar to dip coating. This was achieved by soaking the brush completely with the solution thus forming a droplet like effect which was then passed over the optical fibre.

Initially it was difficult to produce good films using this method. With practice and the right viscosity of the solution good coatings were achieved.

The slope of the edge was measured using a Surtronic 3 + surface texture measuring instrument. The instrument had a resolution of 10 nm. This type of instrument has been used to determine heights of very small steps such as those in deposited coatings (Dagnall 1986).

The Surtronic 3+ is a microprocessor-based instrument for the measurement of surface texture. More information about surface texture measurement can be found in reference (Dagnall 1986). The unit houses the control electronics for controlling the measurement sequence, computing the measurement data and outputting the results to the built-in display or to the RS232 port for use with a printer. The unit also contains a drive motor, which traverses the pickup across the surface to be measured. The traverse length is selectable by the user. Full details of the instrument can be found in the manual (Rank Taylor Hobson Ltd 1993).

The Surtronic 3 + was used to measure the thickness of the optical fibre coating and the shape of the edge. During measurement, the optical fibre was firmly placed parallel, level and directly below the pickup of the instrument as shown in Fig.6.5. As the pickup traverses across the surface, movements of the stylus relative to the skid are detected and converted into a proportional electrical signal. The radius of curvature of the skid (40mm) is much greater than the thickness of the optical fibre coating (few microns). This enabled it to ride across the surface unaffected by the edge of the film, and provided a datum representing the general form of the surface.

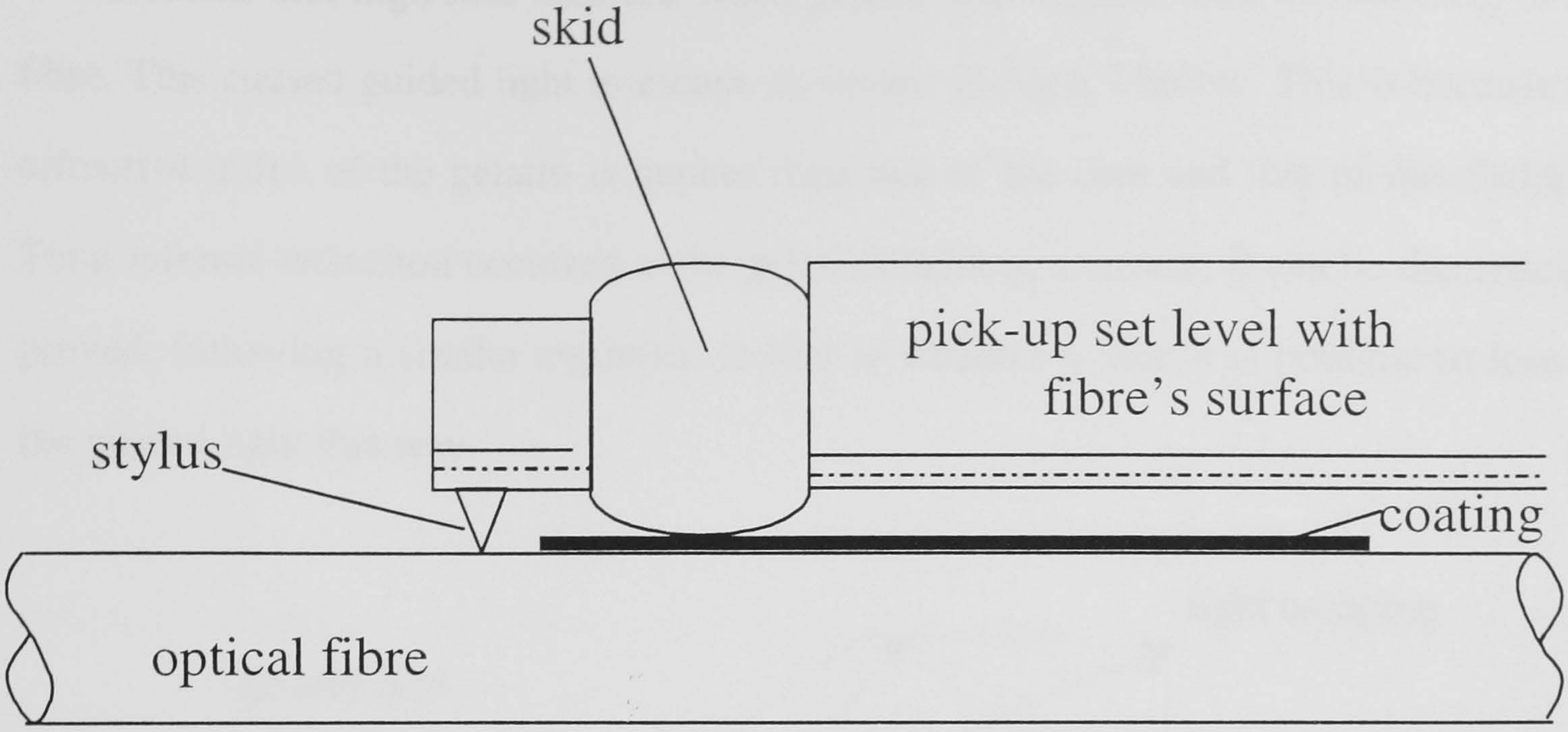

Figure 6. 5 The pickup is supported on the coated optical fibre.

The thickness of the film is given by the parameter Ry, the largest peak to valley height within a single run, which is calculated by the instrument. The slope of the edge can be calculated from the thickness of the film and the traverse distance across the edge as shown in Fig. 6.6. The graph shows typical output results obtained by the instrument when connected to a printer. The measurements were taken at low humidity since gelatin films tend to soften at high humidities.

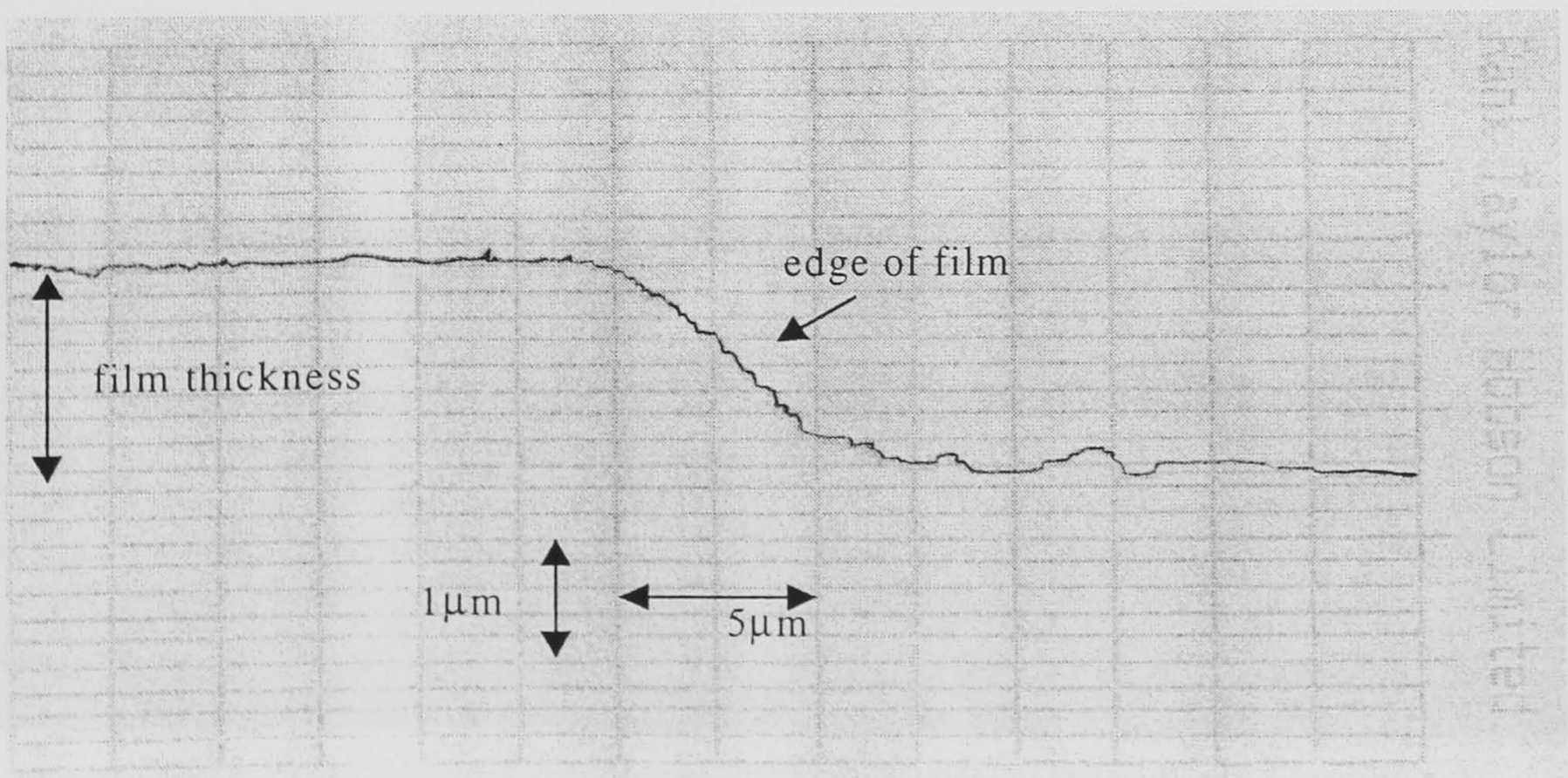

Figure 6. 6 Surface profile of the edge of cobalt chloride/gelatin film on the core of a HCS fibre.

It was found that high loss incurred when gelatin was applied onto the cladding of the fibre. This caused guided light to escape as shown in Fig.6.7 below. This is because the refractive index of the gelatin is greater than that of the core and that of the cladding. Total internal reflection occurred at the gelatin/cladding interface. It can be theoretically proved, following a similar argument to that in Chapter 4, that it is possible to lose all the guided light this way.

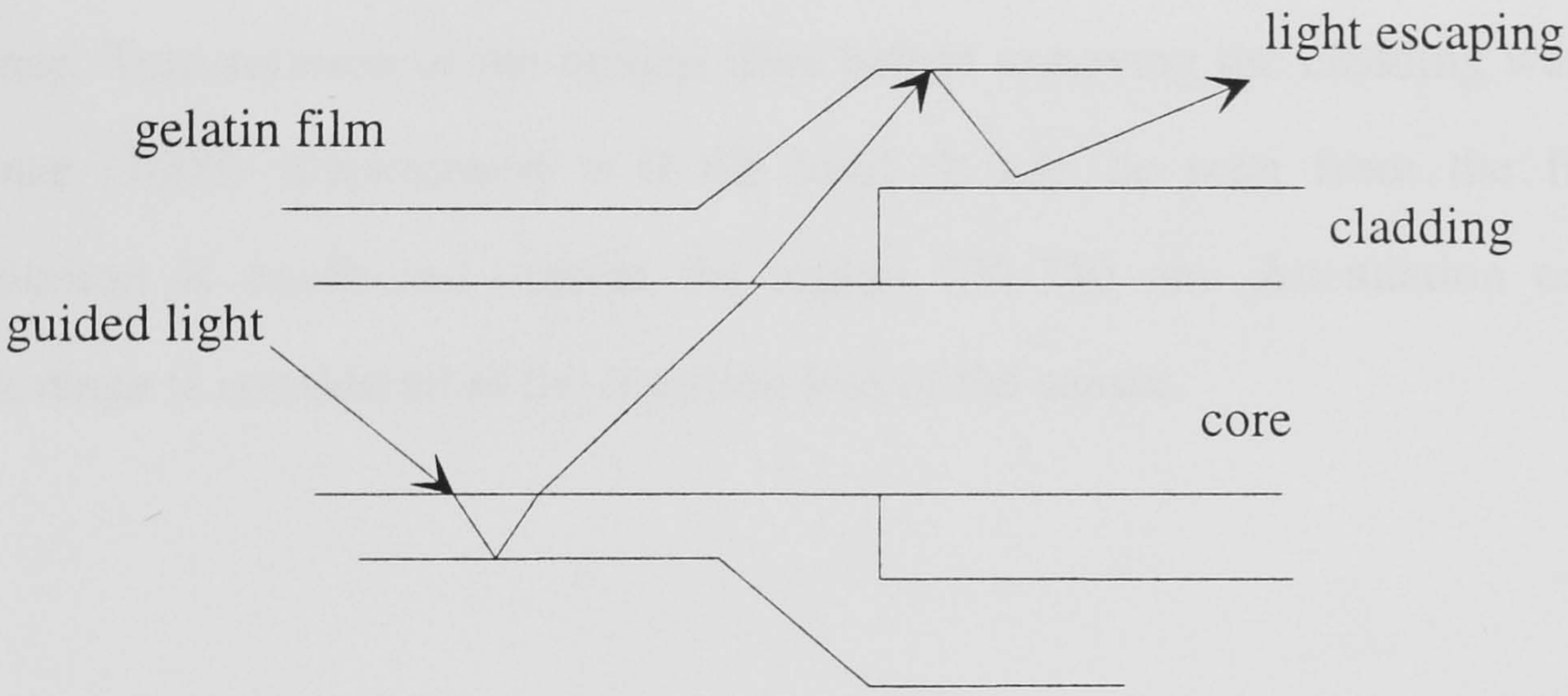

Figure 6. 7 Light loss caused by applying gelatin film over the cladding.

(5) Since the bare optical fibre is brittle and can easily be damaged, a protection arrangement was fitted to the sensing area as shown in Fig. 6.8. The sensor was then left to dry at 60 ^{o}C in an oven. This helps produce an amorphous film as explained in Chapter 5 section 5.4.3.

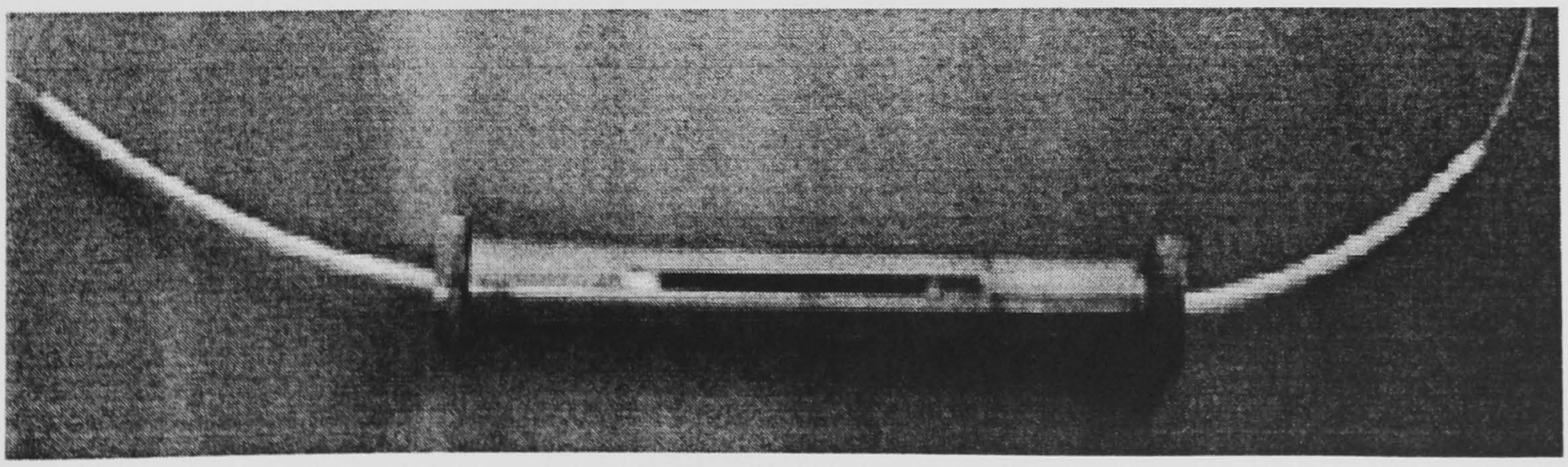

Figure 6. 8 Optical fibre sensing area fitted with protection casing.

The above procedure can equally be applied to different diameter optical fibres. Sensors were built using 200 μm, 400 μm and 600 μm optical fibres. More care was required when using the 200 μm core fibre as it could break more easily once the protective coating was removed. A typical transmission loss curve, at 25 ^{o}C temperature and 40% RH, is shown in Fig.6.9. In this case the reference was taken as the optical power through the optical fibre before the protective coating was removed. At this point the power through the fibre was measured and stored in the instrument and taken as the reference. Transmission of the optical fibre before removing the cladding was taken as reference (100% transmission = 0 dB loss). It can be seen from the figure that transmission is unaffected outside the region 550-750 nm. Attenuation outside the visible range is considered as the insertion loss of the sensor.

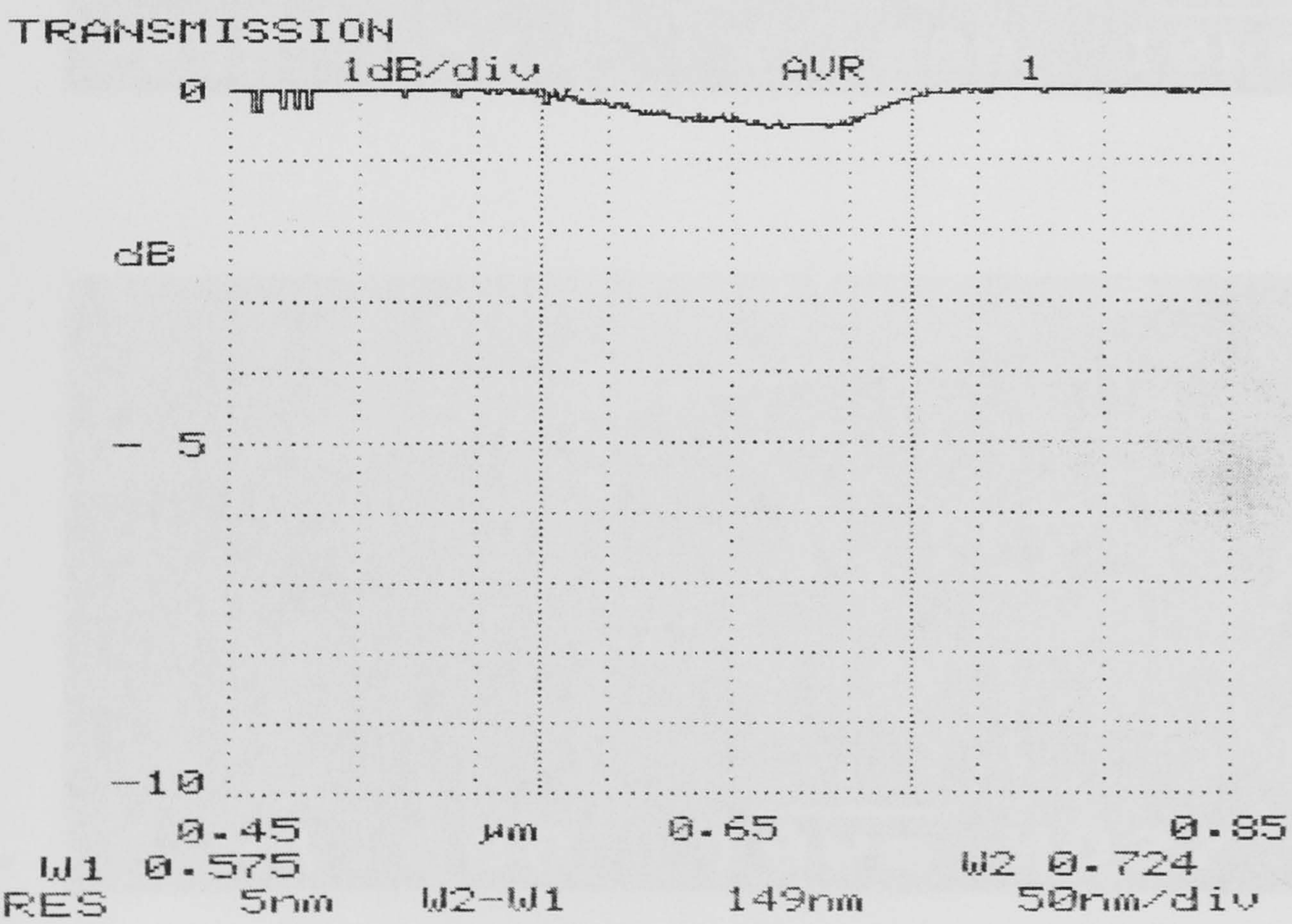

Figure 6. 9 Sensor insertion loss (active sensing area 575-724nm).

Losses outside the active sensing area (at 850nm for example) may be attributed to some irregularities that may be found on the surface of the thin film. This was confirmed by inspecting the film under a microscope.

A cross-section of the coated optical fibre was examined in an electron microscope. It showed that uniform coating was achieved. Fig. 6.10 shows a micrograph of a cross-section of a coated and an uncoated optical fibre.

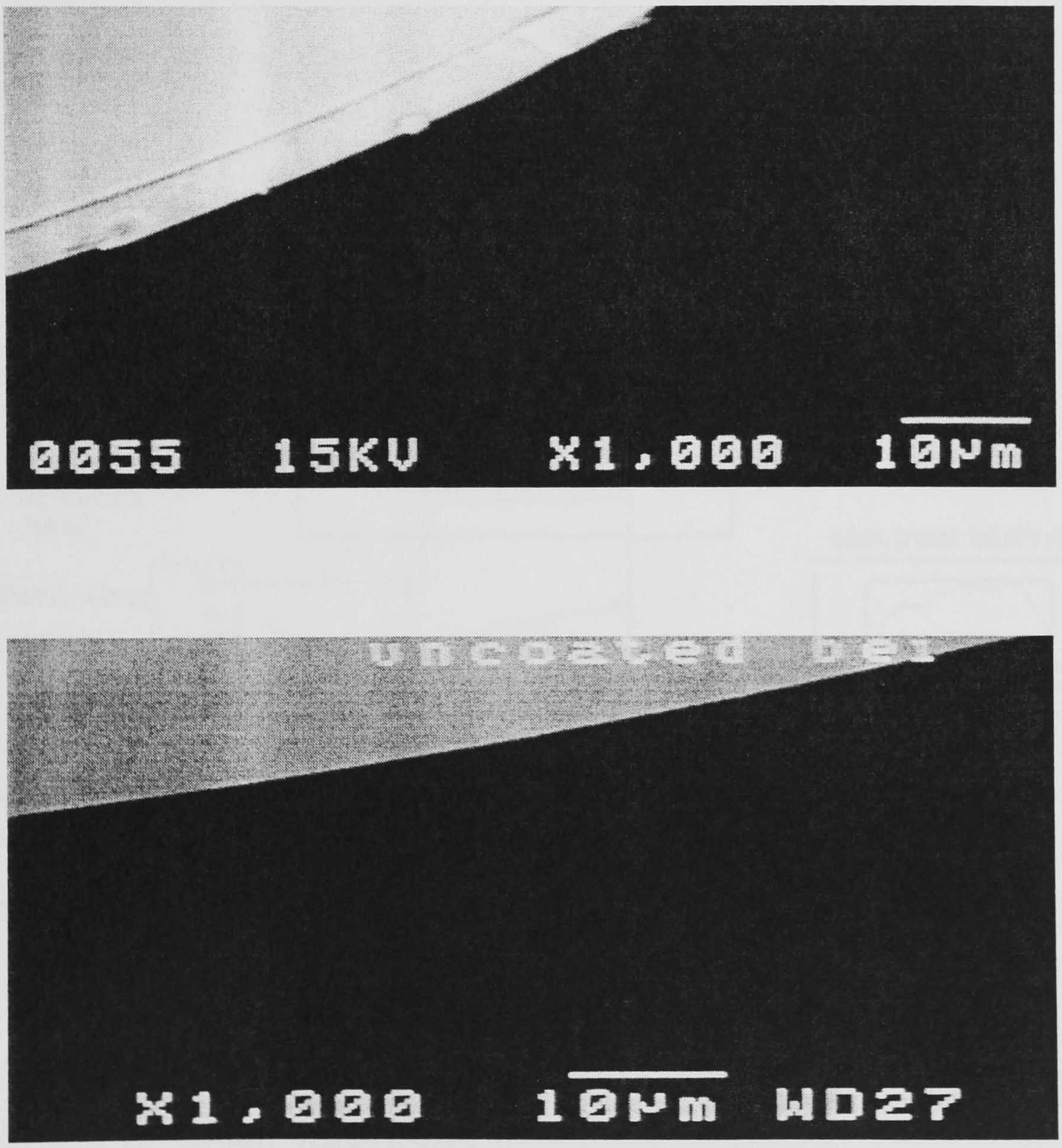

Figure 6. 10 Coated and an uncoated cross-section of unclad optical fibre (sensing area).

6.4 Testing

A stabilised white light was launched into the sensing fibre and the intensities of the collected light were measured using the spectrum analyser. The sensor under test was placed in the environmental chamber very close to the sensing head of the Michael optical dew-point hygrometer as shown in Fig. 6.11 below.

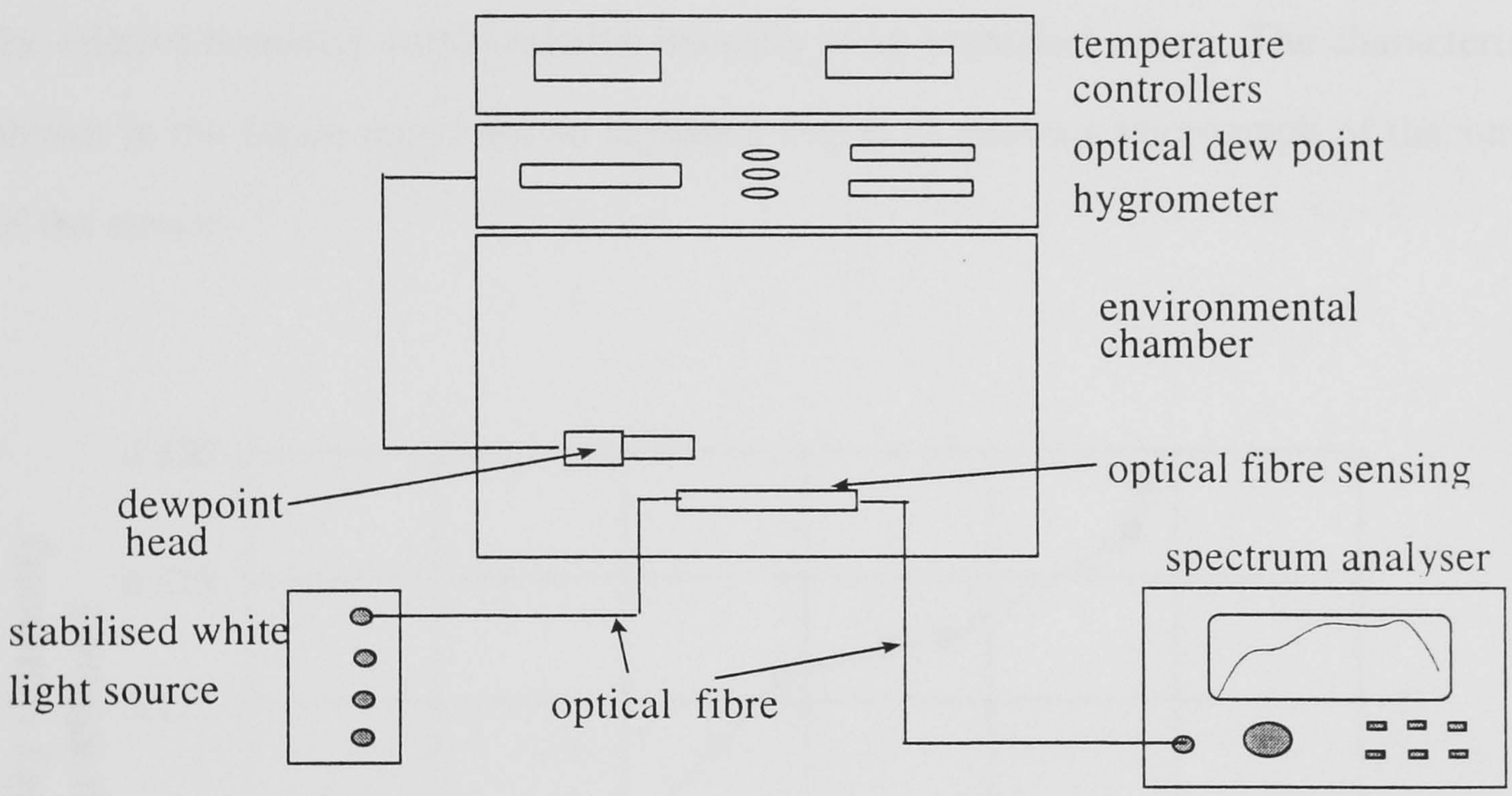

Figure 6. 11 Experimental set-up.

6.4.1 Testing at constant temperature

The relative humidity was varied with the temperature kept constant. At each relative humidity value the intensities of the collected light at the two wavelengths 670nm and

850 nm were noted. The relative intensity (RI) is calculated by dividing the intensity at 670 nm by that at 850 nm.

Several sensors were constructed and tested. Although sensors were monitored at all stages during construction many failed, in different ways, when tested at different humidities. The most common form of failures was sudden fluctuations in the output and extremely poor reproducibility. This was later found to be due to surface imperfection of the coating and perhaps coating failure during operation. It was also found that hot drying, during fabrication, improved sensor reliability. Fig. 6.12 shows the relative humidity versus relative intensity of an imperfect sensor. The characteristics shown in the figure could not be repeated. Fig. 6.13 shows a micrograph of the surface of the sensor.

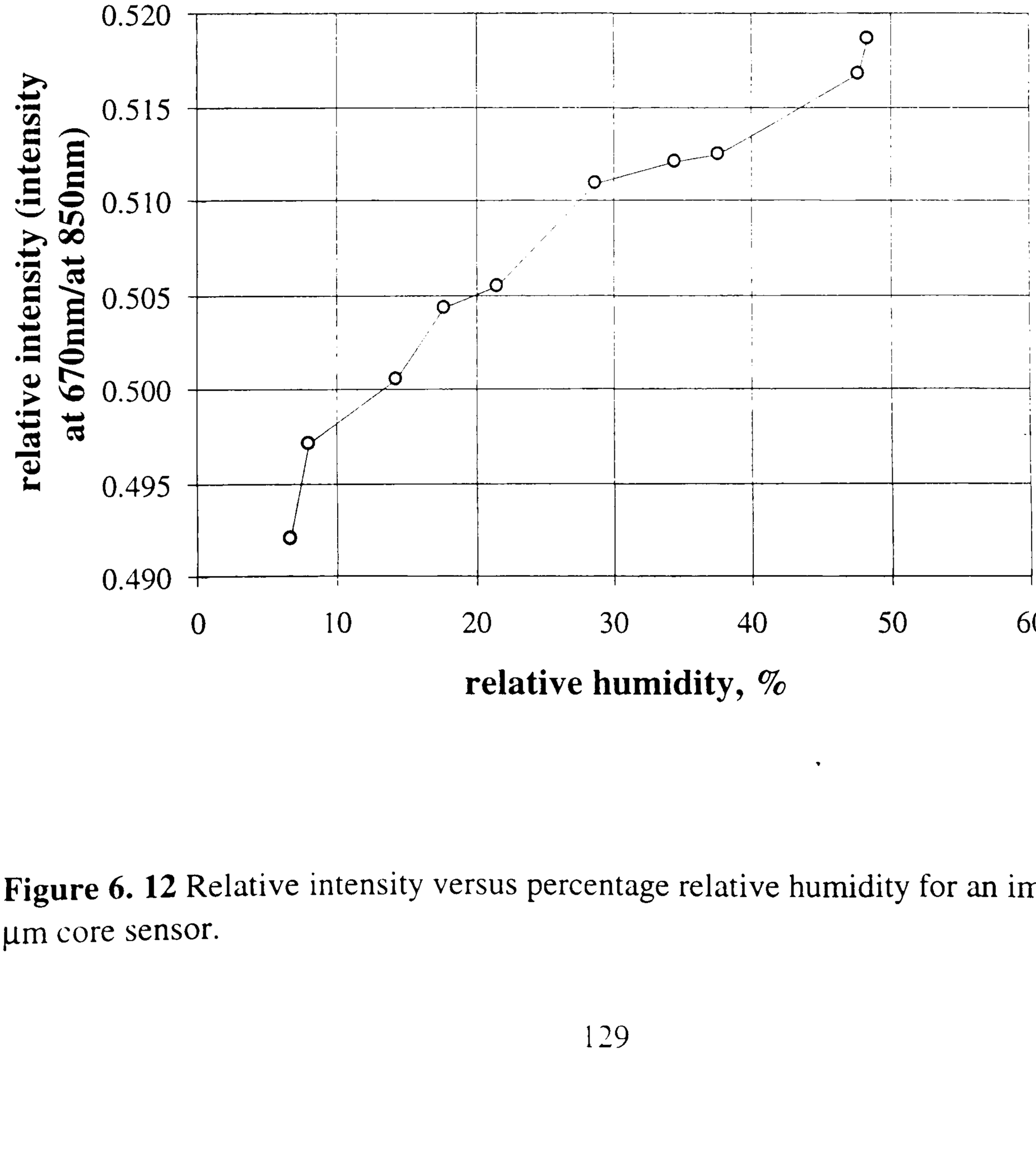

Figure 6. 12 Relative intensity versus percentage relative humidity for an imperfect 600 μm core sensor.

Figure 6. 13 A micrograph of the surface of the above sensor.

Fig. 6.14 shows a graph of relative intensity versus percentage relative humidity for a good sensor. A sensor was considered a good sensor if it had reproducible characteristics. The temperature was kept constant at 24.6 ^{o}C for all readings. During the experiment, heaters within the humidity chamber were switched off to reduce condensation on the cooling pipes hence increasing the efficiency of the dew point generator. This resulted in a temperature of 24.6 ^{o}C in the humidity chamber. This is why this particular temperature was selected. Each reading, on the graph, represents an average of 1000 readings. Error bars are not shown because they are much smaller than the size of the plot symbol on the graph.

The above graph can be considered to have three different operating regions, 20-45, 45-80 and 80-100% RH. The average change in RI per 1% RH change for these three

regions are 0.00054, 0.005188 and 0.00124 RI units. The resolution of the spectrum analyser was found to be 0.001 RI unit. This is based on the resolution of light level and its value for a particular sensor.

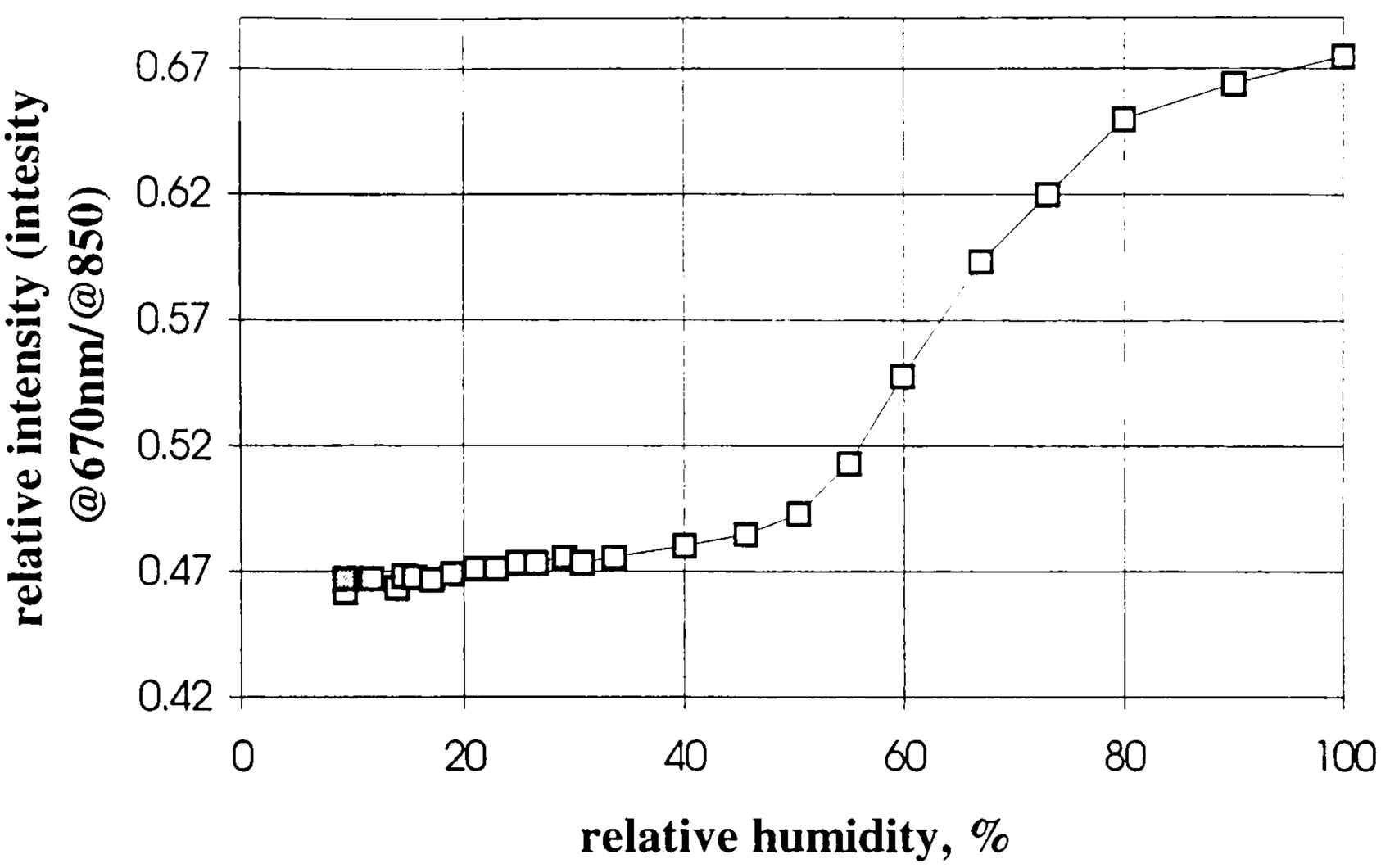

Figure 6. 14 Relative intensity versus percentage relative humidity for a good 600µm core sensor.

The relationship between the moisture content of a sensing film, based on the colorimetric principle, and the light absorption is not a straight forward one. Comparing Fig. 5.1 and Fig. 6.14, we can observe varied correlation over different portions of the graph. A relationship can not be established by examining one immobilising agent only. Several immobilising agents need to be examined in order to establish the type of relationship that might exist.

Repeatability tests had been undertaken over a 3-month period during which time the sensor has been exposed to cycles of humidity change in the operating range 20 to 80%

RH. Repeatability was better than 2% RH for values above 40% RH and 4% for lower than 40%.

In addition to Boots commercial grade gelatin other types of gelatin were considered. Vegetable gelatin, carrageen type 1 and type III commercial grade (product numbers C1013 and C1263), supplied by SIGMA chemical company limited were considered. It was not possible to produce clear film using this type of gelatin.

Gelatin from porcine skin, (product number G2500) and from bovine skin (product number G9382) were also considered. Clear films were successfully fabricated. However sensors constructed were not repeatable especially for RH above 70% and with a concentration ratio of cobalt chloride to gelatin greater than 1:2. Sudden fluctuations in the sensors output were observed. After further examination it was found that the refractive index of the film dropped to below that of the core when relative humidity exceeded about 70% RH. Boots commercial grade gelatin was also found to perform better at low humidity. When using the other types of gelatin frequent cracks were also observed at low humidity.

Using Boots commercial grade gelatin, six sensors were successfully built and tested with two different concentration ratios as shown in Table 6.3 below.

With the sensors placed, in turn, in the environmental chamber, the relative humidity was varied with the temperature kept constant at 24.6 ^{o}C. At each humidity value the intensities of the collected light at 670 nm and 850 nm were noted. The relative intensity was obtained by dividing the intensity at 670 nm by that at 850 nm. Fig. 6.15 shows a graph of the relative humidity versus the relative intensity of 3 sensors fabricated from 200 μm, 400 μm and 600 μm core fibres and of the same film of mixing ratio (0.6g $CoCl_2$):(3g gelatin):(80 ml water).

Table 6. 3 Diameter of the optical fibres used and the mixing ratios.

Sensor No.	*Optical Fibre Core diameter (μm)*	*Mixing ratio $CoCl_2$(g):Gelatin(g):Water(ml)*
1	600	0.6:3:80
2	600	1.5:3:80
3	400	0.6:3:80
4	400	1.5:3:80
5	200	0.6:3:80
6	200	1.5:3:80

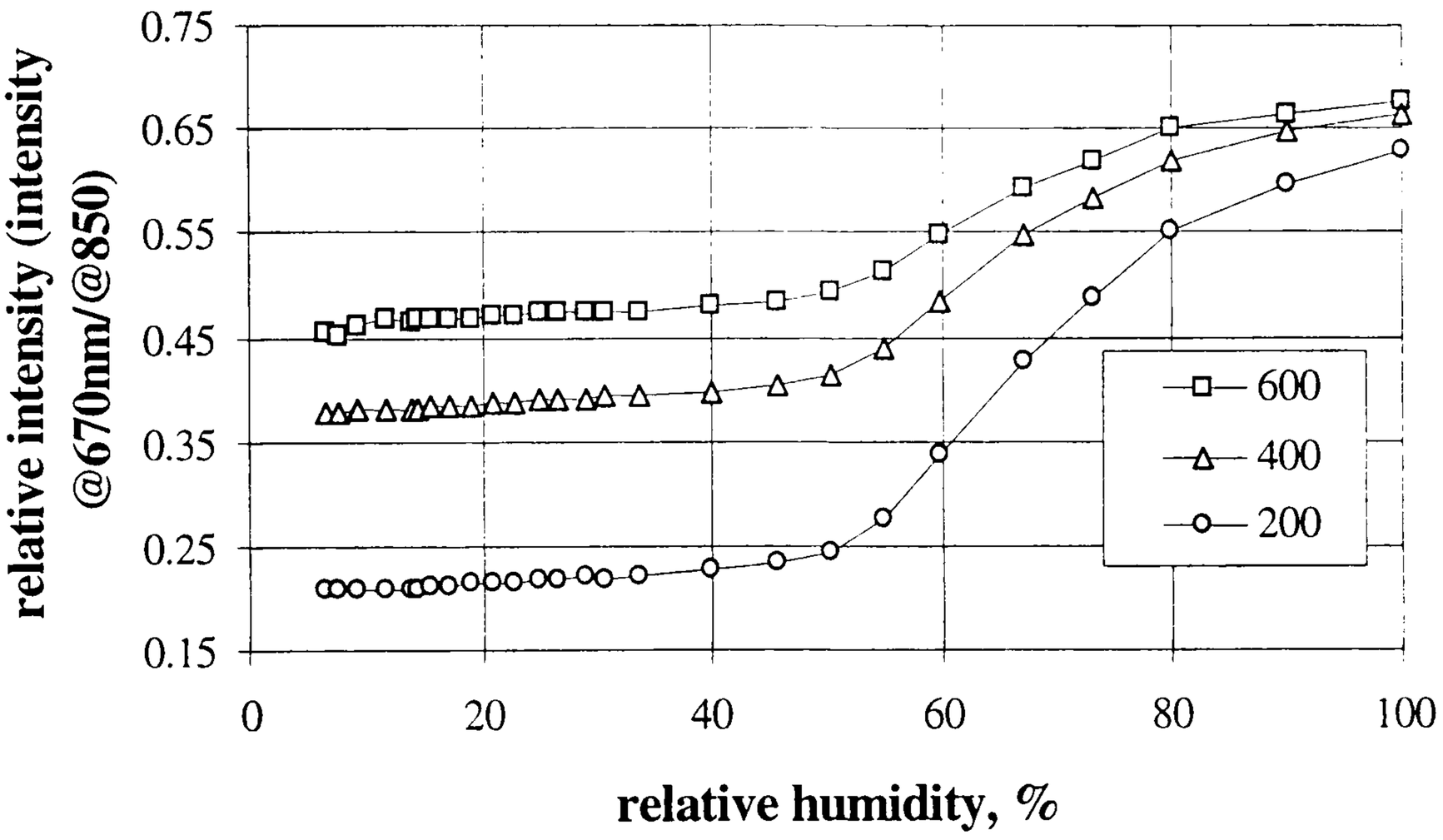

Figure 6. 15 Characteristics of three sensors fabricated from the same thin film mixture and optical fibre with three different diameters, 600 μm, 400 μm and 200 μm. Mixing ratio is (0.6 g $CoCl_2$):(3 g gelatin):(80 ml water).

Fig.6.16 shows a graph of the relative humidity versus the relative intensity of 3 sensors as in above with a different mixing ratio of (1.5 g $CoCl_2$):(3 g gelatin):(80 ml water). It can be seen from the graph that sensitivity increases as concentration increases. For example the sensitivity of the 200 μm core sensor, averaged over the range 50-100% RH, increased from 0.0078 RI per 1%RH to 0.01244 RI per 1% RH as the concentration of the $CoCl_2$ increased from 0.6 g/3 g of gelatin to 1.5 g/3 g.

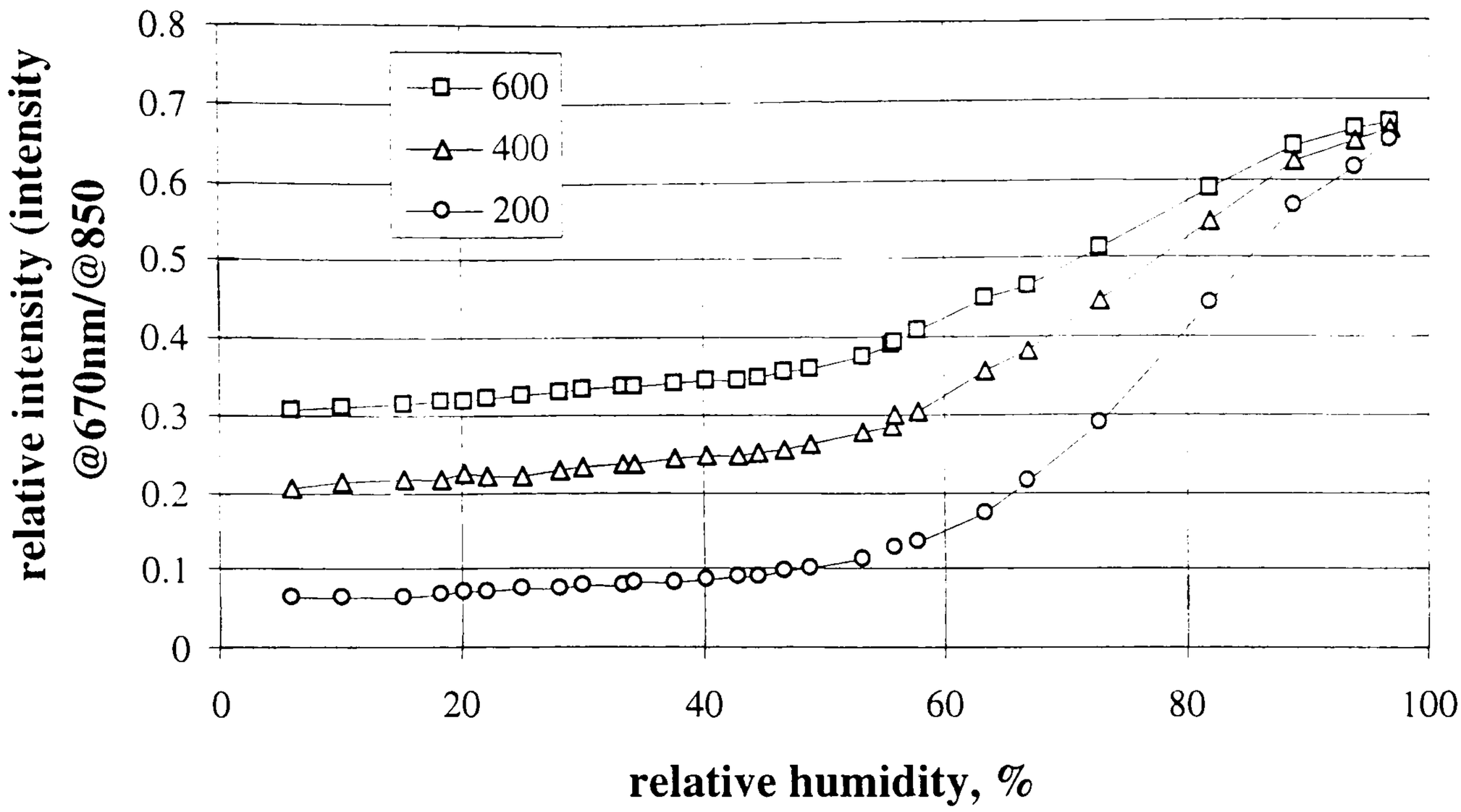

Figure 6. 16 Characteristics of three sensors fabricated from the same thin film mixture of (1.5 g $CoCl_2$):(3 g gelatin):(80 ml water) and optical fibre with three different core diameters, 600 μm, 400 μm and 200 μm.

Cobalt chloride/gelatin sensors were successfully fabricated using 200 μm, 400 μm and 600 μm HCS optical fibres. Special care was required to avoid breaking the fibre when using the 200 μm fibre. They all showed good response and repeatability over the range 20 to 80% RH. It was also found that responsivity increased with decreasing the diameter of the core of the optical fibre. In the next section the effect of temperature on the sensor characteristics is considered.

6.4.2 Effect of temperature variation on the sensor behaviour

For sensor 1 (in Table 6.3) the relative humidity was kept constant and the temperature was varied. This was repeated at a number relative humidies. The mixing ratio used for preparing this sensor was 0.6 g cobalt chloride to 3 g gelatin. The relative intensity obtained is shown in table 6.2. These values are plotted together with previously obtained values for the same sensor (used in Fig. 6.15) as shown in Fig. 6.17.

Table 6. 4 Temperature effect on sensor behaviour.

%RH	*Temperature ^{o}C*	*Relative Intensity*
22.9	24.6	0.4711
22.9	38.3	0.4711
40	24.6	0.4802
40	38.3	0.4806
59.8	24.7	0.5489
59.8	38.3	0.5491

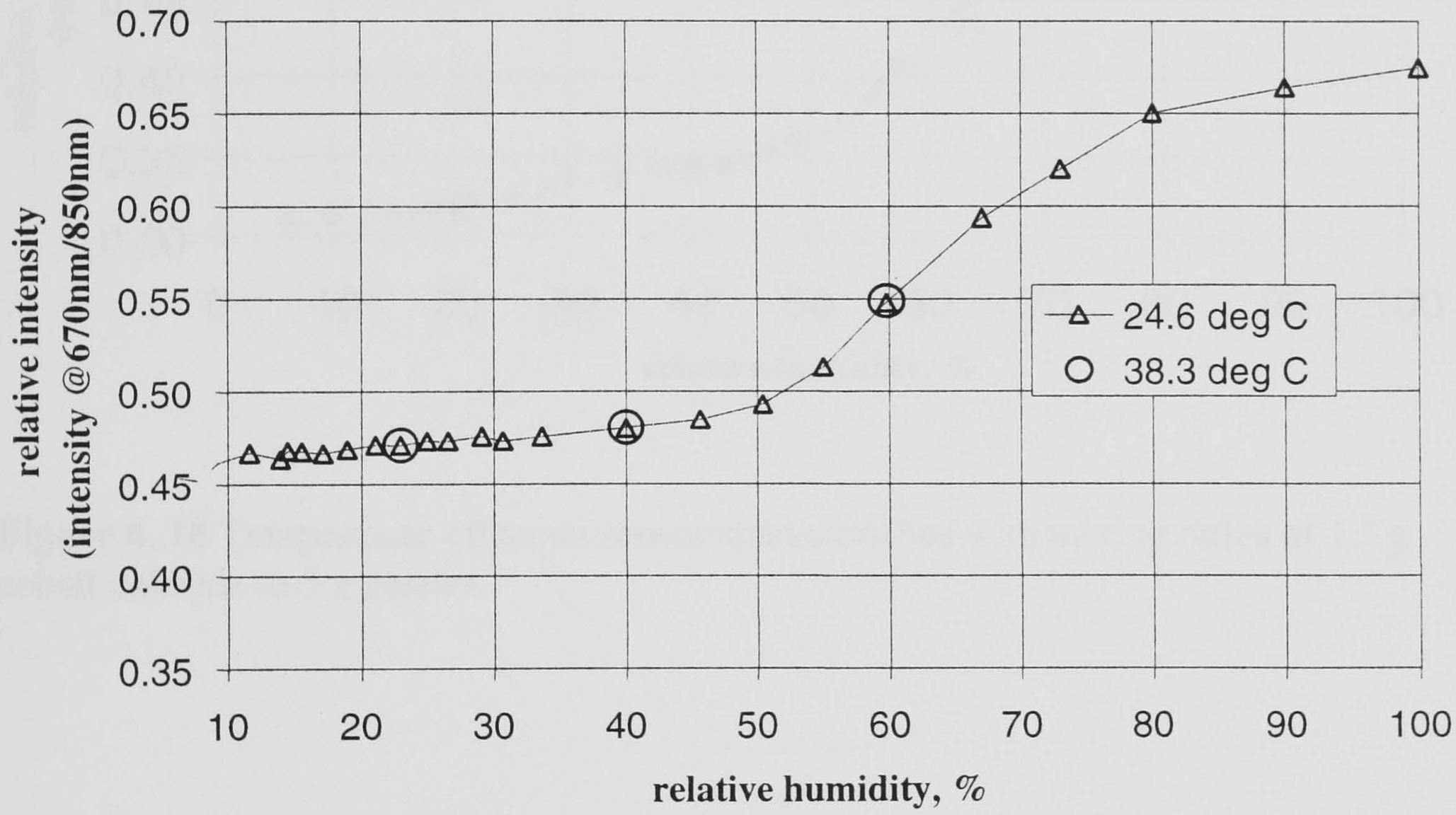

Figure 6. 17 Temperature effect on sensor characteristics with mixing ratios of 0.6 g cobalt chloride to 3 g gelatin. Each point represents an average of 1000 readings.

From Fig. 6.18 it can be seen that the temperature effect is negligible over the temperature operating range.

The same was repeated for sensor 2 with mixing ratio of 1.5 g cobalt chloride to 3 g of gelatin. Again while keeping relative humidity constant the temperature was varied.

Variation of relative intensity was noted. This was repeated at 3 different humidities. These results together with previously obtained data are plotted on the same graph as shown in Fig.18.

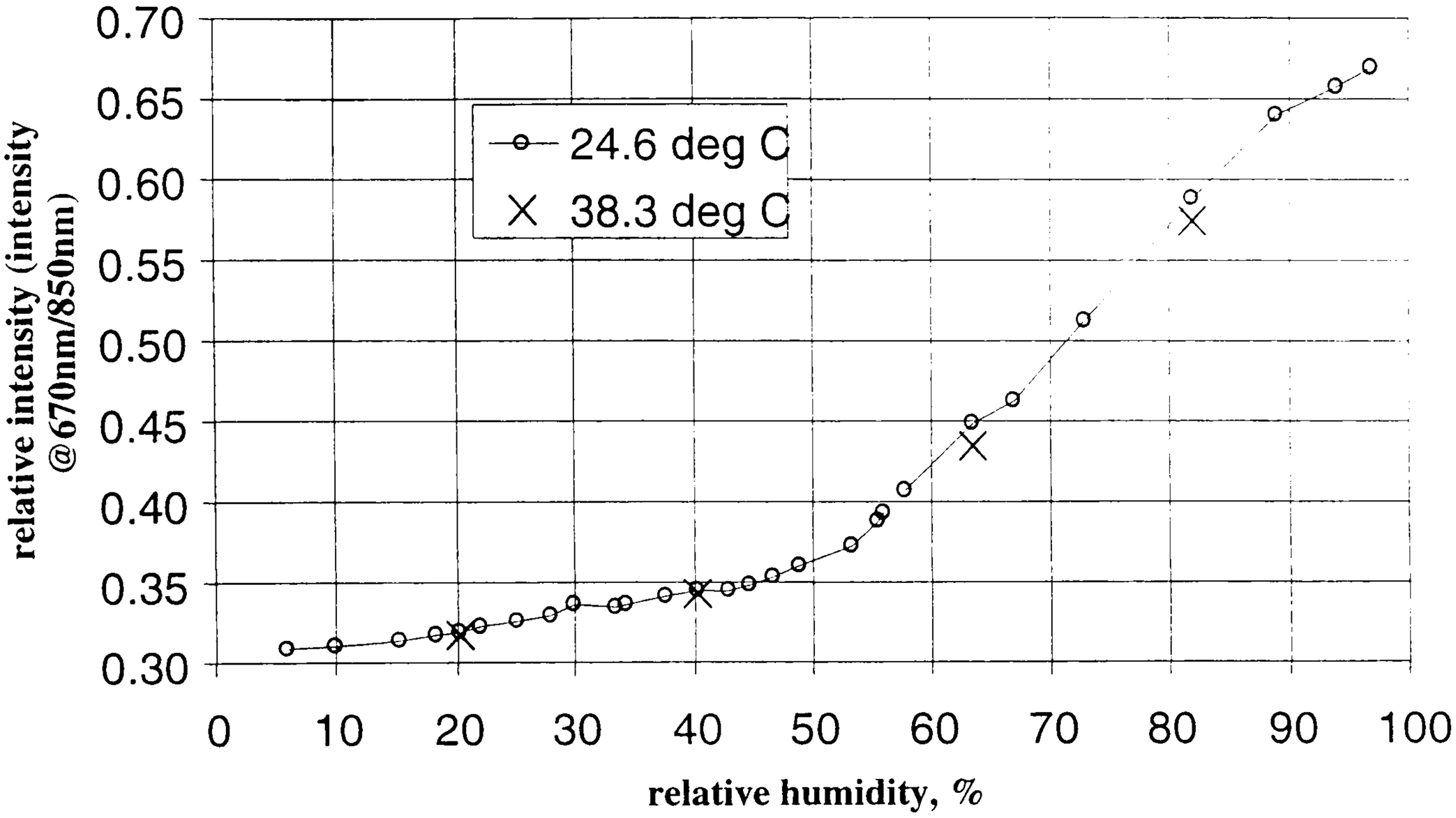

Figure 6. 18 Temperature effect on sensor characteristics with mixing ratios of 1.5 g cobalt chloride to 3 g gelatin.

It can be seen from Fig. 6.17 and Fig. 6.18 that while the temperature had no discernible effect on sensor 1 it showed a slight effect on sensor 2. This could be translated to about 1% RH for every 13.7 °C.

The effect of temperature on the sensor behaviour can probably be explained as follows.

The amount of water molecules available within the film to combine with cobalt chloride is a function of relative humidity with negligible temperature effect in the case of sensor 1. Whereas temperature has some small effect in the case of sensor 2. This

gives a temperature coefficient for sensor 2 of less than 1% RH per about 14 °C. This in a way is similar to the relationship between the equilibrium moisture content (percentage of water weight to the total weight), temperature and relative humidity for various materials.

For example, Agrawal *et a*l found that for peanut pods, the moisture content increased at a given relative humidity as temperature increased (Agrawal *et al* 1971).

Barker reported that as temperature increased, the equilibrium moisture content of lint decreased for constant values of relative humidity up 85%. For temperatures greater than 47 °C and relative humidities above 85%, the moisture content increased with increasing temperature (Barker 1992).

For dried apple, Roman *et al* reported that the equilibrium moisture content decreased for constant values of relative humidities as temperature increased over 20-60°C range (Roman *et al* 1982). Different relationships existed between moisture content and relative humidity for several carbon Phenolic composites as reported by Stoke (Stokes 1992). It has been generally found that the moisture content of nylon-6,6 is a function of relative humidity only i.e. independent of temperature (Hunt 1980). The equilibrium moisture content for epoxy resin film has been found to be strongly dependent on relative humidity but is only marginally dependent on temperature (Davis and Sims 1983) as shown in Fig. 6.20.

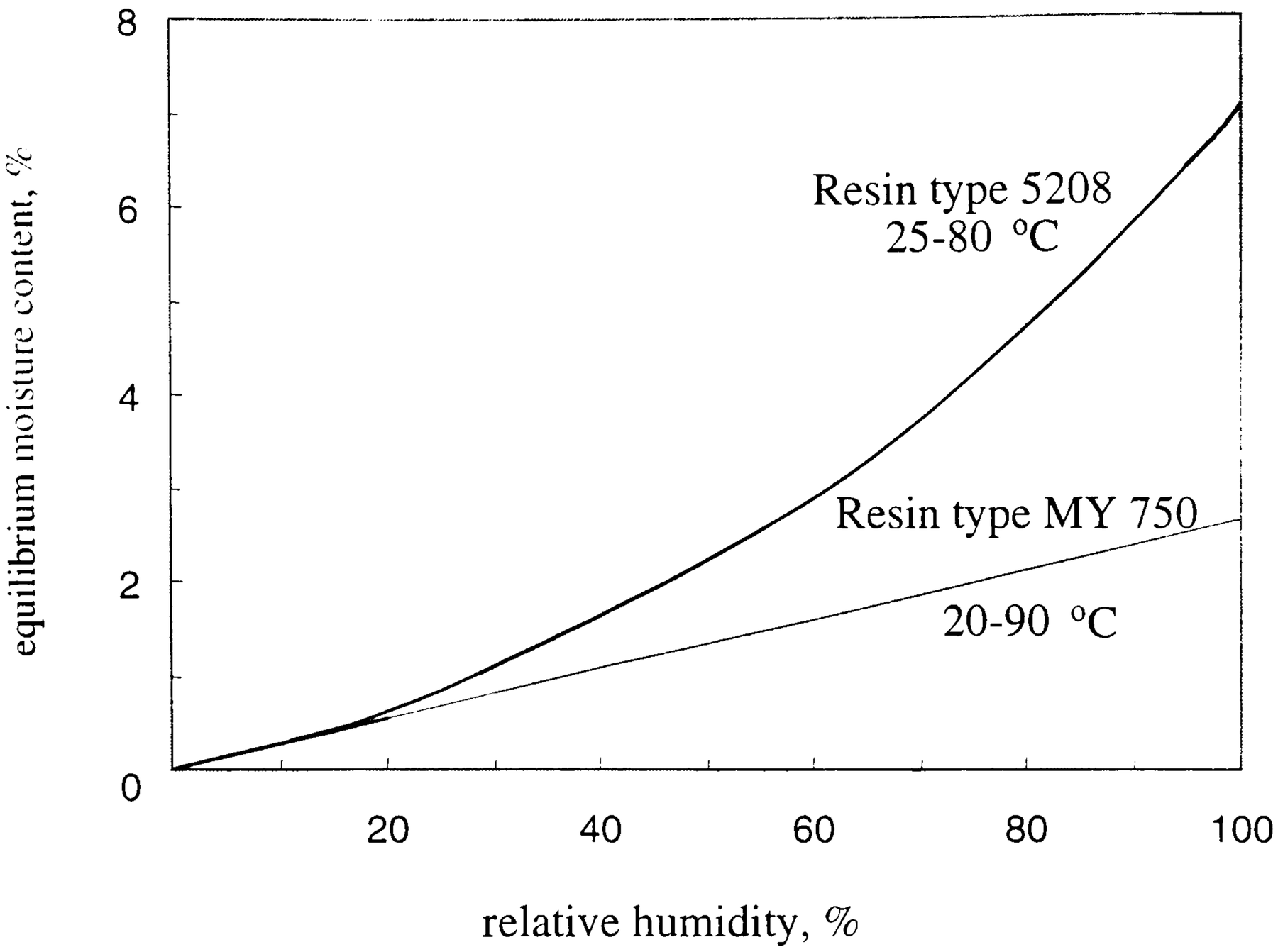

Figure 6. 19 Relationship between equilibrium moisture content, relative humidity and temperature for two epoxy resins (Davis and Sims 1983).

It can be concluded from above that different relationships exit between moisture content and relative humidity, at different temperatures, for different materials. It is possible to have a material whose equilibrium moisture content is a function only of relative humidity and is independent of temperature. This implies that negligible temperature coefficient for a sensor which relies on the equilibrium moisture content to measure relative humidity is possible. However, moisture content behaviour can be taken as a rough guide to predict the viability of a certain material as an immobilising agent. For a colorimetric sensor what matters most is the relationship between relative humidity and the response of the sensor. In such a case the relationship between the sensor response and the equilibrium moisture content could be a complex one. Many more experiments are needed, involving several different materials, to establish such a relationship. Furthermore, as found earlier, the concentration level of the reagent plays

an important role in determining the relationship between the equilibrium moisture content of the resulting film, relative humidity and temperature..

6.4.3 Time constant

A stabilised light source operating at 670nm wavelength and a light detector have been built to measure the time constant of the sensor. Fig. 6.20 shows the circuit diagram of the transmitter and receiver.

The basic function of circuit (a) is to provide a variable stable constant current to LED D3. The current value is controlled by the voltage (V1) present at pin 3 of IC1. This voltage can be adjusted by VR1 to a value in the range 0 to 1.23V thus providing a current in the range 0 to 80 mA. A band gap voltage reference is used to provide a stable voltage reference of around 1.23 V.

Fig.6.20 (b) shows the circuit diagram of the photodetector. The output voltage of the circuit is given by Vout = $I_{pd} \times VR2$. The gain of the circuit can be controlled by VR2.

LED D3 and the photodiode D4 were housed in an SMA receptacle to enable easy connection to the sensor terminals.

The time constant of the sensor, defined as the time taken to reach 90% of its final value, was measured by connecting the sensor to the source and detector above. The output of the detector was connected to an oscilloscope. The sensor was then exposed to two moisture streams (70% RH and 20% RH) alternately. The output of the detector circuit is shown in Fig. 6.13. The graph shows the rise and recovery time of sensor 1 (see Table 6.3). It can be seen that the rise and recovering times are less than 0.5 sec.

The thickness of the film of sensor was 230nm (measured using the surface texture measuring instrument used in section 6.3). Lower time constants could be achieved if thinner film was used.

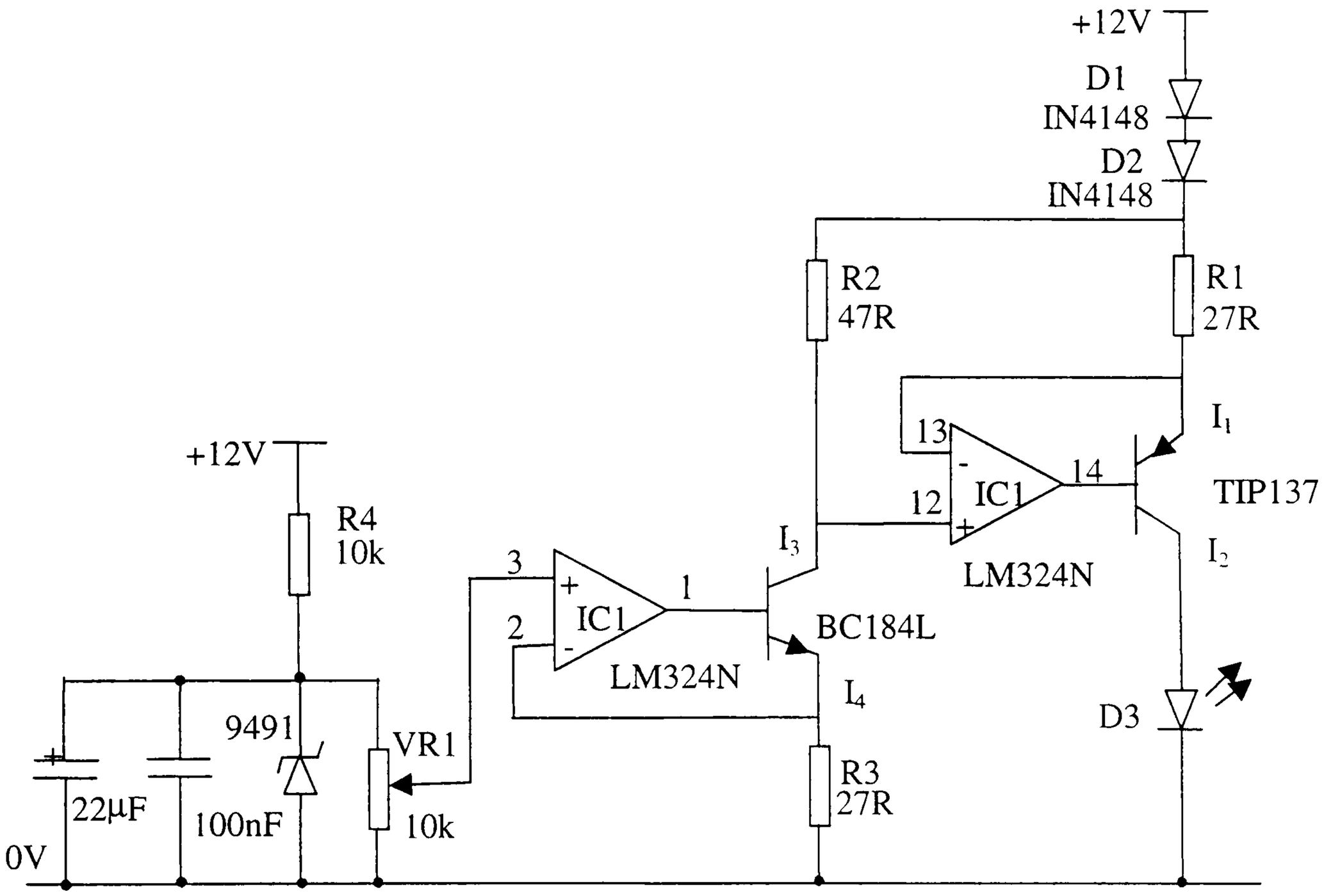

(a)

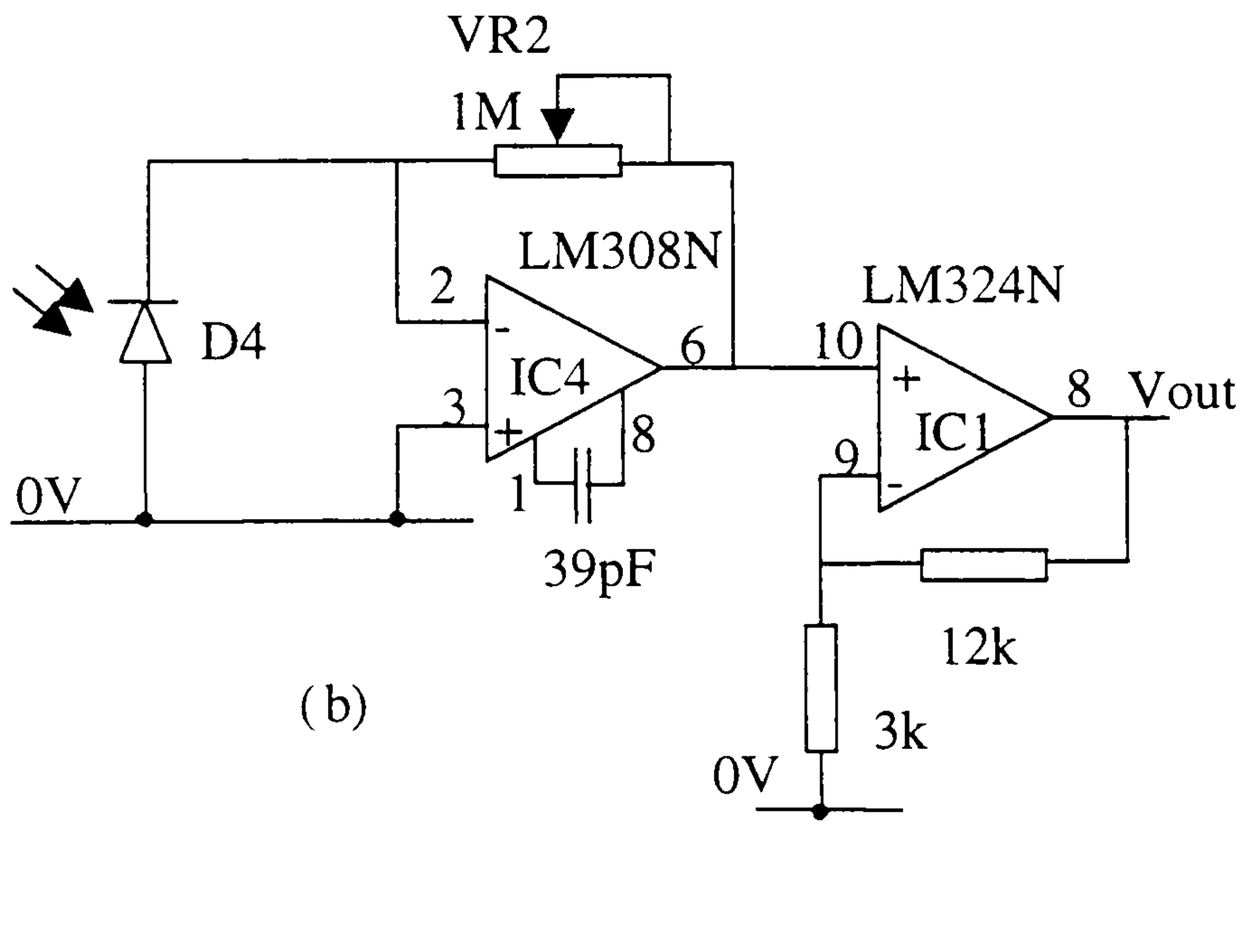

(b)

Figure 6. 20 Circuit diagram of (a) 670 nm source and (b) detector.

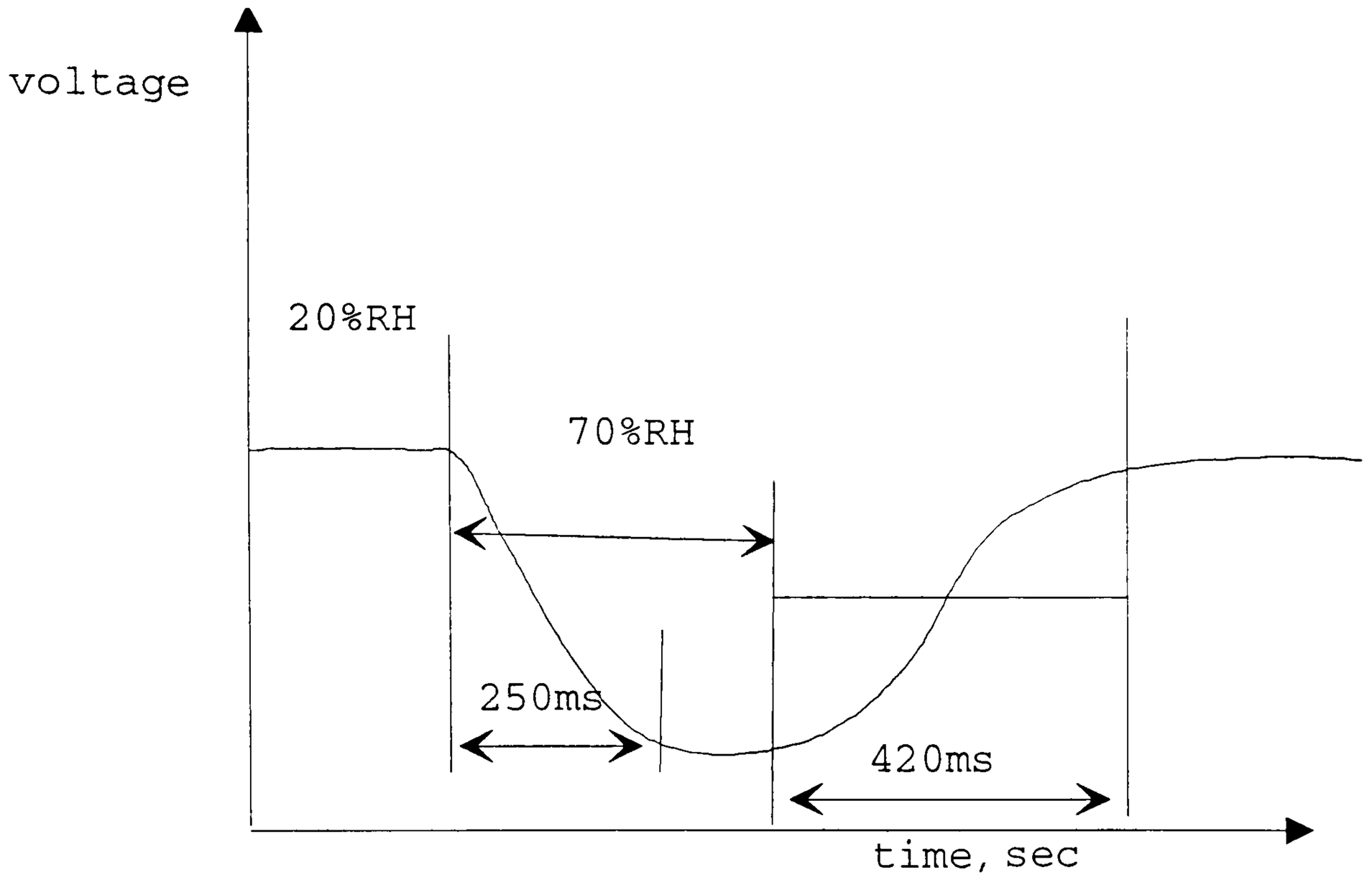

Figure 6. 21 Time response to changes of humidity from 20% to 70% RH.

6.5 Portable sensing system

A system based on LEDs and photodiodes was built to replace the spectrum analyser and the white light source. This provides portability and goes some way in evaluating the commercial viability of an optical fibre sensing system based on colorimetric reagents. Fig. 6.22 shows a block diagram of the system.

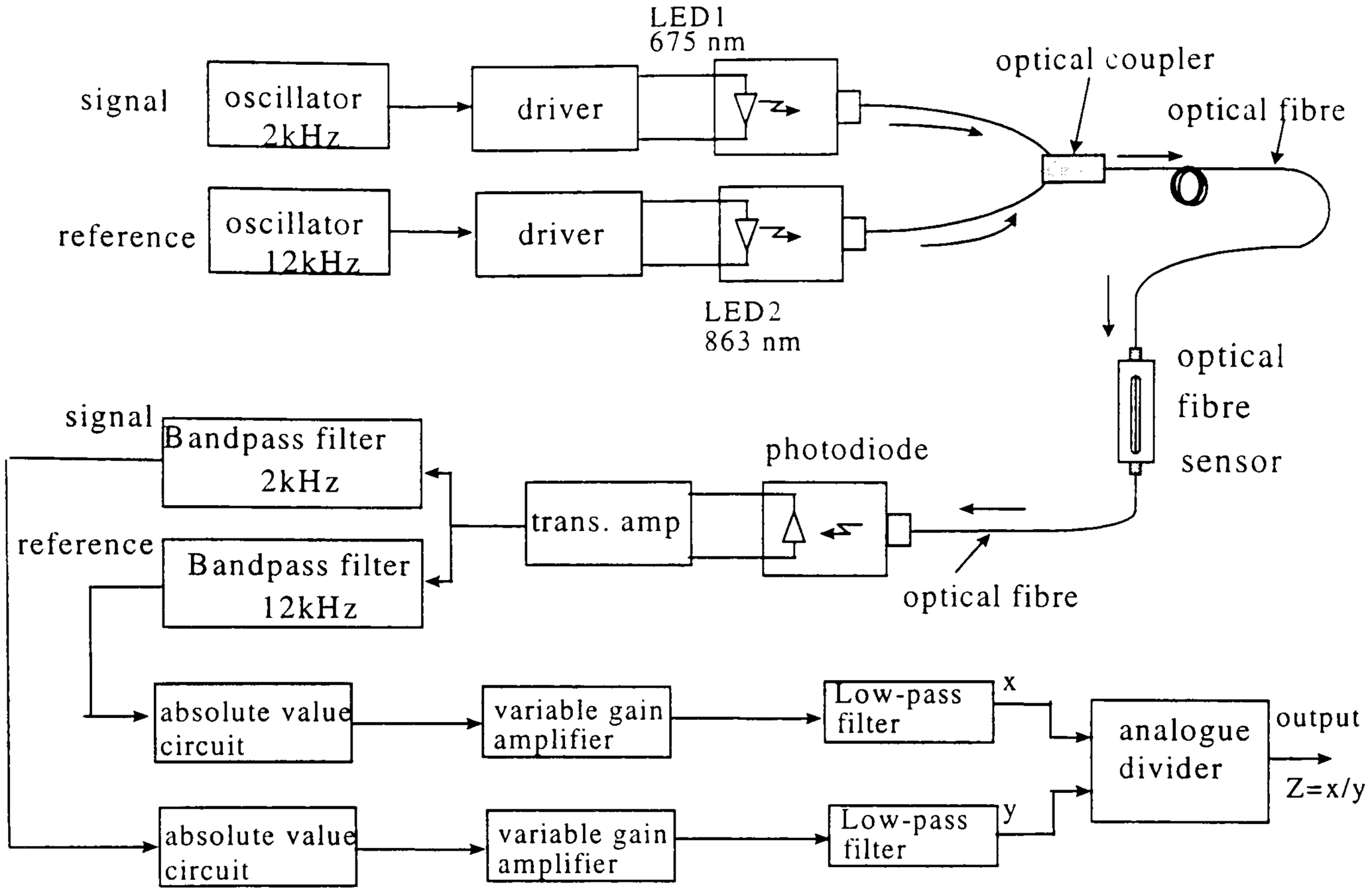

Figure 6. 22 Block diagram of the portable optical fibre humidity sensor.

6.5.1 Source

The light source for the system is provided by two LEDs. One operates at a wavelength of 675 nm (visible) and the other at a wavelength of 863 nm (infra-red). The two LED's are driven by separate accurate voltage-to-current converters and are modulated by two sinusoidal voltages generated by two precision function generators ICs (ICL8038), supplied by Harris Semiconductor. The visible light LED was modulated at 2 kHz, and forms the signal, while the infra-red light LED was modulated at 12 kHz, and forms the reference.

6.5.2 Optical coupler

The outputs of the two LED's are then combined into a single fibre by a 2-to-1 optical coupler. The output of the coupler is connected to a long fibre to ensure equilibrium mode distribution at the sensing point.

6.5.3 Detector

The light leaving the sensor is collected by another optical fibre and fed to a photodiode, as shown figure 6. The photodiode converts the optical signal into an electrical form. Using an 8-pole band pass filters, built around MAX274 IC, supplied by Maxim, the measurand and the reference parts of this signal were separated, i.e. into 2kHz and 12kHz signals. These two signals are then rectified by separate absolute value circuits. The rectified signals are converted into their equivalent dc values (averaged over 0.1 s) by two low-pass filters. The ratio of the two dc values (i.e. the measurand signal divided by the reference signal) was obtained using an analogue divider built around AD538 IC, supplied by Analogue Devices. The output of the divider was a measure of relative humidity.

6.5.4 Sensing element

In order to protect the optical fibre sensing element it was fitted in a protective brass casing as shown in figure 6.23. Two optical fibre SMA connectors were fitted, one at each end of the sensing fibre, and secured in the assembly. Four ventilation slots were incorporated to allow air to get to the sensing fibre. In this way the sensor could be connected to long optical fibres by means of in-line connectors.

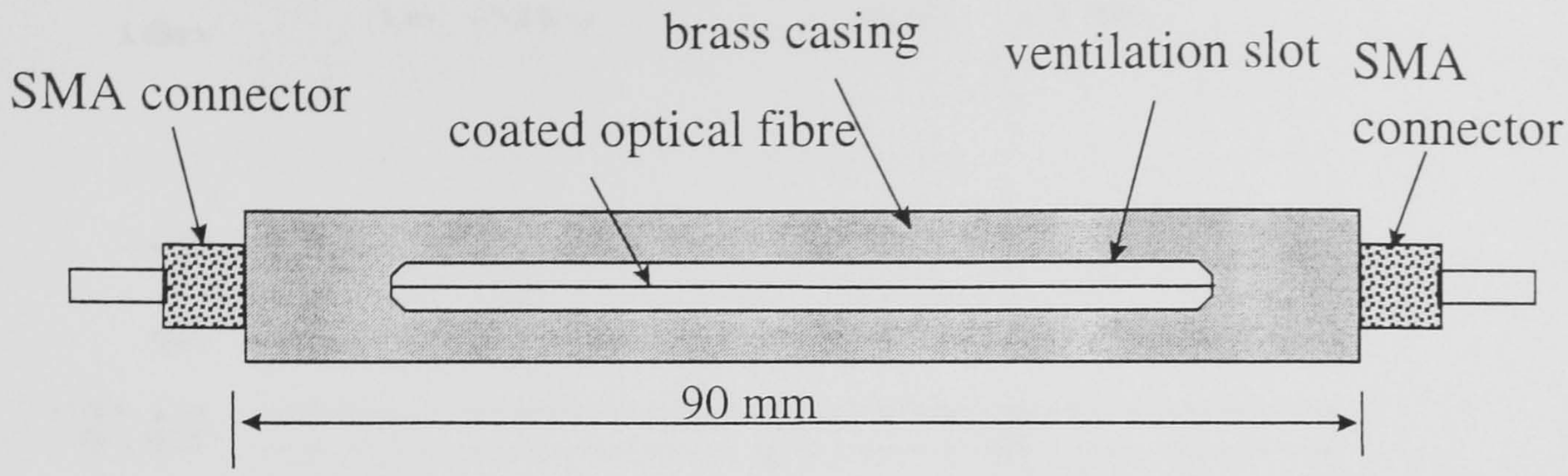

Figure 6. 23 Sensor element.

6.5 Referencing scheme

Two LEDs are used to provide the light source to the system. One operating at the signal wavelength which is modulated by humidity variation while the other is not which is used as a reference. The sensing element was placed in the humidity chamber and the output spectra was recorded. Relative humidity was altered and a second spectra was obtained. It can clearly be seen that while the peak power at 858 nm stayed constant the peak at 676 nm varied with humidity as shown in Fig. 24 below.

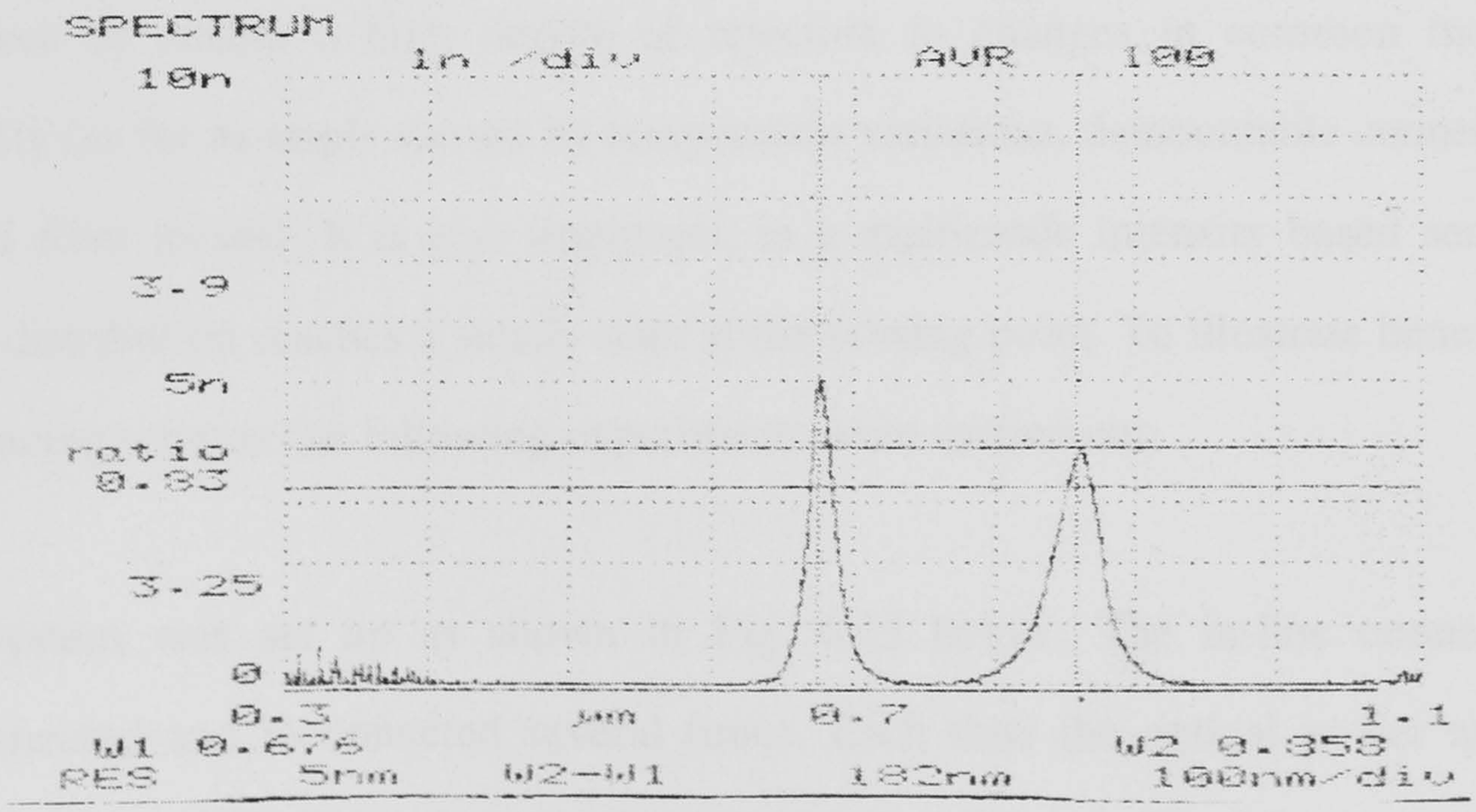

(a)

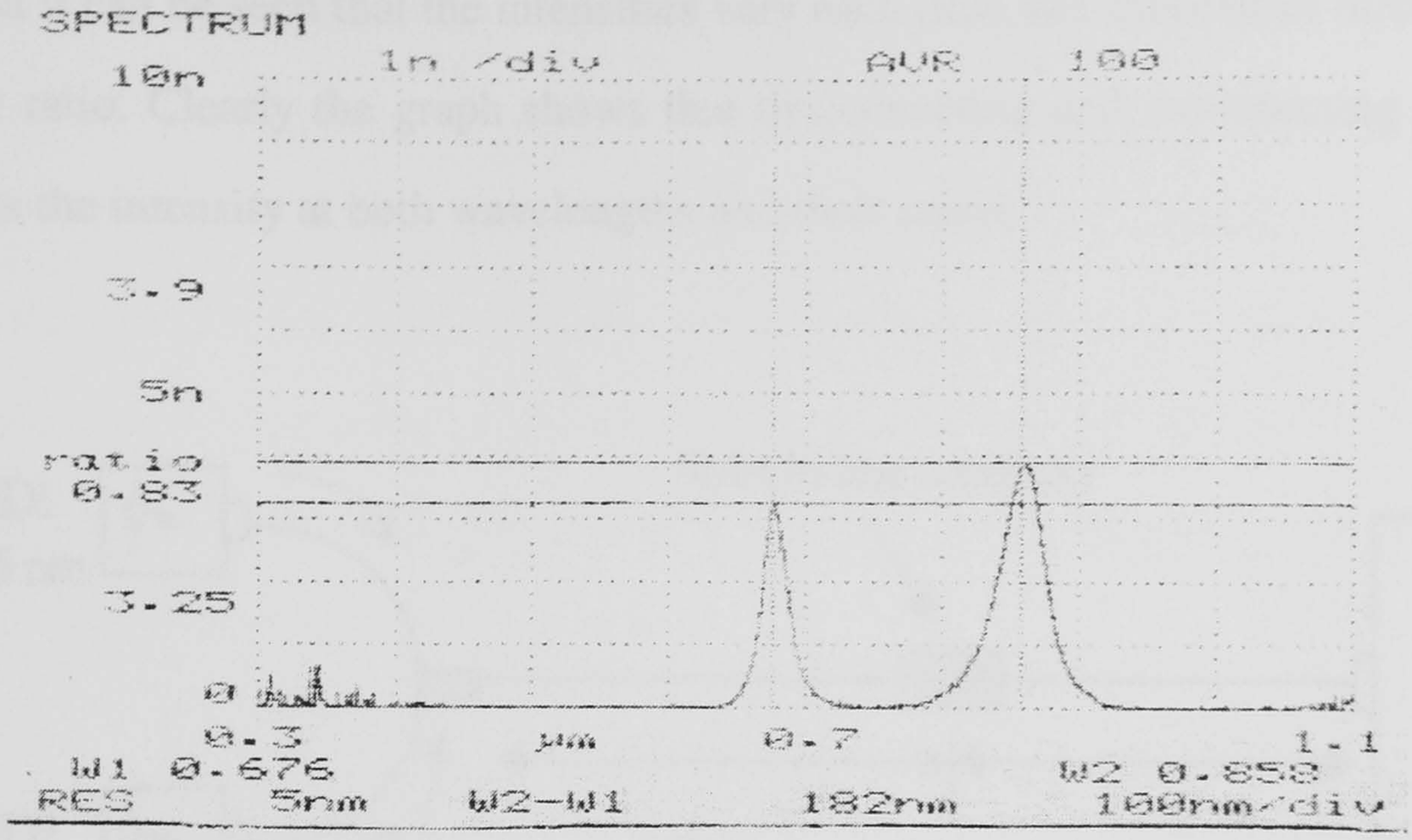

(b)

Figure 6. 24 Spectra of light through the sensor (a) at 70 % RH (b) at 40% RH.

As mentioned earlier, humidity affects the spectral absorption of the sensor in the wavelength region 550-740 nm. This can clearly be seen from Fig. 6.24. Hence a second wavelength outside this region (at, say, 850 nm) can be used to provide an intensity reference to enable a high degree of rejection to changes in common mode light intensity (as for example caused by temperature variations, demountable connectors and optical fibre losses). It is also important, in a multimode intensity based sensor, that mode distribution reaches a steady state at the sensing point. To illustrate benefit of this referencing scheme the following experiments were carried out.

The system was set up as shown in Fig. 6.25 below. The in-line connector was disconnected and reconnected several times. Each time the optical power at the two wavelengths were tabulated. A graph of the intensity obtained and the ratio of the two intensities (intensity at 670 nm/intensity at 850 nm) is shown in Fig. 6.26. From the

graph it can be seen that the intensities vary each time and this causes direct variation in their ratio. Clearly the graph shows that disconnecting and reconnecting the connector alters the intensity at both wavelengths and their ratios.

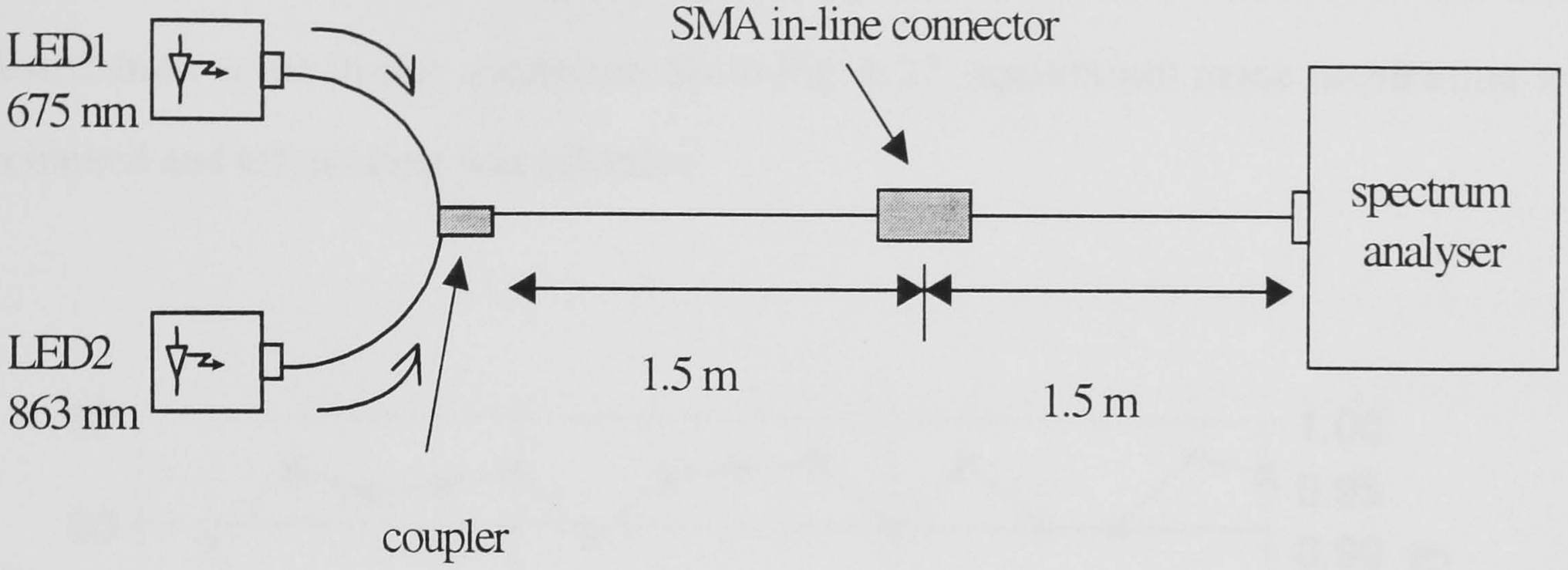

Figure 6. 25 Experiment set up to examine dual wavelength referencing scheme.

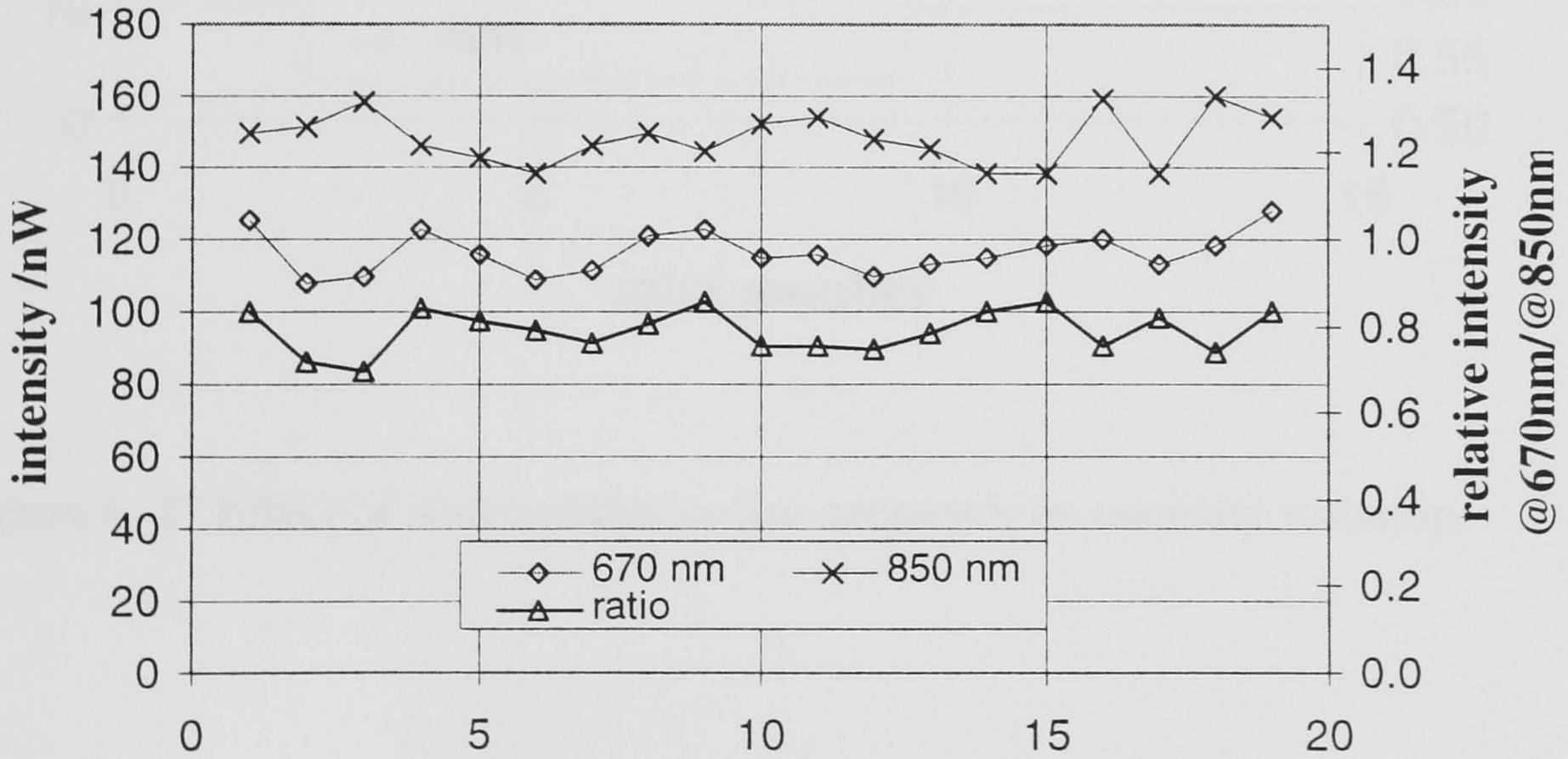

Figure 6. 26 Effect of demountable in-line connector on intensity variations.

Now a 7 m long optical fibre was inserted between the optical coupler and the in-line connector. The results are plotted in Fig. 6.27, It clearly shows that although the intensities vary each time their ratios remain comparatively constant. These results also support the fact that mode equilibrium is necessary before the sensing point. The fact that in Fig. 6.25 no referencing was achieved is due to the random nature of the mode distribution at the in-line connector. So in Fig. 6.27, equilibrium mode distribution was achieved and referencing was effective.

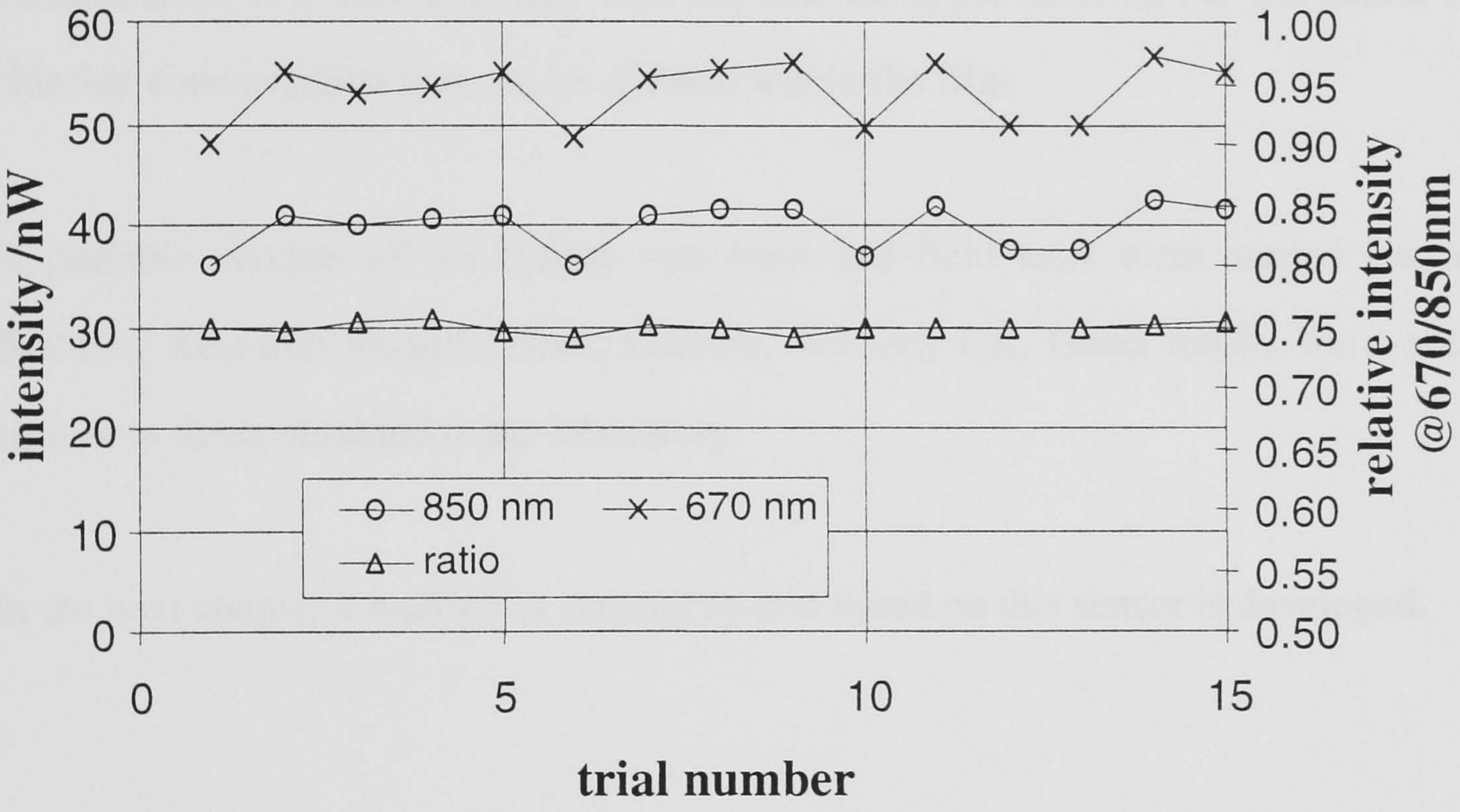

Figure 6. 27 Effect of demountable in-line connector on intensity variation.

The portable system described here was used to carry out humidity measurements in an environmental test room at the Building Research Establishment (BRE), Garston, Watford. The result of these tests were published at the third international symposium on humidity and moisture hosted by NPL. A copy of the paper is in Appendix i. Good and repeatable response was obtained across the whole range including values below 20% RH.

6.6 Summary

In this chapter an optical fibre humidity sensor based on gelatin/cobalt chloride has been developed and tested. The sensor employs two wavelength referencing scheme. Reproducible results were obtained over 20% to 80% range. The temperature coefficient of the sensor was found to be dependant on the concentration of cobalt chloride within the gelatin film and can be made negligible. The responsivity of the sensor increased with increasing the cobalt chloride concentration. However, the refractive index of the cobalt chloride / gelatin film was found to decrease at high humidity with increasing concentration of cobalt chloride. This imposed an upper limit on the maximum cobalt chloride concentration that can be allowed within the film.

A portable version of the system was built and field tests were carried out at the Building Research Establishment, Garston, Watford UK. Good results were obtained similar to those obtained in the laboratory.

In the next chapter a multipoint sensing system based on this sensor is developed.

CHAPTER 7

Design, construction and testing of a distributed sensing system

7.1 Introduction

In the previous chapters a single point dual-wavelength humidity sensor has been developed and evaluated. The aim of this chapter is to demonstrate a dual-wavelength multipoint distributed optical fibre humidity sensing system based on the well known Optical Time Domain Reflectometry (OTDR) technique (Barnoski *et al*, 1976, Mair and Seeger 1995). The theory of operation and the design considerations are detailed in this chapter.

7.2 Backscatter Technique

The basic problem to be solved when producing a distributed optical fibre sensing system is simultaneously to provide information on both the position of the measurement and the quantity to be measured. Most of the truly distributed sensors make use of the differential propagation time of optical signals, in order to determine the distance to the measurement point.

In an OTDR a high intensity, a short duration light pulse is launched into an optical fibre. As the pulse travels through the fibre it gets attenuated due to scattering and absorption (see Chapter 3 section 3.5.1), the scattering occurring in all directions. But mainly in the forward direction. The backscattered amount of scattered light is inversely

proportional to λ^4. A fraction of the backscattered light gets captured and guided back through the fibre (see Fig.7.1). The power backscattered at any point in the fibre depends on the energy of the forward travelling pulse. The pulse experiences some attenuation as it propagates through the fibre thus its power diminishes and so does the received backscatterd power. For a fibre with a constant attenuation along its length an exponential backscattered waveform is observed. Analysis of this backscattered light is widely used to estimate the local fibre attenuation and to locate faults and joints (Barnoski *et al* 1977, Tateda and Horiguchi 1989). It can also be used to reveal information on some fibre parameters such as diameter variation (Condiut *et al* 1981).

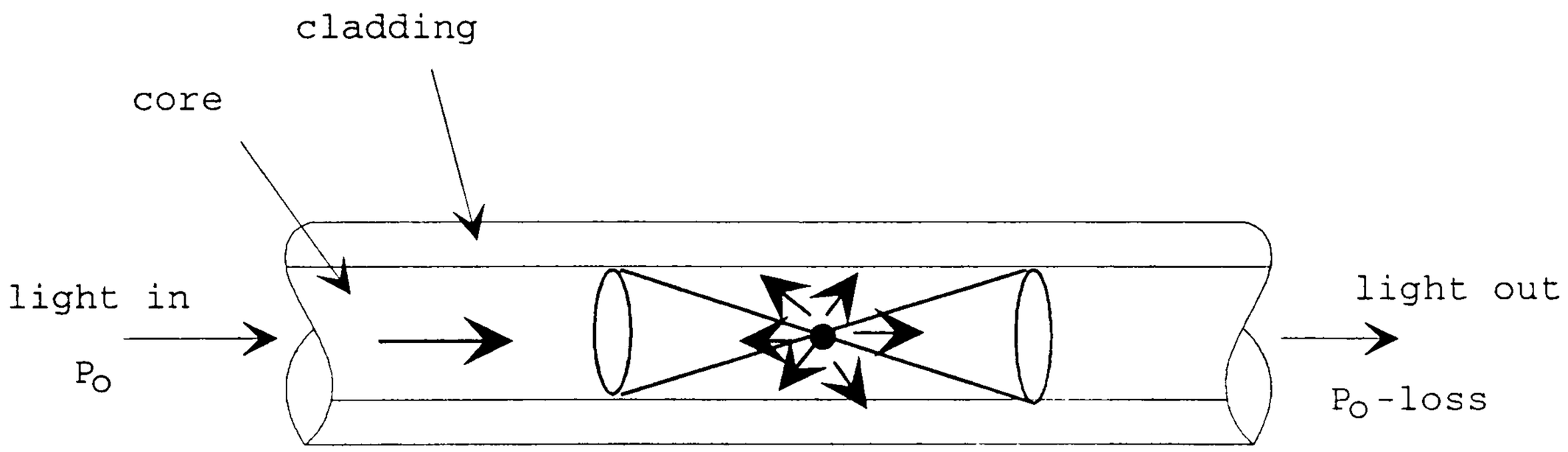

Figure 7. 1 Captured backscattered light

The returned light results from two principal sources:- Fresnel reflections and Rayleigh backscatter reflection.

(i) Fresnel reflections occur whenever there is a change of refractive index within the waveguide (Senior 1992). This is generally caused by poor quality splices or joints, connectors or breaks, etc., along the length of the fibre or fibre ends.

The amount of reflection due to Fresnel reflection, for normal incidence, is given as follows (Keiser 1991):

$$R = \frac{(n_1 - n_2)^2}{(n_1 + n_2)^2} \tag{7.1}$$

where n_1 is the refractive index of the core and n_2 is that of the surround, R is the fraction of the incident light that is reflected.

For silica/air interface the highest possible reflection is from a cleaved fibre is 0.04 or 4%. Non-contacting connectors usually exhibit such a high reflection.

In practice fibre is broken non-uniformly or breaks are soaked in liquid near the refractive index of the fibre core; thus the level of Fresnel reflection varies greatly. Consequently it is inadequate to depend on Fresnel reflection alone for locating faults.

(ii) In modern communication fibres almost all the fibre loss is attributed to the Rayleigh scattering in the glass except in bands associated with an absorbing impurity as mentioned in section 3.2. The Rayleigh scattering coefficient γ_R is given by (Senior 1992) :-

$$\gamma_R = \frac{8\pi^3}{3\lambda^4}(n^8 p^2)(KT_F).\beta_c \tag{7.2}$$

where

n = Refractive Index of core(=n_1 in above)

λ = Optical Wavelength

p = Average Photoelastic coefficient

β_C = Isothermal Compressibility

K = Boltzmann's Constant

T_F = Fictive Temperature.

Based on the above formulae the Rayleigh scattering coefficient was calculated at different wavelengths for a silica optical fibre. The values are plotted against wavelength in Fig. 7.2.

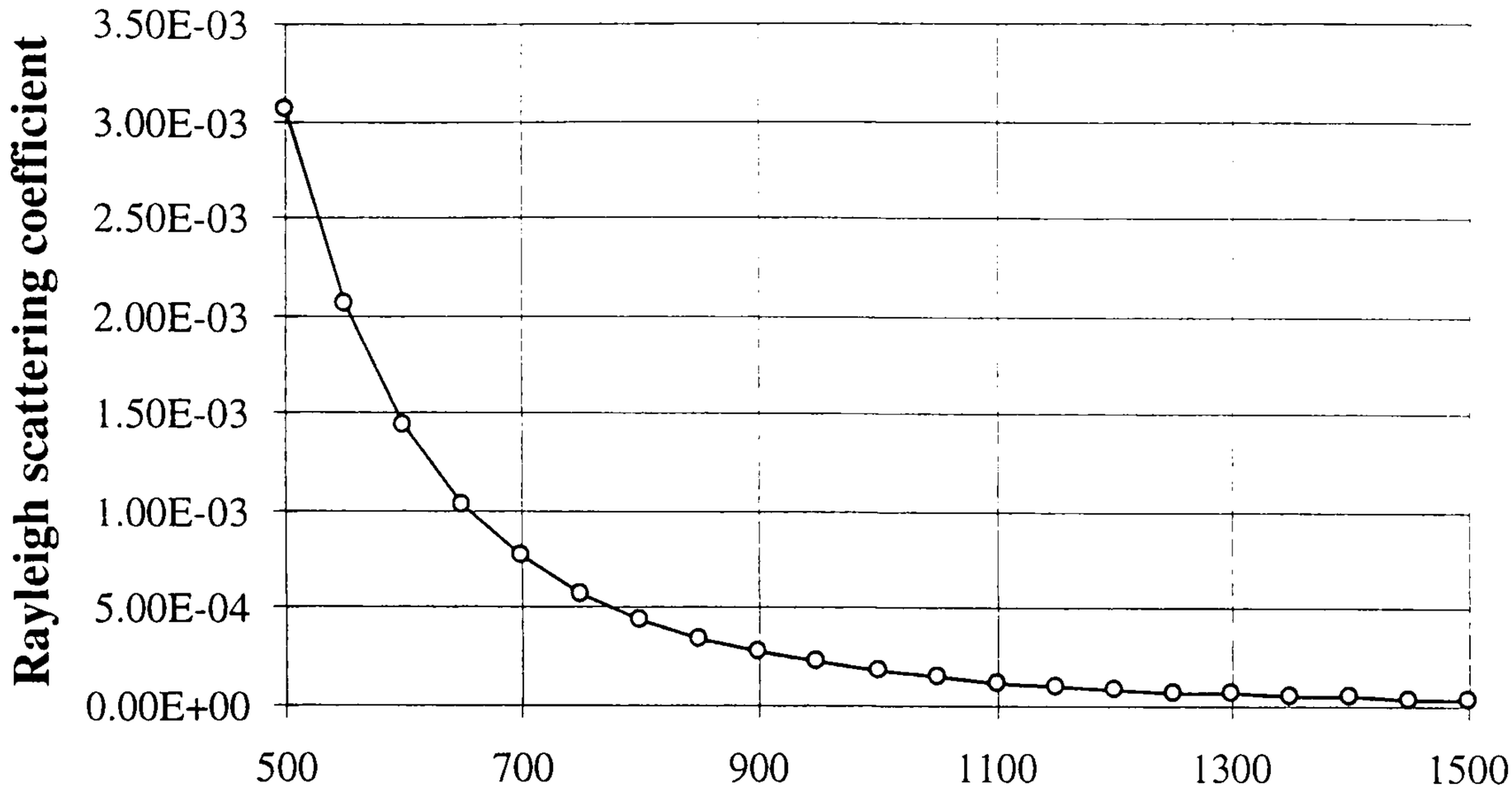

Figure 7. 2 Rayleigh scattering coefficient versus wavelength.

The fibre attenuation, due to Rayleigh scattering is also calculated and plotted against wavelength in Fig.7.3.

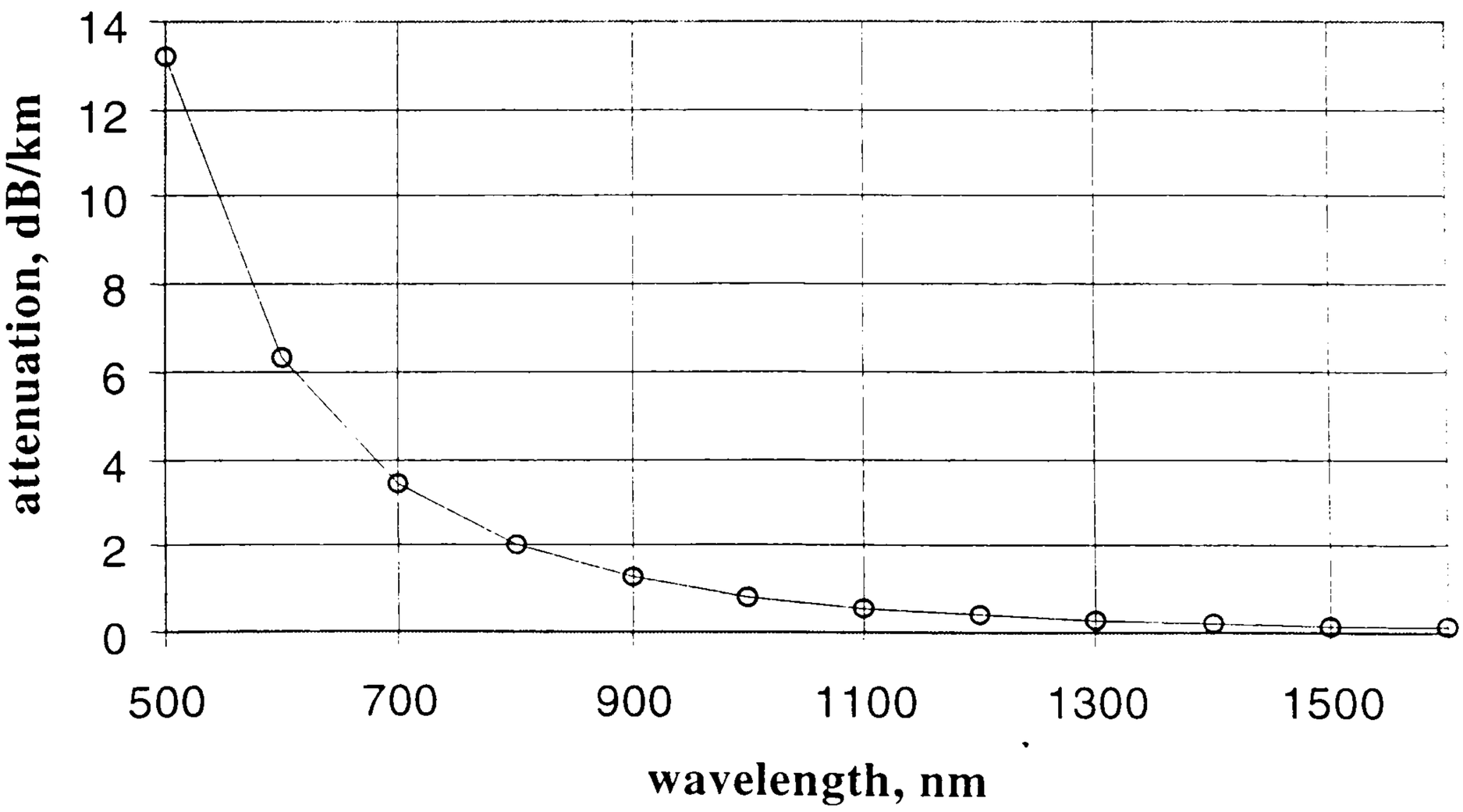

Figure 7. 3 Attenuation of Silica optical fibre, due to Rayleigh scattering, versus wavelength.

The backscatter signal in the fibre is defined by the capture fraction S which, is dependant on the NA of the fibre. The received backscattered light power at time t (P(t)) is defined as follows (Kashima 1995).

$$P(t) = \frac{1}{2} P_0 S \gamma_R W_o v_g \exp(-\gamma_g t) \tag{7.3}$$

$$S = \frac{3}{8} \frac{(NA)^2}{n_1^2} (\text{step} - \text{index multimode fibre})$$

$$S = \frac{1}{4} \frac{(NA)^2}{n_1^2} (\text{graded} - \text{index multimode fibre})$$

$$S = \frac{3}{2} \frac{a^3}{\omega^2 V^2} \frac{(NA)^2}{n_1^2} (\text{single - mode fibre})$$

where P_0 = Peak power of launch pulse

W = Pulse width in seconds

S = Captured fraction of scattered light in the reverse direction.

v_g = Group Velocity in m/s

γ_R = Scattering attenuation

γ = Total attenuation in fibre

n_1 = Refractive Index of core

n_2 = Refractive Index of cladding.

Using the above equations the backscattered light received from various points along an optical fibre is calculated and plotted in Fig.7.4. The calculations are based on the following: Peak power launched 5 mW; pulse width 5 nsec; the optical fibre used is HCS (hard clad silica) with an attenuation of 8 dB/km and 6 dB/km at 670 nm and 850

nm respectively. The refractive index of the core is 1.457 at 633nm (as given by the manufacturer). The refractive indices at 670nm and 850nm were calculated using Selleier formula (Syms and Cozens 1992).

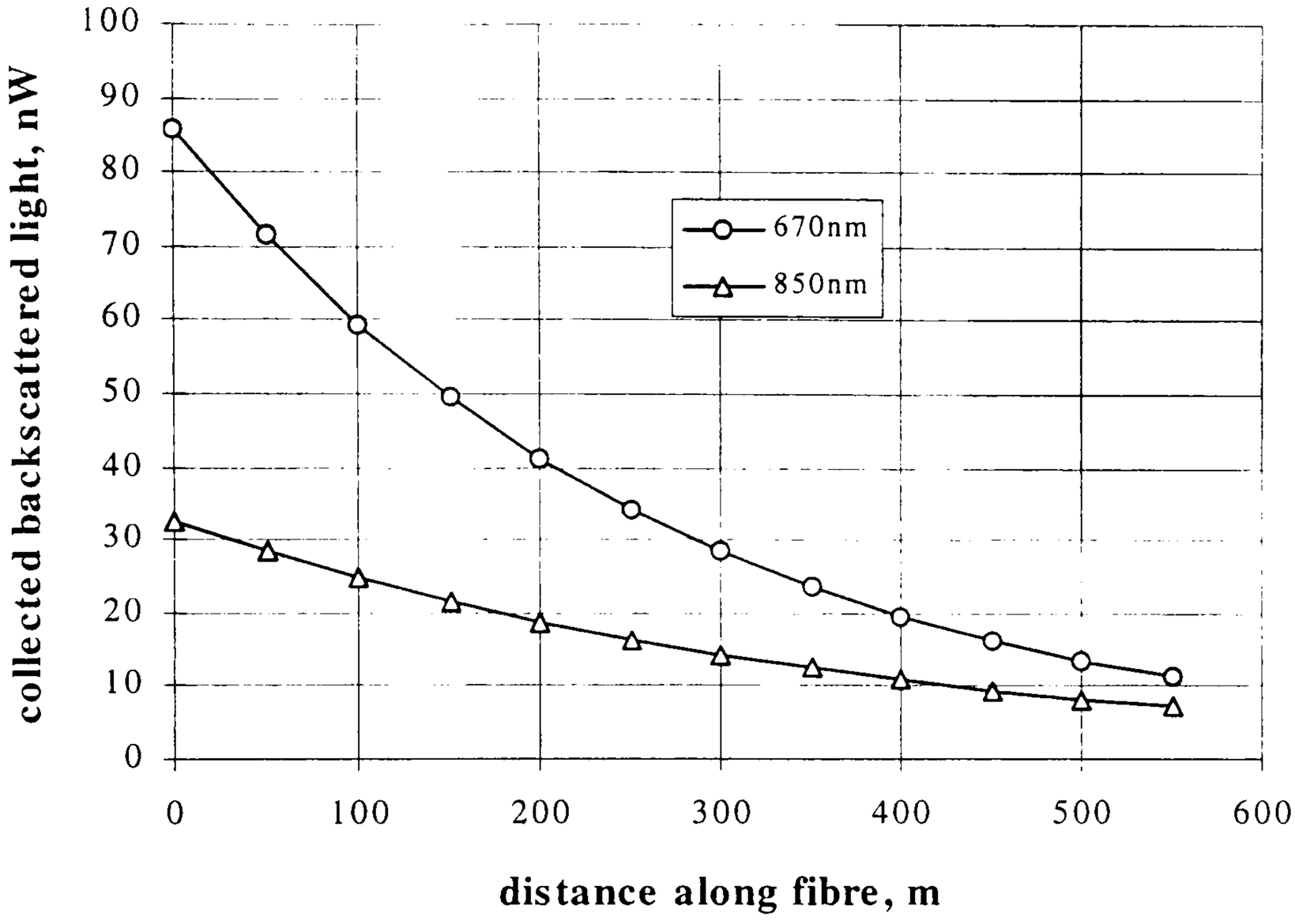

Figure 7. 4 Collected backscattered light along an optical fibre at two different wavelengths.

From the calculations above the following points are noted

1. Backscatter energy is dependent on the energy of the forward travelling pulse at any point.

2. For uniform loss an exponential backscatter waveform is obtained.

3. At joints a sudden drop in backscattered power is obtained.

4. Spikes occur at discontinuities.

5. Collected backscattered signal is strongly dependent on wavelength as illustrated in Fig.7.4.

For an OTDR a decrease in backscatter reduces accuracy. From the Fig.7.4 it can be seen that the received backscattered light, from any point at less than 100 m along the fibre, at 670 nm, is more than 2.5 times that at 850 nm for the HCS fibre used in this work.

6. Mode distribution and launching conditions influence the accuracy of measurement Modes have different path lengths and occupy different parts of the fibre thus having different attenuation.

7. Variation in NA and diameter profile may result in error. The collected backscattered light is a function of both NA and diameter of the fibre.

7.3 Basic operation of OTDR

In section 7.2 above the theoretical background of the backscatter technique was covered. A system that uses the backscattered method is called OTDR. This technique was introduced briefly in Chapter 3 section 3.5.

A basic OTDR configuration is shown in Figure 7.5. The function of the system elements will become clearer over the next few sections. Such a system would produce a signature on an oscilloscope as shown in Fig. 7.6. The horizontal axis is directly proportional to the length of the fibre and the vertical axis is a measure of attenuation. The linear amplitude is usually converted into a logarithmic number and calibrated in dB values.

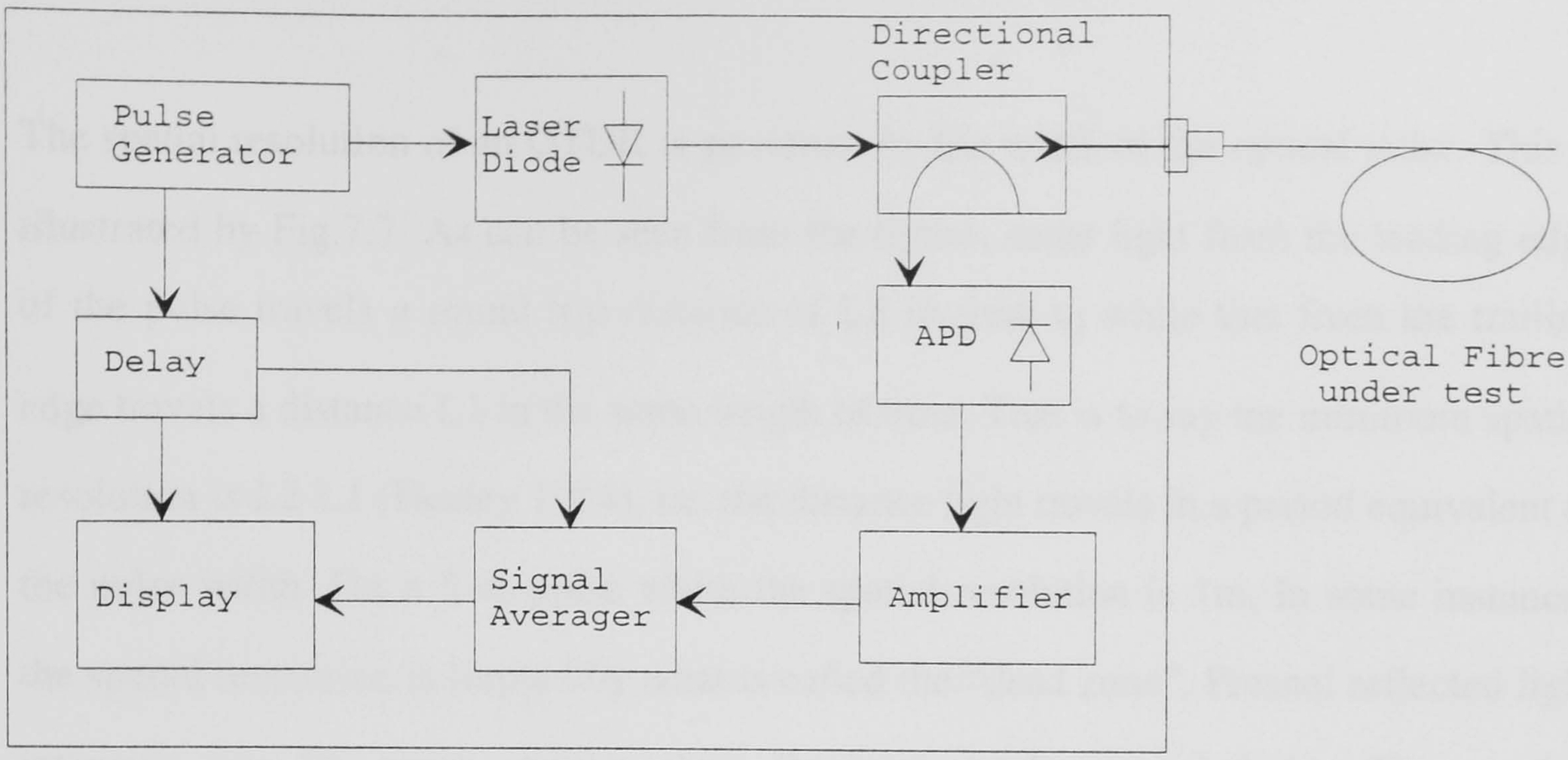

Figure 7. 5 Basic OTDR configuration.

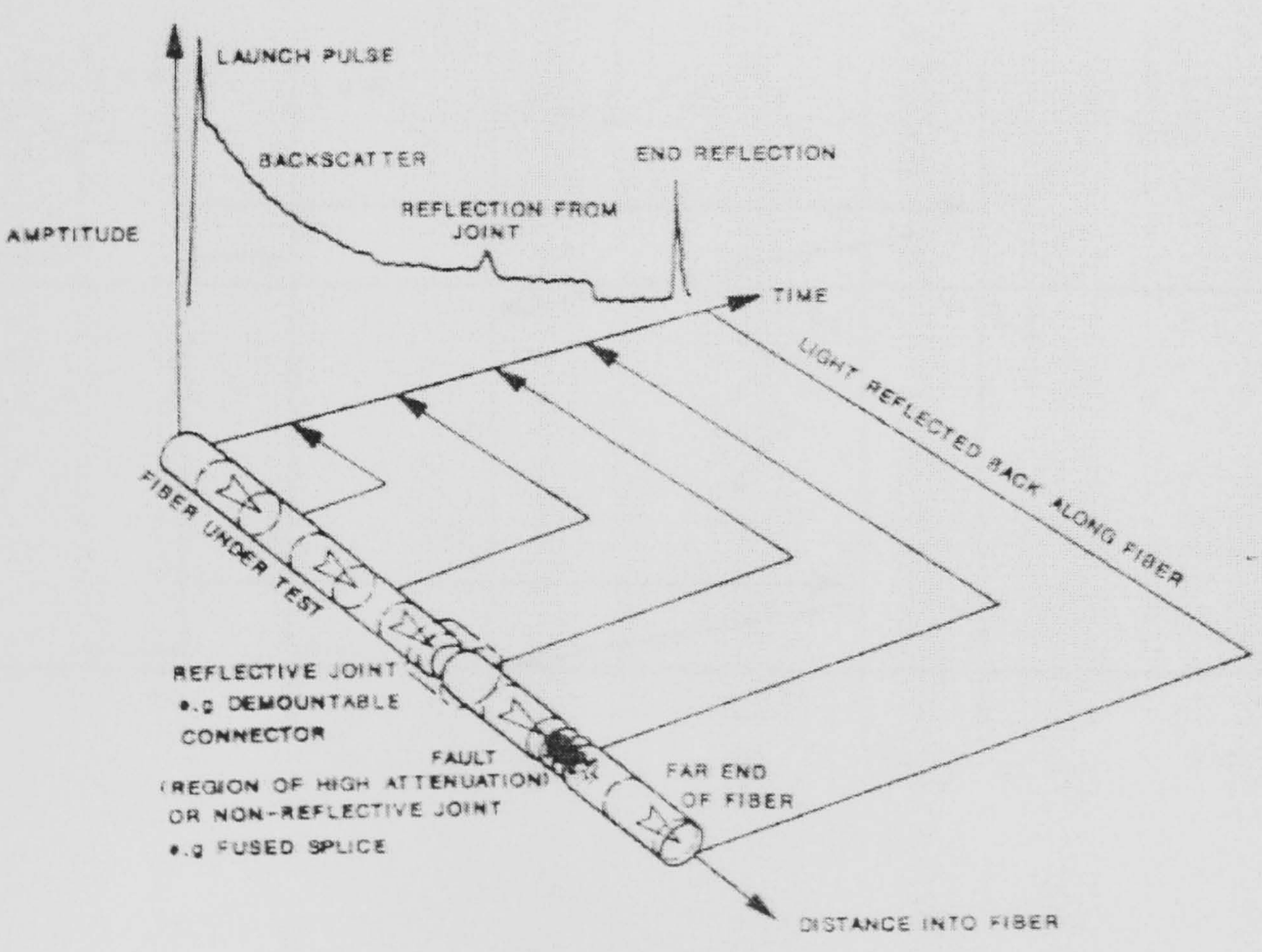

Figure 7. 6 Backscatter signal along the fibre as obtained by the OTDR (Photodyne 1987).

7.3.1 Spatial resolution

The spatial resolution of an OTDR is governed by the width of the optical pulse. This is illustrated by Fig.7.7. As can be seen from the figure, some light from the leading edge of the pulse travels a round trip distance of L2 in time t_0 while that from the trailing edge travels a distance L1 in the same length of time. That is to say the minimum spatial resolution is L2-L1 (Healey 1984), i.e. the distance light travels in a period equivalent to the pulse width. For a 5 ns pulse width the spatial resolution is 1m. In some instances the spatial resolution is limited by what is called the "dead zone". Fresnel reflected light intensity can be much greater than Rayleigh backscattered light. The weaker backscattered light which follows after Fresnel reflected light cannot be detected for a while, and the attenuation characteristics of that region cannot be measured (Tateda and Horiguchi 1989). This region is called a "dead zone".

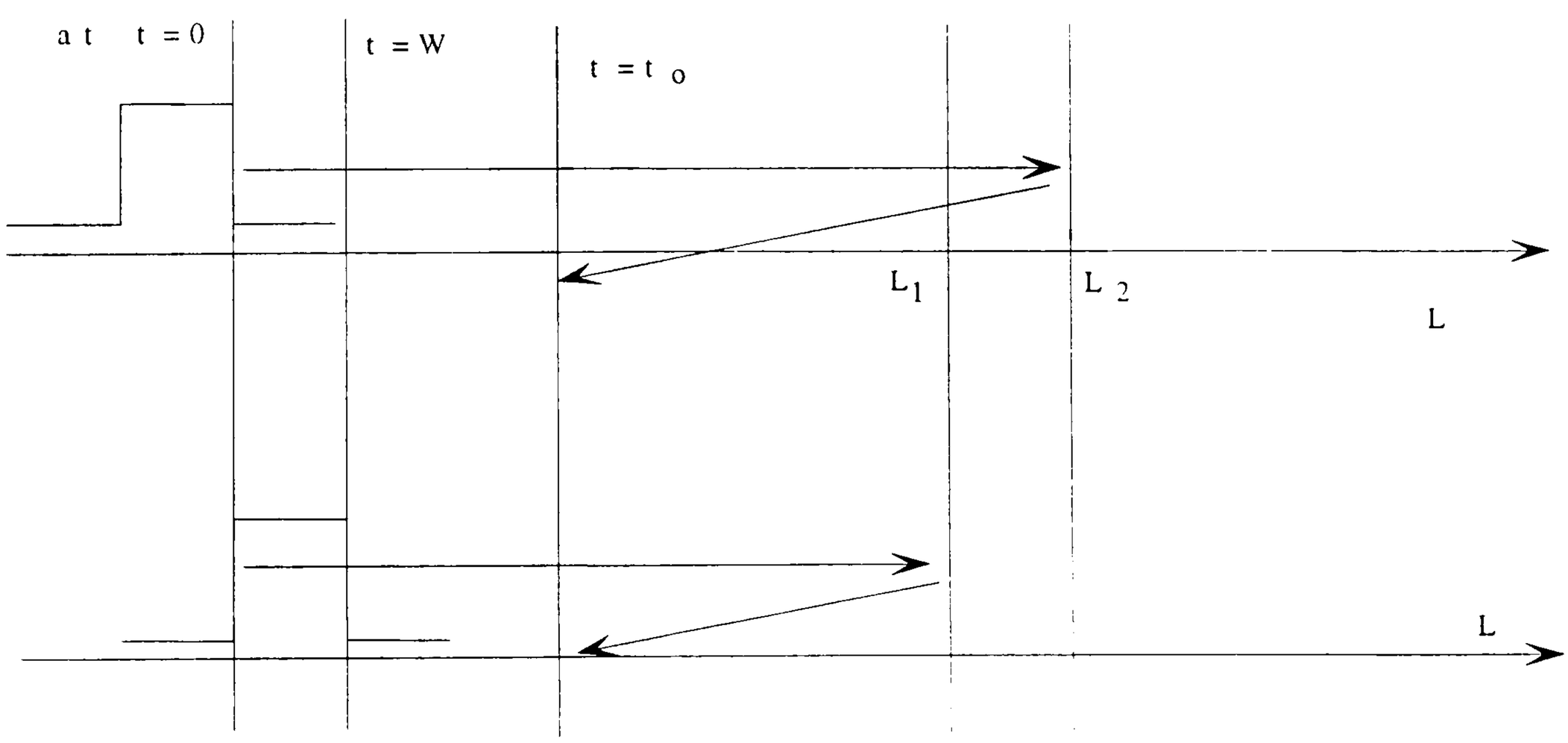

Figure 7. 7 OTDR spatial resolution.

7.3.2 Avalanche photodiode

The avalanche photodiodes came to prominence as a useful device for optical communication once the noise limiting factors of PIN diodes were realised (Wood 1994). This is usually noise in the amplification stage. The avalanche photodiode (APD) has its own built-in gain mechanism, thus providing an increase in sensitivity. This makes them suitable for the detection of the low level backscattering signals involved in OTDR based applications. In APDs, impact ionisation (Bhattacharya 1994) is used as a method of multiplying the photocurrent before it is fed into the next stage of a receiver. However, since the multiplication process is statistical, there is a corresponding increase in the noise level above the level that would result from amplifying only the primary current. For every receiver configuration, an optimum value of the multiplication factor exists which maximises the SNR (Healy 1984). The possible improvement in SNR above a photodiode without internal gain is in excess of 25 dB (Senior 1992).

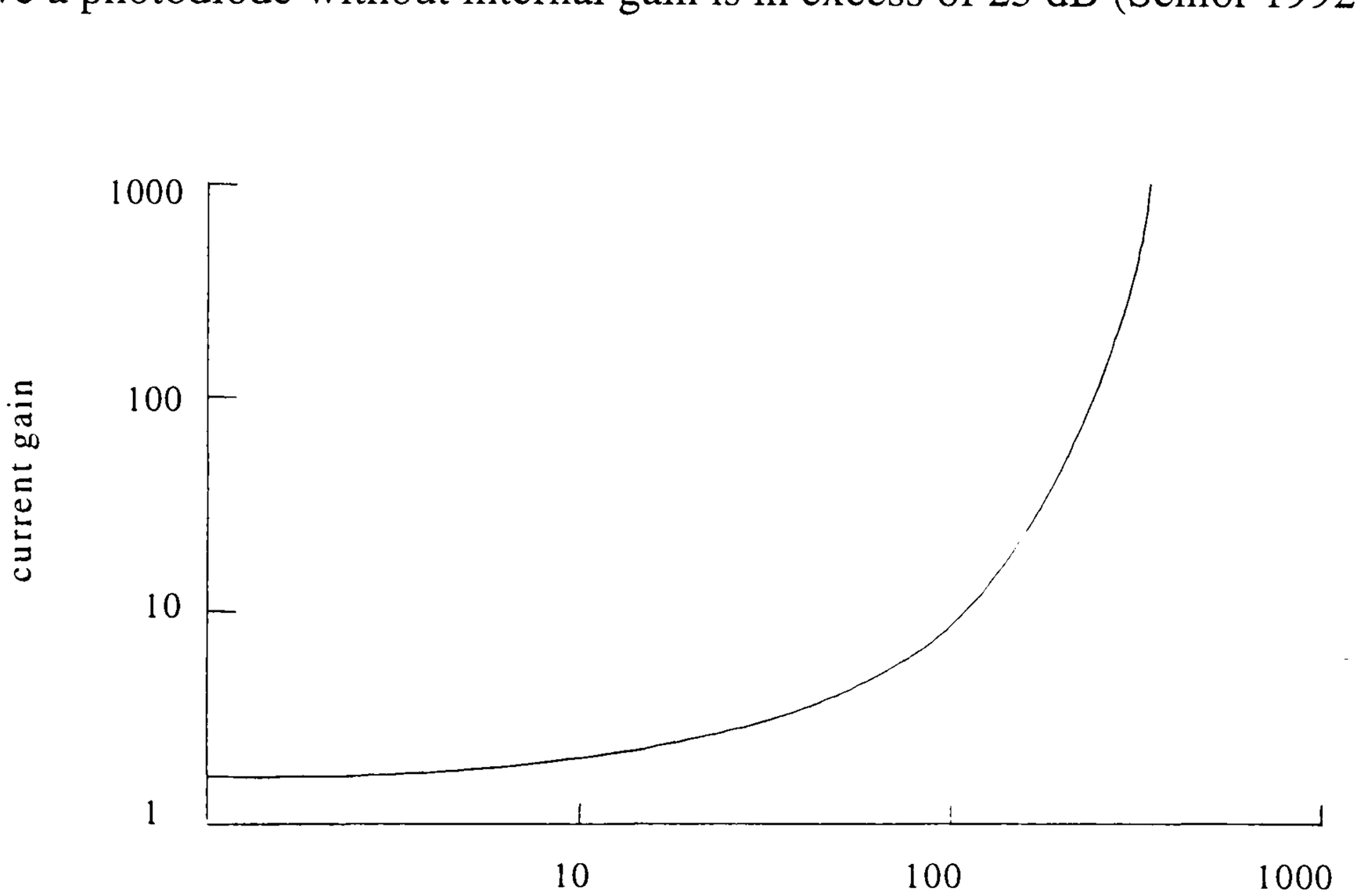

Figure 7. 8 Typical variation of current gain with reverse bias voltage for an avalanche photodiode (Wilson and Hawkes 1983).

The gain of an avalanche photodiode is very sensitive to variation of the bias voltage, as shown in Fig. 7.8, so that it requires the use of a very stable power supply if constant gain is to be maintained. It is also sensitive to temperature change and temperature compensation is normally employed (Wilson and Hawkes 1983). In the work reported here a very stable power supply was used and temperature compensation was employed.

7.3.3 SNR improvement by averaging

The backscattering power level is low so that the signal-to-noise ratio needs to be improved. Applying signal averaging techniques can improve SNR. In this process, SNR can be improved in proportion to the square root of the number of additions, as noise is random (Jones 1978). By using averaging in a digital system, the signal can be recovered with a much greater accuracy than the resolution of the A/D converter (Diebold 1977). Having said that, the digital averaging (digitising signal then averaging) is limited by the quatization noise in the analogue-to-digital converter (A/D). Quantization noise power Δq^2 is given by (Miki *et al* 1977).

$$\Delta q^2 = \frac{2^{-2m}}{12} \tag{7.4}$$

where m is the word length.

The SNR after i times averaging, $(S/N)_A$, is given by (Okada 1982)

$$(\frac{S}{N})_A = -10 log\left[\frac{10^{\frac{-(\frac{S}{N})}{10}}}{i} + \frac{4}{7} i\Delta q^2\right] \tag{7.5}$$

where $(S/N)_i$ is the signal-to-noise ratio before averaging. This shows that a 50dB SNR improvement is possible by averaging when using an 8 bit A/D converter.

The received signals are averaged by adding i-time measurements in the signal averager block to obtain the high SNR signal. For precise measurement, a large number of signal samples is inevitable, however, this requires a long measurement time.

7.4 Dual wavelength OTDR system

Generally, commercial OTDRs operate at wavelengths which are specific to optical fibre communication (i.e. 850 nm 1350 nm and 1550 nm). However, for the purpose of this investigation an OTDR operating at both 670nm and 850 nm was required.

The dual-wavelength OTDR has been developed by modifying a Photodyne Model 5400XQ OTDR. The photodyne system has a mainframe and one slot for an optional plug-in module operating at 850nm or above. The system available has a plug-in module operating at 850nm. A second module operating at 670nm was developed. Fig.7.9 shows a block diagram of the Photodyne 5400XQ system.

The system can be broadly divided into the following subsystems:

(i) Plug-in module

The plug-in module contains all the optical and optoelectronic components necessary for the operation of the OTDR, laser diode and driver, optical receiver and directional optical fibre coupler. All the development work was carried out here in this module as explained in the next section.

(ii) Analogue to digital converter and associated circuits

The function of this system is to convert the captured backscattered analogue signal into its digital form. It is built around a 14-bit, 20 MHz, A/D converter IC. The A/D converter is required to convert analogue pulses of 5 ns width. In order to do that it employs a fast sampler and a delay generator. The delay generator produces the required trigger signal to the sampler to determine the sampling rate and the time when the sample is taken (sampling point). The sampling point can be controlled by the delay generator in steps of 250 ps. Thus enabling analogue signals of 1.2 GHz to be analysed. The control and trigger signals are controlled by the 6800 microprocessor.

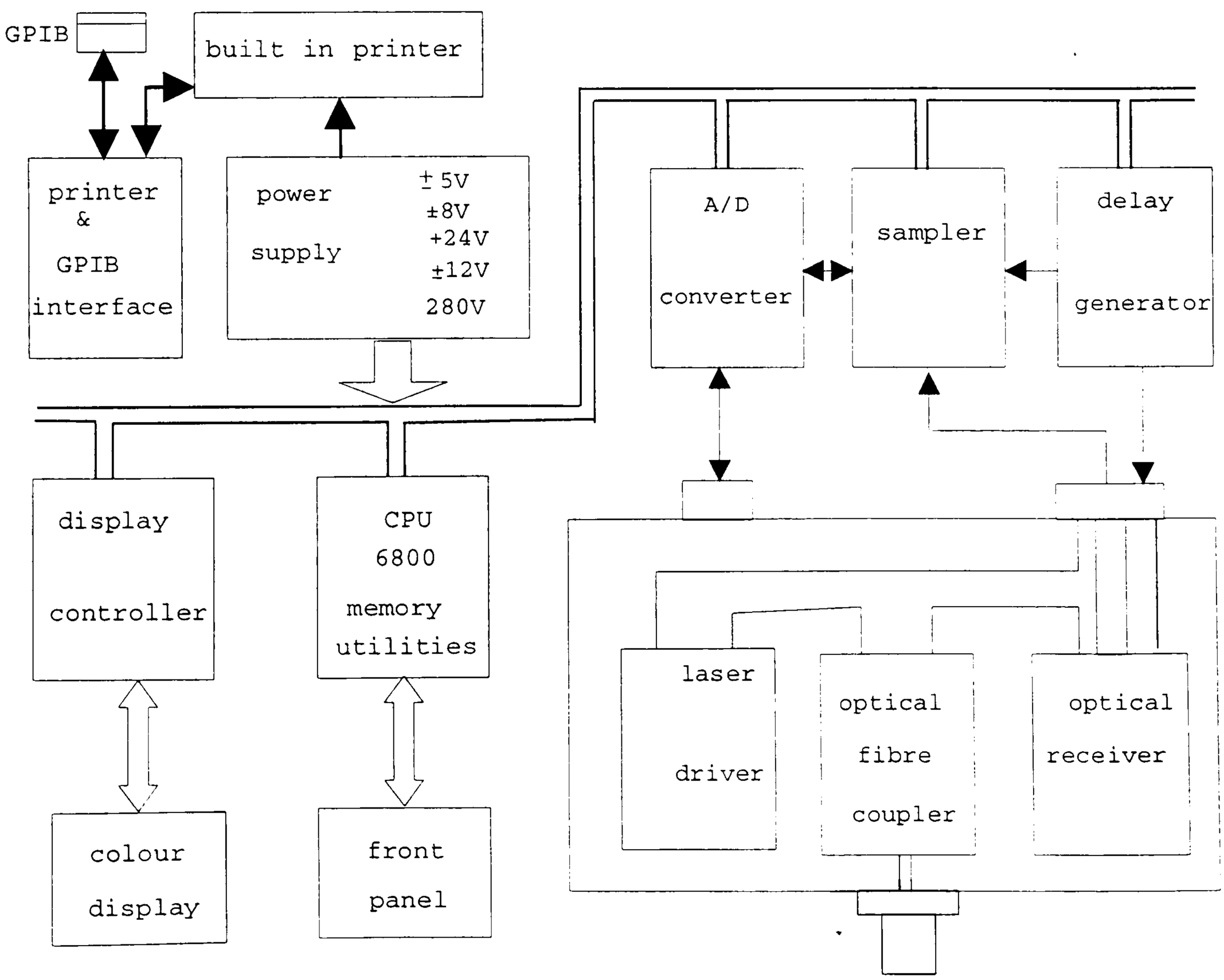

Figure 7. 9 Block diagram the Photodyne OTDR system.

(iii) Central processing unit

The control signals necessary for correct operation of the instrument are monitored and controlled by a Motorola 16 bit microcomputer.

(iv) Display and front panel

The user interacts with the instrument through front panel controls and a 7 inch colour CRT 480 by 640 dots, the operation of all the controls can be found in the manual (Photdyne 1987). Backscattered traces are displayed, measured and analysed on the CRT. The data corresponding to the cursor position in the horizontal and vertical axes are also displayed. A hard copy of the traces and the associated data can be obtained using a built in thermal printer. Two facilities which have been found useful in this work are the "Scale Controls". One allows zooming in at the required location along the optical fibre while the second allows control over the sensitivity of the backscattered light.

7.4.1 Pulsed laser driver

The laser pulser is contained in the plug-in module as shown in Fig.7.9 above. The circuit diagram of the laser pulser is shown in Fig.7.10. It is based on the well known avalanche transistor delay-line pulse generator (Millman and Taub 1965). This technique is very powerful in producing short clean high-power pulses and has been used to build laser diode pulse generators for a number of years (Andrews 1974, Vainshtein 1997). The circuit operates as follows: -

The delay line DL1 (or DL2) is charged, by transistor Q4 through R7, R8 and L1, to V_a which is set by VR1. When a positive trigger pulse is coupled through C5 and R12 into the bases of transistors Q1 & Q2, avalanche breakdown is initiated. Transistors Q1 &

Q2 rapidly switch to their lower breakdown voltage BV_{CEO} (breakdown voltage with base open circuit) and allow the delay line DL1 (or DL2) to discharge through R16 and the laser diode. The current pulse duration is twice the electrical delay time of DL1(or DL2) (Andrews 1972).

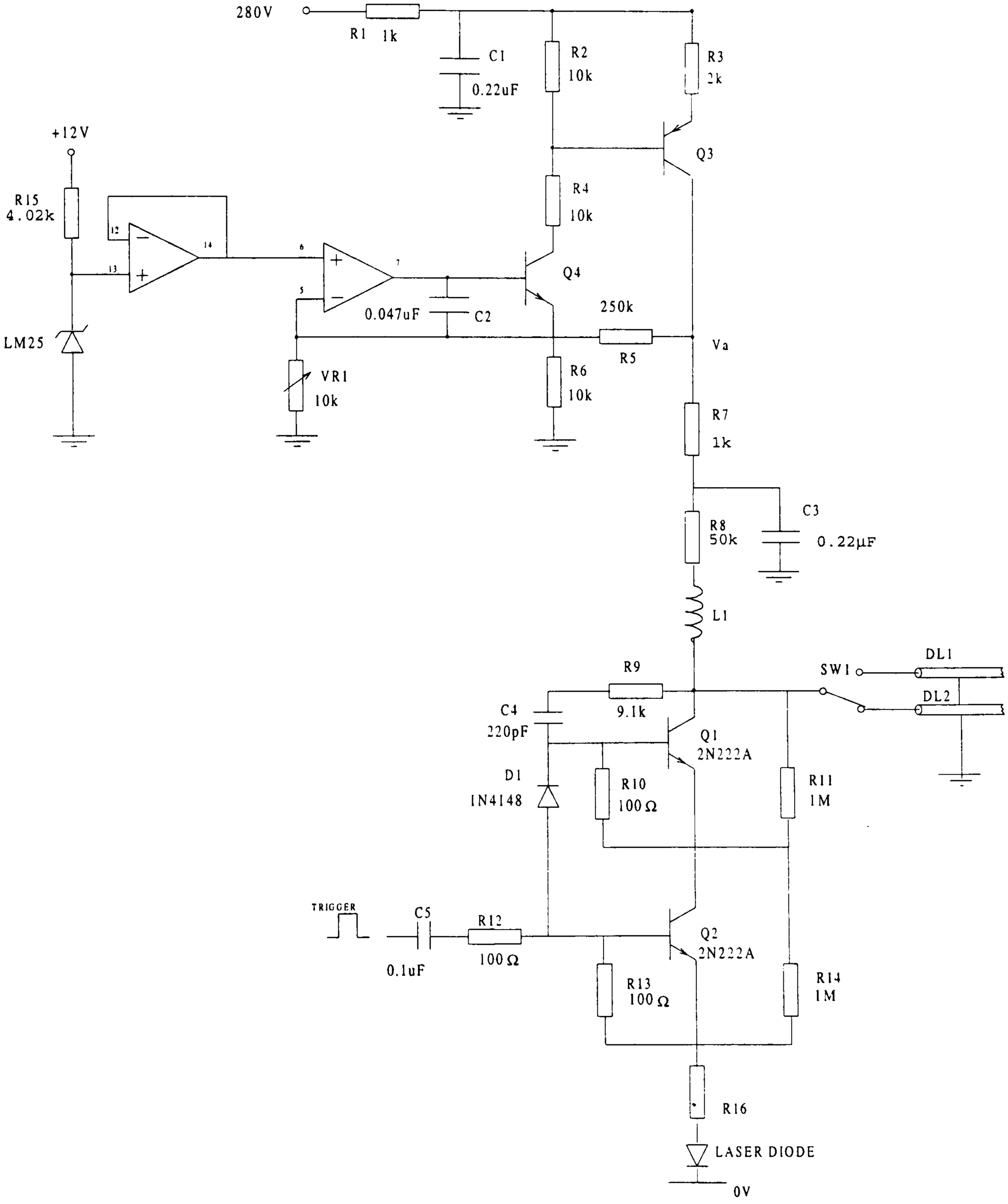

Figure 7. 10 Laser diode pulse driver.

The lengths of DL1 and DL2 are chosen to be 0.5 m and 5 m to give a selectable pulse width of 5 ns and 50 ns respectively. This is achieved by SW1 which is a relay and controlled through the front panel. In the work carried out here a 5 ns pulse was used throughout. A precision 2.5 V shunt regulator diode (LM336Z-2.5) was used to provide a very stable, with low temperature coefficient, voltage reference, V_a, as shown in Figure 7.9. Transistors Q3 and Q4 form part of the feedbackback loop of the noninverting amplifier to maintain V_a at a preset value determined by the ratio of R5 to VR1. Capacitors C1, C2 and C3 are used to reduce noise.

The avalanche transistors Q_1 and Q_2 are type 2N222A which is a general purpose high-speed switch. The maximum breakdown voltage BV_{CEO} given by the manufacturer is 40 V maximum. For any given npn transistor the breakdown voltage between the collector and the emitter can be increased above BV_{CEO} by the insertion of a resistor between the base and the emitter (Millman and Taub 1965). This is the purpose of R_{10} and R_{13} in Figure 7.10.

The peak current may be varied by adjusting VR1. This controls the voltage across the delay line (V_{DL}). Resistor R16 is selected in conjunction with the voltage to set the current through the laser diode. Also R16 is selected to match the characteristic impedance of the delay line to avoid multiple reflections, as shown later in this section. The peak current that can be delivered to the laser diode is given by

$$I_{LD} = \frac{V_d - V_{LD} - BV_{CEO}}{impedance\ of\ delay\ line + R16} \tag{7.6}$$

where

$$V_d = Va \times \frac{R_{11} + R_{14}}{R_7 + R_8 + R_{11} + R_{14} + R_{16}}$$

this is approximated to

$$V_d \approx V_a \tag{7.7}$$

Since $(R_{11}+R_{14})>>(R_7+R_8+R_{16})$.

The repetition rate is set to avoid exceeding the duty cycle limitations of the laser diode (0.025%) and the transistor (0.05%). This is limited, in both cases, by the dissipation rating of both the transistor and the laser diode.

Laser diode reliability is closely related to the junction temperature during operation. An increase in temperature causes an exponential increase in the time rate of change of the operating current (Sharp Corporation 1986).

Fig.7.11 shows a typical curve of current versus optical output power of semiconductor lasers (Philips 1994). It can be seen that the optical output power varies linearly with the input current above the threshold current. The figure also shows that the threshold current decreases as the case temperature decreases. Hence less energy is dissipated in the device resulting in higher efficiency (Hecht 1992). Therefore higher optical output powers are possible with thermoelectric cooling of the laser diode (Danielson 1982). In this work themoelectric cooling was employed to get more optical power output of the laser diode as shown later in this chapter.

The circuit of Fig.7.10, with the component values shown, is suitable for an STC pulsed laser diode LJ1 which operates at 860 nm with a threshold current of 0.7 A and maximum forward current of 3 A. However, a similar circuit is also required to drive a 670nm laser diode to enable the OTDR to operate at 670 nm. The aim was to reduce the power delivered to the laser while keeping all the control lines unchanged.

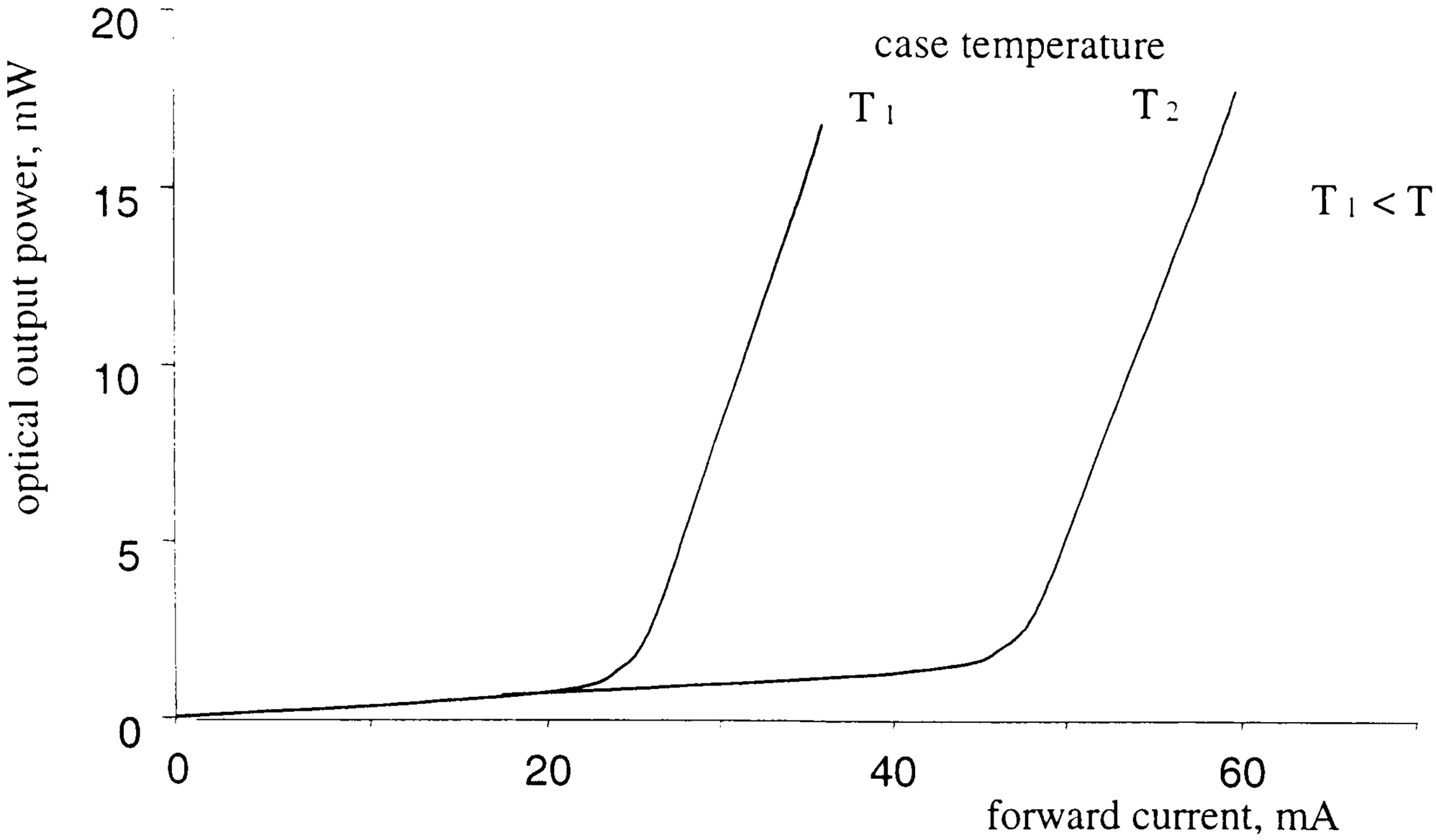

Figure 7. 11 Typical characteristics of laser diode.

The waveform across R16 was monitored using a high speed digital oscilloscope. The result is shown in Fig 7.11.

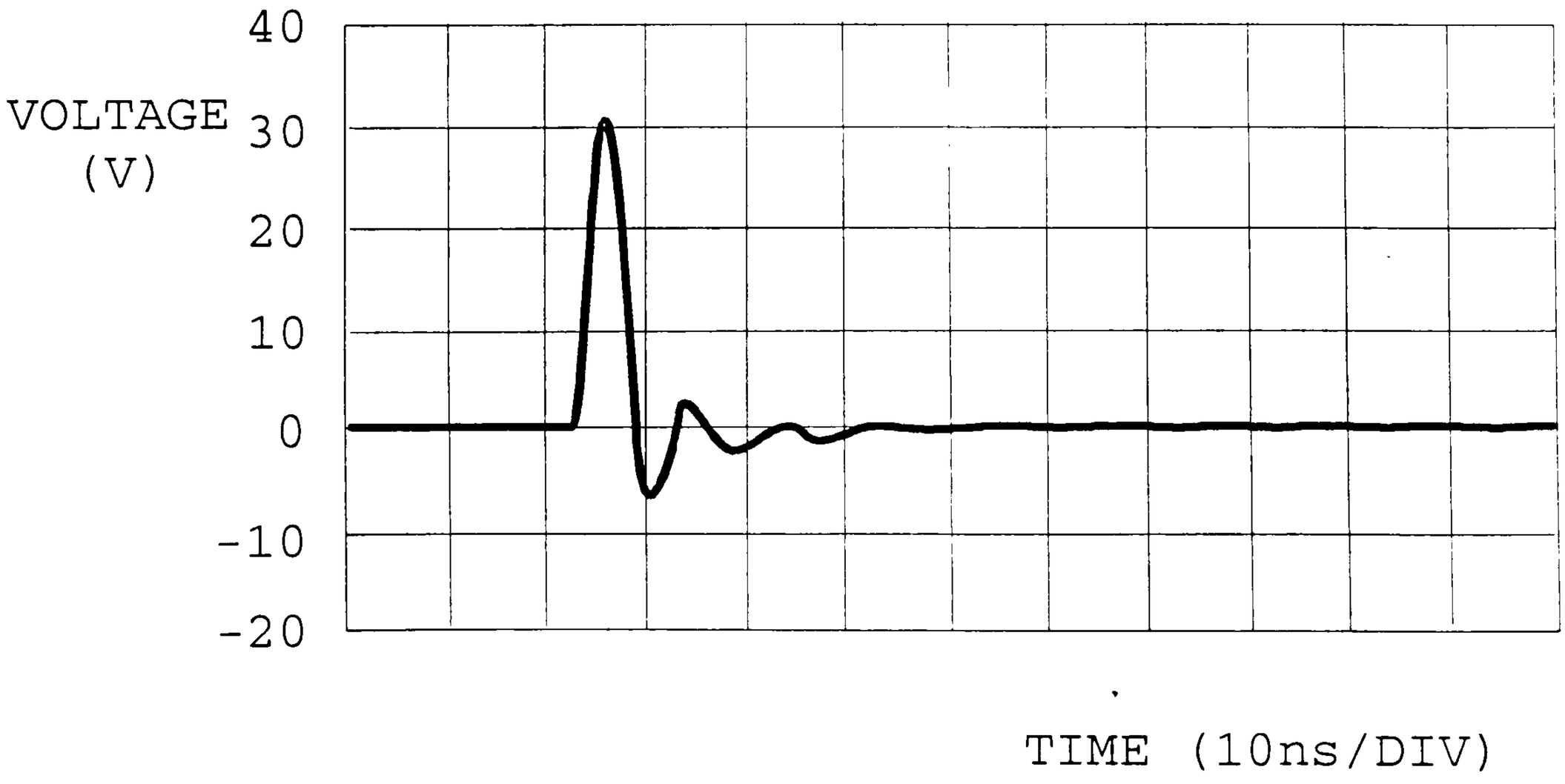

Figure 7. 12 Pulse across R16 under normal operating conditions (i.e. avalanche voltage = 263.86 V).

From Fig. 7.12, the peak current delivered to the laser diode is given by

$$I_{LD} = \frac{peak\ voltage\ across\ R16}{R16} = \frac{30}{5} = 6\ A$$

BV_{CEO} is found to be 34.86 V by substituting the values of I_{LD} and V_{LD} in equation (6).

The voltage V_a was reduced gradually by varying VR1 until avalanche operation ceased. The voltage was found to be 141.08 V. For this condition the peak current delivered to the laser diode was 2.98 A.

The visible laser diode used is a Philips CQL801 with a typical threshold current of 26 mA, a maximum dc forward current of 60mA and a forward voltage of 3 V.

Clearly, a lower supply current was required to operate the CQL801 laser. In the above circuit there were several options available to limit the current to the laser diode: -

(i) Adjusting VR1. The minimum achievable current this way under avalanche condition was 2.98 A.

(ii) Increasing the value of R16. Multiple reflections occurred creating multiple pulses when R16 exceeded the characteristic impedance of the delay line as clearly shown in Fig. 7.13.

(iii) Replacing the transistors with ones which had less breakdown voltages. The two 2N222A transistors were replaced by ZTX313 and the minimum peak current was reduced to 1.16 A which was still too high.

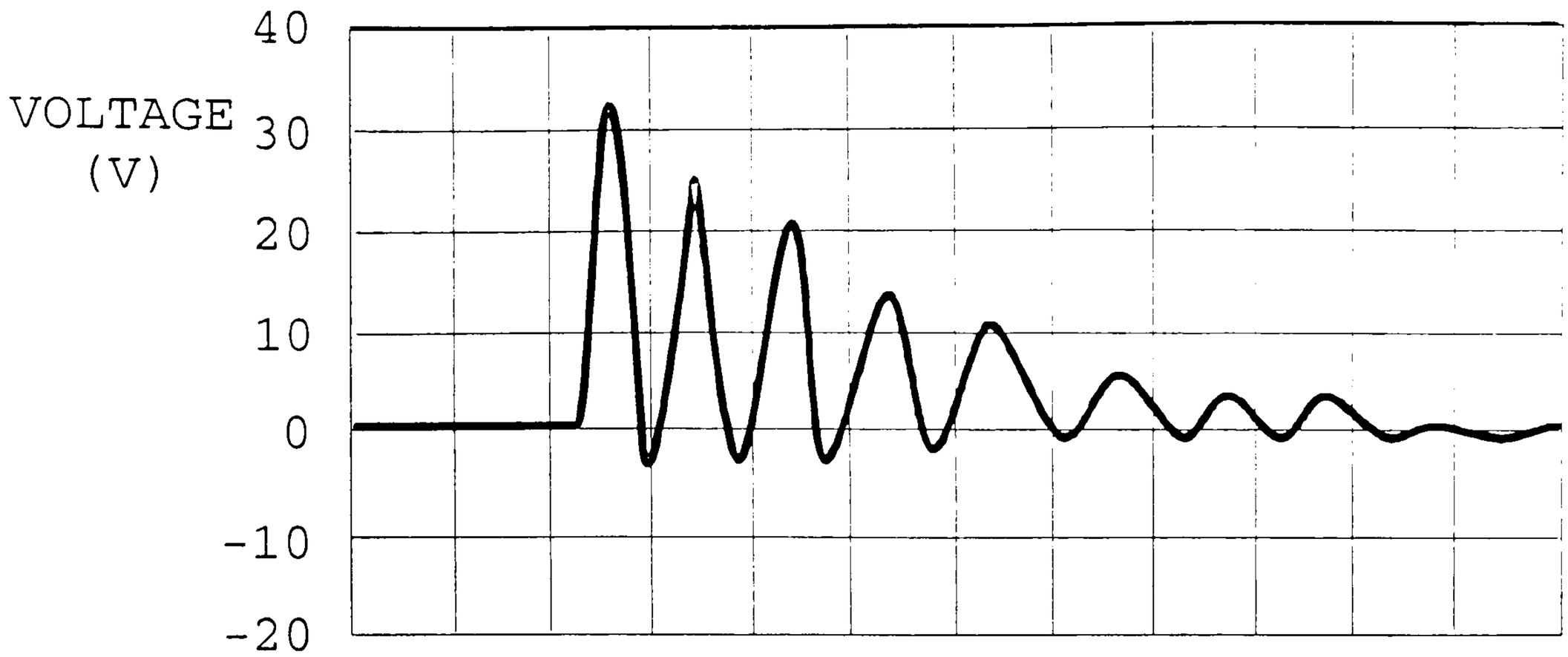

Figure 7. 13 Pulse across R16 (R16 > 1kΩ) greater than the delay line characteristic impedance) under normal operating conditions.

(iv) Removing one of the transistors (Q1). This halved the avalanche voltage and in theory the minimum obtainable current should be 1.35 A, which was still high.

(v) By adding a resistor in parallel with the laser diode. At its maximum operating current the laser diode forward voltage was 3 V at 60mA current. This made the laser diode equivalent to a resistance of 50 Ω. With one avalanche transistor used, ZTX313, this method was adopted for two reasons; first, it gave extra control over the current delivered to the laser diode, second, it reduced the impedance as seen by the delay line thus avoiding multiple reflections.

It was not possible to get specifications from the manufacturer regarding the maximum peak pulsed current allowed through the laser diode. However, it should be possible to apply current pulses with a peak larger than the specified maximum dc current without exceeding the maximum power dissipation of the laser diode. The maximum quoted modulation frequency was 5 GHz.

7.4.2 Directional coupler and laser coupling

The directional coupler used, in conjunction with the visible laser diode (CQL801), was manufactured from a 200 μm core fibre. Fig.7.14 shows how the coupler fitted within the system.

The laser output is launched into one of the arms of the coupler. The NA of the optical fibre is 0.39 which is higher than the NA of the laser beam and the emitting area of the laser diode is much smaller than that of the core of the fibre. This was ideal, with the appropriate use of lenses, to achieve a very high coupling efficiency (Gowar 1984, Buck 1995). The other two arms of the coupler were fitted with SMA connectors to enable connection with the fibre under test (sensor network in the context of this work) and with the receiver.

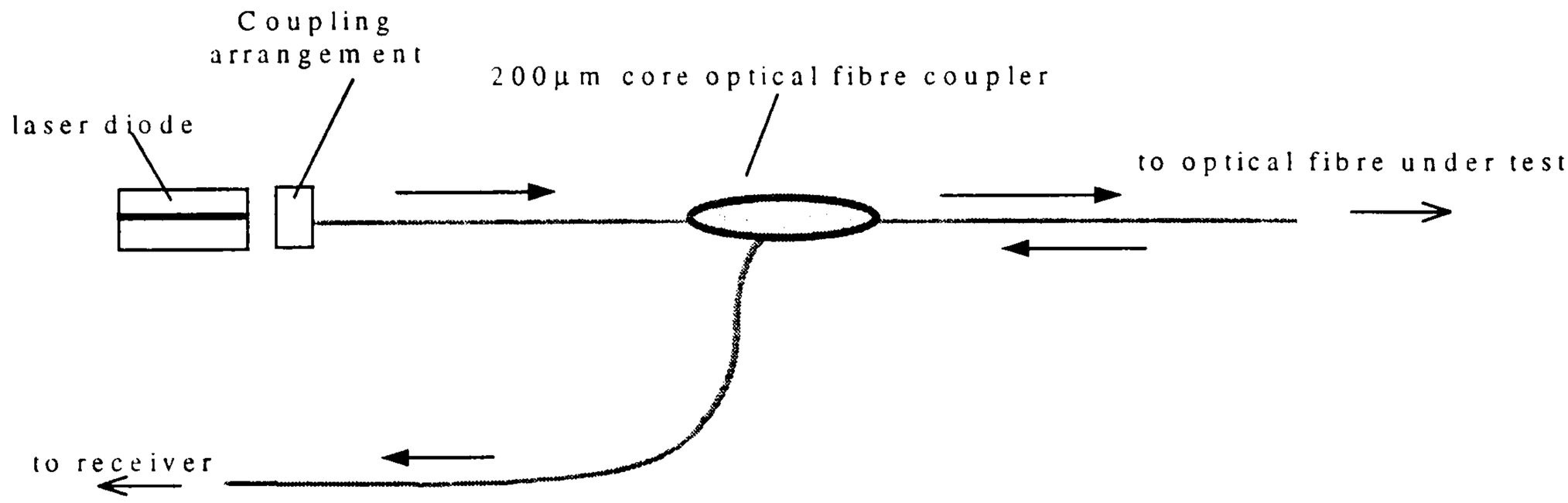

Figure 7. 14 Optical fibre directional coupler arrangement.

The simplest way of coupling a laser diode to an optical fibre is to directly butt the fibre against the laser diode as shown in Fig. 7.15 below. It can be seen that the emitting area is not immediately accessible. The area of the laser beam at the window glass of the diode is of an ellipsoidal shape and much larger than the area of the fibre core. Only light incident within the fibre core area can couple into the fibre. Any light incident

outside this area is wasted. This resulted in reducing the coupling efficiency by an amount proportional to the ratio of the two areas.

For the CQL801 laser diode θ// , the far field angle parallel to the junction, is 10° maximum, and θ⊥, the far field angle perpendicular to the junction, is 40° maximum. The laser beam at the window glass is an ellipsoidal in shape its area can be calculated from dimensions shown in Fig. 7.15. The area of the laser beam at window glass for θ⊥ = 40° and θ// = 10° is 0.151 mm^2. Area of the optical fibre core = 0.031 mm^2.

$$\text{Maximum coupling effiency} = \frac{area\ of\ optical\ fibre\ core}{area\ of\ laser\ beam\ at\ \text{int}erface} = 21\%$$

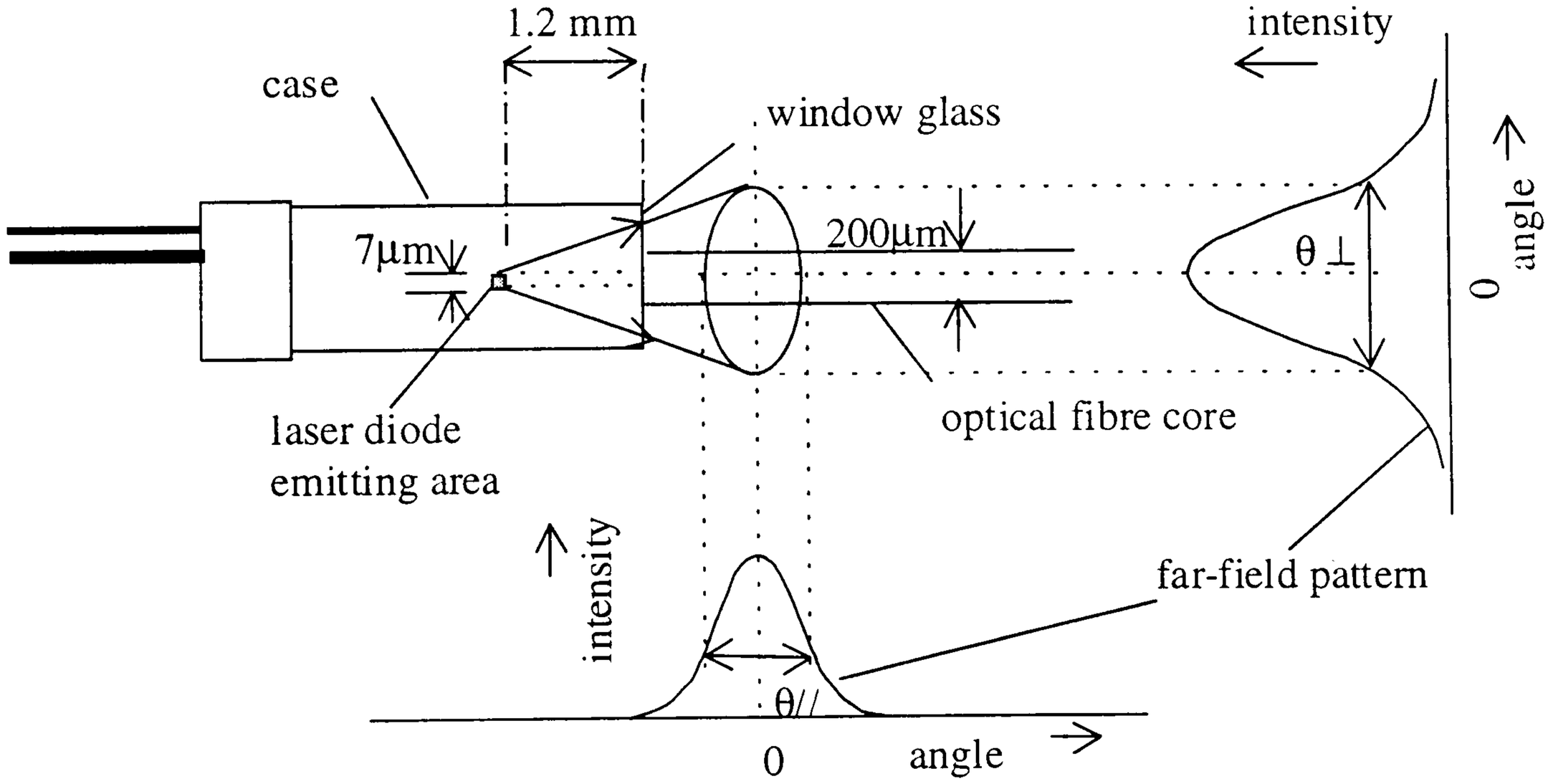

Figure 7. 15 CQL801 laser diode package dimensions and optical output beam characteristics.

The laser diode was connected to a variable dc current source (supplied by Hero Electronics Ltd, UK). Using a power meter, the optical power output of the laser diode directly and through a 200μm core fibre was measured. The maximum efficiency that could be achieved was 17%.

The fact that the emitting area was not immediately accessible could be overcome by using a graded index (GRIN) rod lens of the type shown in Figure 7.16. The advantages of this type of lens lie in the fact that the image is displaced from the end of the lens and therefore makes the emitting area of the laser diode accessible. A GRIN-rod lens of 1.8 mm diameter was used. The coupling efficiency achieved was better than 90%. In the laser diode assembly the GRIN-rod lens was positioned such that its end makes a slight angle with the laser diode window. This was done to stop light from reflecting back into the laser which may cause feedback noise (Hecht 1992). Theoretical analysis of efficiency limits using lens coupling is covered by Nicia (Nicia 1981). At its maximum dc current rating the output power of the laser was found to be 22.5 mW.

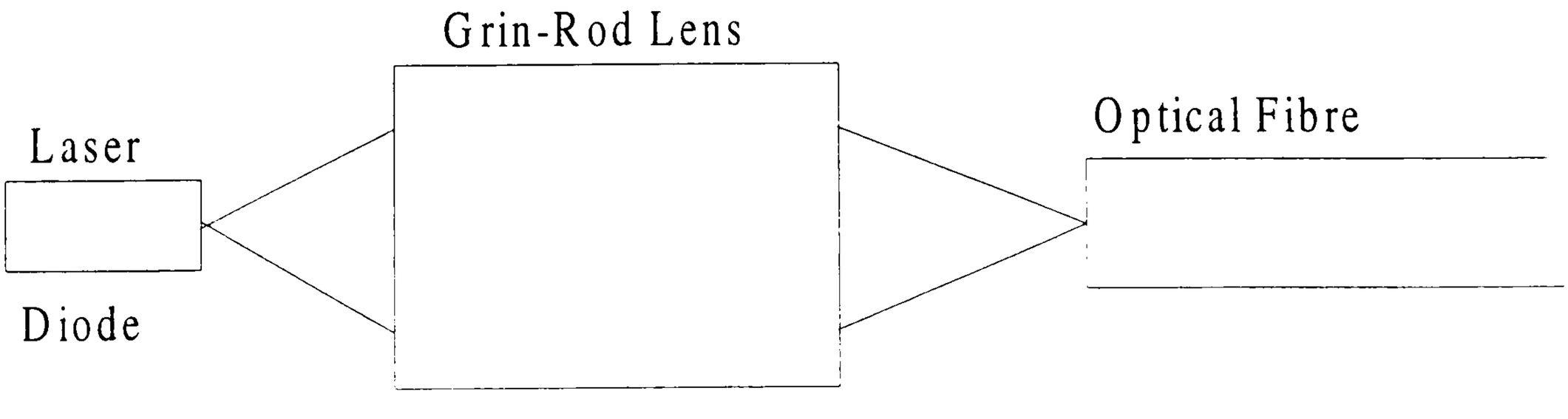

Figure 7. 16 Laser diode-fibre coupling using GRIN-rod lens.

7.4.3 Thermoelectric cooling of the laser diode

The output available from a laser diode is inherently limited by the volume of the devices, the need to remove excess heat, and optical damage to the laser facets. Heat removal becomes a problem as the output power increases. This limits the continuos wave output powers. Higher peak powers are possible from diodes designed for pulsed operation. Lifetime is critically dependent on heat removal (Hecht 1992).

Thermoelctric cooling of the laser diode was used here for two reasons:

1. To reduce the operating temperature of the laser diode thus increasing its operating life.

2. By shifting the case temperature to a lower value consequently lowering the threshold current resulting in an increase in the optical output power for the same input current, see section 7.4.1.

The laser diode was cooled using an 18.8 W Peltier heat pump (supplied by RS components). When the device was connected to a dc source, heat was pumped out of one end of the device, cooling it, while heat was rejected at the other end. Heat generation or absorption rates are proportional to the magnitude of the current and also the temperature of the junction. The device only transfers or pumps heat from one side to the opposite side. At the hot side heat must be removed through the use of heat sink or some other means. (RS data sheet, 1988).

The Peltier effect was discovered in 1834 by Jean Peltier. He discovered that the passage of an electric current through the junction of dissimilar conductors can either cool or heat this junction depends on the direction of current. Practical Peltier effect

heat pumps consist of many such couples connected electrically in series and thermally in parallel.

The laser diode was mounted in the assembly shown in Fig.7.17. The laser diode was fitted in a receptacle and positioned on the cold side of the Peltier device. The other side of the device (hot side) was mounted on a heat sink. The receptacle and the heat sink were fixed together using plastic screws to keep the two sides thermally isolated. Both hot and cold sides were coated with a thin film of heat sink compound before assembly. By varying the supply current to the device the laser diode could be kept at temperature lower than 10^{o}C.

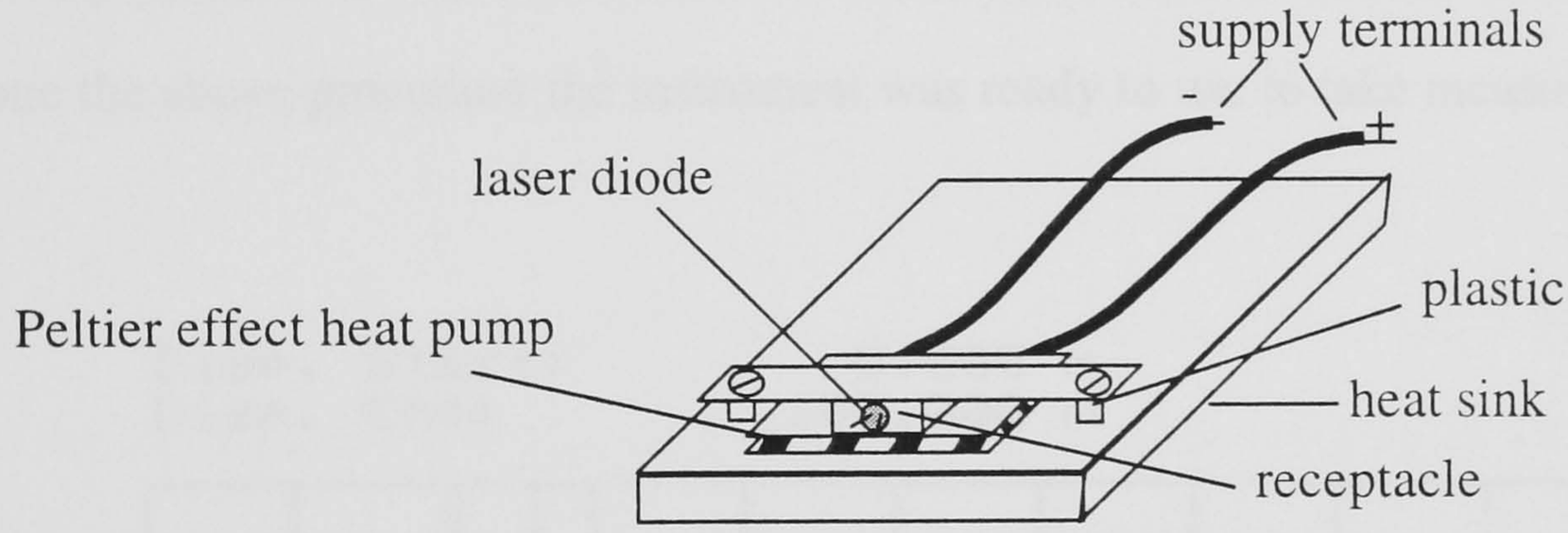

Figure 7. 17 Peltier cooler and laser diode mount assembly.

7.4.4 Setting the system

The 670nm laser (CQL801) was mounted in the assembly shown in Fig.7.17 and it was inserted in the circuit of Fig.10 very close to the avalanche transistor since UHF (ultra high frequency) circuit construction technique for component layout is required. A 50 Ω (VR2) multi-turn pot resistor was connected in parallel with the laser diode. Before

switching the module on, VR2 was turned to minimum and the Peltier cooler was switched on.

Before fitting the Peltier cooler, the laser diode life was less than 1 hour. With the cooler operational the diode life increased to more than 10 hours and the output power was also increased. Although this was an improvement it was not practical and didn't give adequate time to investigate the system. The short life is partly due to the fact that the laser was driven by short current pulses which are larger than the maximum dc current rating.

About 100 m length of 200 μm core HCS fibre was connected to the OTDR. The instrument was then turned on and VR2 was adjusted until a peak appeared which corresponded to a 100 m distance on the OTDR trace as shown in Fig.7.18. Having done the above procedure the instrument was ready to use to take measurements.

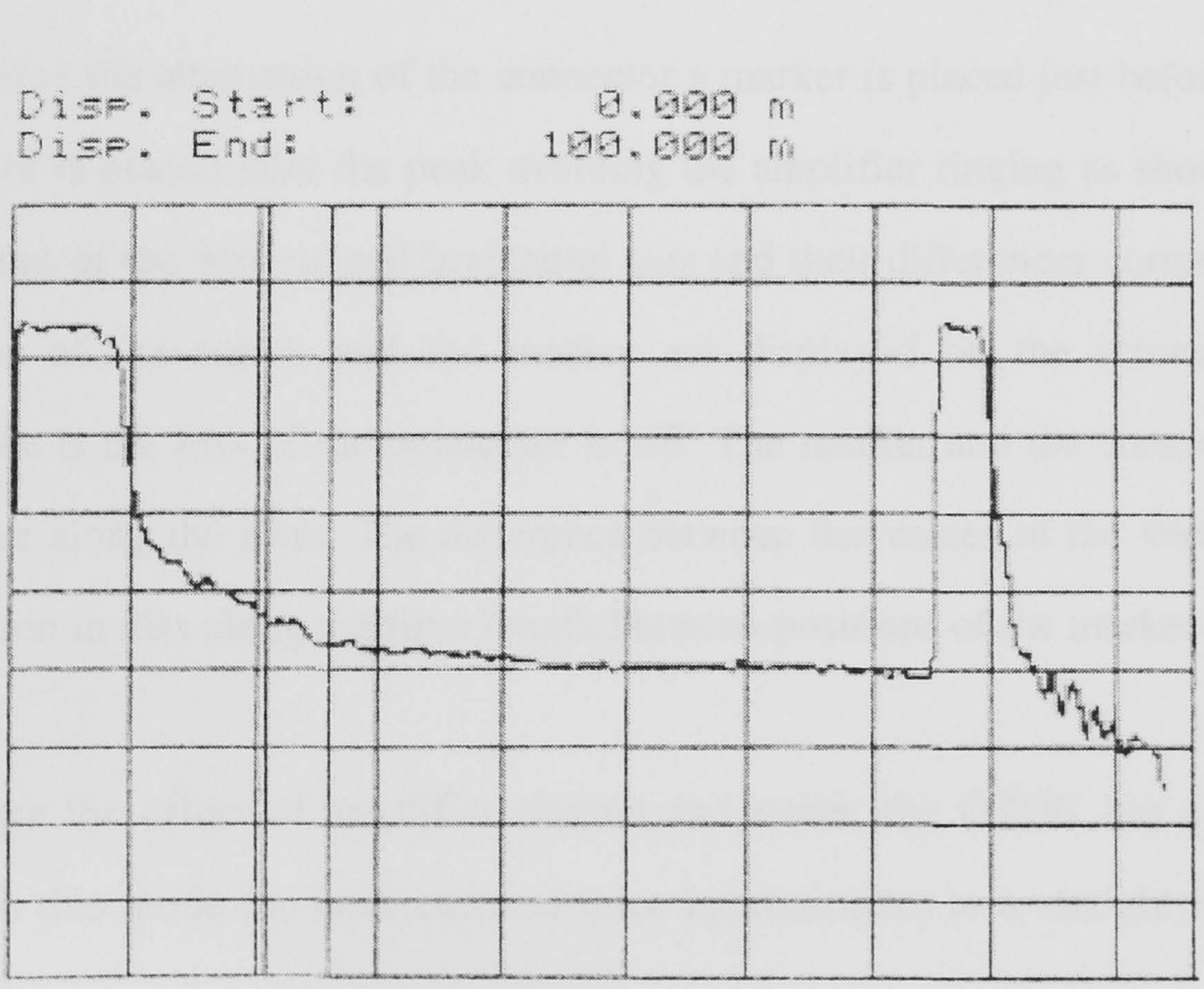

Figure 7. 18 OTDR trace when about 100 m of HCS fibre was connected to it.

The OTDR system could only take one plug-in module at a time. Therefore measurements were taken first using the 850nm module, and then this module was replaced by the 670nm module and a second reading was taken.

7.4.5 Attenuation measurement using the OTDR

Attenuation measurement along an optical fibre can easily be made using the OTDR instrument. Figure 7.19 shows the trace of two optical fibres joined together by a connector. It can be seen from the figure that a peak appears on the trace corresponding to the position of the connector along the fibre. This is due to Fresnel reflection (section 7.2) generated by the connector. The presence of this peak gives rise to amplifier ringing and the creation of a dead zone (section 7.3.1). The second peak is due to reflection from the fibre end.

To measure the attenuation of the connector a marker is placed just before the peak and the cursor is placed after the peak avoiding the amplifier ringing as shown in Fig.7.19. The values of the vertical and horizontal axis and their differences corresponding to the positions of the cursor and the marker are displayed on the screen. The vertical difference is the loss of the connector in dB. The marker and the cursor can be placed anywhere along the fibre. The difference between the values of the vertical axis is the attenuation in dBs along the fibre length between positions of the marker and the cursor.

To reduce the effect of amplifier ringing and noise, the OTDR has a built-in splice mode. In this mode the backscattered trace approximates to a straight line (Photodyne 1987).

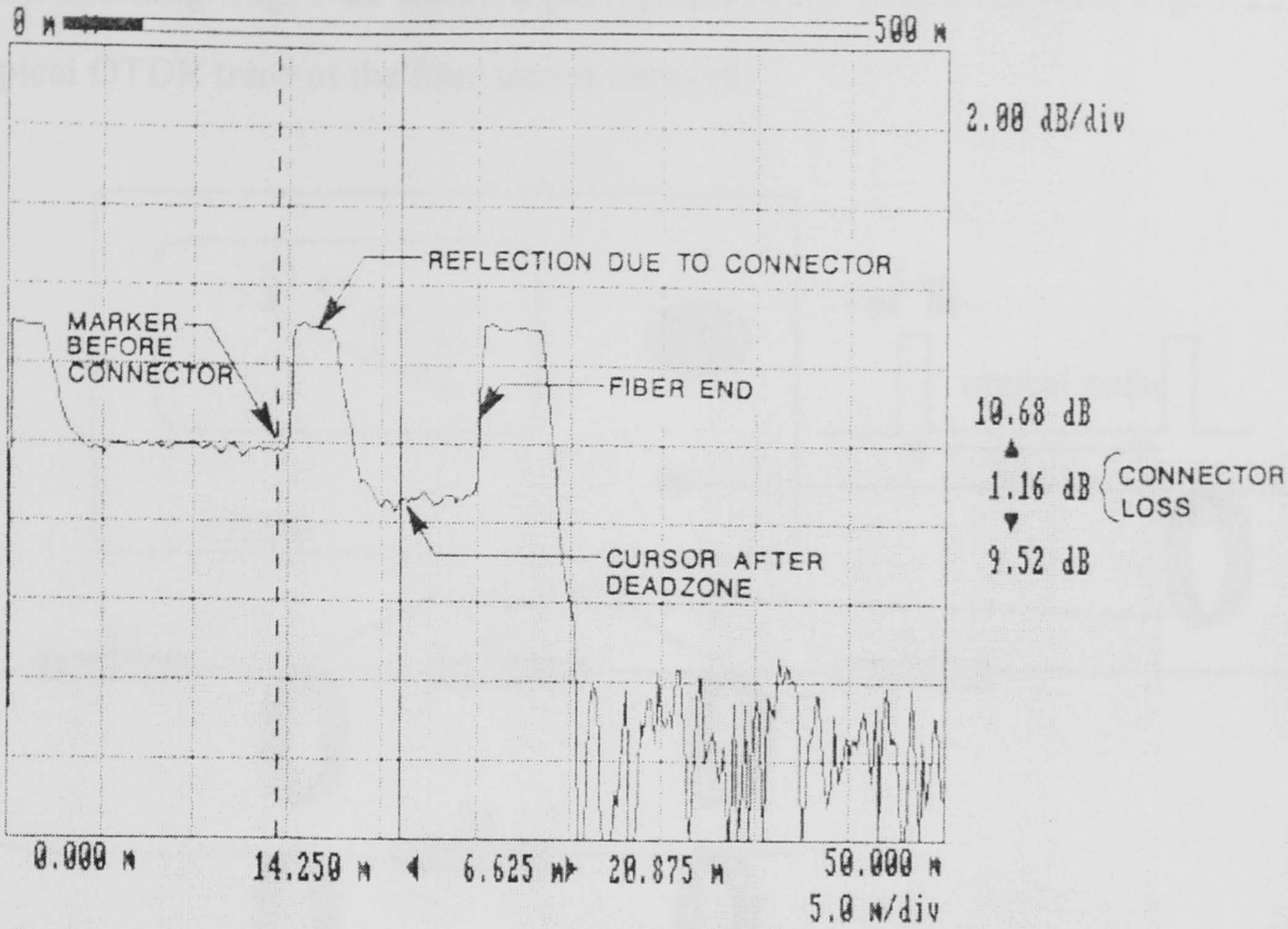

Figure 7. 19 OTDR trace of an optical fibre with an in-line connector (Photdyne 1987).

7.5 A Four-Point Distributed Sensor Network

A four-sensor network has been built along a 100 m long 200 μm core HCS fibre. The sensors were fabricated at about 20m apart. Fig. 7.20 shows the configuration of the complete system.

The optical fibre was fitted with a SMA connector at one end to enable connection to the OTDR. At each sensing point the protective coating was stripped off and the cladding was removed by burning it off using a low temperature flame. The core was then coated with a cobalt chloride/gelatin film (see Chapter 6 for more details on coating). The sensing points were fitted with a protective housing to prevent the fibre

from breaking. Fig. 7.21 shows a photograph of the sensor network. Fig. 7.22 shows a typical OTDR trace of the four-sensor network.

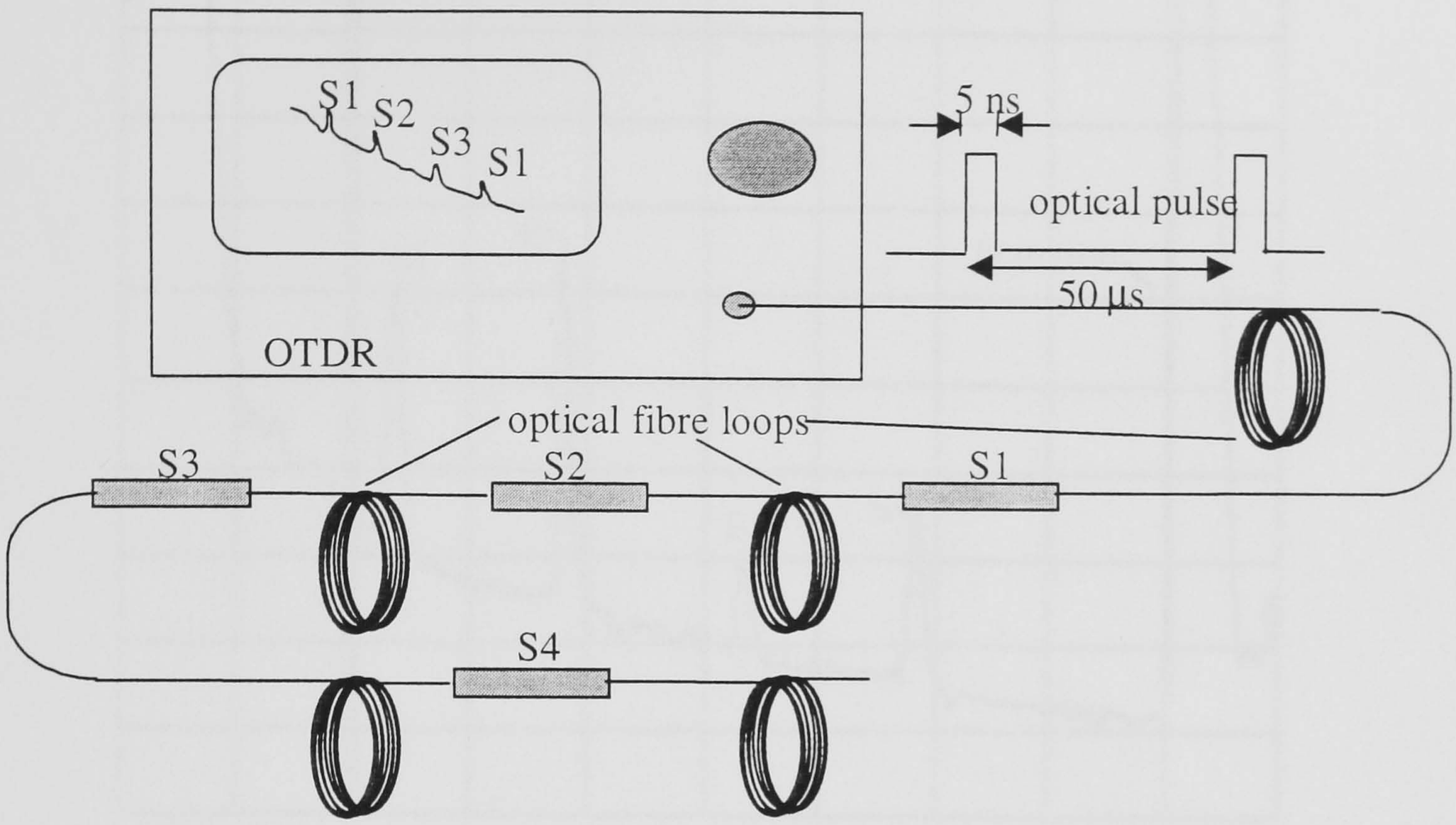

Figure 7. 20 Configuration of the four sensor network system.

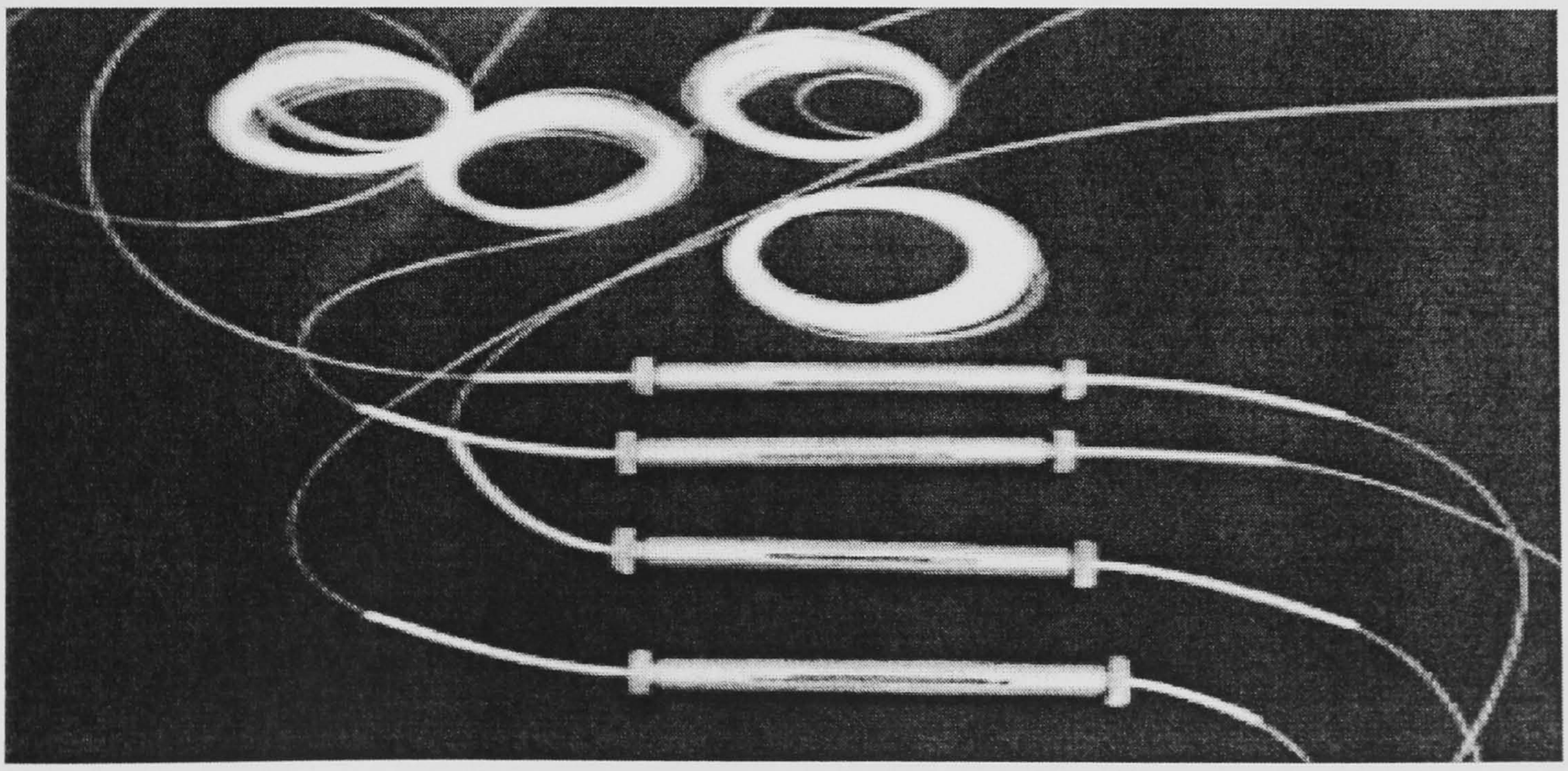

Figure 7. 21 A photograph of the four-sensor network.

Figure 7. 22 An OTDR trace showing the four sensor network. Horizontal axis: Distance along the optical fibre; Vertical axis: backscattering level in dB.

7.5.1 Testing the four-point sensor network

The sensors of the network were placed in the humidity chamber and were exposed to cycles of humidity in the operating range 20 to 80 %RH. At each humidity level the attenuation caused by each sensor was measured at 670 nm and then at 850 nm using the OTDR. From these two values a relative attenuation (RA) in dB was calculated and plotted in Fig. 7.23. The sensors attenuation measured at 850 nm did not vary with the relative humidity and had a value of 0.39, 0.26, 0.19 and 0.3 dB for sensors S1 to S4 respectively. From Fig. 7.23 it can be seen that the sensors characteristics are similar to those of the single sensor shown in Fig. 6.14 in Chapter 6. Note that in Fig. 6.14 the

sensor relative intensity (a measure of optical transmission) was plotted versus RH whereas in Fig. 7.23 attenuation versus RH was plotted.

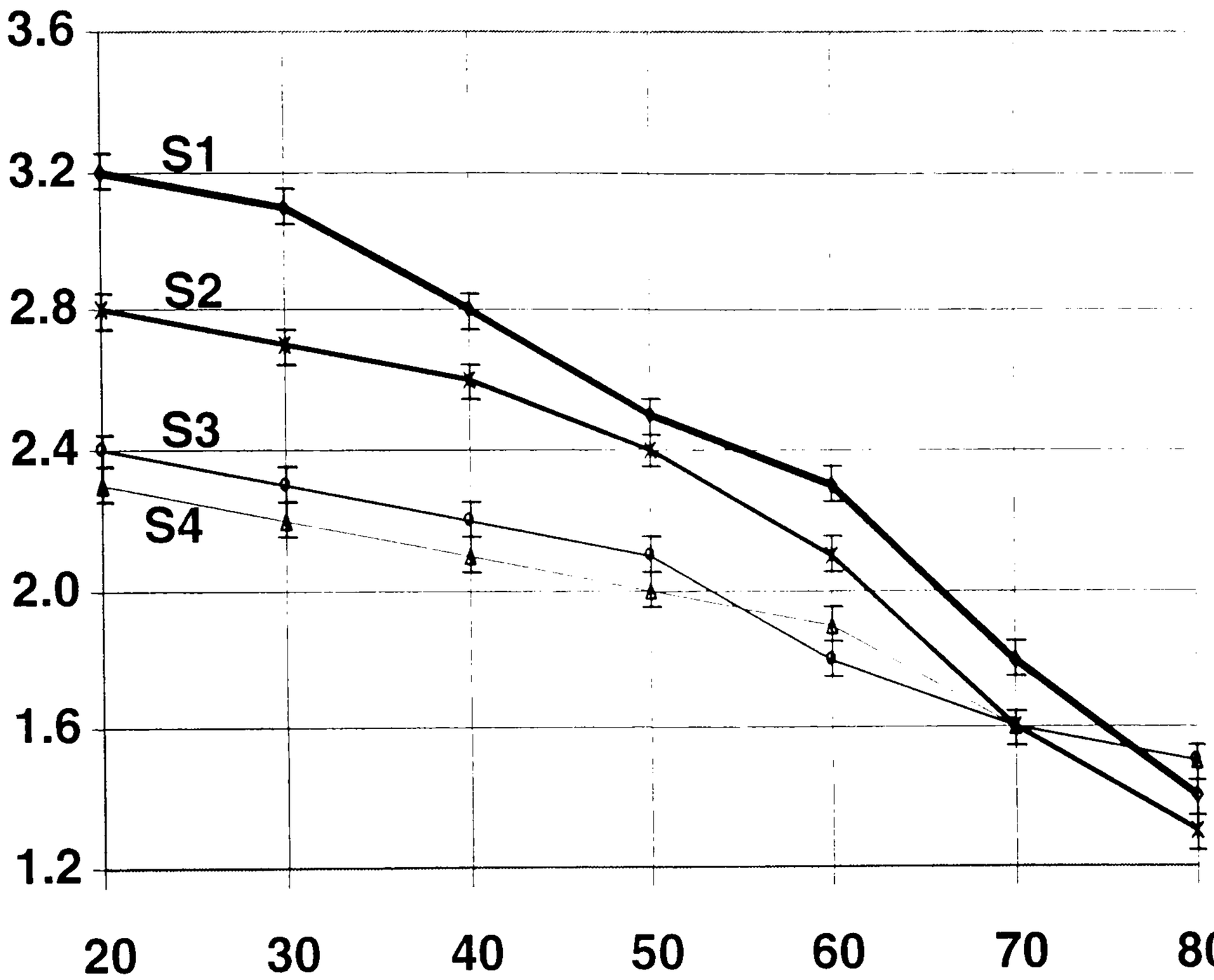

Figure 7. 23 Attenuation of the four-sensor network versus % RH.

The attenuation at each sensing point was measured by expanding the trace around the sensing point as shown in Fig.7.24. The cursor and the marker positions are shown in the figure. The measurements were done in splice mode. The trace is characterised by the presence of peaks each corresponding to a sensing point. The peaks were not expected to be present hence they were further investigated in the next section. Fig. 7.24 also shows the actual trace in solid line and the expected one is indicated by the dotted line.

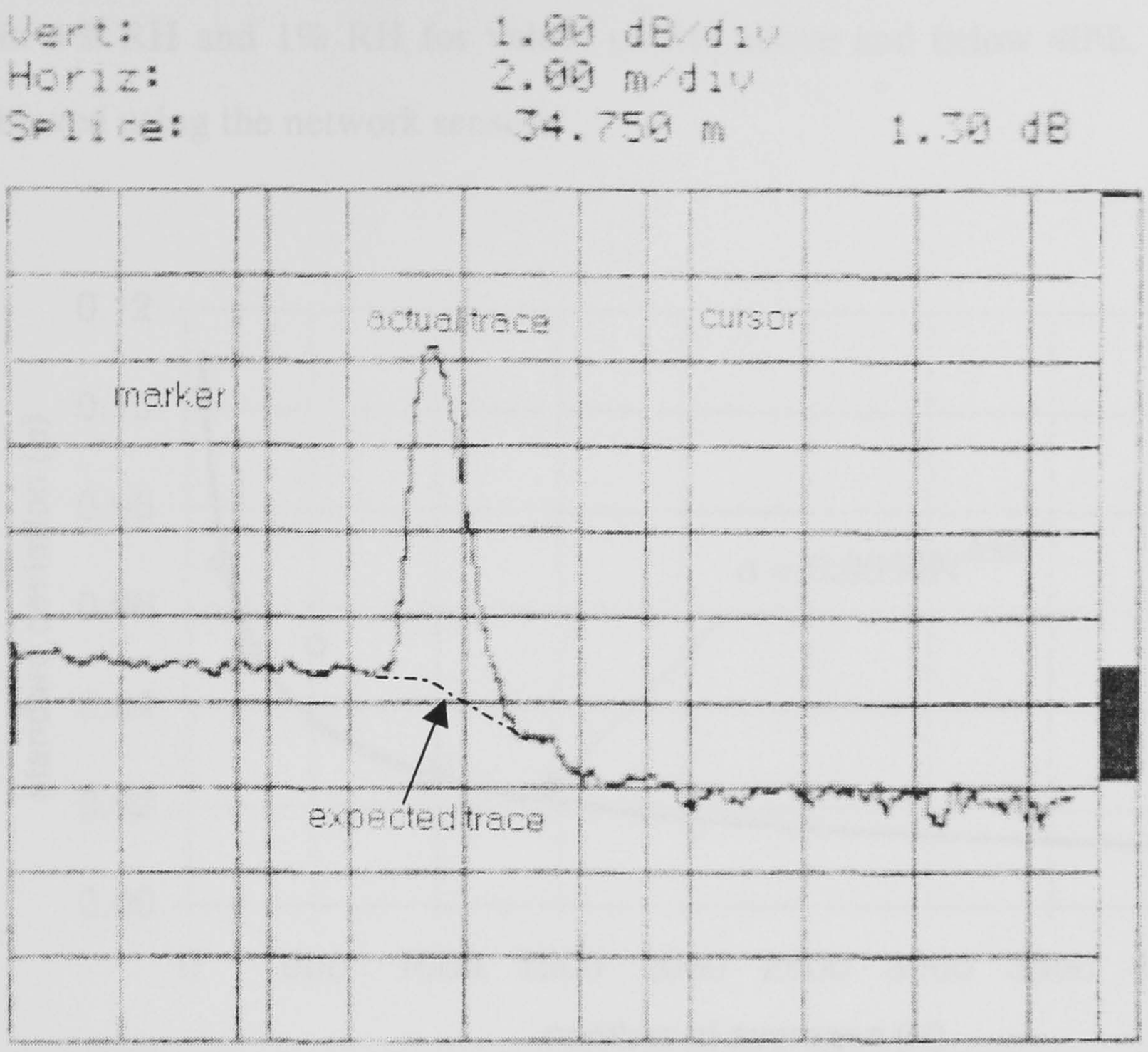

Figure 7. 24 An expanded OTDR trace showing one sensor. The solid line shows the actual trace while the dotted line shows the expected one.

7.5.2 Effect of averaging times on SNR

As mentioned earlier in section 7.3.3, the backscattering level in OTDR systems is low such that the backscattering signal-to-noise ratio needs to be improved by averaging. Fig.7.25 illustrates the measured relationship between the number (N) over which average was taken and the standard deviation. For each value of N twelve readings were taken and the standard deviation was calculated. A best fit curve to the data shows that the SNR improved according to the equation:- standard deviation = $0.9954N^{-0.527}$. This clearly shows an improvement in SNR in proportion to, approximately, the square root of the number N. By taking averages over 4000 times or more a resolution of better

than 4% RH and 1% RH for values of RH above and below 40%, respectively, was achieved using the network sensors.

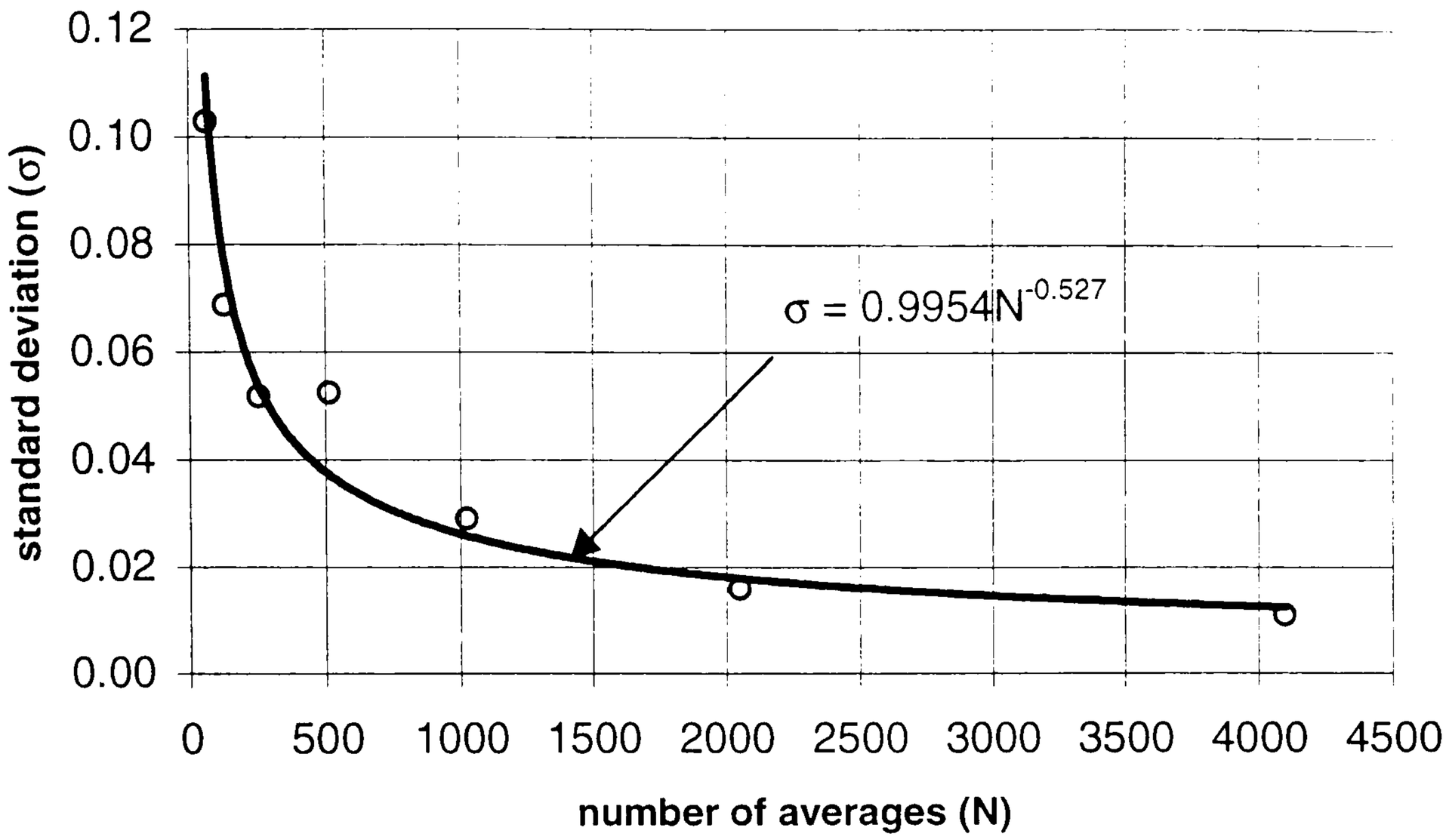

Figure 7. 25 Effect of averaging on the standard deviation (noise) of backscattering signal for the OTDR system.

7.5.3 Excessive reflections associated with the sensors

As mentioned in the previous section the presence of peaks within the OTDR trace, Fig 7.22, of the sensor network was not expected. The height of each peak indicates the value of the reflected power above that of Rayleigh backscatter at the sensing point. The height of these peaks can be several dBs. These peaks occured as a result of Fersnel reflection (see section 7.2). To take this further the values of Fresnel reflection (back into the optical fibre) were calculated by taking different values for the refractive index of the outside medium. Fig. 7.26 shows calculated values of Fresnel reflection in excess of that of Rayleigh backscatred in dB's at points along the optical fibre. Fresnel reflections are calculated for normal reflection for simplicity.

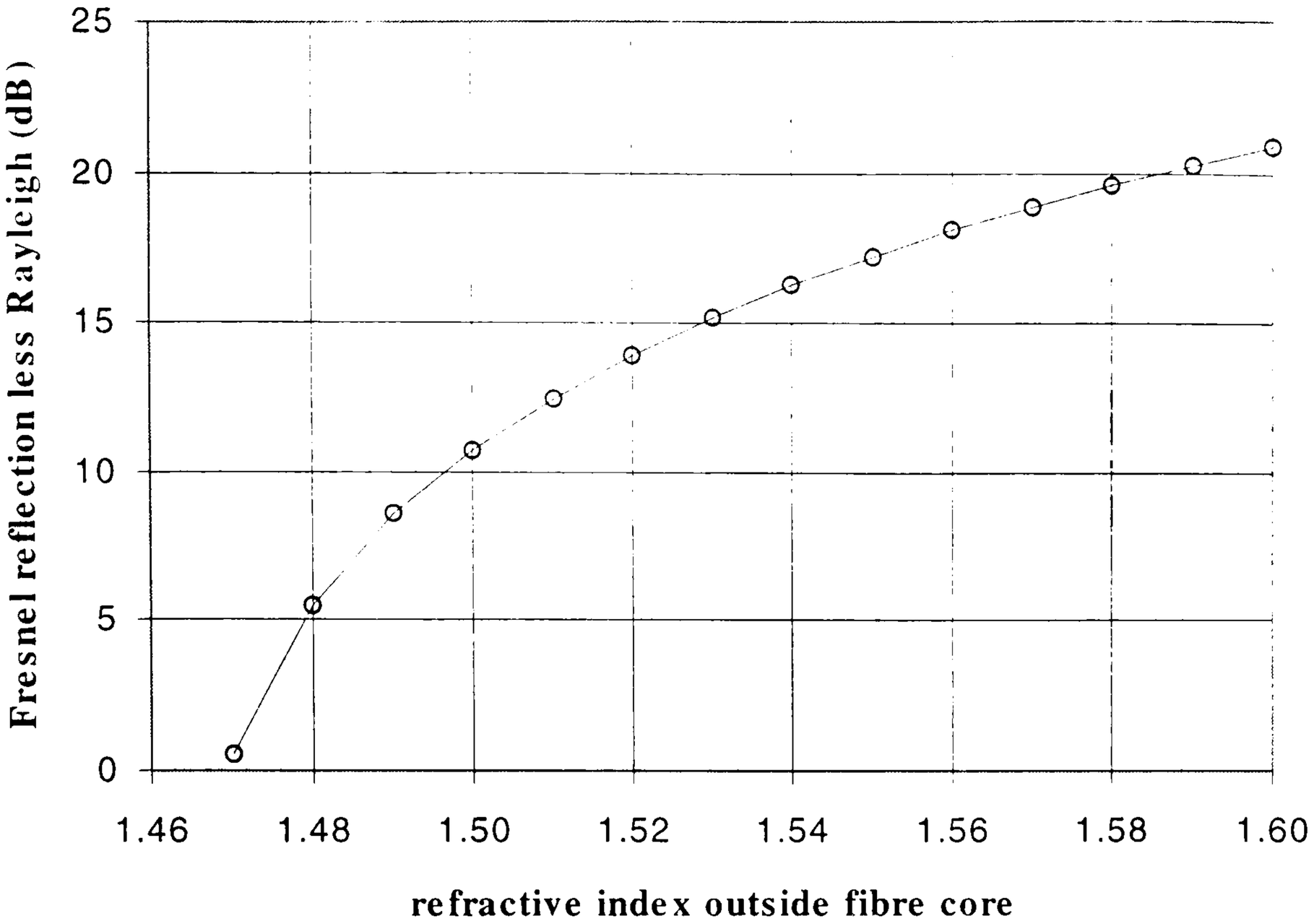

Figure 7. 26 Fresnel (normal) reflection in excess of Rayleigh reflection at any point along the fibre.

It can be seen from the figure that a 0.02 change of the surround refractive index (from 1.47 to 1.49) causes a change of about 10 dB in the value of Fresnel reflection over that of Rayleigh backscattering. From this it is clear that Fresnel reflection can account for the appearance of these peaks.

The following experiments were carried out in order to explain the presence of peaks.

A long 200 μm core fibre was connected to the OTDR. At about 20 m from the launch end the fibre the protective coating along 50 mm was removed. A peak appeared which corresponds to that point on the trace as shown in Fig. 7.27. On further examination of the fibre, under a microscope, scratches on the cladding were observed. This clearly indicated that scratches of the cladding can cause peaks in the OTDR trace. It is interesting to note, from the figure, that the presence of the peak (1.3 dB) did not introduce any discernible loss. The loss measured across the sensing point was 0.01 dB which is the resolution limit of the OTDR.

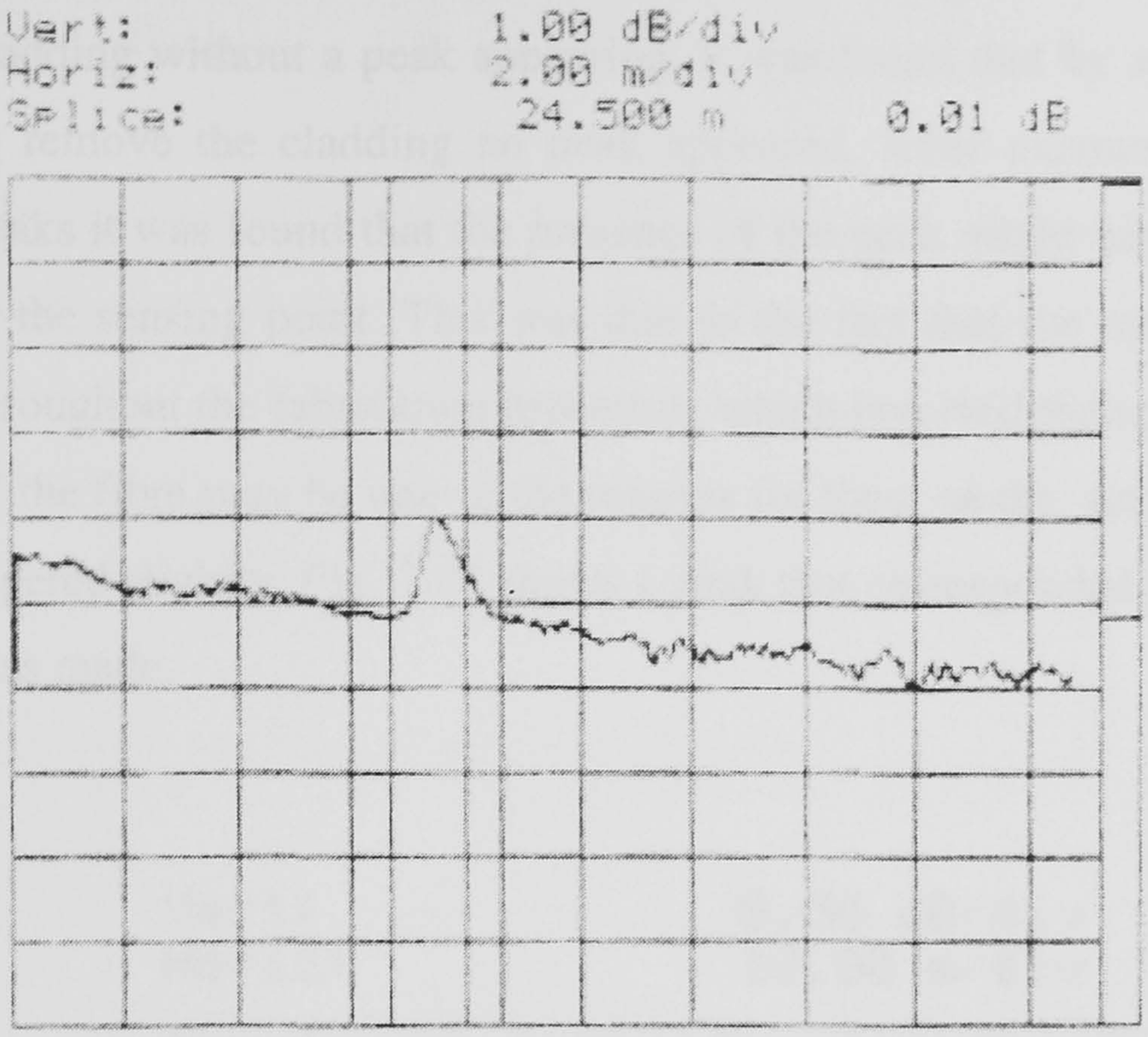

Figure 7. 27 A peak caused by the presence of scratches on the cladding of the optical fibre.

The same area was then completely immersed, in turn, into a number of liquids with different refractive indices ranging from 1.33 to 1.62. The peak did not disappear even when the liquid used had the same refractive index as that of the cladding. Although the peak height varied slightly with the refractive index of the applied liquid, it has never disappeared. This suggests that the peak presence is due to some form of interaction between the cladding the core.

A different optical fibre was used and the protective coating was carefully removed. At this stage no peak was present. When a flame was applied to burn the cladding off a peak appeared. The fibre was then cleaned with acid, alcohol and acetone but the peak was still present. Various liquids of refractive indices over the range 1.3 to 1.65 were applied to the fibre but the peak was still there although with slightly variable amplitude depending on the index of refraction of the liquid.

Using a fresh point every time, several attempts were made to try to remove the cladding without a peak appearing. It was found that by applying short bursts of flame to remove the cladding no peak appeared. After examining the fibres that produced peaks it was found that the presence of the peak might have been due to slight tapering at the sensing point. This was due to the fact that the optical fibre was under tension throughout the fabrication procedure which involved the application of heat. So tapering of the fibre may be one of the reasons for these peaks. An optical fibre was deliberately tapered slightly. Fig. 7.28 shows a peak that corresponded to the point at which tapering was made.

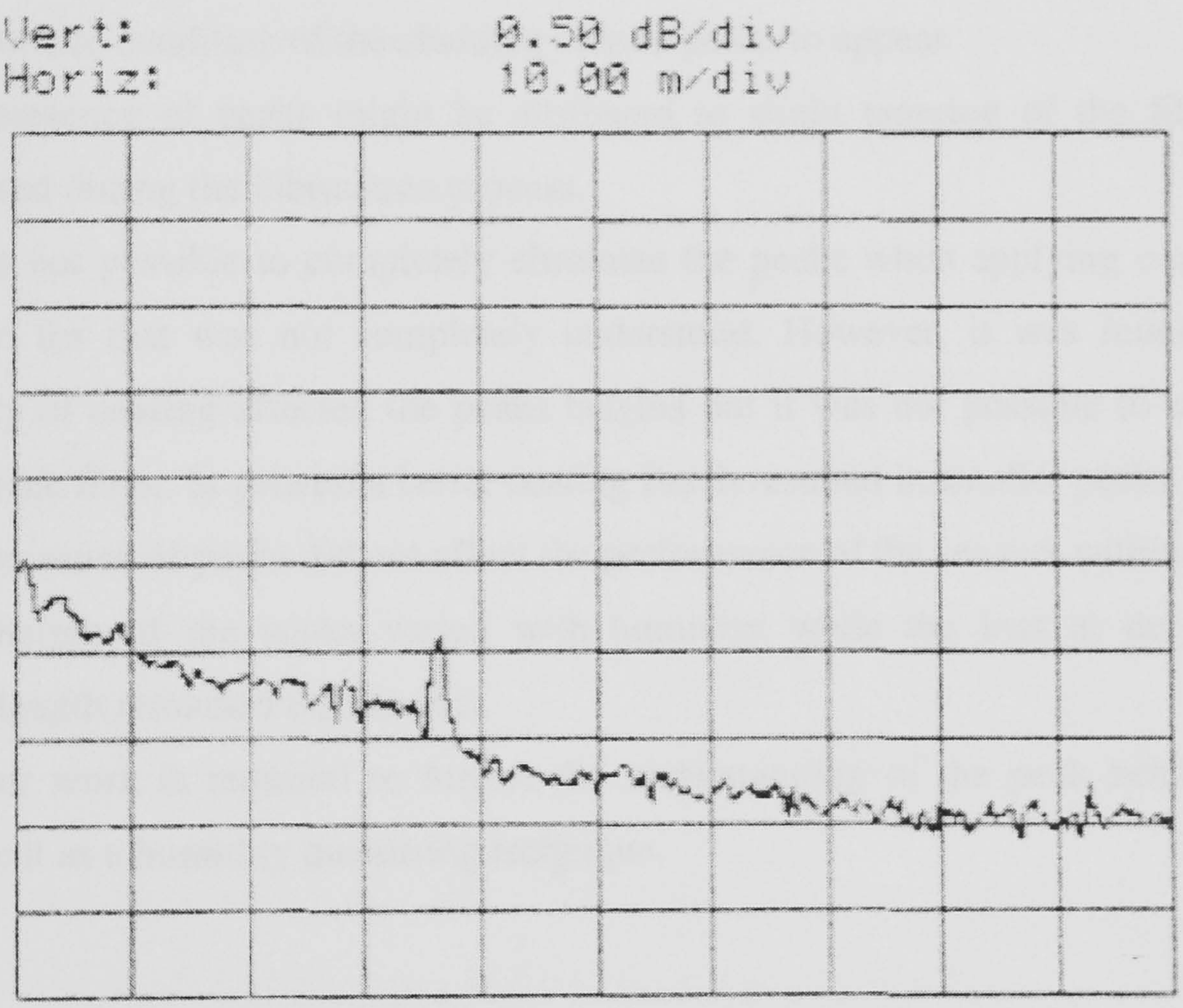

Figure 7. 28 A peak caused by a slight tapering in the optical fibre.

Having achieved a no peak situation when stripping the fibre, when a gelatin coating was applied the peak appeared. Several attempts were made to form a coating with no peak by applying the coating at various temperatures and in different ways like brushing or dipping, a peak still appeared and it was believed that this might be due to the edge of

the film. It was also was found that a slight contamination of the bare core resulted in a peak appearing.

The presence of the peaks did not affect the performance of the sensor. Although the height of the peak varied with RH, at the reference wavelength (850 nm) the attenuation across the sensor was constant. For a particular sensor the attenuation of the sensor was the same (0.2 dB) at 100% RH and 47% RH while the peak height changed from 1.97 dB at 100% RH to 0.72 dB at 45 % RH.

The above can be summarised as follows: -

1. The surface condition of the cladding caused peaks to appear.
2. The presence of peaks might be attributed to slight tapering of the fibre which occurred during the fabrication process.
3. It was not possible to completely eliminate the peaks when applying coating. The reason for that was not completely understood. However, it was found that the quality of coating affected the peaks heights but it was not possible to completely eliminate them. In general a better coating finish resulted in smaller peaks.
4. The presence of peaks did not affect the performance of the sensors within network.
5. The height of the peaks varied with humidity while the loss at the reference wavelength remained unchanged.
6. Further work is required to further the understanding of the peak behaviour and utilise it as a humidity measuring technique.

7.6 Summary

In this chapter the design and construction of a dual wavelength OTDR operating at 670 nm and 850 nm wavelengths has been be detailed. A four humidity sensor network has been constructed along a 200 μm core HCS optical fibre. The characteristics of the sensors within the network were tested at different humidites. Sensors within the network had an accuracy better than 4% RH and this depended on the averaging time.

Averaging was carried out to increase the SNR since the backscattered signal is low. The lifetime of the visible laser was limited. This combined with the difficulty in fabricating the sensors within the network restricted the number of tests. Nevertheless, a multipoint sensing network has been demonstrated which could be developed into a practical system. Each sensing point could have a low insertion loss value associated with it. Using an OTDR with 15 dB range it is possible to accommodate a maximum of 15 sensors each being allowed a dynamic range of 1 dB.

The presence of peaks, at the sensing points, in an OTDR trace was investigated. It was found that the peak height for each sensor varied with RH while the attenuation, at 850 nm, remained unchanged. The variation in peak height could be developed as an RH indicator with the prospect of multiplexing a large number of sensors. This is possible because the insertion loss for each sensor is low, at 850 nm, and remains constant (with undetectable loss) while the peak height varies with RH. In addition there is a potential for high sensitivity. It was shown in Chapter 5 section 5.5.4.3, that the refractive index of gelatin/cobalt chloride film varied from about 1.46 to 1.56, as RH varies from 0 to 100% RH. This would give rise to a large Fresnel reflection as shown in Fig. 7.26 hence high sensitivity in such a sensing system.

This investigation exposed the prospect of developing a reflective multipoint network with the potential of multiplexing a much larger number of sensors.

CHAPTER 8

Conclusions and future work

8.1. Conclusions

The aim of the research reported in this thesis has been to develop a novel optical fibre humidity sensor suitable for use in an optical fibre multi-point distributed sensing system. This allows for the first time multi-point measurements of humidity along an optical fibre which can be distributed within an industrial plant or machine without the need for electrical power supplies. It is believed that such an approach would open-up new prospects for improving manufacturing quality and efficiency as well as energy efficiency in many industrial situations.

The above aim was achieved by following the programme detailed throughout the thesis. As a result, a novel single-point intrinsic optical fibre sensor has been developed. The sensor is based on the principle of using the absorption spectrum of a colorimetric reagent (cobalt chloride) immobilised on the surface of the core of a multimode optical fibre by employing a special thin gelatine film. Two-wavelength detection has been employed to provide referencing to minimise common mode intensity variations.

A low insertion loss, which is very important when multiplexing, was achieved by using a special film design. A two-wavelength optical time domain reflectometer (OTDR) has been developed and a four-sensor network has been built.

The characteristics of the sensor are summarised in the following points: -

(i) Achieved accuracy; better than 2% RH for values below 40% RH and about 1%RH for values above 40% RH.

(ii) The resolution, range and accuracy are functions of the cobalt chloride concentration, length and thickness of the film and optical fibre diameter.

(iii) Insertion loss of the sensor is less than 0.2dB. This is an important parameter in sensor multiplexing.

(iv) Repeatability has always been within 4% RH.

(v) A time constant of less than 0.5 sec was achieved and is a function of the film thickness.

(vi) Temperature coefficient is dependent on the concentration of cobalt chloride within the gelatine film and it is negligible for certain concentration.

(v) The resolution of measurement on the network can be better than 4 % RH, but because of noise in the OTDR the resolution value is dependant on averaging time in the instrument.

(vi) The OTDR responded to changes in the film refractive index which was a direct result of relative humidity. The response was much larger than the Rayleigh backscattered signal with negligible attenuation associated with it.

8.2 Future work

Following the success of the research carried out, a number of future developments areas have been identified. They can be summarised as follow: -

1. There are a number of applications where installation of a distributed humidity sensing system would be far easier than using multiple electronic humidity sensors. As a continuation to this work, a prototype multi-point distributed optical fibre humidity sensor is now being developed for the Building Research Establishment (BRE). The system is to be installed in air conditioning ductwork.

2. Engineering an arrangement to minimise the effect of dust and other particles. This may be solved by adding an additional film with a suitable affinity to water and a refractive index lower than both the sensing film and the core of the optical fibre.

3. As indicated in Chapter 5, some success has been achieved in immobilising cobalt chloride in porous silica using sol-gel process. This should be taken further as this has the potential of increasing the temperature range. Other polymeric materials should also be considered. For example, polyamide film retains usable properties at 300 ^{o}C for months and at 400 ^{o}C for few hours and withstands exposures of a few minutes to temperatures well above 500 ^{o}C (Billmeyer.1971, Lipscomb et al 1992).

4. The sensor developed responds to the moisture content of the immobilising agent. Polymers have varied abilities to retain moisture. Thus it may be possible that by using a number of different polymers as immobilising agents within a single sensing element, the sensitivity may be made uniform across the whole range. This is particularly important in OTDR multiplexing. For example, it was pointed out earlier that the sensor is more sensitive to humidities above 40%. So for example, concentration of the reagent must be increased if low values of humidity were important. This in turn

increases the total attenuation of the sensor across the whole range thus reducing the number of sensors on the network.

5. The availability of a spectrum analyser on a single chip makes it possible to implement a multiple sensor system using a single wide spectral source and a single fibre. A neat solution would be to incorporate a temperature sensor, operating at a different wavelength, within the sensing area.

6. The short lifetime of the laser diode used did not allow a full evaluation of the system. However more powerful visible laser diodes are expensive. It is expected that prices will decrease in the future. That coupled with the availability of very powerful DSP chips, which facilitate many of the signal processing functions required by the OTDR, makes the distributed sensing system a very practical proposition.

7. Developing a more efficient and systematic method of fabrication to produce near identical sensors.

8. Cellulose acetate is not suitable as an immobilising agent for cobalt chloride. It had weak adhesion to glass and suffered from leaching at high humidity.

9. Two water-soluble polymers have been identified as potential immobilising agents for cobalt chloride based sensors. These are HEC (Hydroxyethylcellulose) and HPC (Hydroxypropylcellulose). As a continuation of this work, tests are currently underway at the BRE to establish their viability. A new improved electronic system based on lock-in amplifier has been integrated into the sensing system. Initial results are promising. The variation of moisture content with relative humidity for these two polymers are well documented. Therefore, this work will also shed light on the relationship between the moisture content of the immobilising agent and the sensor characteristics.

10. Explore the prospect of developing a reflective multipoint sensing network with the potential of multiplexing a much larger number of sensors. Such a sensing system would rely on the change of refractive index of the sensing film (gelatin for example) with relative humidity. This was discussed in chapter 7 section 7.5.3.

References

Abeles F (editor), *Optical properties of solids*, North Holland publishing. The Netherlands, 1972.

Agrawal K K, Clary B L and Nelson G L, Investigation into the theories of desorption isotherms for rough rice and peanuts, *Journal of food science*, Vol. 36, pp. 919-924, 1971.

Allison M, Building management systems in the pharmaceutical industry, *Measurement & Control*, Vol. 29, No.10, pp. 300-303, 1996.

Andrews J R, A Frequency Calibrator of Uhf Using an Avalanche Transistor, *QST*, pp. 16-19, 1972.

Arnold C R and Rolls P J, *Applied Photography*, The Focal Press, 1971.

Arnold L K, *Introduction to plastics*, The Iowa State University Press, 1968.

Bakker-Arkema F W, Heat recovery in continuous-flow grain dryers, *International Meeting - Energy Savings in Drying Processes: Applications to Industry and Agriculture. 287th Event of the European Federation of Chemical Engineering*, pp. C9.1-C9.4, 1983.

Barnoski M K and Jensen S M, Fibre waveguide: a novel technique for investigating attenuation characteristic, *Applied Optics*, Vol. 15, pp. 2112-2115, 1976.

Barnoski MK, Rourke M D, Jensen S M and Melville, Optical time domain reflectometer, *Applied Optics*, Vol. 16, No. 9, 1977.

Barker G L, Temperature effect on lint cotton equilibrium moisture content, *Transactions of ASAE*, Vol. 35, No. 5, pp. 1377-1380, 1992.

Barrow G M, *Physical chemistry for the life sciences*, McGraw-Hill, 1979.

Bass H G, *Intrinsic Safety*, Quartermane House Ltd, Sunbury, UK, 1984.

Berkoff, Kersey A and Dandridge, Noise aliasing in interferometeric sensors utilising phase-generated carrier modultion, *Proc. SPIE*, Vol. 1169, p. 80,1989.

Bellingham and Stanley Ltd, *High accuracy Abbe Refractometer operators manual*, 1992.

Berro N, Cook J P D, Ingrey S, Lester T, Shepherd F R, Surridge R, Westwood W D, Airborne contamination on semiconductor wafers traced to humidification plant additives , *Journal of the IES*, Vol. 36, No. 6, pp.15-18, 1993.

Bhattacharya P, *Semiconductor Optoectronic Devices*, Prentice Hall, 1994.

Bhave R R, *Inorganic Membranes*, Van Nostrand Reinhold, New York, 1991.

Billings A, *Optics, Optoelectronics and Photonics, Engineering Principles and Applications*, Prentice Hall, 1993.

Billmeyer F W, *Textbook of Polymer Science*, John Wiley, 2nd Ed., 1971.

Birch K P, Optical fringe subdivision with nanometric accuracy, *Precision Engineering*, Vol. 12, No. 4, pp. 195-198, 1990.

Birch K P and Downs M J, The precise determination of the refractive index of air, *NPL report MOM90*, July 1988.

Blank L C and D M Spirit, Otdr performance enhancement through ebrium fibre amplification, *Electronics Letters*, Vol. 25, No. 25, pp. 1693-1694, 1989.

Bohren C F and Huffman D R, Absorption and scattering of light by small particles, Wiley, New York, 1983.

Boisde G and Harmer A, *Chemical and Biochemical with Optical Fibers and waveguides*, Artech House, 1996.

Bolton W, *Engineering materials*, Heinemann Newnes, 1989.

Bowes K, Fibre connectors: A primer for the wary designer, *Photonics Spectra*, Vol. 23, pp. 115-120, Oct.1989.

Boyle H B, *User's directory of electrical transduces*, Butterworth-Heinemann, 1992.

Bradbury E and Martin C, The effect of the temeprature of preparation on the mechanical properties and structure of gelatin films, *Porc.Roy.Soc. A*, Vol. 214, pp. 183-192, 1952.

Brady G S and Clauser H R, *Materials Handbook*, McGraw Hill, 1992.

Briston J H and Katan L L, *Plastics Films*, Published for The Plastics Institute, ILIFFE Books, London 1974.

Bruce J A, Dupuis S R, Gleason R, Linde H, Effect of humidity on photoresist performance, *Journal of the Electrochemical Society*, Vol.144, No. 9, pp. 3169-3174, 1997.

Brydson J A, *Plastics Materials*, ILIFFE Books Ltd, London, 1969.

BS 1339, *Definitions, formulae and constants relating to the humidity of the air*, 1965.

Bucks J A, *Fundamentals of Optical Fibres*, John Wiley, 1995.

Carr-Brion K, *Moisture sensors in process control*, Elsevier, UK, 1986.

Castelli J A and Tenney A S III, Paper drying control with high performance moisture sensors, *Advances in Instrumentation and Control : International, Conference and Exhibition*, Vol. 51, No.2, pp. 1451-1456, 1996.

Charrier J, *Polymeric Materials and Processing*, Hanser Publishers, 1990.

Cole J, Danver B., and Bucaro J., Synthetic-Hetrdyne Interferometric Demodulation. *IEEE J. Quantum Electron*, Vol. QE-18, p. 694, 1982.

Conduit A J, Hartog A H, Hadley M R, Payne D N, Gold M P, Mansfield R J and Tarbox E J, High-resolution measurement of diameter variations in optical fibres by the backscatter method, *Electronics Letters*, Vol. 17. No. 20, 1981.

Conley M P, Zarobila C.J. and Freal J., Reflection Type Fibre-Optic Sensor, *Proceedings of SPIE, Fibre Optic and Laser Sensors IV*, Vol. 718, pp. 237-239, 1986.

Croft V G, The wet and dry hygrometer, *Con. Proc. on Humidity Sensors and Their Calibration*, NPL 1986.

Culshaw B and Dakin J, *Optical fibre sensors: systems and applications*, Vol. 2, Artech House, 1989.

Dagnall H, Exploring surface texture, Rank Talylor Hobson Ltd, 2nd edn., 1986.

Dakin J P (ed.), *The distributed Fibre optic sensing handbook*, Springer-Verlag, 1990.

Dakin J and Culshaw B, *Optical fibre sensors: principles and components*, Vol. 1, Artech House, 1989.

Dakin J P, Distributed optical fiber sensor systems, in Culshaw B and Dakin J (eds), *Optical fibre sensors: systems and applications*, Vol. 2, Artech House, 1989.

Dandridge A, Tventen and Giallorenzi, Homodyne Demodulation scheme for fibre optic sensors using phase generated carrier, *IEEE J.Quantum Electron*. Vol. QE-18, p. 1647, 1982.

Danielson B L, Backscatter Measurement on optical fibres, *NBS Special Publication*, No. 637, pp. 1-46, 1982.

Davidson R L, *Handbook of Water-Soluble Gums and Resins*, McGraw-Hill, 1980.

Davies D E N, Signal Processing for Distributed Optical fibre sensors, *Proc. 2nd Int. Conf. On Optical Fibre Sensors*, pp. 285-293, 1984.

Davis C, Fibreoptic Sensor Technology Handbook, Optical Technologies, Herndon, Va. 1986.

Davis A and Sims D, *Weathering of Polymers*, Applied science Publishers Ltd, England 1983.

Dean J A, *Lange's Handbook of chemistry*, McGraw-Hill, 1990.

Diebold G J, Effect of A/D converter resolution on signal averaging, *Rev. Sci. Instrum.*, Vol. 48, No. 12, 1977.

Diedling M, Avoiding the ten most common mistakes in garment drying, *American Dyestuff Reporter*, Vol. 78, No. 9, pp. 86-88, 1989.

Dislich H, 'Chapter 4; Thin Films from the Sol-Gel Process', in Klein LC (editor), *Sol-Gel Technology for Thin Films, Fibers, Preforms, Electronics, and Speciality Shapes*, New Jersey 1987.

Downs M J and Birch K P, Bi-directional fringe counting interference refractometer, *Precision Engineering*, Vol. 5, No. 3, 1983.

Eder J M, *History of photography*, Dover Publication, New York 1978.

Fabelinskii I L, *Molecular scattering of light*, Plenum, New York, 1968.

ETSU, Sensors R&D for Energy Efficiency in Industry, *General Report No. 11*, March 1993.

Fowles G R, *Introduction to modern optics*, Holt, Rinehart and Winston Inc., New York 1968.

Garofalini S H, 'Chapter 2; Simulation of Sol-Gel Process', in Klein LC (editor), *Sol-Gel Technology for Thin Films, Fibers, Preforms, Electronics, and Specialty Shapes*, New Jersey 1987.

Gerthsen P, Gilsing J A A and Van Tol M, An automatic dew-point hygrometer using Peltier Cooling, *Philips Tech. Rev.*, Vol. 21, p. 196, 1959.

Gjessing D T, Holm C and Lanes T, Simple Rapid-Response Hygrometer, *Electronics Letters*, Vol. 3 No.4, pp.156-157, 1967.

Goldsmith P and Cox L C, An improved elecrolytic hygrometer. *J. Sci. Instrum.*, Vol. 44, p. 29, 1967.

Gowar J, *Optical Communication Systems*, Prentice Hall, London, 1984.

Graff G, Fiber Optics Analze Chemical Processes, *High Technology*, Vol. 3, No. 2, pp.24-25, Boston, Feb 1983.

Griffiths E and Awbery J H, A hygrometer employing glycerine, *Proc. Phys. Soc.* Vol. 39, p. 79, 1926.

Hadley L N and Dennison D M, Reflection and Transmission Interference filters Part I. Theory, *J. Opt. Soc. Am.*, Vol. 37, No. 6, pp. 451-465, 1947.

Hale K F, Optical Fibre sensors for inspection, *Physics in Technology*, Vol. 15 No. 3, pp.129-135, 1984.

Harbison B B, Roberts W I, and Aggarwal I D, Fusion splicing of heavy metal fluoride glass optical fibres, *Electronics Letters*, Vol. 25, pp. 1214-1216, August 1989.

Harrick N J, *Internal Reflection Spectroscopy*, John Wiley & sons, 1967.

Harrison L P, Fundamental Concepts and Definitions Relating to Humidity, *Int. Symposium on Humidity & Moisture.* Vol. 3, pp. 3-69, Washington DC 1963.

Hayashi I, Panish M B, Foy P W and Sumski S, *Appl. Phys. Lett.*, Vol. 17. p. 109, 1970.

Healey P, Optical Time Domain Reflectometry - A Performance Comparison Of The Analogue And Photon Counting Techniques, *Optical and Quantum Electronics*, Vol. 16, No. 3, pp. 267- 276, 1984.

Healy P and Hensel P, Optical time domain reflectometry by photon counting, *Electronics Letters*, Vol. 16, No.16, pp. 631-633, 1980.

Healy P and Malyon D J, OTDR in single-mode fibre at 1.5 mm using hetrodyne detection, *Electronics Letters*, Vol. 18, No. 20, pp. 862-863, 1982.

Hecht J, *The Laser Guidebook*, McGraw-Hill 1991.

Hedvig P, *Dielectric of Spectroscopy of polymers*, Adam Hilger Ltd, Bristol 1977.

Hench L L and West J K, The Sol-Gel Process, *J. Amer. Chem. Society*, Vol. 90, pp. 33-72, 1990.

Hench L L, Wang S H and Nogues J L, Gel-silica Optics, *Proc. of SPIE Multifunctional Materials*, Vol. 878, pp.76-85, 1988.

Hercules, *Klucel Hydroxypropylcellulose, Natrosol Hydroxyethylcellulose*: *Physical and Chemical Properties*, Aqualon, a Division of Hercules Incorporated, 1994.

Hickman M J, *Notes on Applied Science No.4: Measurement of Humidity*, National Physical Laboratory London, 1970.

HMSO, *Information on concentration and determination procedures in atomic spectrophotometry*, Crown, London, 1992.

Ho Z Z, Chen R T and Shih R, Electro-optic phenomena in gelatin-based poled polymer, *Appl. Phys. Lett.*, Vol. 61 part 1, 1992.

Horowitz P and Hill W, *The Arts of Electronics*, Cambridge University Press, 1989.

Huglin M B, *Light scattering from polymer solutions*, Academic press, 1972.

Hunt D G, Prediction of sorption and diffusion of water vapour by nylon-6,6, *Polymer*, Vol. 21, 1980.

Inamatsu T and Takashi C, A Dew-Point Hygrometer by Quartz Crystal, *Proceedings of the International Symposium on Moisture and Humidity*, pp.379-388, Washington D.C., 1985.

Itaya Y and Hasatani M, R & D needs -drying of ceramics, *Drying Technology* , Vol. 14, No. 6, pp. 1301-1313, 1996.

Jones B E, *Instrumentation, measurement and feedback*, Tata McGraw-Hill, 1978.

Jones B E, Simple optical sensors for the process industries using incoherent light, *Proc. Inst. Measurement and control sysmposium* (Optical Sensors and Optical Techniques in Instrumentation), London, 1981.

Jones B E, Medlock R S, and Spooncer R S, Intensity and wavelength-based sensors and optical actuators, in Culshaw B and J Dakin, (Eds), *Optical fibre sensors: Systems and Applications*, Vol. 2, Artech House, 1989.

Jones B E and Spoonser R C, An optical fibre pressure sensor using a holographic shutter modulator with two-wavelength Intensity referencing, *Proc. 2nd Int. Conf. on Optical fibre sensors, Stuttgart (Proc. SPIE 514)*, pp. 223-226, 1984.

Jones B E, Optical Fibre Sensors And Systems for Industry, *J. Phys. E: Sci. Instrum.*, Vol. 18, pp. 770-782, 1985.

Jones T P and Porter M D, Optical Sensor Based on Infrared Spectroscopy, *Applied Spectroscopy*, Vol. 43, No. 6, pp. 908-911, 1989.

Kao K C and Hockham G A, Dielectric-fibre surface waveguides for optical frequencies, *Proc. IEE*, Vol. 113, No. 7, pp. 1151-1158, 1966.

Kashima N, *Passive Optical Components for Optical Fiber Transmission*, Artech House, 1995.

Kazovsky L, Benedetto S and Willner A, *Optical Fibre Commuinication Systems*, Artech House 1996.

Keck D B, Morrow A J, Nolan D A and Thomson D A, Passive Components In The Subscriber Loop, *J.Lightwave Tech.*, Vol. 7, pp. 1630-1633, Nov. 1989.

Keiser G, *Optical fibre communications*, McGraw-Hill 1991.

Keitz H.A.E., *Light calculations and measurements*, Macmillan, 1971.

Kemp I C, The Importance of Humidity in Solids Drying Processes, *Proc. Third international symposium on humidity & moisture, Hosted by NPL London*, Vol. 1 pp. 18-25, April 1998.

Kenchington A W and Lauder W E, Reactions of gelatin bifunctional reagents, *Proc. of a conf. on Recent Advances in Gelatin and Glue Research*, University of Cambridge, pp. 191-196, 1958.

Kesting R. E., *Synthetic polymeric membranes*, McGraw Hill, New York, 1971.

Kharaz A. and Jones B.E., A distributed optical-fibre sensing system for multi-point humidity measurement, *Sensors and Actuators A*, Vol. 46-47, pp.491-493, 1995.

Kharaz A. and Jones B.E., A intrinsic optical fibre sensor, *Intern. Conf. on Moisture and Humidity Measurements (Sira Ltd, Chislehurst)* Vol. 1, p. 1.1, 1993.

Kist R, Point sensor multiplexing, in Culshaw B and Dakin J, *Optical fibre sensors: systems and applications*, Vol. 2, Artech House, 1989.

Komatsu T and Tanaka T, Development Of Sensors For Noodle Manufacturing Process, *Japanese Technology Reviews. Section E, Biotechnology*, Vol. 4, No. 2, pp.109-112, 1994.

Krohn D A, Intensity Modulated Fibre Optic Sensors Overview, *Proceedings of SPIE, Fibre Optic and Laser Sensors IV*, Vol. 718, pp. 2-11, 1986.

Krohn D A, *Fibre Optic Sensors: Fundamentals and Applications, Instrument Society of America*, Research Triangle Park, N.C., 1988.

Kuisma H, Instrumentation For Improving Drying Processes, *ISA Transactions*, Vol. 27, No.2, pp. 31-35, 1988.

Laude J P, *Wavelength Division Multiplexing*, Prentice Hall, 1993.

Lemstra P J and Kleintjens L A, *Integration of Fundamental Polymer Science and Technology*, Elsevier, England, 1989.

Lipscomb G.F., Lytel R., Ermer S., Valley J.F., Van Eck T.E., Girton D.G. and Ticknor, Organic Electro-optic Devices for optical interconnection, *SPIE Nonconducting Photopolymers and Applications,* Vol. 1774, pp. 76-86, 1992.

Loughlin C, *Sensors For Industrial Inspections*, Kluwer Academic Publishers, 1993.

Maier F A and Seeger H, Automation of optical time-domain reflectometry measurements, *Hewlett-Packard Journal*, pp. 57-62, 1995.

Magariños J R and Coleman D J, Holographic mirrors, *Optical Engineering*, Vol. 24 No. 5, pp. 769-180, 1985.

Macleod H A, *Thin-film optical filters*, Adam Hilger, London 1969.

Mason L F A, *Photographic Processing Chemistry*, The Focal Press, 1975.

McKellar J F and Allen N S, *Photochemistry of Man-Made Polymers*, Applied Science, England, 1979.

Meteorological Office, *Handbook of Meteorological Instruments*, Volume 3: Measurement of Humidity, HMSO, London, 1981.

Miki T, Yamaguchi H and Yoshiro N, An Accurate Wide-Band Automatic Waveform Analzer, *IEEE Transactions on Instr. and Measurement,* Vol. IM-26, No. 4, pp. 279-291, 1977.

Millman J and Taub H, *Pulse, digital, and switching waveforms*, McGraw-Hill, 1965.

Miller H H and Hirschfeld T B, Fibre Optic Chemical Sensors for Industrial and Process Control, *Proceedings of SPIE, Fibre Optic and Laser Sensors IV,* Vol. 718, pp. 237-239, 1986.

Milton K, *The scattering of light and other electromagnetic radiation*, Academic Press, 1969.

Misra A, David D J, Snelgrove J A and Matis, *J. of Appl. Polymer Scienece*, Vol. 31, pp. 2387-2398, 1986.

Mitschke F, Fiber-Optic Sensor for Humidity, *Optics Letters*, Vol. 14, No. 17 pp.967-969, 1989.

Miya T, Terunuma Y, Hosaka T and Miyashita T, Ultimate low-loss single mode fibre at 1.55 μm, *Electron. Lett.*, Vol. 15, p. 107, 1979.

Morisawa M, Uematsu H and Muto S, Optical Humidity Sensor with a Fast Response Time Using Dye-Adsorbed Langmuir-Blodgett Films, *Jpn. J. Appl. Physics*, pp.1202-1205, 1992.

Murtaza G and Senior J M, Referencing strategies for intensity modulated optical fibre sensors: a review, *Optics and Laser Technology,* Vol. 25, No. 4, pp. 235-245, 1993.

Narayanaswamy R and Sevilla III F, Optical fibre sensors for chemical species, *J. Phys. E: Instrum,* Vol. 21, pp. 10-17, 1988.

Nelson A R, McMahon D H and Gravel R L, Passive multiplexing system for fibre optic sensors, *Applied Optics*, Vol. 19, pp. 2917-2920, 1980.

Nevell T P and Zeronian S H, *Cellulose Chemistry and its applications*, Horwood, England, 1985.

Nicia A, Practical low-loss lens connector for optical fibres, *Electronics Letter*, vol. 14, pp. 511-512, August 1978.

Nicia A, Lens Coupling in Fiber Optic Devices: Efficiency Limits, *Applied Optics*, Vol. 20, No. 18, pp. 3136-3145, 1981.

Norton H N, *Handbook of Transducers for Electronic Measuring Systems*, Prentice-Hall, 1969.

Nussbaum A and Phillips R A, *Contemporary optics for scientists and engineers*, Prentice-Hall Inc., 1976.

Ogawa K, Tsuchiya S, Kawakami H and Tsutsui T, Humidity-sensing effect of optical fibre with microporous SiO_2 cladding, *Electronics Lett.* Vol. 24, No. 1, 1988.

Okada K, Backscattering Measurment, Japan Annual Reviews in Electronics, Computers & Telecommunications; in Suematsu Y, *Optical Devices & Fibers*, pp.299-313, 1982.

Park H S and Day D E, Corrosion of evaporated Ag Films on Glass by saturated water vapor, *Solar energy Materials*, Vol. 13, pp. 351-365, 1986.

Perkowitz S, *Optical Characteristics of Semiconductors*, Academic Press, London, 1993.

Perry's chemical engineers' handbook, McGraw-Hill, 1984.

Personick S D, *Fibre Optics Technology and Applications*, Plenum Press, 1985.

Phillips, Optoelectronics Centre, Shortwavelength semiconductor *Lasers reference data*, 1994.

Photodyne, *Model 5400XQ High Resolution Optical Time Domain Reflectometer Instruction Manual*, 1987.

Potyrailo R and Golubkov, Optical Waveguides In Analytical Chemistry: Recent Advances, *Sensors Review: The interntional Journal of sensing for industry*, 1992.

Poulter K F, Hales J L, Forton A G and Pragnell R F, The UK National Humidity Standard-Justification and concept, *Proceedings of the International Symposium on Moisture and Humidity*, pp.7-13, Washington D.C., 1985.

Powell G R, Crosby P A, Fernando G F, France C M, Spooncer R C and Waters D N, Optical Fiber Evanescent Wave Cure Monitoring of Epoxy Resins, *Proceedings of SPIE - The International Society for Optical Engineering*, Vol.2718, pp.80-92, 1996.

Pragnell R F, Review of humidity sensors, *Conf. Proc. Humidity Sensors and their Calibration*, pp.*3-11*, NPL 1986.

Psaila D C, Poole S B and Screats M G, An Optical fibre Humidity Sensor, *Proc. 7th Optical Fibre Sensors*, pp.59-62, Sydney 1990.

Rank Taylor Hobson Ltd, *Surtronic 3+ user manual*, 1993.

Rabinovich E M, Johnson D W, MacChesney J B and Vogel E M, Preparation of High-Silica Glasses from Colloidal Gels: I, Preparation for Sintering and Properties of Sintered Glasses, *J. Amer. Ceramic Society*, Vol. 66, No. 10, pp.681-688, 1983.

Ramaswany R V, Chia T, Srivastava, Milliou A and West J., Gel Silica Waveguides, *Proc. of SPIE Multifunctional Materials*, Vol.878, pp.86-93, 1988.

Reay D and Pilavachi P A, *Energy: Needs for Strategic R&D in support of improved energy efficiency in the processing industries*, Report No. GP-EUR/11920, Commission of the European Communities, 1989.

Roman G N, Urbicain M J and Rotstein E, Moisture Equilibrium in Apples at Several Temperatures: Experimental Data and Theoretical Considerations, *Journal of food science*, Vol.47, pp. 1485-1507, 1982.

RS data sheet, Peltier heat pumps, No. F9192, RS components UK, 1988.

Rudolf Seitz W, Chemical Sensors Based on Fibre Optics, *Analytical Chemistry*, Vol. 56, No. 1, pp. 16-34, 1984.

Russell A P and Fletcher K S, Optical sensor for the determination of moisture, *Anal. Chim. Acta.*, Vol. 170, pp. 209-216, 1989.

Sadaoka Y, Sakai Y and Murata Y, Optical Humidity and ammonia gas sensor using calcein-based films, *Sensors and Actuators B*, pp. 420-423, 1993.

Saunders P R and Ward A G, The physical properties of gelatin and its degradation products, *Proc. of a conf. on Recent Advances in Gelatin and Glue Research*, University of Cambridge, pp. 197-203, 1958.

Senior J M, *Optical Fiber Communications Principles and Practice*, Prentice Hall 2nd ed. 1992.

Sharp Corporation, Laser diode user's manual, 1986.

Sheem S K, Giallorenzi T G, Koo K, Optical techniques to solve the signal Fading problem in Fibre interferometers, *Applied Optics*, Vol. 21, No.4, pp.689-693, 1982.

Shi R and Jannson T, Chapter 5: Integrated Optical Waveguide Routing–Micro-optics, in Tocci C and Caulfield H J (editors), *Optical Interconnections Foundations and Applications*, Artech House, 1994.

Shih R, Chen R and Ho Z Z, Travelling-Wave Modulator Using a Gelatin-based EO Polymer, *Proceedings of SPIE, Nonconducting Photopolymers and applications*, Vol. 1774, pp. 111-117, 1992.

Sira, *Communications Course Notes on Humidity and Moisture Measurement, Techniques and applications in Industry, the Laboratory and environmental testing*, 1991.

Slater K, Control Of The Drying Process In Textile Production, *CCAC, Can Conf. on Autom. Control*, McGill Univ., Montreal, Que, p.20 1979.

Smith F G and Thomson J H, *Optics*, John Wiley 1971.

Smith P I, *Glue and Gelatine*, Sir Isaac Pitman & Sons Ltd, London 1929.

Snyder A W and Love J D, *Optical Waveguide Theory*, Chapman and Hall, 1983.

Solomon S, *Introduction to General, Organic, and Biological Chemistry*, McGraw Hill, 1991.

Spooncer R C, Al-Ramadhan F A and Jones B E, A Humidity Sensor Using a Wavelength-Dependent Holographic Filter With Fibre Optic Links, *Int. J. of optoelectronics*, Vol. 7 No. 3 pp. 449-452, 1992.

Spooncer R C, *Optical fibre sensors course notes*, BCMM, Brunel University, 1989.

Stainby G, Proc. of a Conference on Recent Advances in Gelatin and Glue research, held at University of Cambridge July 1957, Published by Pergamon Press in 1958.

Stewart G and Johnstone W, Evanescently Coupled Components, in Culshaw B and Dakin J, *Optical fibre sensors: Components and subsystems*, Vol. 3, Artech House, 1996.

Stokes E H, Equilibrated moisture content of several carbon phenolic composites, Vol. 30, No. 6, pp. 1597-1601, 1992.

Stuart A D and Grazier P E, A fibre optic relative humidity sensor, *Int. J. of Optoelectronics*, Vol.3 No. 2 pp. 177-186, 1988.

Sydenham P H (editor), *Handbook of measurement science; Practical fundamentals* Vol.2, Wiley,1983.

Syms R and Cozens J, *Optical Guided Waves and Devices*, McGraw-Hill, 1992.

Tachibana T, Inokuchi K and Kakiyama H, Tanning of gelatin monolayers, *Proc. of a conf. on Recent Advances in Gelatin and Glue Research*, University of Cambridge, pp. 243-245, 1958.

Takeo T and Hattori H, U-shaped fibre optic refractive index sensor and its applications, *EPIE Miniature and Micro Optics: Fabrication and system Applications*, Vol. 1544 pp. 282-286, 1991.

Tanaka K and Iwata M, Effect of water vapour on the switching phenomena in silver thin film produced by electroforming, *Thin solid films*, Vol. 81, pp. L85-L87, 1981.

Tateda M and Horiguchi T, Advanaces in Optical Time-Domain Reflectometry, *Journal of Lightwave Technology*, Vol. 7, No.8, 1989.

Theocharous E, Flourescence displacement transducer with a reference channel, *Third international conference on optical fibre sensors*, pp. 148-149, 1985.

Thomas I M, 'Chapter 1; Multicomponent Glasses from Sol-Gel Process', in Klein LC (editor), *Sol-Gel Technology for Thin Films, Fibers, Preforms, Electronics, and Specialty Shapes*, New Jersey 1987.

Tiefenthaler K and Lukosz W, Sensitivity of Grating Couplers As Integrated-Optical Chemical Sensors, *J. Opt. Soc. Am. B*, pp.209-220, 1989.

References

Toropainen A P and Vainikainen P V, Measurement of Humidity in Harsh Environmental Conditions, *Proc. of the Third international symposium on humidity & moisture, Hosted by NPL London,* Vol. 1, pp. 299-306, 1998.

Udd E, *Fibre optic sensors*, Wiley, New York, 1991.

Vainshtein S, Kostamovaara J, Kilpela A and Maatta K, Novel compact 35 A/150 ps current pulse generator for a new generation of the laser radars, *Proceedings of the 40th Midwest Symposium on Circuits and Systems.* Vol.1, pp.148-151, 1997.

Van Krevelen D W, *Properties of polymers*, Elsevier, The Netherlands, 1972.

Visscher G J W and Kornet J G, Long-Term Tests of Capacitive Humidity Sensors, *Meas. Sci. Technol.*, Vol 5 pp. 1294-1302, 1994.

Walker J A J and Campion P, The Use Of Electrolytic Hygrometers for The Determination of Water and Hydrogen, *Analyst*, Vol. 90, p 199, 1965.

Wang J, Cylindrical waveguide evanescent field ellipsometry, *Optical Engineering*, Vol.31 No. 7, pp. 1432-1435, 1992.

Ward A.G., The Chemical Structure and Physical Properties of Gelatin, *The Journal Of Photographic Science*, Vol. 3, pp. 60-67, 1955.

Ward A G, Recent Progress in Gelatine Research, *The British Food Manufacturing Industries: Scientific and Technical Surveys No. 31*, Leatherhead 1958.

Ward A G and Court A, *The science and technology of gelatin*, Academic Press, 1977.

Waynant R and Ediger M, *Electro-optics Handbook*, McGraw-Hill, 1993.

Wilson J and Hawkes J F B, *Optoelectronics: An Introduction*, Prentice-Hall, 1983.

Wolf H F, *Handbook of Fibre Optics:Theory and Applications*, Granada, 1979.

Wood D, *Optoelectronic Semiconductor Devices*, Prentice Hall 1994.

Young R A and Rowell R M, *Cellulose Structure, Modification and Hydrolysis*, Wiley, 1986.

Zhu C, Bright F V, Wyatt W A and Hietftie G M, A New Fluorescence Sensor for Quantification of Atmospheric Humidity, *J. Electrochem. Soc.*, Vol. 136 No. 2 pp.567-570, 1989.

APPENDIX I

Publications

1. A paper published on this work in the Proceedings of the Third International Symposium on Humidity & Moisture, Hosted by NPL London, Vol. 1, pp. 358-365 April 1998.

2. A paper published on this work in Sensors and Actuators A, Vol. 46-47, pp. 491-493, 1995.

DEVELOPMENT AND FIELD TRIALS OF AN OPTICAL FIBRE RELATIVE HUMIDITY SENSOR

Ahmad Kharaz[1], Ken Bromley[2], Ken Hale[3] and Barry Jones[3]

[1]The Open University, Milton Keynes, United Kingdom
[2]Building Research Establishment Ltd , Watford, United Kingdom
[3]Brunel University, Uxbridge, United Kingdom

Abstract: This paper describes the fabrication and the principle of operation of an optical fibre relative humidity sensor based on a cobalt chloride/ gelatine film. The sensor was first fabricated and characterised in the laboratory. Based on the laboratory results, a prototype sensor was then designed and constructed for evaluation in an environmental test room at the Building Research Establishment. The sensor together with a conventional thin film capacitance sensor were placed in the environmental test room and data were collected over a six week period. Results obtained are reported in this paper.

Keywords: optical fibre, humidity, colorimetric, sensor

1 INTRODUCTION

Humidity is an important quantity to control in many manufacturing environments. At the same time it is quite a difficult quantity to measure. With the advent of optical fibres and their availability at reasonable prices, a number of optical fibre sensors (OFS) for humidity measurement have been reported in an effort to overcome some of the problems of the presently available electronic sensors, most notably drift and the need for regular calibration [1-5]. Humidity OFS would not only have the advantages of freedom from electromagnetic interference, intrinsic safety and remote monitoring, but they also offer the prospect of a distributed sensing system using the fibre itself as the sensor and therefore providing means for multiple points of humidity measurement without the need for localised electrical power supplies [7].

This paper reports on the development and field trials of an optical fibre relative humidity sensor based on the colorimetric interaction of cobalt chloride with water molecules [6].

2 PRINCIPLE OF OPERATION

The sensor described here is based on the colorimetric interaction of cobalt chloride (reagent) with water molecules. The anhydrous salt is blue and turns pink as water of hydration converts the salt to hexahydrate [1]. In the sensor cobalt chloride is immobilised on the surface of the core of the optical fibre using gelatine film with a slightly higher refractive index than that of the fibre core, as shown in figure 1. Because of this, most of the light launched through the fibre will traverse the film thus interacting with cobalt chloride molecules and giving good responsivity to changes in atmospheric moisture. As the external humidity level alters so does the moisture content of the film and the light absorption in the sensitive wavelength region. Thus attenuation experienced by the wavelength signal in this region will give an indication of humidity level, while a second

wavelength signal outside the light absorption wavelength region is used to eliminate the common mode variations, notably temperature variation. Because the optical fibre itself is used to make the measurement the sensor is an intrinsic optical fibre device.

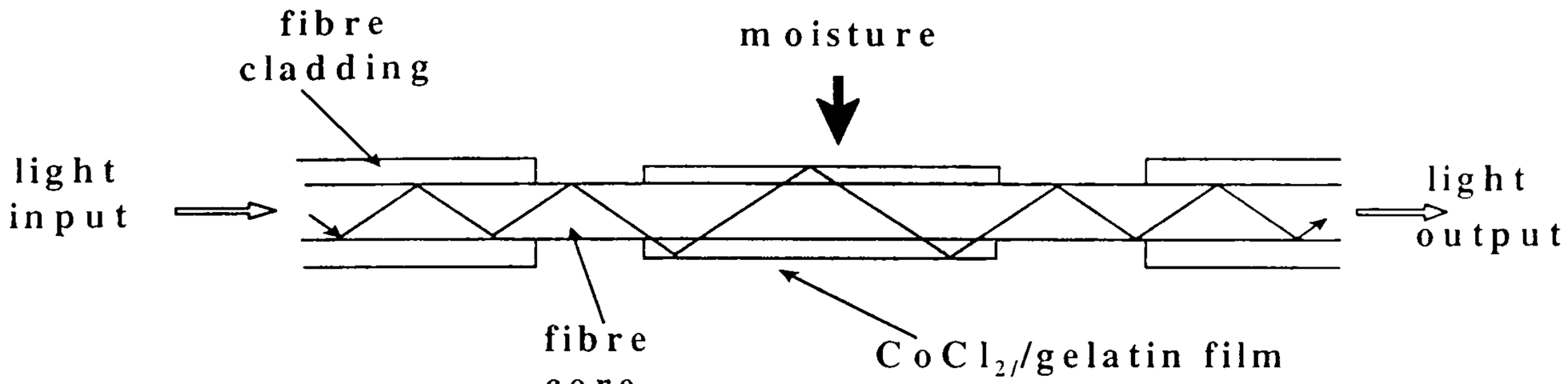

Figure 1 Basic sensor configuration

The change in light intensity due to absorption is determined by the type of the reagent in the optical path and is related to the concentration (C) via the Beer-Lambert relationship. This law describes an exponential reduction of light intensity with distance (and concentration) along the optical path. The relationship can be expressed logarithmically as follows:

$$A = log\frac{I_o}{I} = \varepsilon lC \qquad (1)$$

where A is the optical absorbance
ε is the molar absorptivity
l is the path length of the light
I_O is incident light intensity.
and I is transmitted light intensity.

The above equations can be rearranged as follows:

$$I = I_o e^{-\varepsilon lC} \qquad (2)$$

For the sensor in figure 1, light traverses the film as shown, thus the light path length is a function of both its thickness and its length.

3 EXPERIMENTAL

3.1 Laboratory tests

A single optical fibre sensor was constructed using 400 μm core HCS (hard clad silica) optical fibre. At the sensing point along the fibre the cladding was removed over 50 mm and replaced by the cobalt chloride-gelatine film, as shown in figure 1. A protective casing was fitted to the sensing part to prevent the fibre from breaking. White light was launched into the sensing fibre and the intensities of spectra of the collected light were measured using a spectrum analyser. The sensor was placed in an environmental chamber, as shown in figure 2, and two spectral responses of the sensor were obtained at two different

percentage relative humidity (% RH) values, at constant temperature of 25 °C (figure 3). It can be seen that a

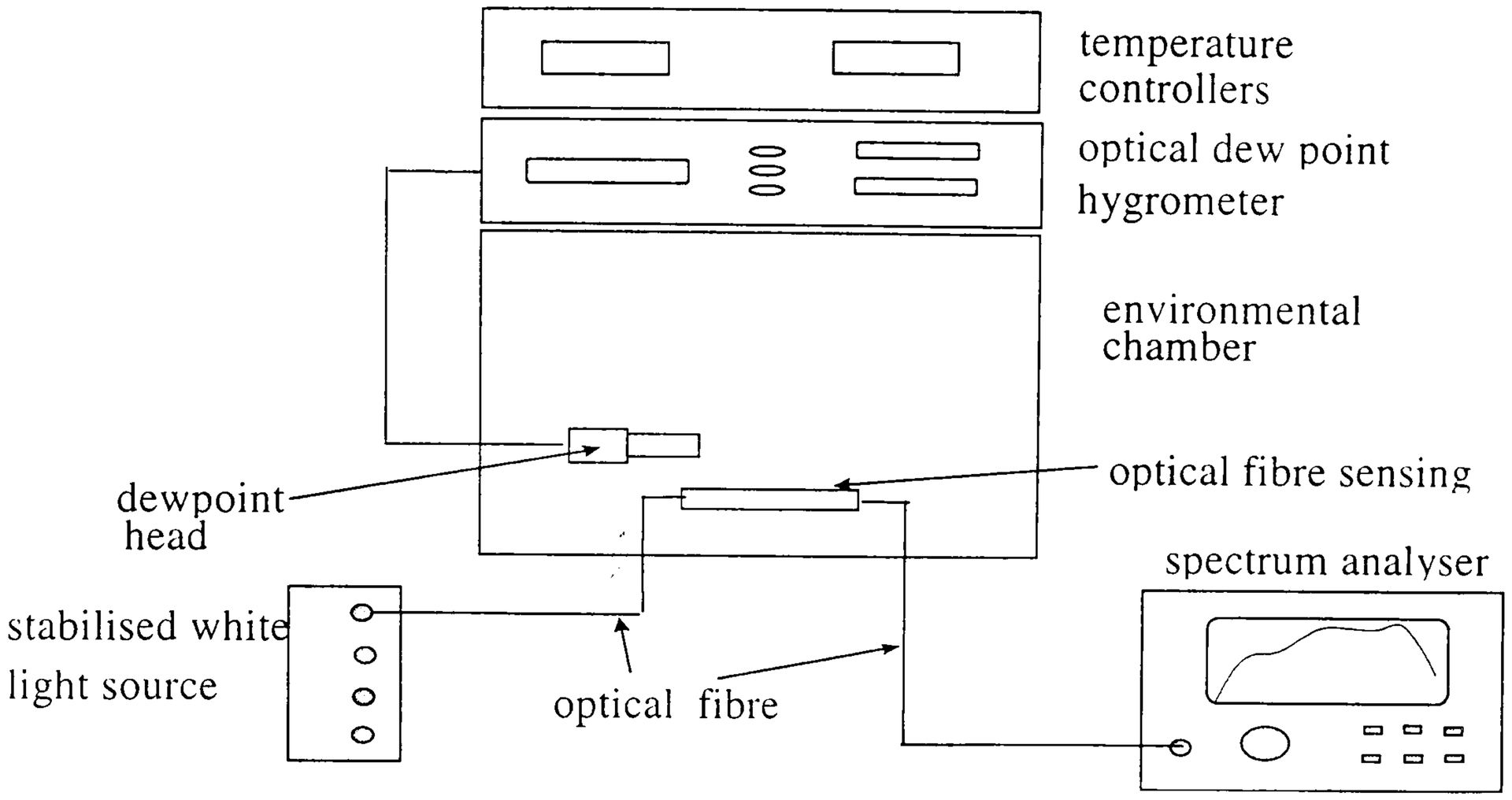

Figure 2 Experimental set-up

change of relative humidity affects the spectral absorption of the sensor in the wavelength region 600-740 nm. Hence a second wavelength outside this region (at, say, 850 nm) can be used to provide an intensity reference to enable a high degree of rejection to changes in common mode light intensity (as for example caused by temperature variations and demountable connectors). The attenuation of light by the sensor at a wavelength of 850 nm is 0.2 dB.

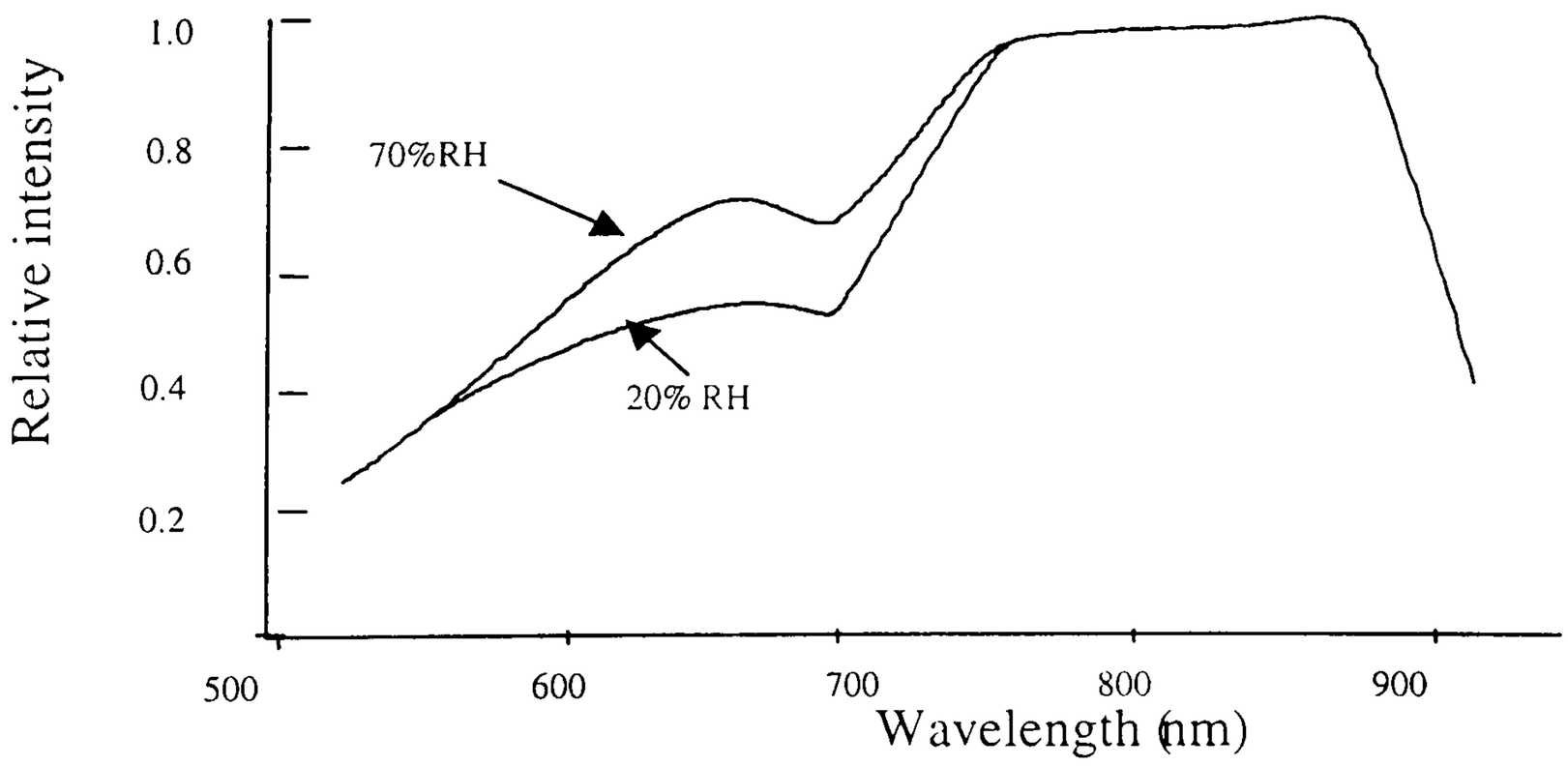

Figure 3 Spectral response of the sensor at two %RH values

With the sensor placed in the environmental chamber, the relative humidity was varied again with the temperature now kept constant at 25°C. At each humidity value the intensities of the collected light at the two wavelengths 670 nm and 850 nm were noted. The relative intensity curve plotted in the graph of figure 4 was obtained by dividing the intensity of light at 670 nm by that at 850 nm.

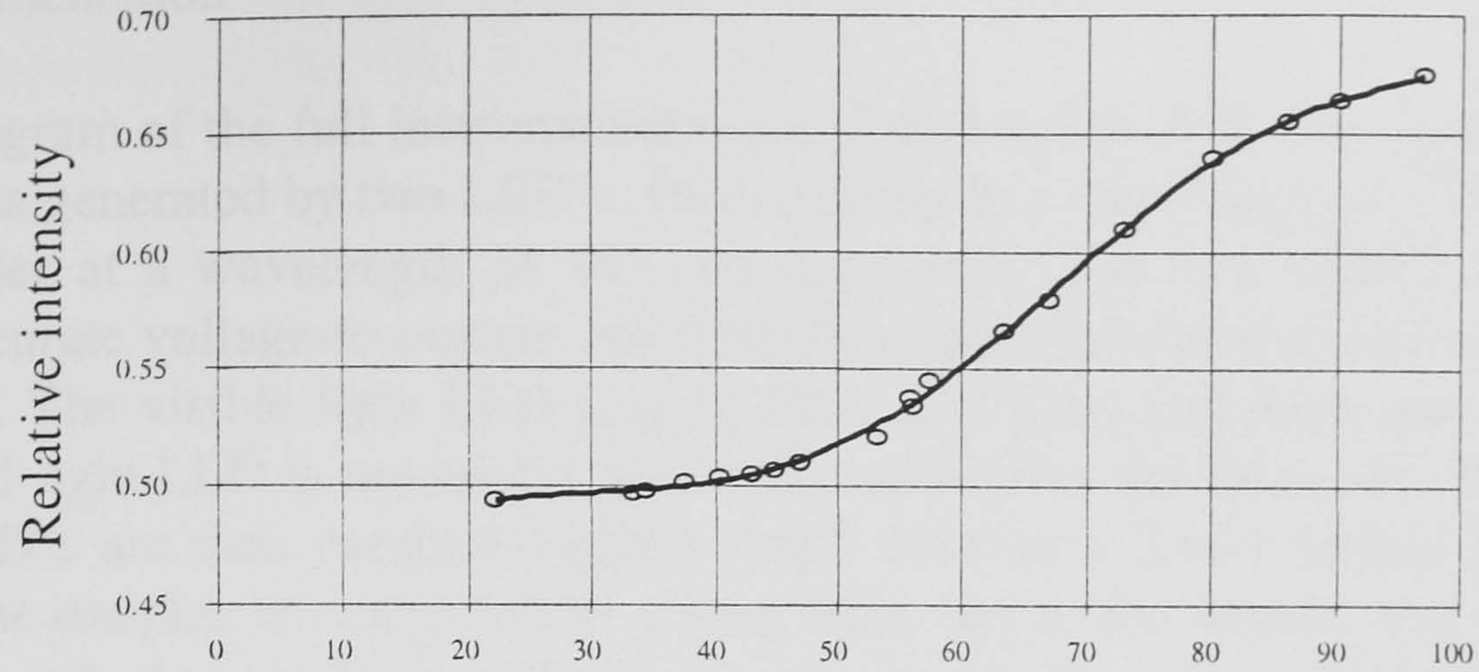

Figure 4 Sensor characteristic

It can be seen from the graph that the sensor has a higher sensitivity for relative humidity above 40% RH. Repeatability tests were undertaken over a 3-month period during which time the sensor was exposed to cycles of humidity change in the operating range 20 to 80% RH; repeatability was always within the resolution limit. The time constant of the sensor, defined as the time taken to reach 90% of the final value, was found to be approximately 1 second. This measurement was achieved by applying two moisture streams (70% RH and dry 20% RH) alternatively at the sensor. The resolution of the sensor, which is a function of the $CoCl_2$ concentration within the film and the length of the sensing area, was found to be better than 2% at greater than 40% RH, and better than 4% below 40% RH.

3.2 Field trials

A portable prototype sensor was designed and built in order to carry out humidity measurements in an environmental test room at the Building Research Establishment (BRE).

3.2.1 Sensing element

In order to protect the optical fibre sensing element it was fitted in a protective brass casing as shown in figure 5. Two optical fibre SMA connectors were fitted, one at each end of the sensing fibre, and secured in the assembly. Four ventilation slots were incorporated to allow air to get to the sensing fibre. In this way the sensor could be connected to long optical fibres by means of in-line connectors.

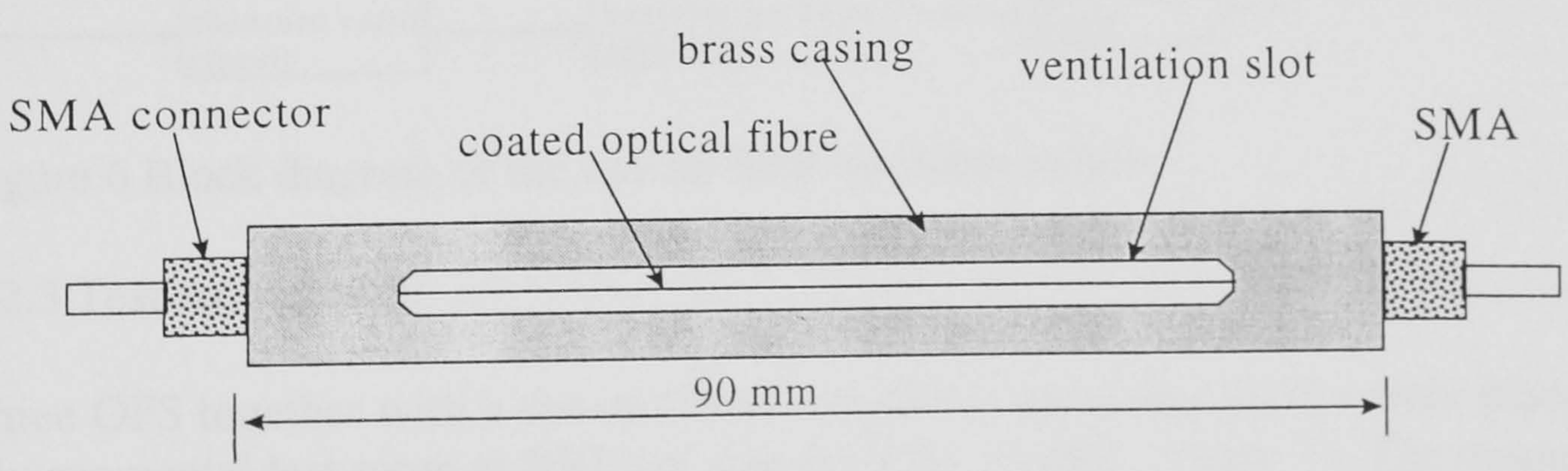

Figure 5 Sensor assembly

3.2.2 Instrumentation

A block diagram of the full instrumentation is shown in figure 6. The optical source for the system is generated by two LED's. One operates at a wavelength of 675 nm (visible) and the other at a wavelength of 863 nm (infra-red). The two LED's are driven by separate accurate voltage-to-current converters and are modulated at different sinusoidal frequencies. The visible light LED is modulated at 2 kHz, and forms the signal, while the infra-red light LED is modulated at 12 kHz, and forms the reference. The outputs of the two LED's are then combined into a single fibre by a 2-to-1 optical coupler. The output of the coupler is connected to a long fibre and to the sensor; this input fibre is made into a coil of about 20 mm diameter to ensure equilibrium mode distribution at the sensing point.

The light leaving the sensor is collected by another optical fibre and fed to a photodiode, as shown in figure 6. The photodiode converts the optical signal into an electrical form. Using electronic band-pass filters, the measurand and the reference parts of this signal are separated, i.e. into 2kHz and 12kHz signals. These two signals are then rectified by separate absolute value circuits. The rectified signals are converted into their equivalent dc values (averaged over 0.1 s) by two low-pass filters. The ratio of the two dc values (i.e. the measurand signal divided by the reference signal) is obtained using the analogue divider circuit. The output of the divider is between 0 to 10 V and varies with relative humidity.

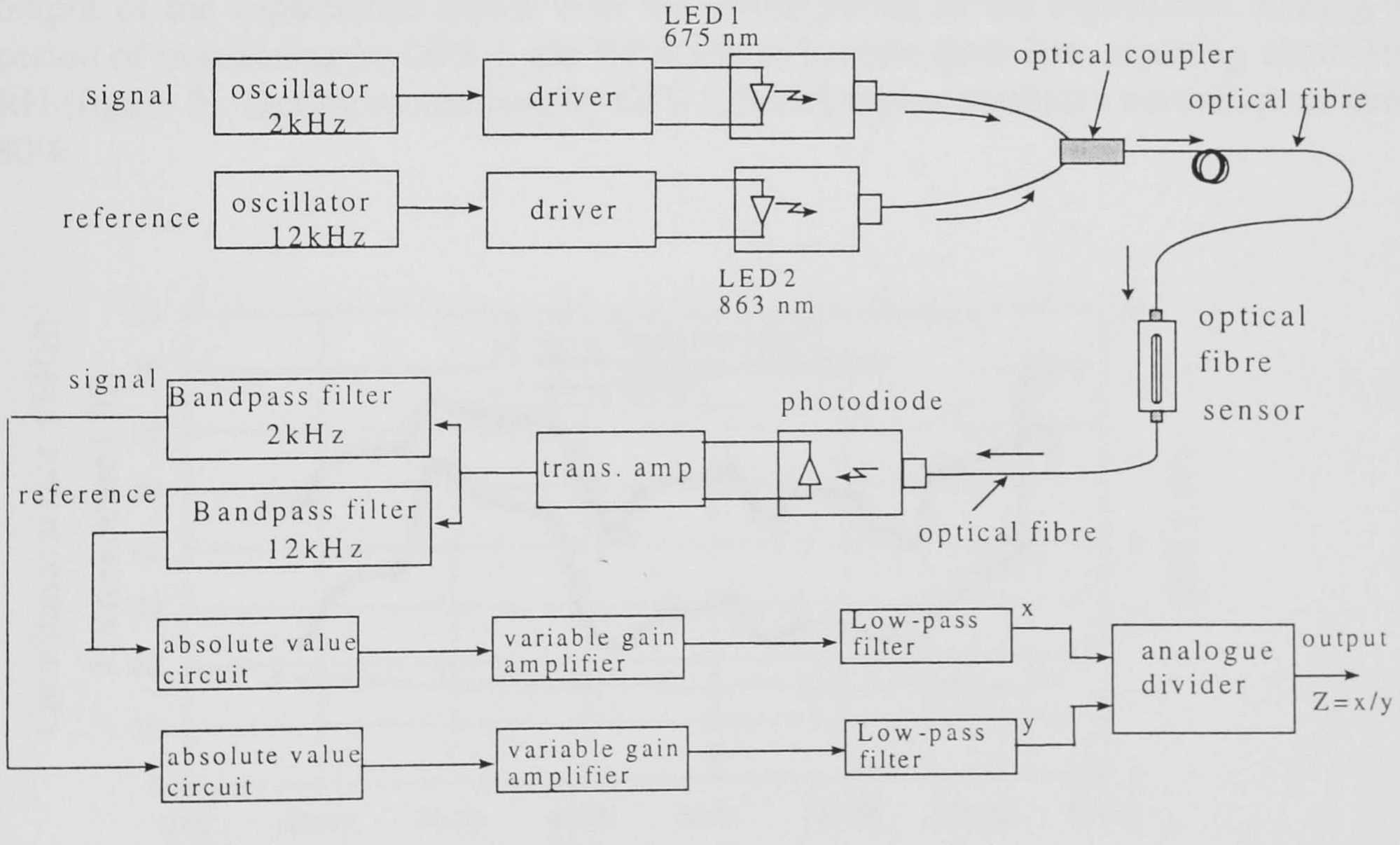

Figure 6 Block diagram of the optical fibre humidity sensor

3.2.3 Test arrangement

Three OFS together with a conventional thin-film capacitance sensor were placed in the environmental test room at BRE (of size 4m x5m x2.4m) (figure 7). The outputs of the sensors were connected to a data logger as shown. Relative humidity and temperature readings from the capacitance sensor, and the OFS output voltage were recorded every 5

minutes over a two week period for each sensor. A different OFS was selected for each of the three two-week test periods.

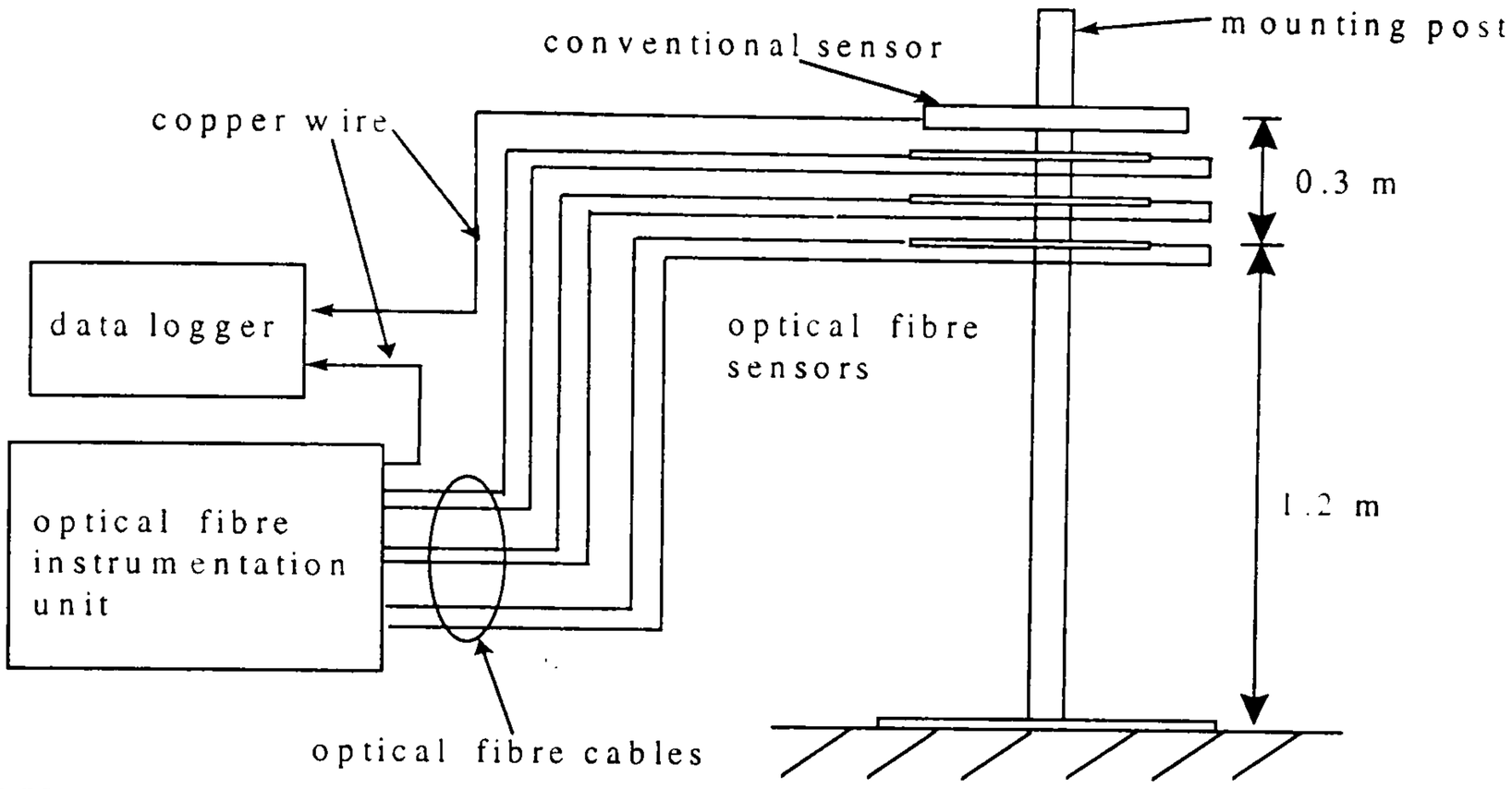

Figure 7 Test arrangement

3.2.4 Results

It can be seen from figures 8, 9 and 10 that the outputs of the three OFS followed the output of the capacitance sensor over the whole period of the experiment. During the period of monitoring by OFS 2, the %RH values became quite low, reaching about 16% RH (figure 9). During monitoring by OFS 3, %RH values reached a maximum of about 80%.

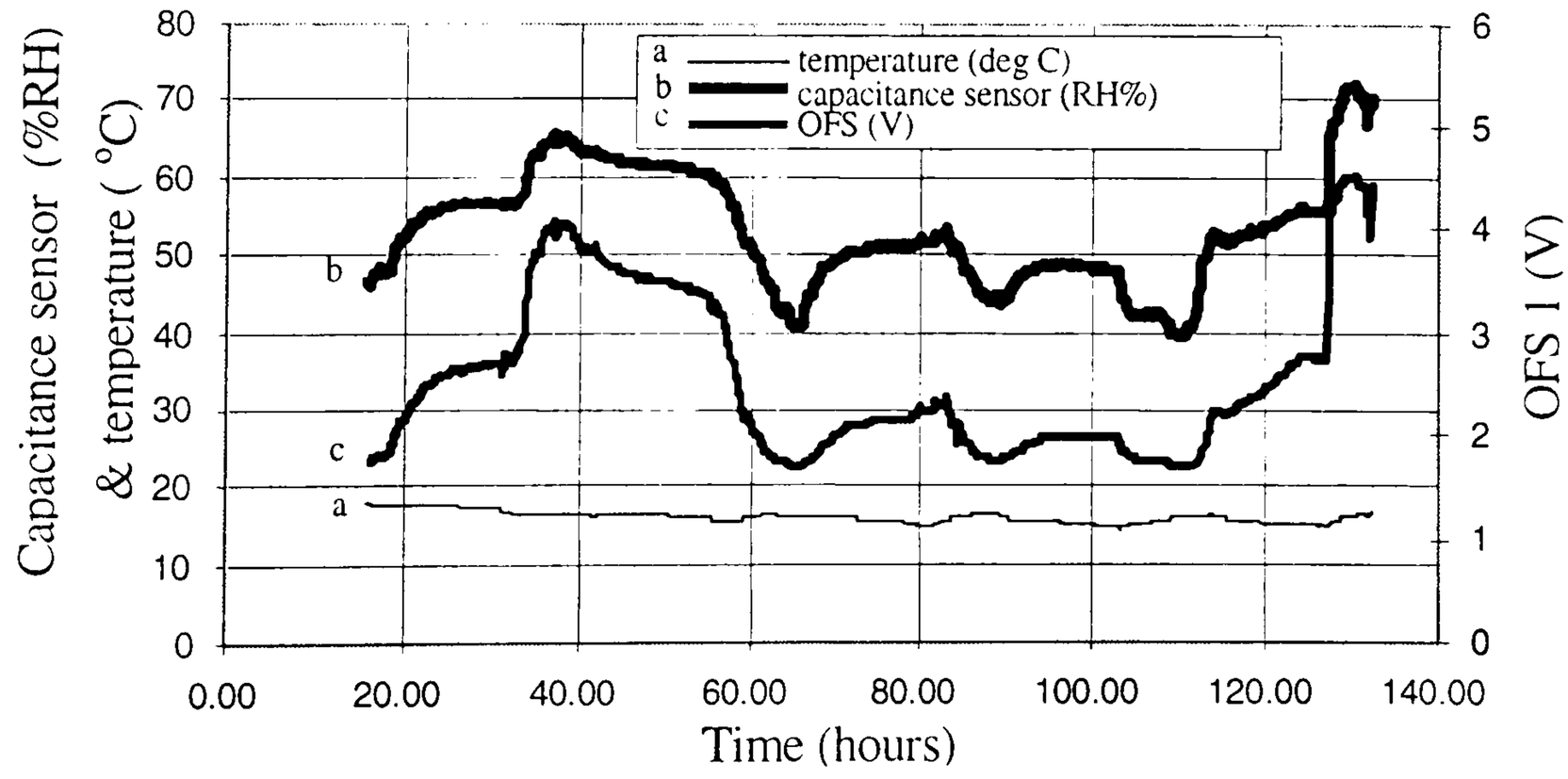

Figure 8 OFS 1, capacitance sensor %RH and temperature, versus time

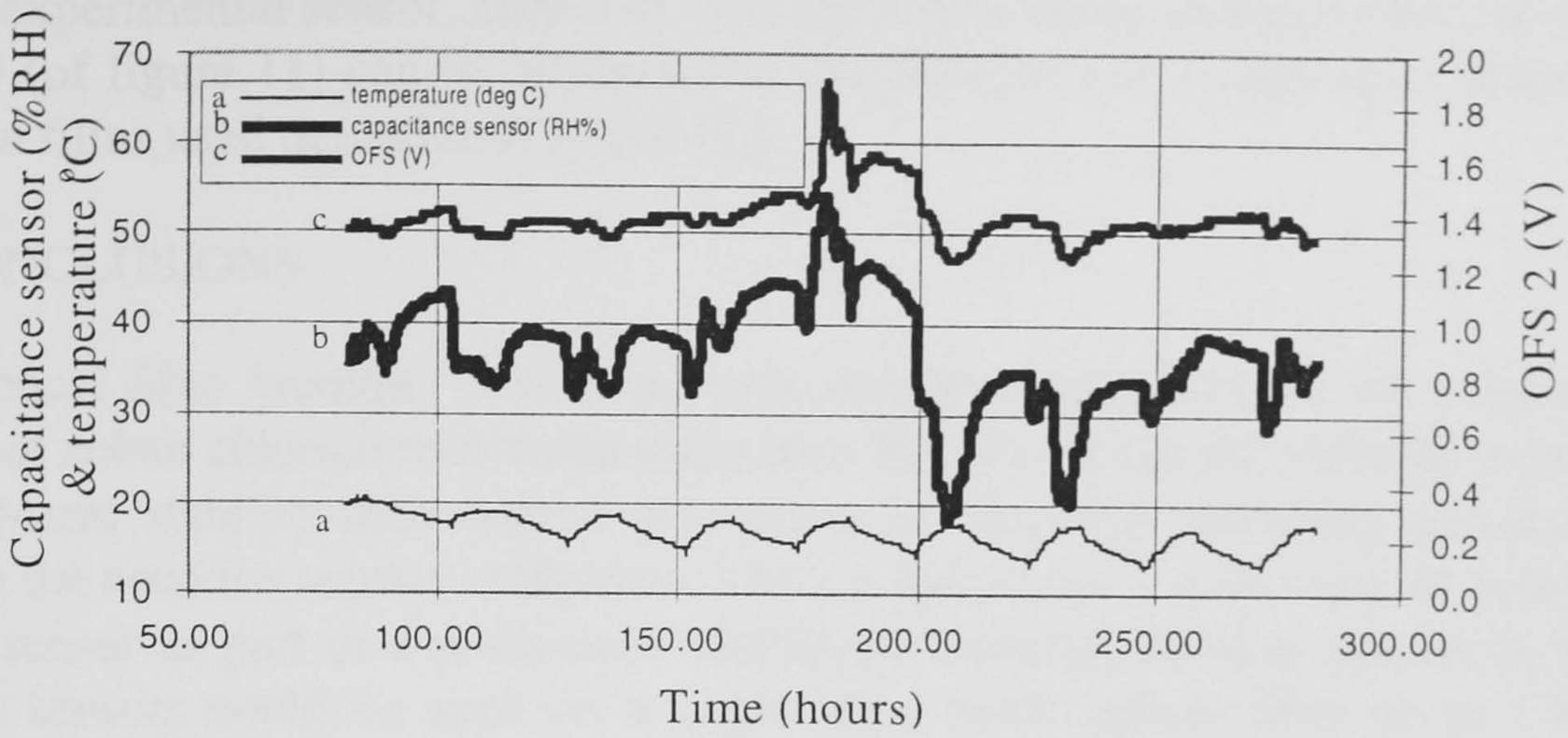

Figure 9 OFS 2, capacitance sensor %RH and temperature versus time

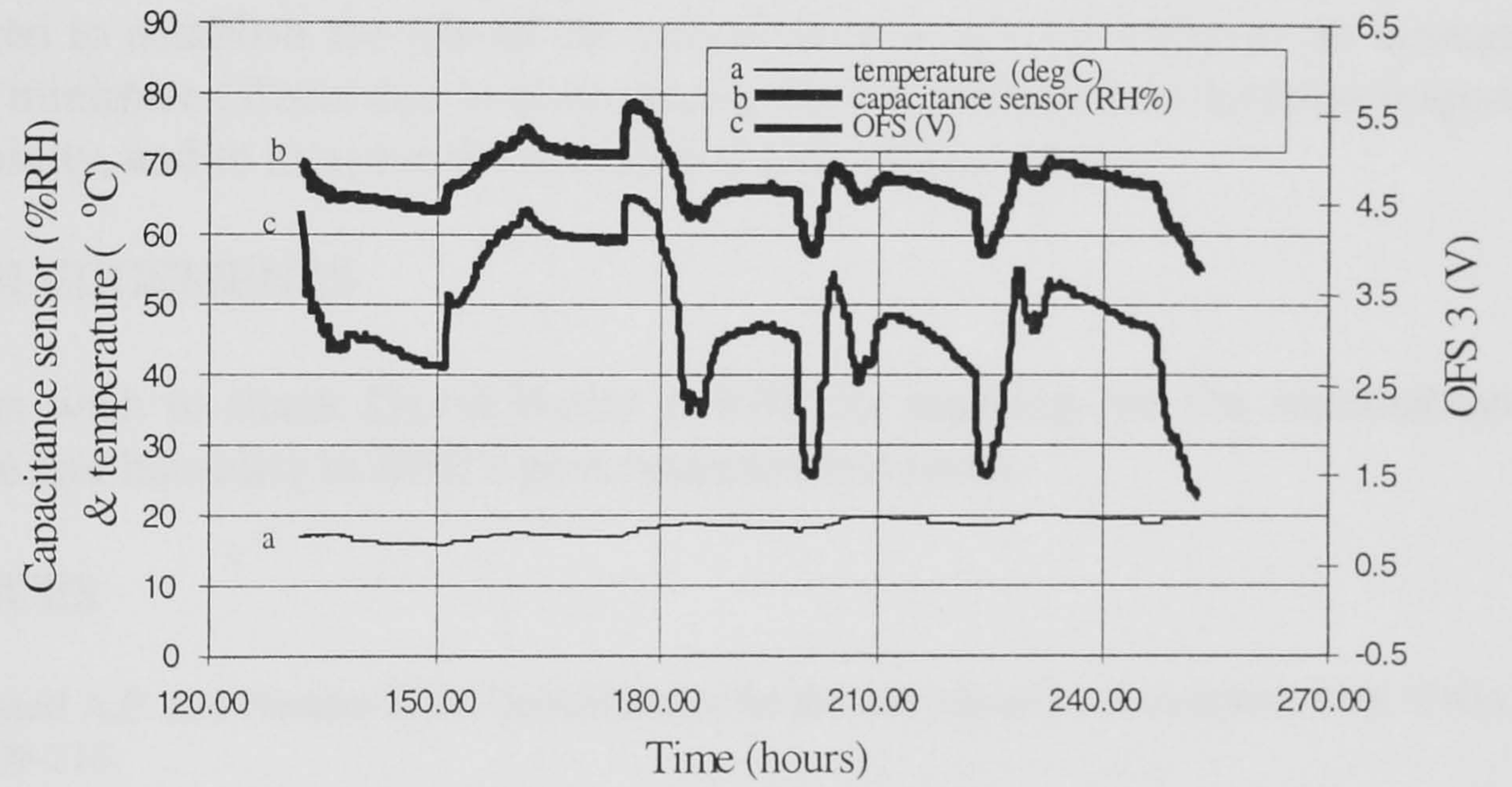

Figure 10 OFS 3, capacitance sensor %RH and temperature versus time

In figure 11, OFS 1 and OFS 3 outputs have been plotted against the %RH measured by the capacitance sensor.

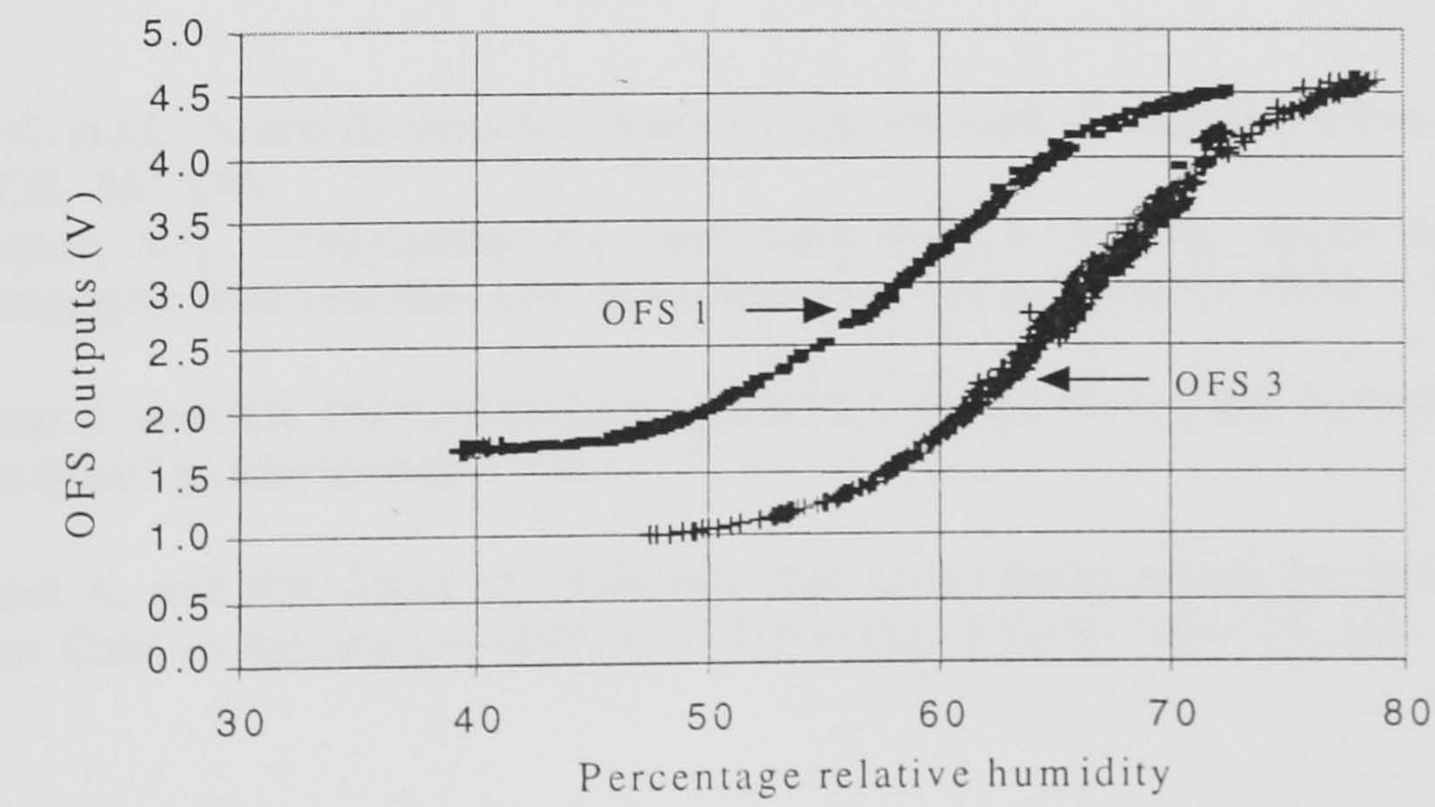

Figure 11 OFS 1 & OFS 3 outputs versus %RH as measured by capacitance sensor

The characteristics of these sensors show that they behaved in a same manner to that of the earlier experimental sensor (figure 4). The difference in the characteristics of OFS 1 and OFS 3 (of figure 11) can be attributed to the difference in length and thickness of the two thin films used (equations (1) and (2)).

4 CONCLUSIONS

A novel optical fibre humidity sensor has been demonstrated based on the colorimetric interaction of cobalt chloride with water molecules. The sensor has the potential to provide better long-term stability than current generations of electronic humidity sensors, thus eliminating the need for regular calibration. There is the prospect, moreover, of being able to use the sensor as part of a multi-point distributed humidity sensing system, in which perhaps 10 sensors could be sited on a single multi-mode optical fibre up to 1 km in length, with sensors placed within several meters of one another if necessary. There are a number of applications where a distributed humidity sensing system of this type would be far more cost-effective than using separate electronic humidity sensors. Further work is now required to establish the life of the optical fibre sensor, to engineer an arrangement which will minimise effects due to atmospheric dirt and pollution, to increase responsivity at low humidity, and to increase the operational temperature range.

ACKNOWLEDGEMENTS

The authors wish to thank David Butler at BRE for carrying out the measurements of temperature and humidity in BRE's environmental test room.

REFERENCES

1 Russell A.P. and Fletcher K.S., Optical sensor for the determination of moisture, Anal. Chim. Acta., 1985, 170, 209-216.

2 Stuart A.D. and Grazer P.E., A fibre-optic relative humidity sensor, Intern. J. of Optoelectronics, 1988, 3, 177-186.

3 Mitschke F., Fibre-optic sensor for humidity , Optics Letters, 1989, 14, 967-969.

4 Zhu C. *et al.*, A new fluorescence sensor for quantification of atmospheric humidity, J. Electrchem. Soc., 1989, 136, 567-570.

5 Spooncer R.C., Al-Ramadhan F.A. and Jones B.E., A humidity sensor using a wavelength-dependent holographic filter with fibre optic links, Intern. J. of Optoelectronics, 1992, 7, 449-452

6 Kharaz A. and B.E. Jones, A intrinsic optical fibre sensor, Intern. Conf. on Moisture and Humidity Measurements (Sira Ltd, Chislehurst), 1993, 1, 1.1.

7 Kharaz A. and B.E. Jones, A distributed fibre optic sensing system for humidity measurement, Intern. Conf. on Applications of Photonic Technology, Canada, 1994, 335-338.

Contact point:
Professor Barry E Jones, Brunel Centre for Manufacturing Metrology, Brunel University, Uxbridge Middlesex, UB8 3PH, UK.
Tel.: +44 (0)1895-274 000 Ext. 2637, Fax: +44 (0)1895-812 556, Email: barry.jones@brunel .ac.uk

Ahmad Kharaz, Department of Telematics, The Open University, Walton Hall, Milton Keyenes, MK7 6AA, UK. Tel.: +44 (0)1908-652 510, Fax +44(0)1908-653 658, Email: a.kharaz@open.ac.uk.

Ken Bromley, Building Research Establishment Ltd , Garston, Watford, Herts, WD2 7JR, UK. Tel.: +44 (0)1923-664 840, Fax: +44 (0)1923-664 781, Email: bromleyk@bre.co.uk.

ELSEVIER

Sensors and Actuators A 46–47 (1995) 491–493

SENSORS AND ACTUATORS A PHYSICAL

A distributed optical-fibre sensing system for multi-point humidity measurement

A. Kharaz, B.E. Jones

The Brunel Centre for Manufacturing Metrology, Brunel University, Uxbridge, Middlesex UB8 3PH, UK

Abstract

A novel multi-point distributed humidity-sensing system has been constructed based on the principle of using the absorption spectrum of a colorimetric reagent (cobalt chloride) immobilized on the surface of the core of a multimode optical fibre by employing a thin gelatin film. Two-wavelength detection is employed to provide intensity referencing. Light attenuation at the reference wavelength is only 0.2 dB. The basic design, construction and testing of an experimental sensor in the humidity region 20–80% RH and temperature range 25–50 °C is described. Resolution can be better than 2% RH and the time constant is about one second. Repeatability is at least as good as the resolution of measurement. A two-wavelength optical time-domain reflectometer (OTDR) has been developed and a four-sensor network has been built. The resolution of measurement on the network can be better than 4% RH, but because of noise in the OTDR the resolution value is dependent on the averaging time in the instrument.

Keywords: Humidity measurement; Optical-fibre sensors

1. Introduction

The measurement of relative humidity (RH) is rapidly increasing in importance in physical, chemical and biological processes as industry attempts to improve quality and production rates by better control of RH. Typical examples occur in the food, textile, chemicals, electronics and pharmaceutical industries. Fibre-optic humidity sensors would not only have the advantages of freedom from electromagnetic interference, intrinsic safety and remote monitoring, but offer the prospect of distributed sensing using the fibre itself as the sensor, and so it is not surprising that several optical-fibre humidity-sensing methods have been reported. These methods are mainly based on one of the following phenomena: colorimetric reagents that change colour with relative humidity [1]; change in physical size with humidity [2]; change of refractive index with humidity [3]; change of reflectivity of thin metal films with humidity [4]; change of fluorescence intensity with humidity [5].

2. Basic scheme

The sensor described here [6] is based on the colorimetric interaction of cobalt chloride with water molecules. The anhydrous salt is blue and turns pink as water of hydration converts the salt to hexahydrate [1]. In the sensor cobalt chloride is immobilized on the surface of the core of the optical fibre using a gelatin film with a slightly higher refractive index than that of the fibre core. Because of this, light in the optical fibre will travel through the film. As the external humidity level alters so does the moisture content of the film and the light absorption in the sensitive wavelength region. Thus attenuation experienced by the wavelength signal in this region will give an indication of the humidity level, while the second wavelength signal is used to eliminate the common-mode variations, notably temperature variation. Because the optical fibre is used to make the measurement, this novel humidity sensor is an intrinsic optical-fibre device.

A single optical-fibre sensor was constructed using 600 μm core HCS (hard clad silica) optical fibre. At the sensing point along the fibre the cladding was removed over 50 mm and replaced by the cobalt chloride–gelatin thin film, as shown in Fig. 1. Since the refractive index of the film is greater than that of the fibre core, practically all light launched through the fibre will transverse the film, thus interacting with cobalt chloride molecules and giving good sensitivity to changes in atmospheric moisture.

0924-4247/95/$09.50
SSDI 0924-4247(94)00948-H

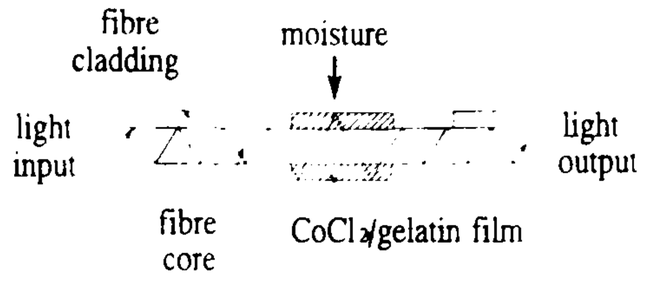

Fig. 1. Basic sensor construction.

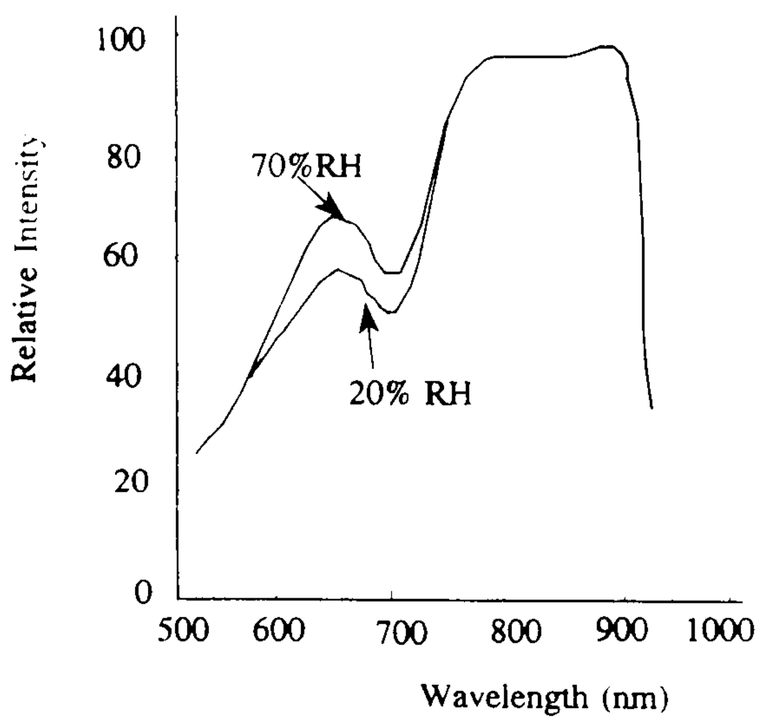

Fig. 2. Spectral response of sensor at two RH% values.

A distributed sensing network can be constructed for a series of measurands that affect the attenuations of the optical fibre at various points along its length [7]. Thus a series of humidity sensors as previously described can be sited at various points along the optical fibre. An optical time-domain reflectometer (OTDR) technique can be used to establish the optical attenuation values of the multiple sensors and thus to establish humidities at the various points. In this method a pulsed laser diode is coupled to the optical fibre via a directional coupler, which also allows the return backscattered light (a function of the localized attenuations) to be collected by a photodiode detector.

An OTDR utilizing two pulsed laser diodes operating at 670 and 850 nm, respectively, has been developed. For demonstration purposes a four-sensor network has been constructed using a 200 μm core HCS optical fibre; the length of optical fibre from the OTDR to the first sensor is 20 m and the distance between sensors is 20 m.

3. Experiments and results

White light was launched into the sensing fibre and the intensities of spectra of the collected light were measured using a spectrum analyser. The sensor (using 600 μm core) was placed in an environmental chamber of size 0.3 m × 0.3 m × 0.3 m, and two spectral responses were obtained at two different RH% values, while keeping the temperature constant at 36 °C (Fig. 2). It can be seen that a change of relative humidity affects the spectral absorption of the sensor in the wavelength region 600–740 nm. Hence a second wavelength outside this region (at, say, 850 nm) can be used to provide an intensity reference to enable rejection of changes in common-mode light-intensity variations (such as those caused by temperature variations). The light attenuation of the sensor at a wavelength of 850 nm is 0.2 dB.

With the sensor placed in the environmental chamber, the relative humidity was varied again with the temperature now kept constant at 25 °C. At each humidity value the intensities of the collected light at the two wavelengths 670 nm and 850 nm were noted. The relative intensity (RI) plotted in Fig. 3 was obtained by dividing the intensity of light at 670 nm by that at 850 nm.

This graph can be considered to have three different operating regions, 0–40, 40–70 and 70–100 %RH. The average changes in RI per 1% RH change for these three regions are 0.001, 0.007 and 0.002 RI units per 1% RH, respectively. The resolution of relative intensity measurement was about 1% RI, determined by the resolution of the spectrum analyser. When the experiment was repeated for the temperature range 25–50 °C no discernible change in these results was noted.

Repeatability tests have been undertaken over a three month period during which the sensor was exposed to cycles of humidity change in the operating range 20–88 %RH; repeatability has always been within the resolution limit. The time constant of the sensor, defined as the time taken to reach 90% of the final value, was found to be approximately one second. This measurement was achieved by applying two moisture streams (70% RH and dry 20% RH) alternately at the sensor. The resolution of the sensor is a function of the cobalt chloride concentration within the film and was found to be better than 2% above 40% RH, and better than 4% below 40% RH.

The sensors of the network were placed in the humidity chamber and exposed to cycles of humidity in the operating range 20–80% RH. At each humidity level the attenuation caused by the sensors was measured at 670 nm and then at 850 nm using the OTDR. A typical OTDR trace is shown in Fig. 4. From these

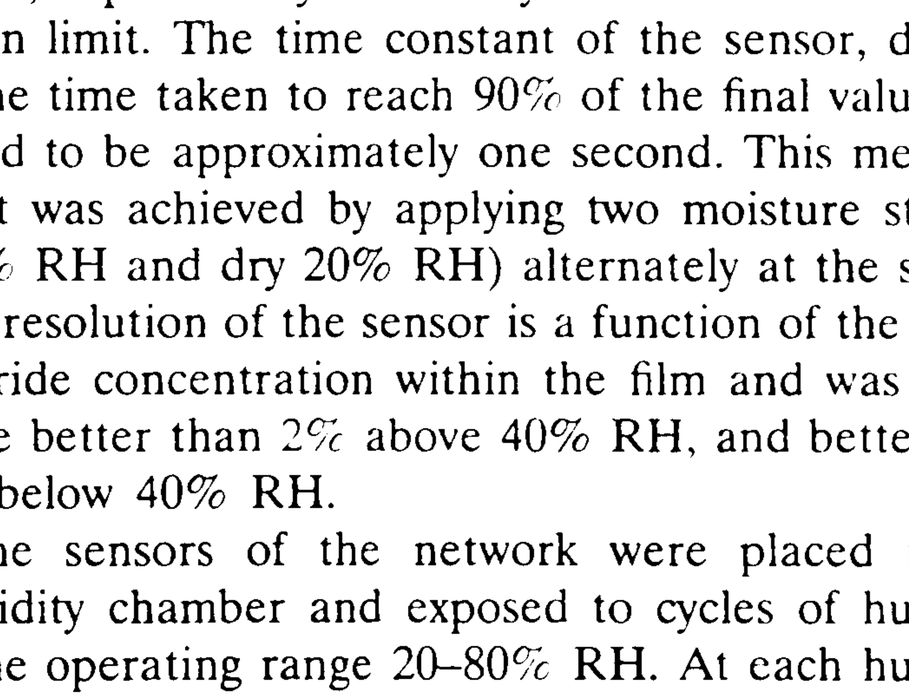

Fig. 3. Sensor characteristics.

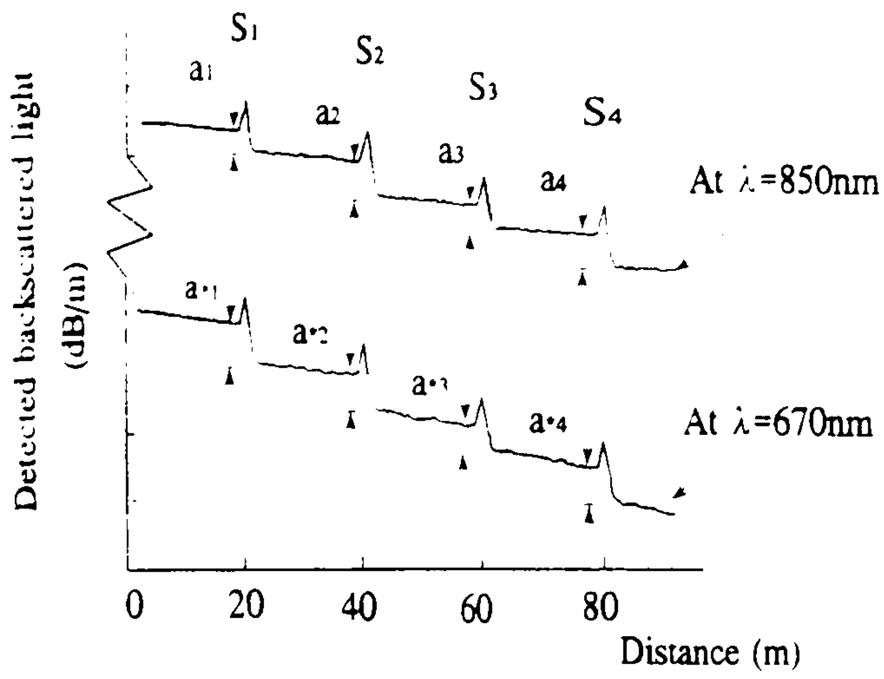

Fig. 4. Typical OTDR trace: a_1–a_4 and a^*_1–a^*_4 are optical attenuations of sensors S_1–S_4 at wavelengths of 850 and 670 nm, respectively.

Table 1
Characteristics of the four-sensor network

RH%	RA of S_1 (dB)	RA of S_2 (dB)	RA of S_3 (dB)	RA of S_4 (dB)
20	3.2	2.8	2.3	2.4
30	3.1	2.7	2.2	2.3
40	2.8	2.6	2.1	2.2
50	2.5	2.4	2.0	2.1
60	2.3	2.1	1.9	1.8
70	1.8	1.6	1.5	1.6
80	1.4	1.3	1.6	1.5

two values a relative attenuation (RA) in dB has been calculated and tabulated in Table 1; the standard deviation had a value of 0.3 dB, caused by noise, when averaging over 1 s, but when averaging was taken over 2 min the standard deviation was reduced to 0.03 dB. The peaks of reflected light at each sensor are due to Fresnel reflections.

4. Conclusions

A novel multi-point distributed humidity-sensing system has been developed. It is expected that more than 10 sensors can be sited on the single multimode optical fibre which might be, for example, 1 km in length; the sensors could be placed within several metres of one another, if necessary. There are a number of applications where installation of a distributed humidity-sensing system would be far easier than using multiple electronic humidity sensors. Further work is required to establish the long-term life of the sensor and to engineer an arrangement to minimize any effects due to atmospheric dirt and pollution, to improve the signal-to-noise ratio, to increase the operational temperature range and to allow operation at low humidity levels.

Acknowledgements

The authors wish to acknowledge support for this work received from the UK Science and Engineering Research Council, the UK National Physical Laboratory and Professor R.C. Spooncer.

References

[1] A.P. Russell and K.S. Fletcher, Optical sensor for the determination of moisture, *Anal. Chim. Acta, 170* (1985) 209–216.
[2] R.C. Spooncer, F.A. Al-Ramadhan and B.E. Jones, A humidity sensor using a wavelength-dependent holographic filter with fibre optic links, *Int. J. Optoelectron., 7* (1992) 449–452.
[3] F. Mitschke, Fibre-optic sensor for humidity, *Optics Lett., 14* (1989) 967–969.
[4] A.D. Stuart and P.E. Grazer, A fibre-optic relative humidity sensor, *Int. J. Optoelectron., 3* (1988) 177–186.
[5] C. Zhu, F.V. Bright, W.A. Wyatt and G.M. Hieftje, A new fluorescence sensor for quantification of atmospheric humidity, *J. Electrochem. Soc., 136* (1989) 567–570.
[6] A. Kharaz and B.E. Jones, An intrinsic optical fibre sensor, *Int. Conf. Moisture and Humidity Measurements (Sira Ltd, Chislehurst),* 1993, Vol. 1, pp. 1.1–1.4.
[7] M.K. Banoski and S.M. Jensen, Fibre waveguide: a novel technique for investigating attenuation characteristic, *Appl. Opt., 15* (1976) 2112–2115.

APPENDIX II

A selection of humidity related British Standards

1. BS 903:Part A35:1985

Methods of testing vulcanized rubber. Humidities and times for conditioning pieces.

2. BS 1006:B02:1973

Formerly BS 1006:HTC:1961. Methods of test for colour fastness of textiles and leather.

3. BS 1051:1981

Glossary of terms relating to the conditioning and mass determination of textiles.

4. BS 1133:Section 19:1968

Packaging code. Use of desiccants in packaging. Function, choice, method of calculating quantity of desiccant.

5. BS 1339:1965

Definitions, formulae and constants relating to the humidity of the air. Includes tables of saturation vapour pressures and bibliography.

6. BS 1706:1960

Specification for electroplated coatings of cadmium and zinc on iron and steel purity, appearance, thickness and adhesion. Corrosion resistance for passivated coatings. Tests for local and average thickness, adhesion by burnishing, humidity for passivated coatings, presence and adherence of chromate film

7. BS 1706:1951

Basic environmental testing procedures. Composite test procedure for component type specimens to determine in an accelerated manner their resistance to deteriorative effects of high temperature/humidity and cold conditions.

8. BS 2011:Part 2.2C & D:1981

Basic environmental testing procedures. Guidance for damp heat tests. Guidance for specification writers on the use of tests described in BS 2011:Parts 2.1Ca, 2.1Da, 2.1Db and 2.1 Z/AD.

9. BS 2844:1972

Memorandum on conditioning of solid electrical insulating materials prior to and during testing. Standard conditions of temperature, atmospheric humidity and immersion in liquid for use in testing electrical insulating materials.

10. BS 3156:Part 5:1969

Methods for the analysis of fuel gases. Techniques for high pressure gases determination of water and hydrocarbon dew points, dust and oil fog, sulphur compounds and other constituents of gases at pressures above 1.7 bar; includes observations on the determination of density.

11. BS 3292:1960

Specification for direct reading hygrometers. Two grades of non-recording direct reading hygrometers are specified, both calibrated for use over the range 20 to 100 per cent relative humidity. Permissible error, temperature correction, drift, response time and constructional requirements are specified and methods of test described.

12. BS 3431:1973

Method for the conditioning of paper and board for testing. Defines the conditioning

atmosphere and method of conditioning paper and board before and during testing.

13. BS 3718:1964

Specification for laboratory humidity ovens.

14. BS 3898:1965

Specification for laboratory humidity ovens (injection type). Humidity-sensitive device controls admission of moisture from external source. Temperature variation (from point to point); temperature fluctuation (with time); RH fluctuation; stability of oven conditions; time of recovery; absence of droplets; reproducibility of oven conditions; rates of heating and cooling.

15. BS 3900:Part F9:1982

Methods of test for paints. Determination of resistance to humidity (continuous condensation). Specifies a method for determining resistance to high humidity under continuous condensation conditions.

16. BS 4443:Part 4:1970

Methods of test for flexible cellular materials. Method 10. Determination of solvent swelling. Method 11. Humidity ageing at an elevated temperature. Method 12. Heat ageing.

17. BS 4533:Part 1:Section 1.9:1971

Specification for electric luminaires (lighting fittings). General requirements and tests. Resistance to the ingress of moisture and dust.

18. BS 4672:Part 1:1.971

Guide to hazards in the transport and storage of packages. Climatic hazards. Climatic conditions likely to be encountered by packages, worldwide, aboard ship, in aircraft.

in road or rail vehicles and during storage.

19. BS 4682:Part 2:1972

Methods of test for the dimensional stability of textile floor coverings. Determination of dimensional changes due to changes in ambient humidity. Applicable to all textile floor covering.

20. BS 4826:Part 2:1972

Methods of test for complete, filled transport packages. Conditioning for testing. Preferred atmospheric temperatures and relative humidities, preferred minimum times of conditioning, and procedure.

21. BS 4864:1973

Recommendations on the design and testing of enclosures for environmental testing.

22. BS 5369:1976

Methods of testing doors behaviour under humidity variations of door leaves placed in successive uniform climates. Applicable to all flat and rigid doors containing hygroscopic materials.

23. BS 5579:1978

Specification for standard reference conditions for measurement of petroleum liquids and gases. Conditions of temperature and pressure for petroleum measurement identical with ISO 5024 are specified with an additional UK requirement for humidity of gases.

24. BS 5687:1979

Recommendations for storage conditions for silver image photographic plates for record purposes. Defines terms and recommends practices for the storage of black-

and-white silver image photographic plates having integral photographic layers and intended for record purposes.

25. BS 5967:Part 1:1980

Operating conditions for industrial-process measurement and control equipment. Specification for temperature, humidity and barometric pressure.

26. BS 1195:Part 1:1973

Specification for kitchen fitments and equipment. Imperial units with metric equivalents. Dimensional equivalents of kitchen fitments for domestic kitchens. Performance, protection, storage and installation.